

PROJECT ADMINISTRATION DATA SHEET

ORIGINAL REVISION NO. 11

Project No. G-35-651 (R6020-0A0) GTRC ~~XXX~~ DATE 8 / 28 / 85

Project Director: Tim Long Leland Timothy Long School ~~XXX~~ Geo Sci

Sponsor: U. S. Nuclear Regulatory Commission

Type Agreement: Contract No. NRC-04-85-122

Award Period: From 8/1/85 To 7/31/88 (Performance) 7/31/88 (Reports)

Sponsor Amount:	<u>This Change</u>	<u>Total to Date</u>
Estimated: \$	<u>100,000</u>	\$ <u>278,921</u>
Funded: \$	<u>100,000</u>	\$ <u>100,000 (Through 7/31/86)</u>

Cost Sharing Amount: \$ may be added later Cost Sharing No: G-35-324

Title: Georgia/Alabama Regional Seismographic Network

ADMINISTRATIVE DATA

OCA Contact Brian J. Lindberg X4820

1) Sponsor Technical Contact: Dr. Andrew Murphy ^{querry} Dr. ERNST ZURFLUEH

U. S. Nuclear Regulatory Commission Ronald D. Thompson
Contracting Officer

Mail Stop: 1130-SS Division of Contracts

Washington, DC 20555 U. S. Nuclear Regulatory Commission

(301) 427-4078 Mail Stop: AR-2223

Washington, DC 20555

Defense Priority Rating: N/A Military Security Classification: N/A

(or) Company/Industrial Proprietary: N/A

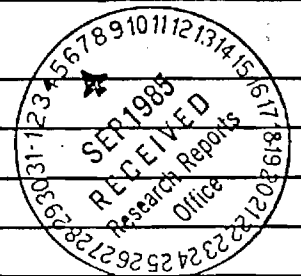
RESTRICTIONS

See Attached N/A Supplemental Information Sheet for Additional Requirements.

Travel: Foreign travel must have prior approval - Contact OCA in each case. Domestic travel requires sponsor approval where total will exceed greater of \$500 or 125% of approved proposal budget category.

Equipment: Title vests with GIT

COMMENTS:



COPIES TO: SPONSOR'S I. D. NO. 02.106.000.86.001

Project Director	Procurement/GTRI Supply Services	GTRC
Research Administrative Network	Research Security Services	Library
Research Property Management	<u>Reports Coordinator (OCA)</u>	Project File

GEORGIA INSTITUTE OF TECHNOLOGY
OFFICE OF CONTRACT ADMINISTRATION

NOTICE OF PROJECT CLOSEOUT

Closeout Notice Date 08/29/90

Project No. G-35-651_____

Center No. R6020-0A0_____

Project Director LONG L T_____

School/Lab E & A SCI_____

Sponsor NUCLEAR REGULATORY COMM/GENERAL_____

Contract/Grant No. NRC-04-85-122_____

Contract Entity GTRC

Prime Contract No. _____

Title GA/AL REGIONAL SEISANOGRAPHIC NETWORK_____

Effective Completion Date 900731 (Performance) 900731 (Reports)

Closeout Actions Required:	Y/N	Date Submitted
Final Invoice or Copy of Final Invoice	Y	_____
Final Report of Inventions and/or Subcontracts	N	_____
Government Property Inventory & Related Certificate	Y	_____
Classified Material Certificate	N	_____
Release and Assignment	Y	_____
Other _____	N	_____
Comments _____		

Subproject Under Main Project No. _____

Continues Project No. _____

Distribution Required:

Project Director	Y
Administrative Network Representative	Y
GTRI Accounting/Grants and Contracts	Y
Procurement/Supply Services	Y
Research Property Management	Y
Research Security Services	N
Reports Coordinator (OCA)	Y
GTRC	Y
Project File	Y
Other _____	N
_____	N

GEORGIA INSTITUTE OF TECHNOLOGY
OFFICE OF CONTRACT ADMINISTRATION

NOTICE OF PROJECT CLOSEOUT

Closeout Notice Date 03/04/91
Original Closeout Started 08/29/90

Project No. G-35-651 _____ Center No. R6020-0A0 _____

Project Director LONG L T _____ School/Lab E & A SCI _____

Sponsor NUCLEAR REGULATORY COMM/GENERAL _____

Contract/Grant No. NRC-04-85-122 _____ Contract Entity GTRC

Prime Contract No. _____

Title GA/AL REGIONAL SEISANOGRAPHIC NETWORK _____

Effective Completion Date 900731 (Performance) 901031 (Reports)

Closeout Actions Required:	Y/N	Date Submitted
Final Invoice or Copy of Final Invoice	Y	_____
Final Report of Inventions and/or Subcontracts	N	_____
Government Property Inventory & Related Certificate	Y	_____
Classified Material Certificate	N	_____
Release and Assignment	Y	_____
Other _____	N	_____
Comments _____		

Subproject Under Main Project No. _____

Continues Project No. _____

Distribution Required:

Project Director	Y
Administrative Network Representative	Y
GTRI Accounting/Grants and Contracts	Y
Procurement/Supply Services	Y
Research Property Management	Y
Research Security Services	N
Reports Coordinator (OEA)	Y
GTRC	Y
Project File	Y
Other _____	N
_____	N

G-35-651

NUREG/

GEORGIA/ALABAMA REGIONAL SEISMOGRAPHIC NETWORK

Annual Report
July 1, 1986 -- June 30, 1987

Prepared by L. T. Long
Georgia Institute of Technology

Prepared for
U. S. Nuclear Regulatory Commission

NUREG/

GEORGIA/ALABAMA REGIONAL SEISMOGRAPHIC NETWORK

Annual Report
July 1, 1986 -- June 30, 1987

Manuscript Completed: December 1989
Date Published: March 1990

Prepared by L. T. Long
Georgia Institute of Technology
School of Geophysical Sciences
Atlanta, Georgia 30332

Prepared for
Office of Nuclear Regulatory Research
U. S. Nuclear Regulatory Commission
Washington, D.C. 20555

Under Contract No. NRC 04-85-122

EXECUTIVE SUMMARY AND ABSTRACT

OBJECTIVE:

The objective of this study is to contribute data and analyses conducive to the development of criteria for establishing earthquake hazard potential in the southeastern United States.

TASKS:

The first task is to install and maintain the Georgia/Alabama seismic network. The seismic network consists of about 21 stations in Alabama, Georgia, and adjoining regions of southeastern Tennessee and South Carolina. The seismic net includes three three-component short period stations and operates completely on solar power.

The second task is to monitor the seismic activity in southeastern Tennessee, northern Alabama, and Georgia. The data are to be used in appropriate topical studies.

RESULTS:

Five topical studies achieved notable conclusions or were completed during the reporting period of July 1986 to June 1987. The principal conclusions are summarized below and presented in detail in Appendices A-E.

During the first quarter of 1987 a swarm of small earthquakes occurred in the Lake Sinclair, Georgia, vicinity. The events occurred in three main shocks of magnitude 2 and their aftershocks. The third event had an unusually rapid decay in aftershock activity suggesting complete release of stress.

A solid sphere in a fluid or a fluid-filled sphere in a solid elastic or viscoelastic media affects the scattered waves. For the first case, only a scattered P wave can exist, but the properties of the elastic scatterer affect the scattering coefficient, i.e. the quality factor due to the scattering. In the second case, the spectral response of the scatterer is much more complicated because of resonances in the fluid-filled obstacle. Resonance of the scatterer plays an important role in the calculations of the scattering coefficients, especially for wavelength shorter than the diameter of the scatterer. The viscosity of the solid material affects the scattering coefficients; it smooths its shape and it shifts the resonant eigenfrequency.

The P-wave coda is generally interpreted as P wavelets scattered from heterogeneities in the lithosphere. The spectral signature of an individual P wavelet can depend on absorptive attenuation and scattering along its propagation path. In particle velocity records, the Brune source model generates a wavelet with a spectral peak near the corner frequency. With increased time, absorptive attenuation systematically shifts the corner frequency toward lower frequencies. The spectra of wavelets scattered from heterogeneities can be complex and depends on the size of the heterogeneity. For corner frequencies below the fundamental resonance of the heterogeneity, the corner frequency is systematically shifted to higher frequencies. In moving window high-resolution spectral analysis of P-wave coda, systematic

increases and decreases in spectral peaks are observed that may be explained by shifts in the corner frequency caused by absorptive attenuation and scattering.

Coda Q is a measure of the scattering and attenuation properties of the crust between a source and recording station. In southeastern Tennessee, the coda of earthquakes appears to be dependent on direction to the epicenter. In order to determine whether the coda are controlled by crustal structure, we computed synthetic finite difference seismograms for the complex structure of southeastern Tennessee. The comparison of synthetic and observed seismograms suggest that a zone of low Q exists near station CBT and that the structure alone can not explain the scattering properties. The addition of a random velocity variation of 5 percent improved the comparison, but the coda Q values were still significantly lower for the synthetic seismograms.

The location method used at Georgia Tech computes the origin time independent of location. The location and depth are then computed with a fixed origin time. The basis for this separation can be derived from a consideration of the covariance matrix used to weight arrivals used in earthquake location. Normally the off diagonal elements are not used and set to zero. In the case of S and P phases recorded at the same station, however, the off diagonal elements are significant. By including the off diagonal elements, one can show that the proper inverse separates origin time computations from location when S and P times are available. The resulting location precision is better than normally computed using standard methods.

TABLE OF CONTENTS

	page
Executive Summary and Abstract.....	iii
Table of Contents.....	v
List of Figures.....	vi
List of Tables.....	viii
I. Introduction.....	1
A. Objectives.....	1
B. Summary of Results and Findings.....	2
Network maintenance and seismic monitoring.....	2
Graphical representation of operational status.....	2
Plans for next year.....	2
C. Abstracts of Presentations.....	2
Results of topical studies.....	5
Appendix A.....	7
Appendix B.....	12
Appendix C.....	19
Appendix D.....	28
Appendix E.....	41

LIST OF FIGURES

	page
Figure 1. Seismic stations maintained or monitored.....	7
Figure 2. Graphical representation of station coverage.....	8
Appendix A	
Figure 1. Number of events versus time for the Lake Sinclair swarm of 1 January, 1987 - 31 March, 1987.....	11
Figure 2. Number of events in 0.5 magnitude increments for the Lake Sinclair swarm of 1 January, 1987 - 31 March, 1987.....	12
Figure 3. Cumulative number of events versus time for the Lake Sinclair swarm of 1 January, 1987 - 31 March, 1987.....	13
Appendix B	
Figure 1. Model parameters for a plane P wave incident on the south pole of a scattering sphere.....	17
Figure 2. Scattering cross section of the scattered P wave for an elastic sphere in sea water.....	18
Figure 3. Scattering cross section of the scattered P wave for a fluid-filled sphere in an elastic media.....	19
Figure 4. Scattering cross section of the scattered S wave for fluid-filled sphere in an elastic media.....	20
Appendix C	
Figure 1. Spectra of a Brune type displacement showing effects of intrinsic attenuation.....	25
Figure 2. Influence of scattering on the velocity spectra of a seismic wavelet. Top diagram shows the effects on a low-frequency wavelet. Bottom diagram shows the effects on a high-frequency wavelet. In these examples the spectral response of the scatterer dominates the scattered wavelet.....	26
Figure 3. Moving window spectra of a P wave coda showing the effects of attenuation, creating a gradual decrease in the peak frequency.....	27

List of Figures (continued)

Figure 4.	Moving window spectra of a P wave coda showing the effects of attenuation. Note the gradual decrease in the peak frequency of the spectral maximums at 5.5 Hz...	28
Figure 5.	Moving window spectra of a P wave coda showing systematic jumps to higher frequencies which may be due to scattering.....	29
Appendix D		
Figure 1.	Seismograms recorded at station CBT showing variation in coda with azimuth.....	33
Figure 2.	Location of events and Bouguer gravity anomalies near station CBT.....	34
Figure 3.	Projection of crustal structure onto northwest trending line (figure 2). The Bouguer anomalies are modeled by two zones of low density. (NY-AL = New York-Alabama Lineament, GS = Great Smoky Fault, and BZ = Brevard Zone).....	35
Figure 4.	Scattering of an incident P-wave on a layered random velocity zone. The traces compare analytical results with the finite difference synthetic traces.....	36
Figure 5.	Crustal model used to generate synthetic traces. The S1, S2, and S3 are location of compressional sources...	37
Figure 6.	Synthetic traces for homogeneous media and a media with a five percent random perturbation in velocity....	38
Figure 7.	Event 8 showing the variation in Q obtained when examining different portions of the coda.....	39
Figure 8.	Outline of zone of apparently anomalous Q in southeastern Tennessee.....	40
Appendix E		
Figure 1.	Autocorrelation functions for two seismic refraction lines. The reduced travel time curves are shown below. The reduced velocity for the RBR data was 6.05 km/s and is typical of crystalline Piedmont rocks in Georgia and South Carolina. The southeastern Tennessee data has a reduced velocity of 5.95 km/s and represents Blue Ridge metasediments.....	51

List of Figures (continued)

Figure 2.	Analysis of travel time residuals for earthquakes recorded at station CBT. a) epicenter map showing the magnitude of the travel time residuals superimposed on isostatic gravity anomalies. b) autocorrelation function of travel time residuals assuming radial symmetry. c) projection of residuals onto a line perpendicular to the strike of the basement structures. d) one dimensional autocorrelation function for projection in c.....	52
Figure 3.	Autocorrelation function from gravity data and its conversion to equivalent travel time residuals using the relation from Olsen et al., (1986).....	53
Figure 4.	Stations (solid circles) and epicenter (hexagon) for the event of January 8, 1986.....	54

LIST OF TABLES

Appendix A

Table I. Constants for Omori's Law for two events..... 9

Appendix D

Table 1. Coda Q computed for observed and synthetic seismograms..... 32

Appendix E

Table I. Data from event of January 8, 1986..... 55

I. INTRODUCTION

A. Objectives

The objective of this study is to contribute data and analyses conducive to the development of criteria for establishing earthquake hazard potential in the southeastern United States. The main tasks are to install and maintain a seismic network and monitor the seismic activity in eastern Tennessee, northern Alabama, and Georgia. The data are to be contributed to the southeastern U. S. regional bulletin. Also, available information will be used in appropriate topical studies.

Specific objectives for network maintenance and seismic monitoring are as follows:

- * Install or provide about 16 short-period seismograph stations deployed in Tennessee, Alabama, and Georgia. This network is to be operated with a maximum of 5 percent downtime.
- * Obtain and/or reaffirm use permits and telemetry service to convey the data to a central recording point.
- * Provide all seismic phase readings and hypocenter locations to the Southeast U. S. Seismographic Network Bulletin.
- * Provide a recording medium with on-line digital recording at the Central Recording Facility.
- * Report any significant earthquake within the study region to the Nuclear Regulatory Commission within 24 hours.
- * Relocate and/or establish new seismograph stations as it becomes necessary after approval of the Nuclear Regulatory Commission.

Objectives for topical studies are as follows:

- * Study the spatial and temporal distributions, including earthquake recurrence rates, of seismicity and relate them to structural features.
- * Identify parameters that influence seismic processes within the network area and use these in defining seismogenic/tectonic provinces.
- * Study crustal and upper mantle velocity structure in the United States based on the current data from the network.
- * Study the magnitudes of historic events using magnitude-felt area relationships and obtain the magnitude-frequency relationships.
- * Evaluate the relative significance of results obtained in each of the above analyses as they impact the determination of seismic hazards.

B. Summary of Results and Findings

Network maintenance and seismic monitoring

During the period of 1 July, 1986, to 30 June, 1987, the Georgia/Alabama Regional Seismic Net consisted of 22 stations located as shown in Figure 1. The Clarks Hill Reservoir Area and the area of Lake Richard B. Russell were monitored by five stations. The state of Georgia is monitored by five additional stations. Seven stations are located in Alabama and five in southeastern Tennessee. The Alabama, Tennessee and northwest Georgia stations constitute coverage for the termination of the Southern Appalachian seismic zone.

All stations in the Georgia/Alabama Regional Seismographic Network were converted to solar power to minimize the field maintenance and to eliminate the need for battery changes every six to nine months.

Graphical representation of the operational status of the network

The high level of station down time in the late spring was caused by heavy thunder storm activity and lightening damage. The graphical representation of the operational status of the network is given in the form of the daily log of recording and is given in Figure 2.

Plans for next year

The study of the location of Lake Sinclair seismicity will continue to be the primary concern of a M.S. Thesis.

Digital data accumulating for the southeastern Tennessee area is showing evidence of a highly variable coda Q. Plans for next year include the development of an inversion technique for coda Q in southeastern Tennessee.

Focal mechanisms will be compared to crustal structure to evaluate consistency with selected linear features or the development of a distinctive pattern related to the seismicity.

The zone of induced seismicity in the Clarks Hill Reservoir will be studied for distribution of fractures and a comparison of these joints or fractures with seismicity.

C. Abstracts of Presentations

The following are abstracts of talks which were made possible by data and research related to the Georgia/Alabama seismographic network.

SPECULATION CONCERNING THE EFFECTS OF ATTENUATION AND SCATTERING ON THE SPECTRAL SIGNATURE OF WAVELETS COMPRISING THE P-WAVE CODA

LONG, L. T. and ALEXANDER, C. S., School of Geophysical Sciences, Georgia Institute of Technology, Atlanta, Georgia 30332-0340

The P-wave coda is generally interpreted as P wavelets scattered from heterogeneities in the lithosphere. The spectral signature of an individual P wavelet can depend on absorptive attenuation and scattering along its propagation path. In particle velocity records, the Brune source model generates a wavelet with a spectral peak near the corner frequency. With increased time, absorptive attenuation systematically shifts the corner frequency toward lower frequencies. The spectra of wavelets scattered from heterogeneities can be complex and depends on the size of the heterogeneity. For corner frequencies below the fundamental resonance of the heterogeneity, the corner frequency is systematically shifted to higher frequencies. In moving window high-resolution spectral analysis of P-wave coda, systematic increases and decreases in spectral peaks are observed that may be explained by shifts in the corner frequency caused by absorptive attenuation and scattering.

THE SCATTERING OF A SEISMIC WAVE BY A SPHERICAL INCLUSION

AN, TIE and LONG, L. T., School of Geophysical Sciences, Georgia Institute of Technology, Atlanta, GA 30332-0340

We have investigated two models in which a plane P-wave is incident on a spherical inclusion. The first model is an elastic spherical obstacle in a fluid medium. The second model is a fluid sphere in an elastic medium. The computational procedure used is the resonance scattering theory developed by Uberall and his co-workers (1978-1985). For the first case, only a scattered P wave can exist, but the properties of the elastic scatterer affect the scattering coefficient, i.e. the quality factor due to the scattering. In the second case, the spectral response of the scatterer is much more complicated because of resonances in the fluid-filled obstacle. Resonance of the scatterer plays an important role in the calculations of the scattering coefficients, especially for wavelength shorter than the diameter of the scatterer. The viscosity of the solid material affects the scattering coefficients; it smooths its shape and it shifts the resonant eigenfrequency. The background scattering coefficients, which are computed by subtraction of the portion due to the resonance from the scattering cross section, can be strong frequency dependent.

A STUDY OF CRUSTAL HETEROGENEITY IN THE SOUTHEASTERN TENNESSEE AREA BY FINITE DIFFERENCE WAVE SIMULATION

JEIH-SAN LIOW and Leland Timothy Long (Both at: School of Geophysical Sciences, Georgia Institute of Technology, Atlanta, GA 30332)

The character of seismograms recorded at station CBT depend on azimuth. Events located to the east and southeast show clean impulsive arrivals.

Events located to the west exhibit greater scattering. In order to evaluate the influence of local crustal structures on scattering, a two dimensional finite difference method was used to simulate the elastic wave propagation in a crustal model for southeastern Tennessee. The model consists of a lower-velocity sedimentary basin embedded in the continental crust with both overlaid by the Paleozoic sediments of the Valley and Ridge Geologic Province. A compressional line source was placed at depths of 7 to 15 km and at different locations relative to the structure. The waves from sources that are closer to or behind the subsurface sedimentary basin show more scattering than those from sources that are located away from the sedimentary basin. The synthetic seismograms suggest that the azimuthal variations observed at station CBT may be attributed to the existence of a southwest trending sedimentary basin located to the northwest of station CBT.

A DISCUSSION OF PRECISION IN HYPOCENTER DETERMINATION

LONG, L. T., School of Geophysical Sciences, Georgia Institute of Technology, Atlanta, GA.

The weighting matrix used in location programs contains important information concerning the uncertainty in earthquake hypocenters. The off-diagonal elements which are usually ignored have significant values for P- and S-wave arrivals at the same station and at stations close together. For these arrivals the ray paths are similar and the travel time errors will be strongly correlated. The larger off-diagonal elements increase the weights that should be applied to their respective arrivals. In the special case of S- and P-wave arrivals at the same station and small reading errors, the weighting matrix is nearly singular and the resulting weights make the origin time computation virtually independent of the location. Where data are inadequate to estimate the elements of the covariance matrix, the elements may be estimated from an autocorrelation function of travel time residuals along refraction lines or from gravity data. Use of the properly formulated weighting matrix yields consistent estimates of location errors which are independent of the precision implied by station residuals. The near-singularity of the weighting matrix for P- and S-wave arrivals at the same station suggests an alternate computation method whereby the location equations containing S and P waves at each station can be transformed to isolate the origin time computation from the epicenter computations.

SCATTERING BY A SPHERICAL OBSTACLE AND IMPLICATIONS FOR P-WAVE SCATTERING AND ATTENUATION

AN TIE and L. T. Long, School of Geophysical Sciences, Georgia Institute of Technology, Atlanta, GA 30332

The scattering of a plane longitudinal wave incident on a spherical obstacle for elastic and viscoelastic host and scattering media was investigated. The spherical obstacles considered included a rigid sphere, a spherical cavity, a liquid filled cavity and an elastic sphere. The computational technique utilized an orthogonal function expansion. Numerical results were obtained for wave number-radius products of 0 to 10, extending well beyond the region

of validity of the Rayleigh scattering approximation. The analysis of the scattering cross sections and back and forward scattering coefficients have shown that (1) there exists a significant contribution to scattering at the shorter wavelengths which is not consistent with the Born approximation, (2) the variation in the shear modulus is the most important factor in determining the scattering amplitudes, (3) the velocity models predict the greatest influence of scattering to be in the shallow crust, (4) negative contrasts give a stronger scattering response than positive contrasts at the same percent deviation, (5) scattering functions can be separated into continuous scattering coefficients for the background and discrete scattering frequencies for resonances, (6) in viscoelastic media the scattering coefficients are a function of Q in both media and they can be separated into background scattering, resonances, the interference due to the viscosity and their contrasts of the host media and scatterer, and (7) the total Q is not a simple linear combination of absorptive and scattering Q .

Results of topical studies

Five topical studies achieved notable conclusions or were completed during the reporting period of July 1986 to June 1987. The principal conclusions are summarized below and presented in detail in Appendices A-E.

A. Lake Sinclair Swarm

During the first quarter of 1987 a swarm of small earthquakes occurred in the Lake Sinclair, Georgia, vicinity. The events occurred in three main shocks of magnitude 2 and their aftershocks. The third event had an unusually rapid decay in aftershock activity suggesting complete release of stress.

B. Scattering by a spherical obstacle

A solid sphere in a fluid or a fluid-filled sphere in a solid elastic or viscoelastic media affects the scattered waves. For the first case, only a scattered P wave can exist, but the properties of the elastic scatterer affect the scattering coefficient, i.e. the quality factor due to the scattering. In the second case, the spectral response of the scatterer is much more complicated because of resonances in the fluid-filled obstacle. Resonance of the scatterer plays an important role in the calculations of the scattering coefficients, especially for wavelength shorter than the diameter of the scatterer. The viscosity of the solid material affects the scattering coefficients; it smooths its shape and it shifts the resonant eigenfrequency.

C. High-resolution studies of the seismic coda.

The P-wave coda is generally interpreted as P wavelets scattered from heterogeneities in the lithosphere. The spectral signature of an individual P wavelet can depend on absorptive attenuation and scattering along its propagation path. In particle velocity records, the Brune source model generates a wavelet with a spectral peak near the corner frequency. With increased time, absorptive attenuation systematically shifts the corner

frequency toward lower frequencies. The spectra of wavelets scattered from heterogeneities can be complex and depends on the size of the heterogeneity. For corner frequencies below the fundamental resonance of the heterogeneity, the corner frequency is systematically shifted to higher frequencies. In moving window high-resolution spectral analysis of P-wave coda, systematic increases and decreases in spectral peaks are observed that may be explained by shifts in the corner frequency caused by absorptive attenuation and scattering.

D. Finite Difference simulation of scattering and earthquake signature in southeastern Tennessee.

Coda Q is a measure of the scattering and attenuation properties of the crust between a source and recording station. In southeastern Tennessee, the coda of earthquakes appears to be dependent on direction to the epicenter. In order to determine whether the coda are controlled by crustal structure, we computed synthetic finite difference seismograms for the complex structure of southeastern Tennessee. The comparison of synthetic and observed seismograms suggest that a zone of low Q exists near station CBT and that the structure alone can not explain the scattering properties. The addition of a random velocity variation of 5 percent improved the comparison, but the coda Q values were still significantly lower for the synthetic seismograms.

E. Theory of earthquake error estimation.

The location method used at Georgia Tech computes the origin time independent of location. The location and depth are then computed with a fixed origin time. The basis for this separation can be derived from a consideration of the covariance matrix used to weight arrivals used in earthquake location. Normally the off diagonal elements are not used and set to zero. In the case of S and P phases recorded at the same station, however, the off diagonal elements are significant. By including the off diagonal elements, one can show that the proper inverse separates origin time computations from location when S and P times are available. The resulting location precision is better than normally computed using standard methods.

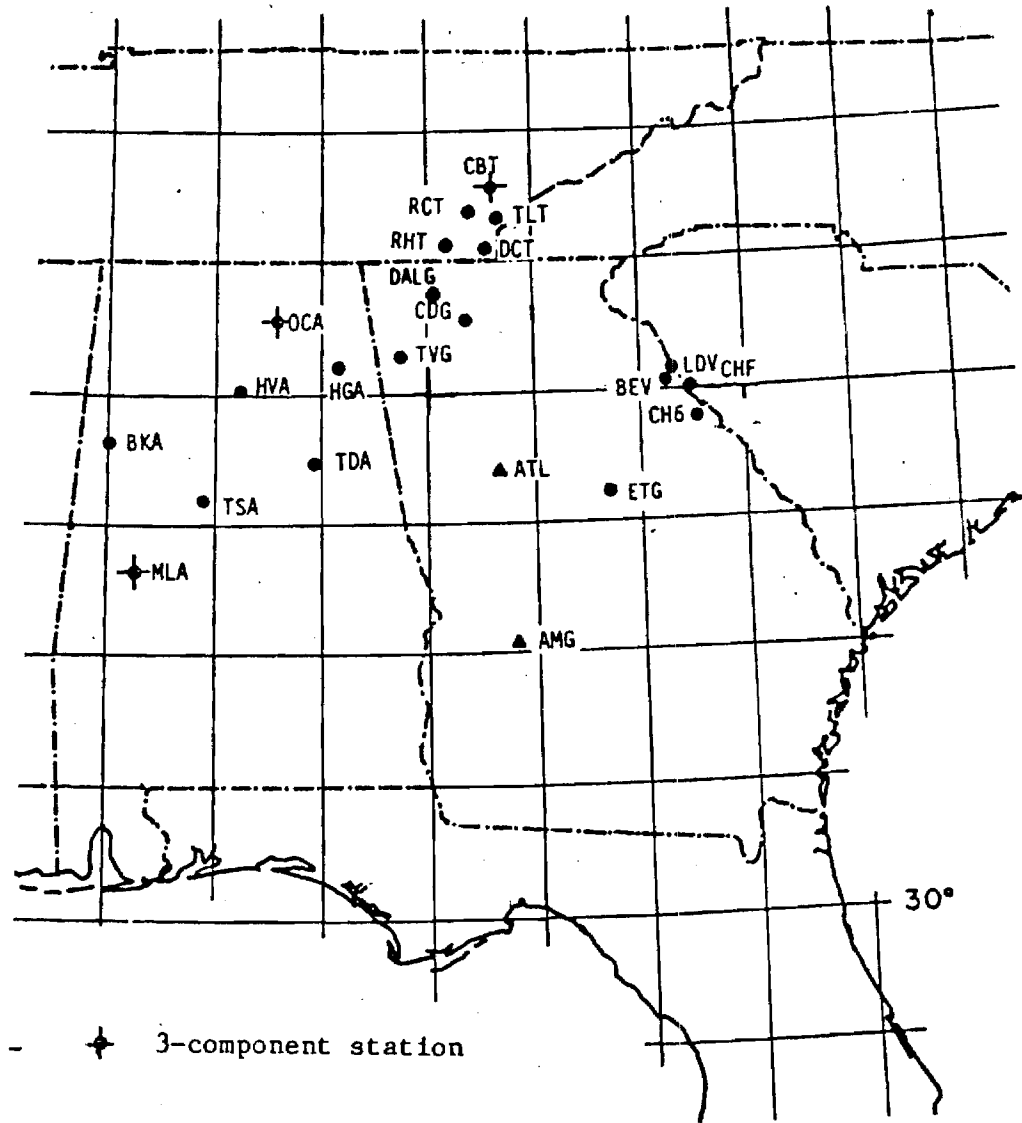
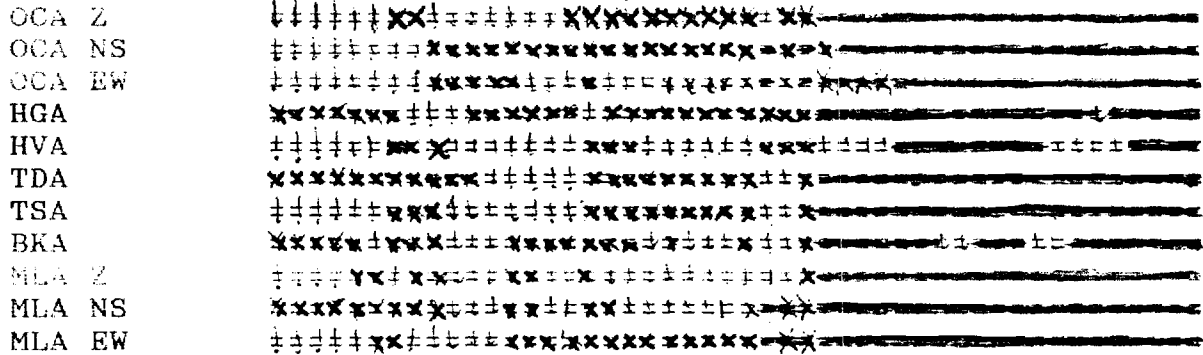


Figure 1. Seismic stations maintained or monitored.

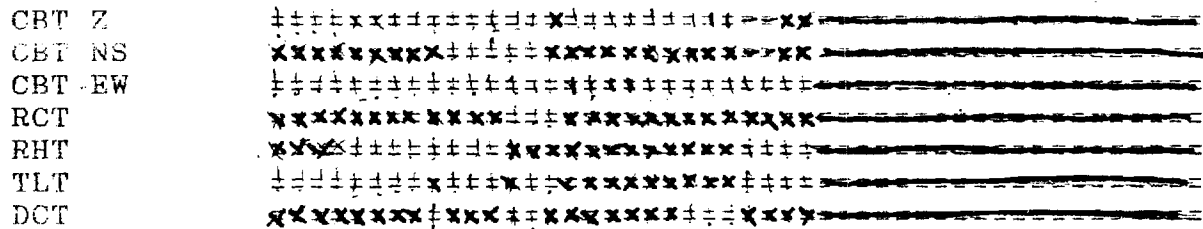
GRAPHICAL REPRESENTATION OF STATION COVERAGE

Station JUL AUG SEP OCT NOV DEC JAN FEB MAR APR MAY JUN

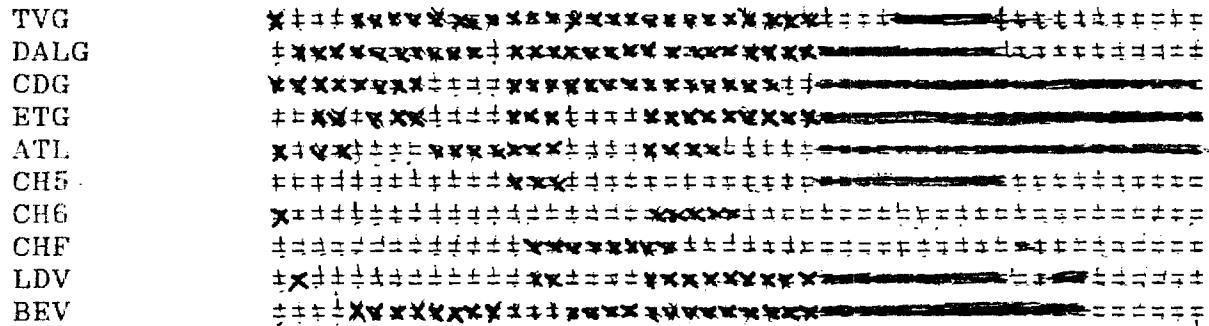
Alabama Stations



Tennessee Stations



Georgia Stations



- x Indicates station recorded on analog recorder.
- = indicates station recorded on digital recorder.
- ! Indicates station not operating.

Figure 2. Graphical representation of station coverage.

APPENDIX A

THE LAKE SINCLAIR, GEORGIA, EARTHQUAKE SWARM:
1 JANUARY-31 MARCH, 1987

During the period of January 1, 1987, to March 31, 1987, a swarm of 57 minor earthquakes were detected by the Georgia Tech Seismic Network in the vicinity of Lake Sinclair, Georgia. The largest event was a magnitude 2.1; but, it was one of three greater than magnitude 2.0. The details of these events are presented in the Georgia Institute of Technology, Quarterly Earthquake Bulletin for 1 January, 1987 - 31 March, 1987 and SEUSSN Bulletin. An additional 25 microearthquakes with magnitudes less than 0.0 were detected but were not listed. These earthquakes are believed to be reservoir induced. The activity level before January 1987 and after March 1987 was typically one to two events per month.

The number of events occurring in five-day time increments (Figure 1) shows three peaks, each corresponding to the three largest events and their aftershock sequence. Their magnitudes are 2.1, 2.0 and 2.05 and occurred on days 13, 29, and 50, respectively.

The number of events in magnitude bands of width 0.5 (Figure 2) indicate a b value 1.0 in the Gutenberg-Richter recursion relation in the magnitude range of 1.0 to 2.0. Figure 3 shows the cumulative number of events versus time in days. Three swarms are evident from 0 to 20, 20 to 50, and 50 to 80 days; however, the magnitude 2.0 events are in the middle of the swarms, not at the beginning. The time periods marked in Figure 3 for the second and third large event were modeled using Omori's law for the number of events versus time. The constants in Omori's Law (see Table I) were determined using maximum likelihood estimators to Omori's Law in the form:

$$N(t) = \int_0^t \frac{k}{(t+c)^p} dt.$$

Table I. Constants for Omori's Law for two events.

No.	Time Period	No. of events	k	c	p
1	18.6 - 35.6	26	62	16.3	1.18
2	23.0 - 35.0	18	12	6.87	0.79
3	44.0 - 64.0	19	72	7.92	1.63
4	44.0 - 71.0	20	57	7.72	1.54

where k = rate of earthquakes in 1st day
c = lack of detection coefficient
p = rate of decay
and N(t) = cumulative number of events at time t.

The constants determined for the aftershock sequences using Omori's Law are typical of constants observed for aftershocks in general. The third sequence observed in time samples 3 and 4 in Figure 3 gave high values for p suggesting a rapid decay of activity. A high p value may be interpreted as a virtual complete release of stress, signaling the termination of this sequence of events.

LAKE SINCLAIR, GEORGIA
1 Jan. - 31 March 1987

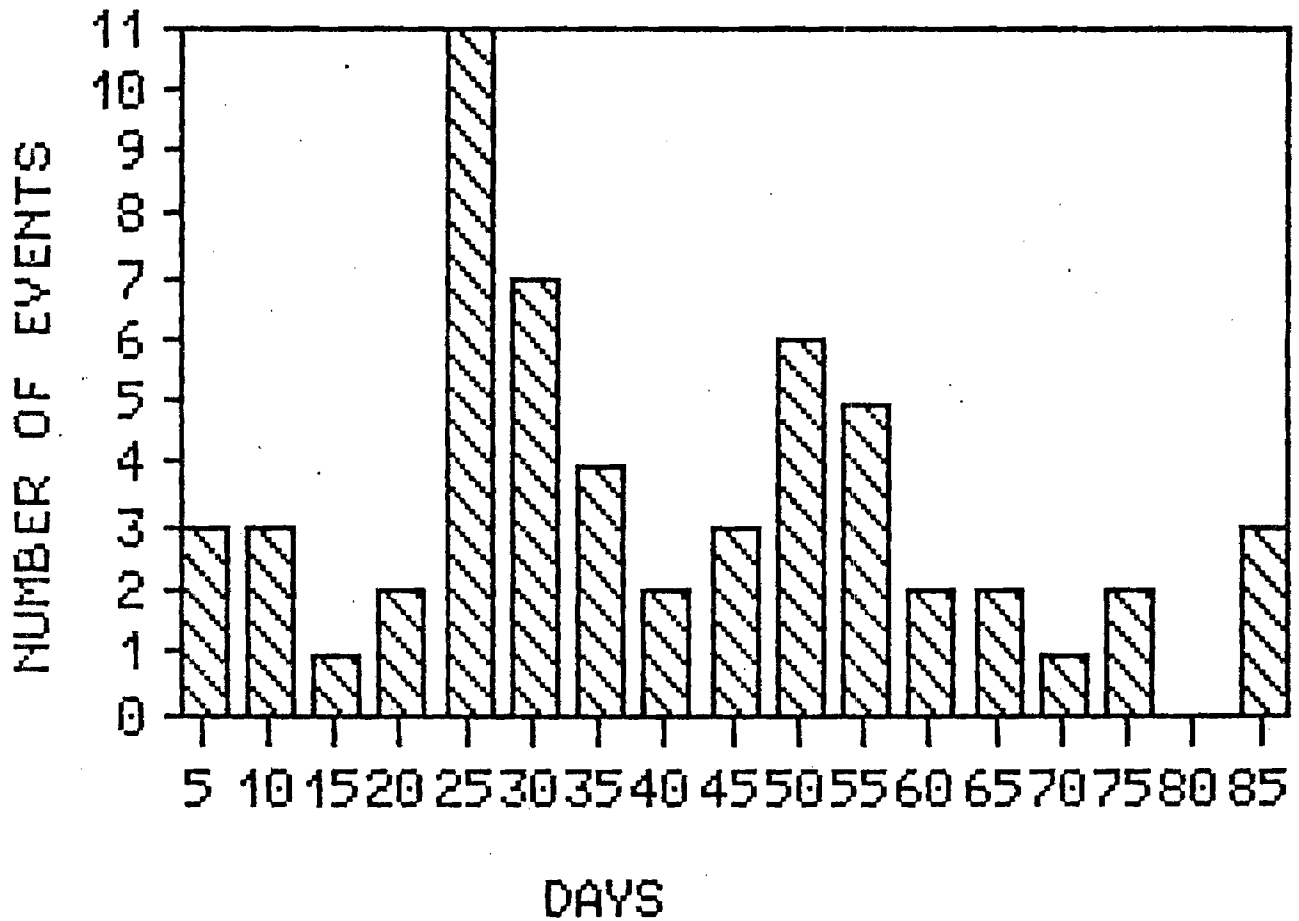


Figure 1. Number of events versus time for the Lake Sinclair swarm of 1 January, 1987 - 31 March, 1987.

LAKE SINCLAIR, GEORGIA
1 Jan. - 31 March 1987

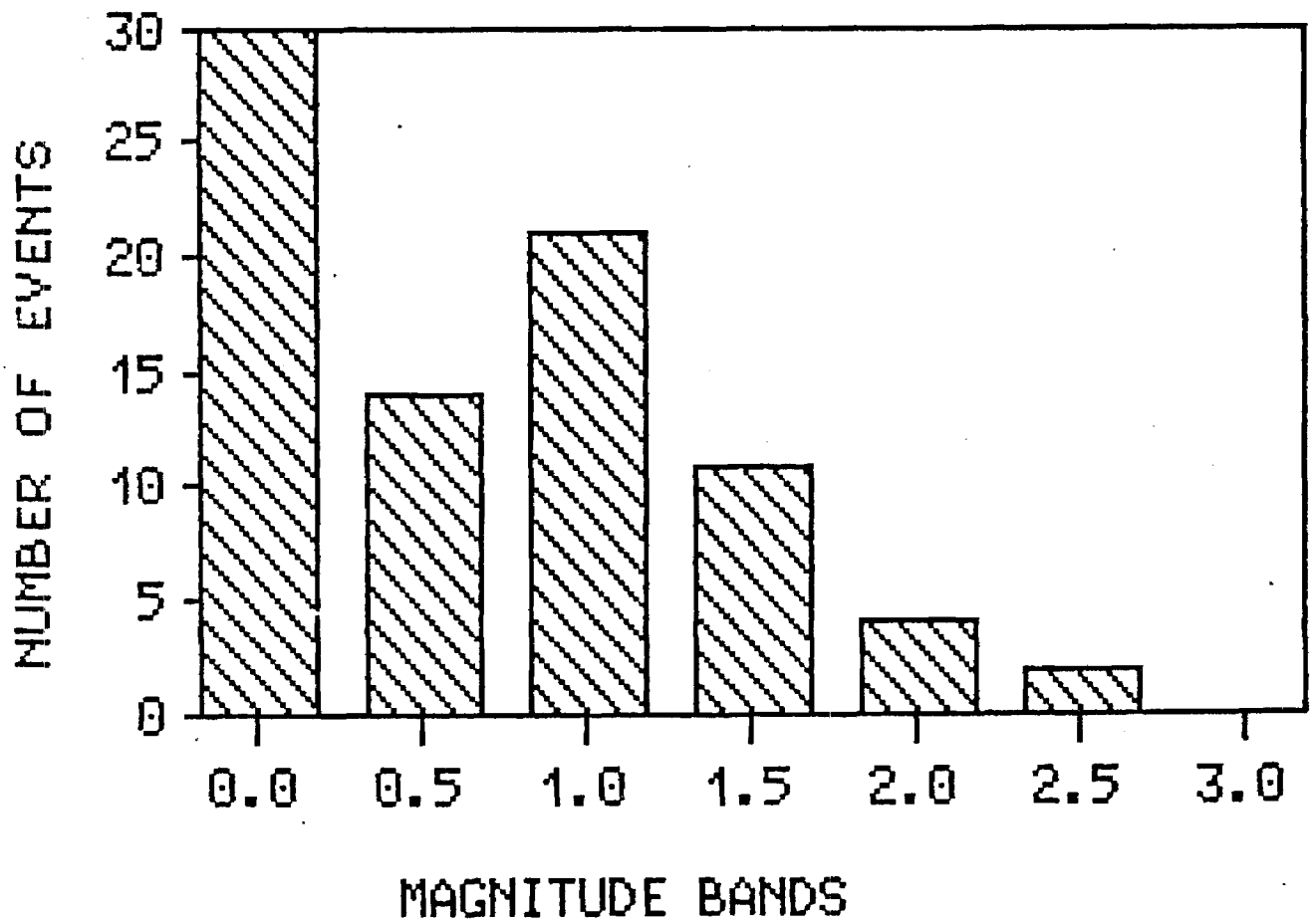


Figure 2. Number of events in 0.5 magnitude increments for the Lake Sinclair swarm of 1 January, 1987 - 31 March, 1987.

Lake Sinclair, Georgia
January 1, - March 31, 1987

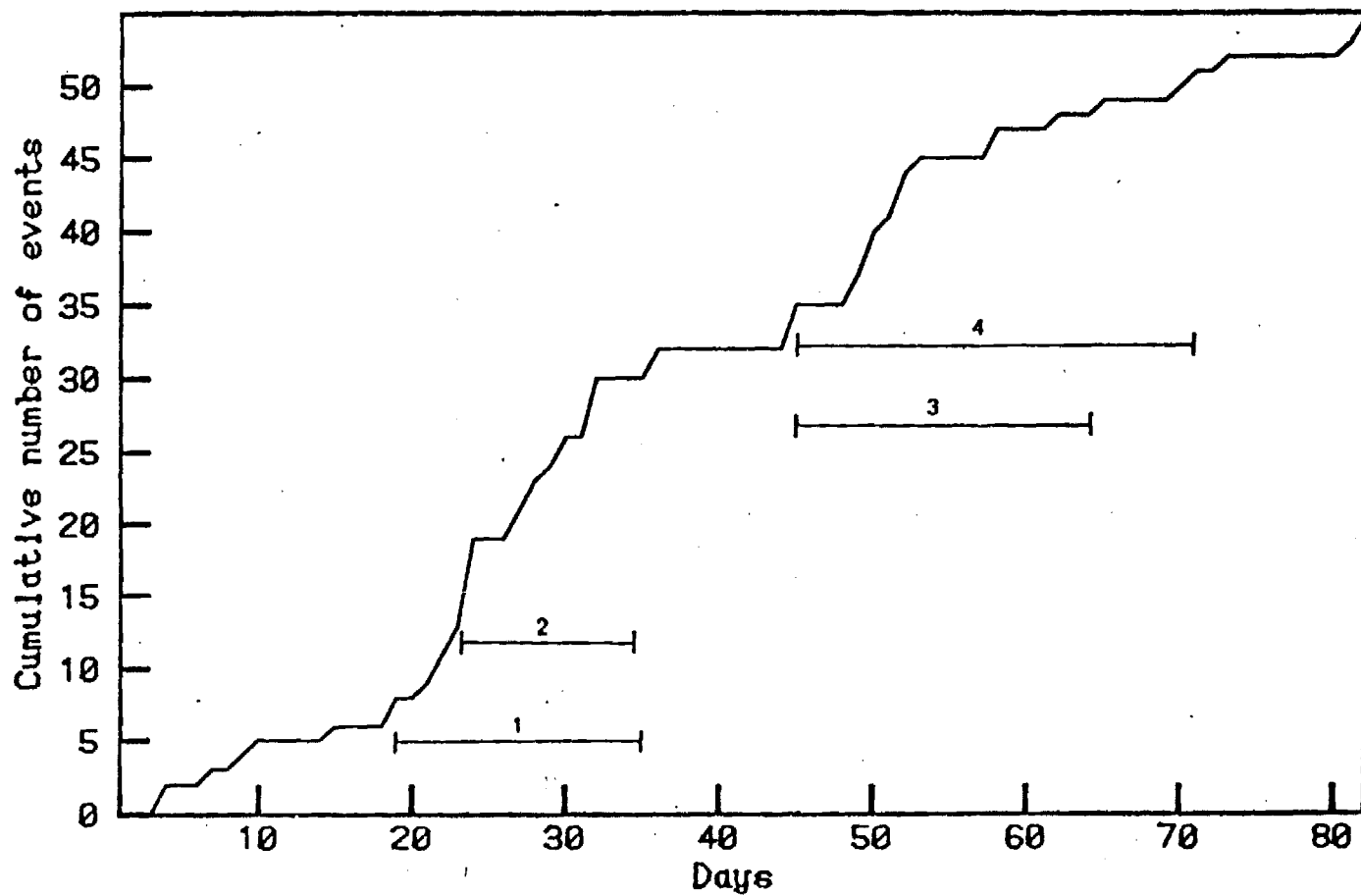


Figure 3. Cumulative number of events versus time for the Lake Sinclair swarm of 1 January, 1987 - 31 March, 1987.

APPENDIX B

THE SCATTERING OF SEISMIC WAVES BY A SPHERICAL INCLUSION

An Tie and L. T. Long

ABSTRACT: We have investigated two models in which a plane P-wave is incident on a spherical inclusion. The first model is an elastic spherical obstacle in a fluid medium. The second model is a fluid sphere in an elastic medium. The computational procedure used is the resonance scattering theory developed by Uberall and his co-workers (1978-1985). For the first case, only a scattered P wave can exist, but the properties of the elastic scatterer affect the scattering coefficient, i.e. the quality factor due to the scattering. In the second case, the spectral response of the scatterer is much more complicated because of resonances in the fluid-filled obstacle. Resonance of the scatterer plays an important role in the calculations of the scattering coefficients, especially for wavelength shorter than the diameter of the scatterer. The viscosity of the solid material affects the scattering coefficients; it smooths its shape and it shifts the resonant eigenfrequency. The background scattering coefficients, which are computed by subtraction of the portion due to the resonance from the scattering cross section, can be strong frequency dependent.

INTRODUCTION

The character of seismic waves may be affected by scattering and absorptive attenuation. The scattering of seismic waves is related to the manner in which inhomogeneities in the elastic material interact with the incident wave. Absorptive attenuation depends on the inelastic properties of the material. When scattering and absorptive attenuation occur together, they interact in a complex manner to attenuate the seismic waves. This study was prompted by the possibility of developing the complete analytical expression for scattering from an elastic media that also exhibits absorptive attenuation. The properties of scattering and attenuation related to an elastic sphere and host media are discussed by An Tie (1987). In this report we present the scattering and the attenuation due to a fluid-filled obstacle in elastic or viscoelastic host and an elastic or viscoelastic inclusion embedded in liquid host material. In both cases, either the host or the scatterer is liquid, and the other is elastic or viscoelastic. Our method is the orthogonal function expansion technique presented by Ying and Truell (1956). For simplicity, only some results of the calculations are discussed.

THE MODEL

We considered a plane P wave incident on a spherical obstacle. Figure 1 presents the geometry of the problem. A plane P wave traveling through a liquid medium is incident on a spherical obstacle at its south pole. In the second case the host is elastic and the scatterer is liquid. The coordinate axes are shown in Figure 1 and the sphere has a radius of "a".

ELASTIC SPHERE IN A FLUID

The scattering cross section was computed for an elastic and viscoelastic obstacle embedded in a fluid host, sea water. The properties of sedimentary rocks were used for the elastic media. In Figure 2 the horizontal axis is a non-dimensional wave number, ka ; and the vertical axis is the scattering cross section, which is the dimensionless ratio of the scattered wave energy to the incident wave energy integrated on the obstacle surface and normalized to unit radius. The lower line in Figure 2 presents the results for a viscoelastic sphere with viscosity about 0.03, implying an intrinsic quality factor of about 130. The top line is for perfect elasticity. From Figure 2 it is apparent that the viscosity does not influence the scattering cross section at the low non-dimensional wave numbers, and its effect is concentrated in the high non-dimensional wave numbers. The viscosity plays a role of smoothing the shape of the scattering cross section. The maximum difference is about five percent for weak viscosity in elastic inclusion of about 0.03. The viscosity tends to reduce the scattering cross section.

FLUID FILLED SPHERE IN ELASTIC HOST MEDIA

Figures 3 and 4 exhibit the scattering cross section of a fluid-filled obstacle in an elastic or viscoelastic host material. Since the host is solid, the scattered P and S waves are excited. The host medium considered is sedimentary rock and we assume its viscosity is equal to 0.08. Figure 3 shows the scattering cross section for the P waves in a pure elastic and viscoelastic host. The viscosity affects the scattering cross section at the high non-dimensional wave numbers. The amount is about 10 percent for the sedimentary rock and sea water material combination.

Figure 4 shows the scattering cross section for the S wave. The attenuation affects the S wave significantly more than it affects the P wave (compare Figure 3 and 4). If the non-dimensional wave number is less than one, a smooth line is coincident with the Born approximation, but the rapid vibration in the higher wave numbers is not predicted by the low frequency approximation. These details are due to the inclusion of the higher order terms in this complete solution.

CONCLUSIONS

The conclusions based on a study of the fluid-filled sphere in an elastic host and the elastic sphere in a liquid host are as follows:

- 1) The fluid-filled scatterer gives a more complicated response to an incident plane wave as indicated by the scattering cross section. The complexity of the response suggests that such a response may be a good indicator to predict the type of the scatterer. The scattering cross section exhibits a vibrational behavior in the high non-dimensional wave number range.

- 2) Viscosity affects the scattering cross section only at the higher frequencies. It is about 10 percent even for weak viscosity in the solid material. The influence of viscosity is much stronger for the fluid inclusion

in a viscoelastic host that for a viscoelastic scatterer in a fluid host. Additional conclusions can be derived from a comparison of these results with those of the study of an elastic scatterer and elastic host media.

3) The variation in complexity of the scattering cross section within the high frequency range is seen from the comparison of the positive contrast scattering and the negative contrast scattering and the scattering due to a fluid-filled inclusion. The negative contrast scatterer or the liquid-filled scatterer cause relative enrichment of the scattered wave energy within the high frequency range.

4) The intrinsic viscosity interacts with the local inhomogeneities on the scattering cross section. The influence of the viscosity depends on the different material combinations. For positive contrasts in an inclusion, an increase in viscosity or a lower Q will generate a larger scattering cross section. On the other hand, a negative contrast in an inclusion, such as sedimentary rock in granite, an increase in viscosity or low Q will generate a smaller scattering cross section.

REFERENCES

Tie, An, 1987. On scattering of seismic waves by a spherical obstacle, Ph.D. Thesis, Georgia Institute of Technology, Atlanta, Georgia, 126 pp.

Ying, C.F., and R. Truell, 1956. Scattering of a plane wave by a spherical obstacle in an isotropically elastic solid, J. Appl. Phys., 27, 1086-1097.

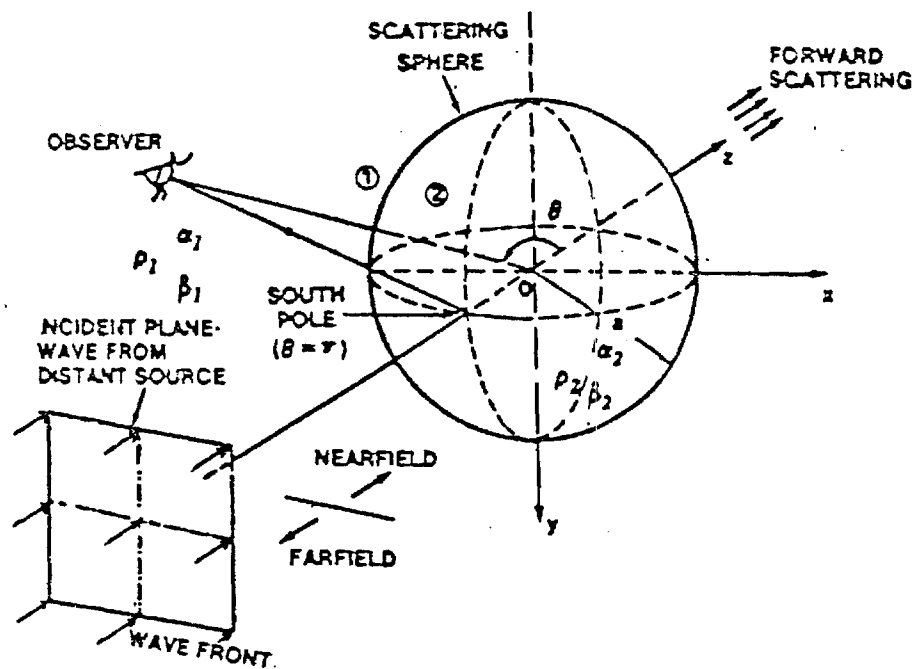


Figure 1. Model parameters for a plane P wave incident on the south pole of a scattering sphere.

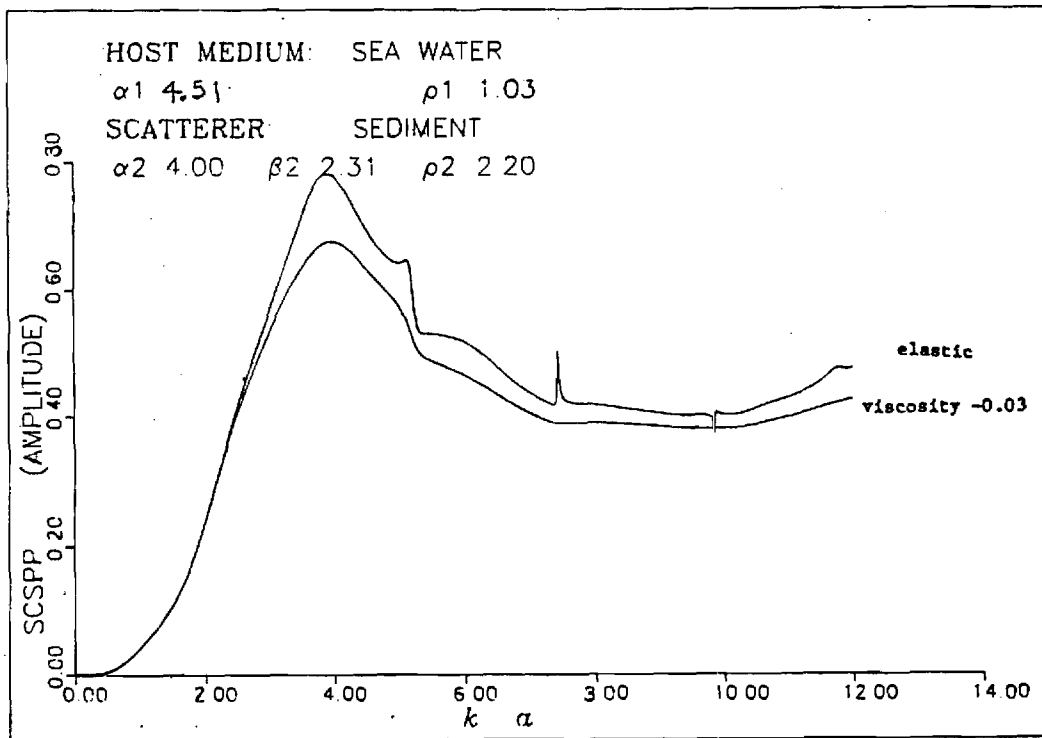


Figure 2. Scattering cross section of the scattered P wave for an elastic sphere in sea water.

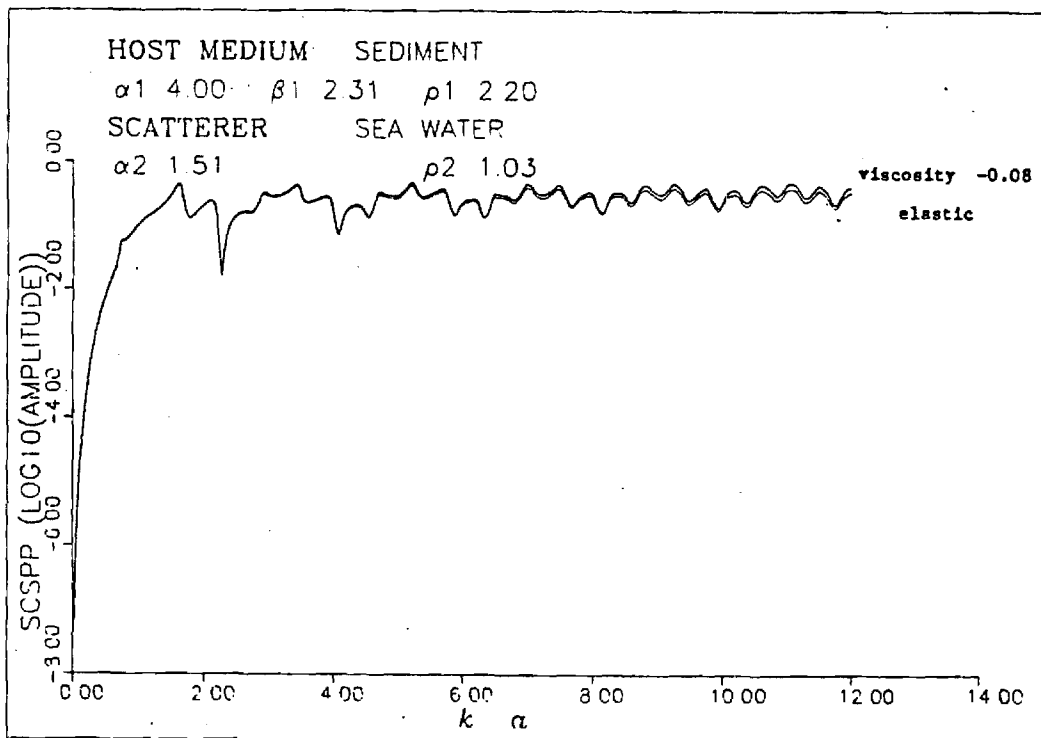


Figure 3. Scattering cross section of the scattered P wave for a fluid-filled sphere in an elastic media.

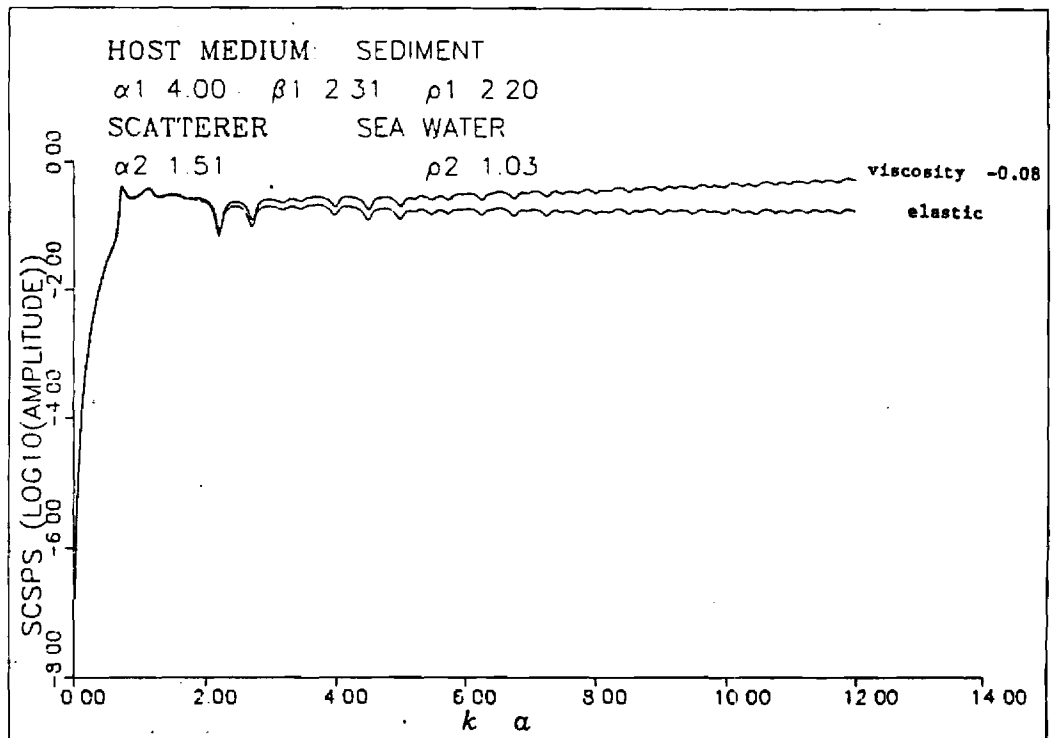


Figure 4. Scattering cross section of the scattered S wave for fluid-filled sphere in an elastic media.

APPENDIX C

SPECULATION CONCERNING THE EFFECTS OF ATTENUATION AND SCATTERING ON THE SPECTRAL SIGNATURE OF WAVELETS COMPRISING THE P-WAVE CODA

L. T. Long and C. S. Alexander

ABSTRACT: The P-wave coda is generally interpreted as P wavelets scattered from heterogeneities in the lithosphere. The spectral signature of an individual P wavelet can depend on absorptive attenuation and scattering along its propagation path. In particle velocity records, the Brune source model generates a wavelet with a spectral peak near the corner frequency. With increased time, absorptive attenuation systematically shifts the corner frequency toward lower frequencies. The spectra of wavelets scattered from heterogeneities can be complex and depends on the size of the heterogeneity. For corner frequencies below the fundamental resonance of the heterogeneity, the corner frequency is systematically shifted to higher frequencies. In moving window high-resolution spectral analysis of P-wave coda, systematic increases and decreases in spectral peaks are observed that may be explained by shifts in the corner frequency caused by absorptive attenuation and scattering.

INTRODUCTION

In traditional methods for the analysis of seismic codas, the codas are assumed to obey the single independent scattering theory developed by Aki (1969). The theory and its more recent improvements predict equations showing exponential decay with increased time in the amplitudes of scattered phases. The exponential decay defines a scattering, Q_s . If the medium also attenuates anelastically, then this intrinsic Q_i is combined with the scattering Q to give a total Q that determines the exponential decay of the coda. In most studies, the total Q and exponential decay are determined as a function of frequency. The total Q can be used to provide information on crustal attenuation, source spectrum, and, more recently, temporal changes in crustal properties.

The existence of a coda is generally accepted to be a consequence of the scattering of seismic waves by inhomogeneities. An statistical approach is assumed in most analyses because it has a simpler theoretical basis and the inhomogeneities are considered too complex to be handled by deterministic methods. In distinct contrast to this statistical approach, the theories of reflection seismology assume that the back scattered waves are derived from distinct reflectors in quasi-layered sediments and that the location and distribution of layers can be determined from the data. The fact that the scatterers in reflection seismology are more often planar and in earthquake coda crustal scatters are more likely to be three dimensional adds 3-dimensional complexity to the analysis of seismic coda. However, the 3-dimensional complexity leads to a greater variability in spectral signatures for scattered objects than would be expected for layered media.

In reflection seismology, the spectral content of the reflecting wavelets often contains significant information, such as the thickness or size of reflectors and attenuation properties of zones or layers. In this study we have examined wavelets in the P-wave coda by using high-resolution spectral analysis methods. These methods are optimal for detecting shifts in the peak spectral amplitude of wavelets on the trace. In essence, we examine discrete scatters and their scattered waves rather than their statistical properties, (e.g. the average decay with time).

THE WAVELET

For the purposes of examining the effects of scattering and attenuation on wavelets in the coda, we assume that the source conforms to the displacement spectra proposed by Brune (1970). Since most short period seismograms closely simulate particle velocity traces, the model for displacement spectra is converted to particle velocity. In particle velocity records the corner frequency is a peak or maximum in the spectra, a fact that we can use to advantage in this analysis. We use the particle velocity model to study the changes in spectral content caused by attenuation and scattering by examining the shifts in the corner frequency, which is equivalent to the peak frequency.

EFFECTS OF ATTENUATION ON SOURCE SPECTRA

In a particle velocity trace, the corner frequency is a maximum in the spectra. The exponential intrinsic attenuation operator ($\exp(-\omega t/2Q)$) was multiplied by the source velocity spectra and the shift in the spectral peak noted. The shift in spectral peaks is evident in Figure 1. At high values of Q the spectral shift is minimal and the spectral peak of the wavelet will be dominated by the corner frequency of the source spectra. At low values of Q , the spectra are dominated by the attenuation. These shifted peaks were used to define curves of constant Q as a function of time in spectral data.

The curves defining spectral peaks for a constant Q depend on the corner frequency of the source. However, as will be shown below, an earthquake source may contain high-frequency spectral peaks not consistent with the source model. Their origin could be in secondary features of the source or in near source scatters.

EFFECTS OF SCATTERING ON SOURCE SPECTRA

The change in spectral content due to scattering is significantly more complex and has been defined only for very simple structures, for example the sphere. A typical response is shown in Figure 2 as a function of the product of the radius and wave number. For long wave lengths, the spectral cross section increases with frequency. The response peaks at a wave length close to the radius of the sphere. The case shown here is for material properties consistent with a sediment in a granite. For shorter wave lengths, the response of a sphere is a complex interaction of multiple internal

reflections, intrinsic attenuation and resonances. However, in the crust, the shorter wave lengths will be of minimal significance because they are more readily attenuated and more randomly scattered by the irregular shapes of crustal inhomogeneities. The expected spectra of the scattered wavelet for two cases are shown in Figure 2. We look first at the spectral content of a scattered wavelet when the radius of the scatterer is small compared to the wave length of the corner frequency. The shift in the spectral peak of the scattered wavelet to frequencies higher than in the incident wavelet suggests that scattering will have an effect on the coda that is opposite that of intrinsic attenuation. For large scatters, only the low frequencies are distorted and resonances corresponding to the corner frequency and the radius of the scatterer are observed.

OBSERVATIONAL DATA

The auto-regressive spectral analysis, or Berg maximum entropy spectral analysis, used in this study has some very useful characteristics. In effect, maximum entropy spectra sacrifice precision in amplitude for resolution in frequency when applied to short data segments. Hence, the response of this type of analysis is to enhance or exaggerate the spectral peaks. In Figure 3 the spectra appear to be made up of many very sharp spectral peaks. These result from the use of a prediction filter on a short segment of data that may be dominated by the peak spectra of the wavelet. By using the moving window technique with the maximum entropy spectra, we are able to track shifts in spectral peaks of scattered and attenuated wavelets.

Figure 4 shows an example of systematic shifts in the frequency that probably corresponds to attenuation by intrinsic Q. The events most likely shared a common source spectra, although whether it was part of the source or a scattered wave is unknown. In this example, the event had a corner frequency near 2 Hz so the higher frequency peaks are anomalous.

Figure 5 shows an example of systematic increases in frequency of the spectral peaks that one might attribute to scattering. In Figure 5 the spectral peaks jump to systematically higher frequencies following the first arrival in time.

CONCLUSION

A P-wave coda, in the form of moving-window maximum-entropy spectra, shows evidence that the seismic P-wave coda can be resolved into scattered and attenuated wavelets. The attenuation is seen as a systematic shift in spectral peaks. The observation that these spectral peaks concentrate in bands, suggests that they may be related to a limited number of single scatters and layers or propagation paths of constant Q. The theory and data suggest that the coda can be modeled in detail and this method of examining the coda may provide greater understanding of the relation between scattering Q and intrinsic Q.

REFERENCES

Aki, K. (1969). Analysis of the seismic coda of local earthquakes as scattered waves, J. Geophys. Res., 74, 615-663.

Brune, J. N. (1970). Tectonic stress and the spectra of seismic shear Waves from earthquakes, J. Geophys. Res., 75, 4997-5009.

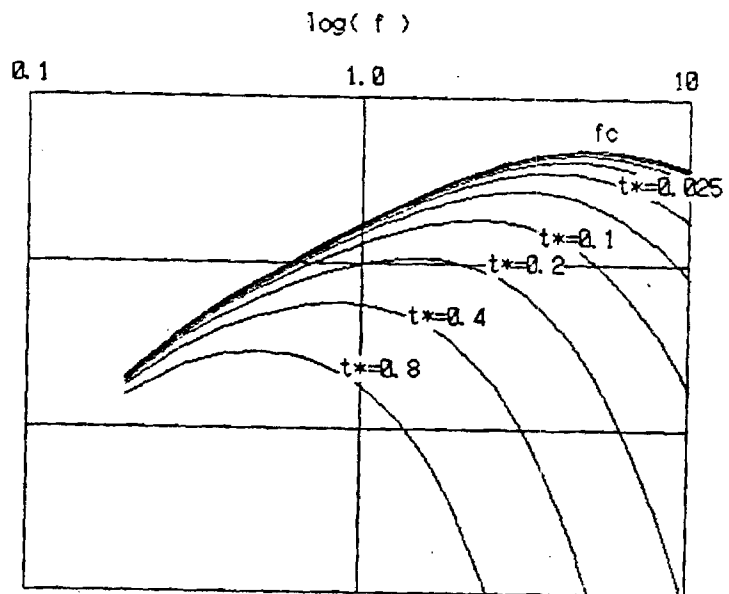


Figure 1. Spectra of a Brune type displacement showing effects of intrinsic attenuation.

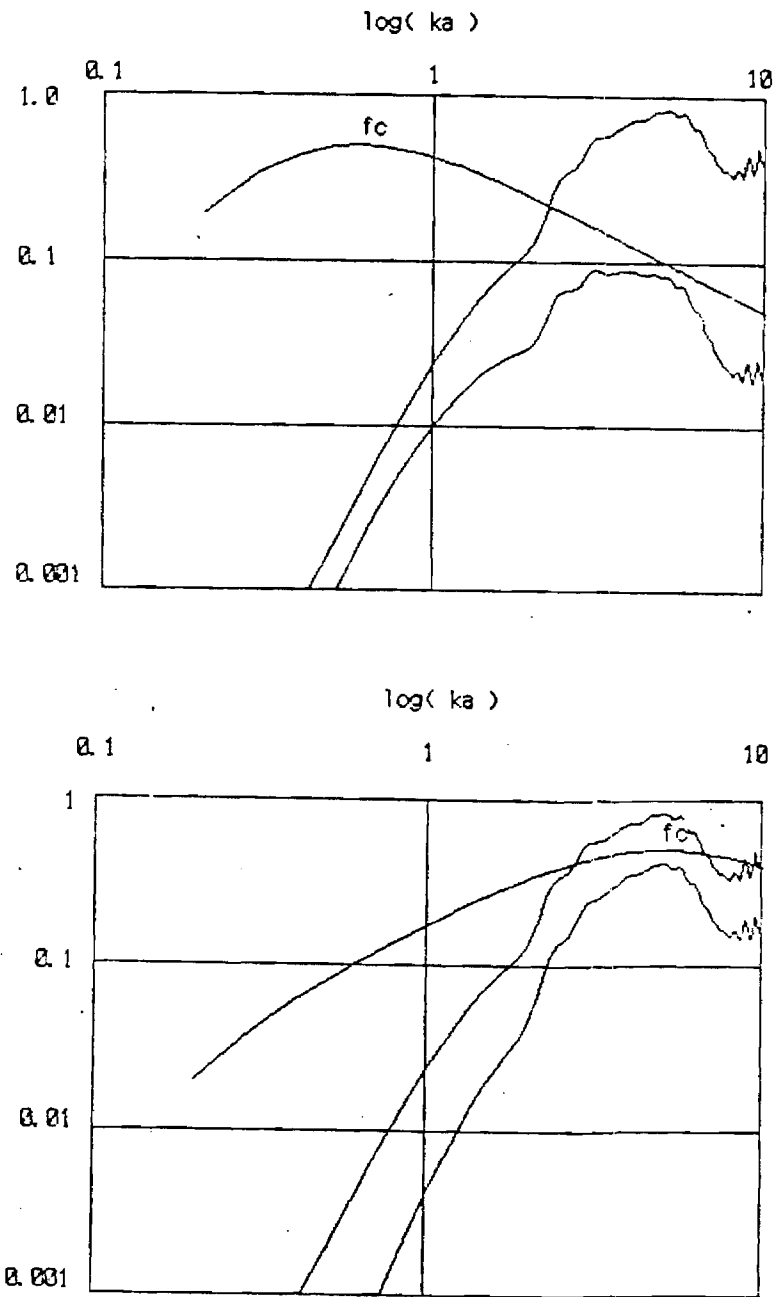


Figure 2. Influence of scattering on the velocity spectra of a seismic wavelet. Top diagram shows the effects on a low-frequency wavelet. Bottom diagram shows the effects on a high-frequency wavelet. In these examples the spectral response of the scatterer dominates the scattered wavelet.

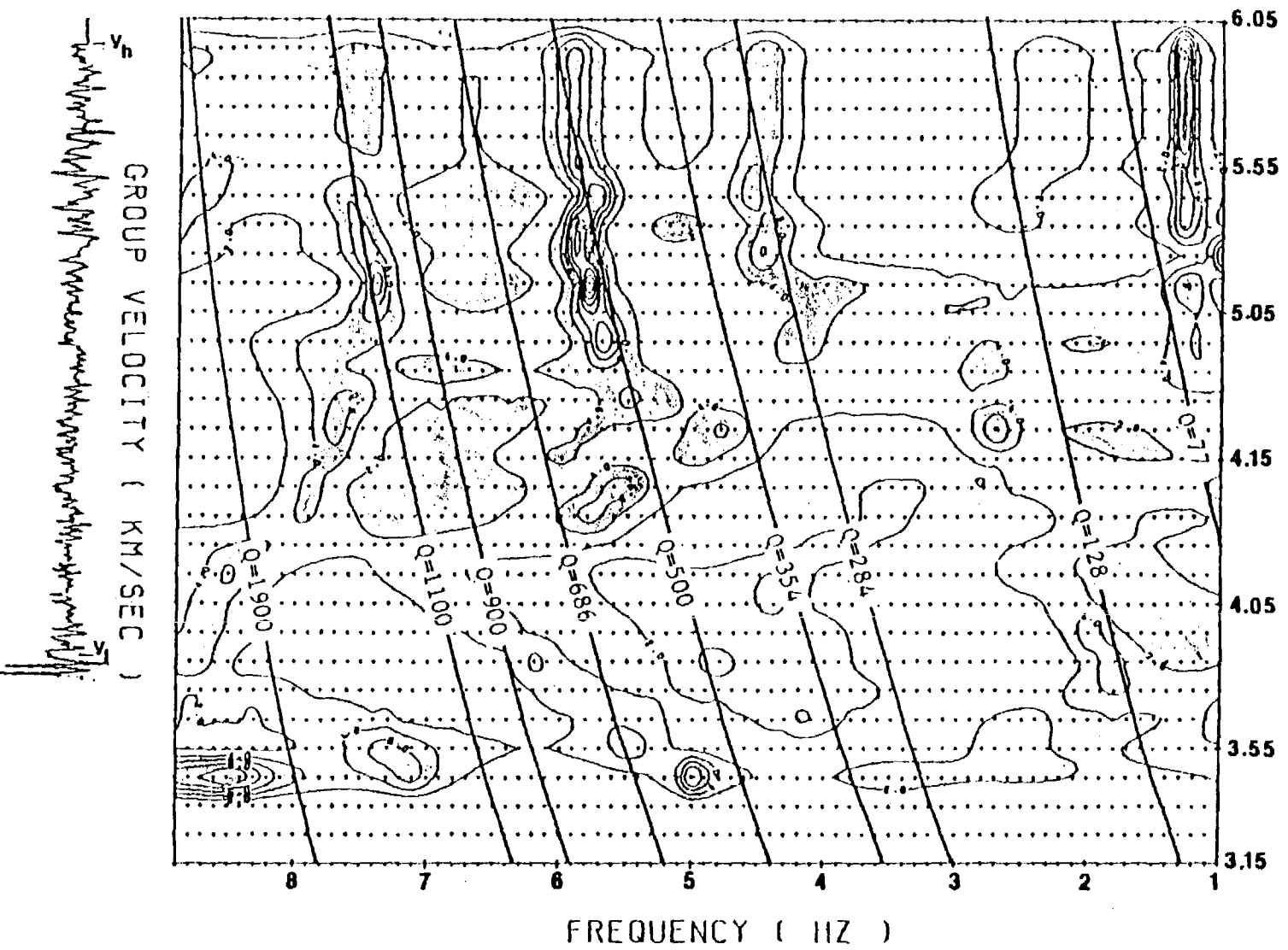


Figure 3. Moving window spectra of a P wave coda showing the effects of attenuation, creating a gradual decrease in the peak frequency.

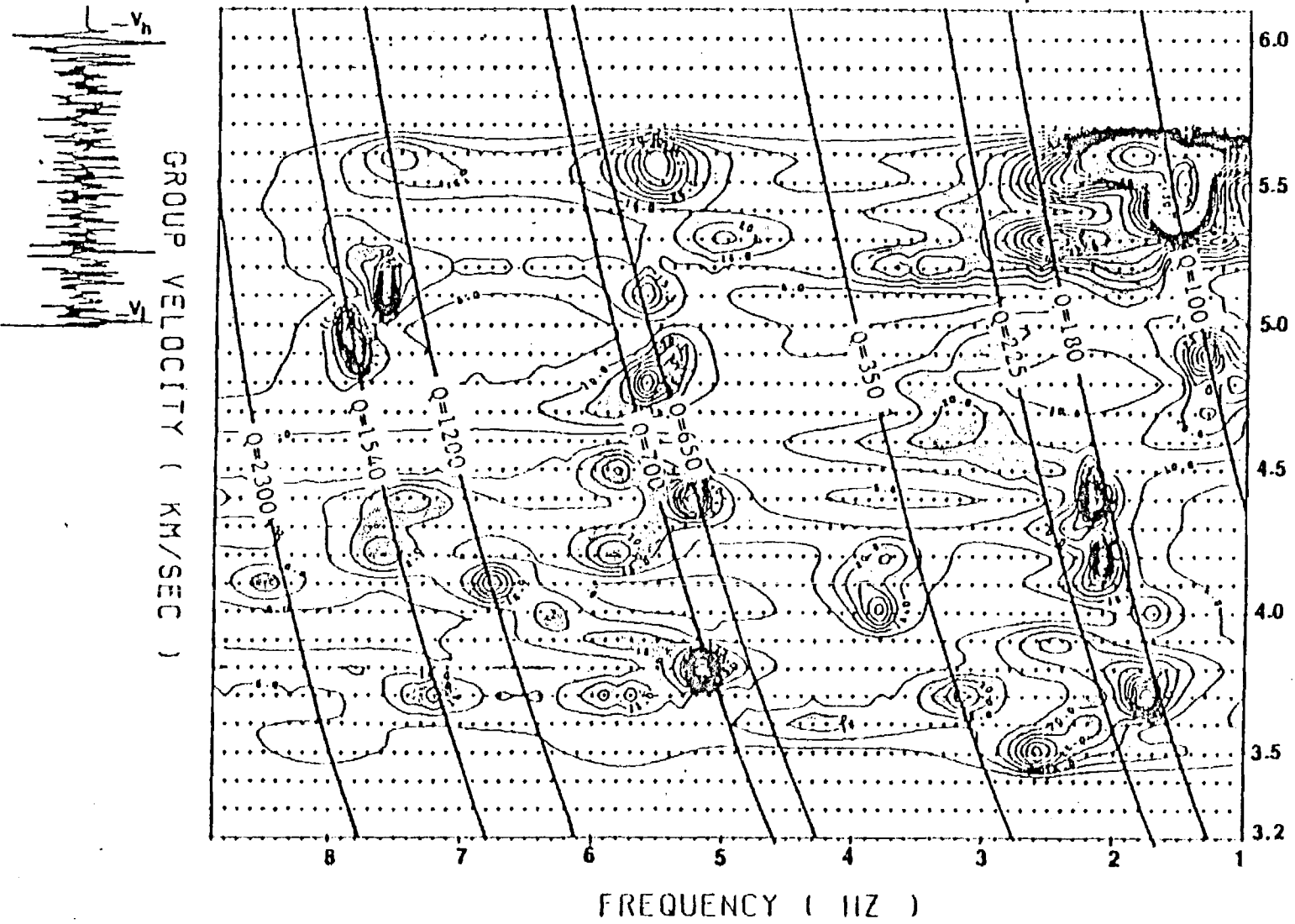


Figure 4. Moving window spectra of a P wave coda showing the effects of attenuation. Note the gradual decrease in the peak frequency of the spectral maximums at 5.5 Hz.

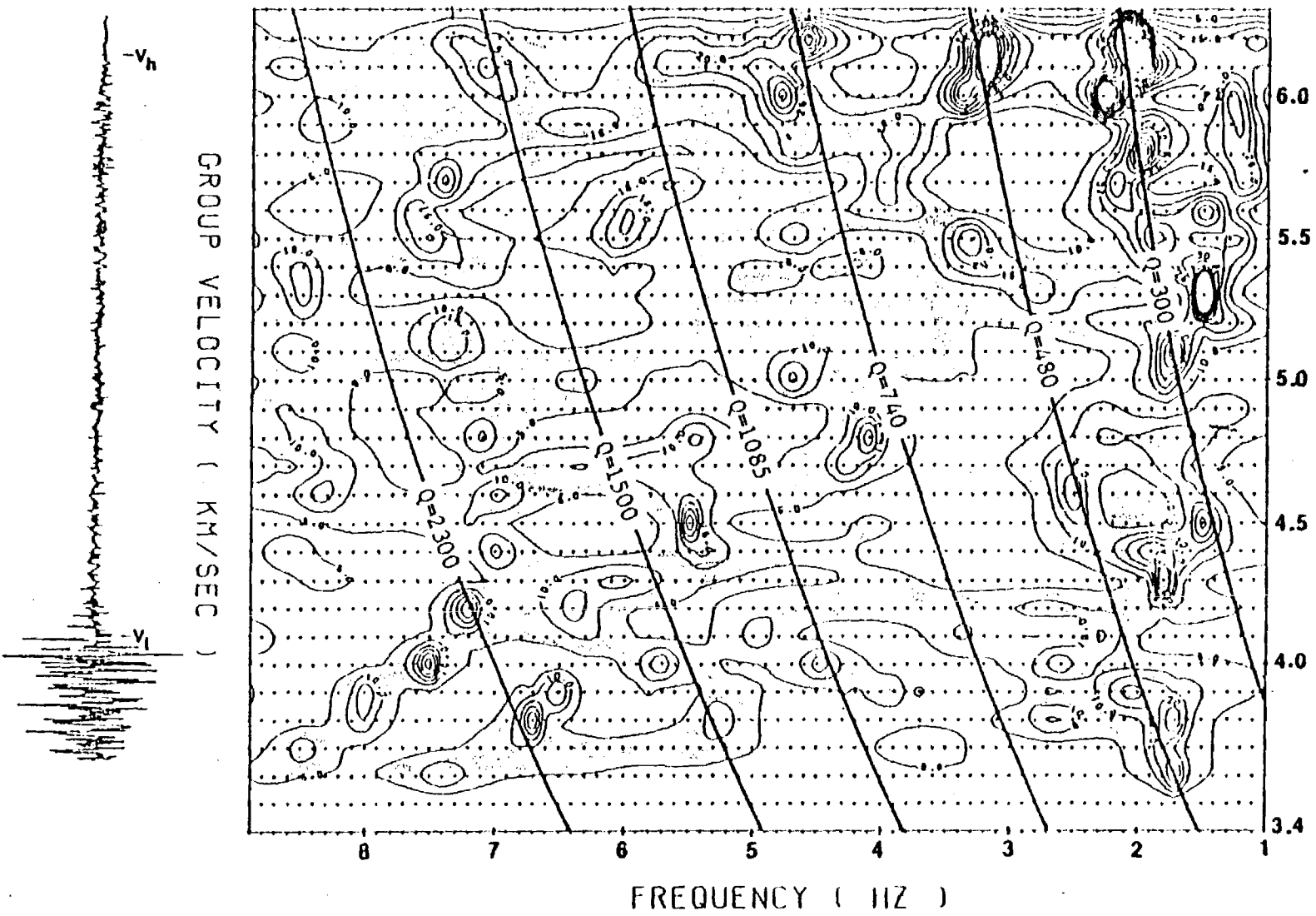


Figure 5. Moving window spectra of a P wave coda showing systematic jumps to higher frequencies which may be due to scattering.

APPENDIX D

FINITE DIFFERENCE SIMULATION OF SCATTERING AND EARTHQUAKE SIGNATURE IN SOUTHEASTERN TENNESSEE.

Jeih-San Liow and L. T. Long

ABSTRACT: The character of seismograms recorded at station CBT depend on azimuth. Events located to the east and southeast show clean impulsive arrivals. Events located to the west exhibit greater scattering. In order to evaluate the influence of local crustal structures on scattering, a two dimensional finite difference method was used to simulate the elastic wave propagation in a crustal model for southeastern Tennessee. The model consists of a lower-velocity sedimentary basin embedded in the continental crust with both overlaid by the Paleozoic sediment of the Valley and Ridge Geologic Province. A compressional line source was placed at depths of 7 to 15 km and at different locations relative to the structure. The waves from sources that are closer to or behind the subsurface sedimentary basin show more scattering than those from sources that are located away from the sedimentary basin. The synthetic seismograms suggest that the azimuthal variations observed at station CBT may be attributed to the existence of a southwest trending sedimentary basin located to the northwest of station CBT.

INTRODUCTION

The digital data for 12 earthquakes in the southeastern Tennessee area recorded at our seismic station CBT show that earthquakes occurring to the east of the station exhibit less scattering than those occurred to the west of the station (Figure 1). The Bouguer gravity anomaly map suggests a north-east south-west trending negative gravity anomaly to the west of CBT (Figure 2). This gravity anomaly, which implies a mass deficiency at depths of 2 to 7 km has been interpreted as a subsurface sedimentary basin embedded between the upper crust and the overlying Paleozoic sediments (Figure 3). The approximate P-wave velocity of the subsurface sedimentary basin ranges from 5.5 to 5.9 km/s, in contrast with the P-wave velocity of the upper crust and the overlying sediments, which are 6.15 and 4.5 km/s, respectively.

We suspected that the azimuthally dependent pattern of scattering in the observed data might be related to the seismic waves traveling through the structural anomaly to the west of the station. In order to test this hypothesis we use a second order two-dimensional finite difference method to simulate the propagation of P wave in a crustal model which simulates the structure of the basin.

THEORETICAL MODELS

Before we apply our second order finite difference method to the problem, a test of using a plane wave source vertically incident upon a 50-layered transitional zone is performed to examine the accuracy of the finite difference technique. The velocity varies randomly for each layer within the transitional zone (Figure 4). The hypothetical crustal model, shown in Figure

5, consists of a sedimentary layer from 0 to 3.5 km and the crust extending from the depth of 3.5 to 10 km. The width of the model is 20 km. The station is located at the surface 10 km away from $x=0$. The embedded sedimentary basin is placed to the left of the station from the depth of 3.5 to 7 km. The grid spacing and time increment used in this study are 0.1 km and 0.01 s respectively. The finite difference synthetic seismograms were computed for a compressional line source being placed at 8 km deep and three different horizontal positions: 0, 10 and 20 km from $x=0$, namely S1, S2 and S3. The central frequency of the line source is 2.5 Hz. Free surface boundary condition is applied to the top of the model. Transparent boundary condition is applied to the bottom, the left and the right edge. The transparent boundary condition, similar to the absorbing boundary condition which eliminates artificial reflections from the grid boundary, is based on theoretically propagating the displacements of the P and the S wave in the direction of their maximum gradient with their velocities.

SYNTHETIC TRACES

Figure 6a shows the vertical component of the synthetic traces at a station for three different source positions. The amplitudes of the scattered arrivals are larger for source positions S1 and S3 than on the waves for source position S2; however, the scatterings for all the three source positions, regardless of the path, are similar and they are all smaller than the amplitudes of the scattered phases on the observed data. In order to evaluate an increased inhomogeneity along the path, a five percent random variation is added to the velocity at each grid point and synthetic seismograms are recomputed. The randomness of velocity increases the scattering of all the traces as can be seen in Figure 6b.

In order to quantitatively compare the results between the theoretical and the observed data, we measure the Q (quality factor) value, which characterizes the exponential decay of the amplitude with respect to time, for all the events used in this study. Standard methods are used in measuring the coda Q except that we have included the initial pulse and selected only very limited length of the coda. Our reason for this is that we are looking for the effect which is more likely representative of the scattering properties of a small area surrounding the direct wave path. Using the full length of the coda would give the average characteristics of scattering for a large area. Figure 7 illustrates an example of different Q values being obtained from the same event with selection of different lengths of coda and the inclusion of the direct pulse. We have not made any correction for the distance and depth of focus for each event which may have some effects on the amplitude of the initial pulse for different events.

COMPARISON WITH DATA

Since the central frequency of the source used in the finite difference simulation is 2.5 Hz and the spectra of the synthetic data show that most of their energy are within the frequency range of 1-5 Hz, we filter both the observed data and the synthetic data with a 1-5 Hz band pass filter before we measured and compared the Q values. We attempted to measure the Q values from

both P- and S-coda for the observed data. The Q values of the unfiltered observed data were also measured simply for comparison. The Q values of the synthetic data ranges from 16-22 for homogeneous models and 24-35 for models with 5 percent randomness (Table 1). Both show slightly higher Q values for source position S3. Among the Q values of the P coda measured from the observed data, only event 1 (25) is consistent with the synthetic data. The shear wave Qs of the filtered traces for the observed data range between 37-81 in this area (Table 1) except for two zones:

Table 1. Coda Q computed for observed and synthetic seismograms.

Event No.	Q	Event No.	Q	Event	Q	Q(5%)
1	10	7	10	S1	16	24
2	37	8	49	S2	17	23
3	72	9	43	S3	22	35
4	570	10	11			
5	62	11	81			
6	74	12	496			

(1) Event 4 and 12, which are located to the west of the subsurface sedimentary basin, show a high Q value of 721 and 496 respectively. Although this is not comparable with the theoretical result of S1, the effect of the structural anomaly on the scattering of the propagating waves is obvious.

(2) Event 1, 7 and 10, which are located to the southeast of CBT, all show low Q values between 10-11. The distinct characteristics of scattering for the zone defined by these three events may imply that the crustal structure in this zone is different from the surrounding area. For unfiltered observed data, the average shear wave Q is between 100-300 except for the events located to the west of zone 1 (721) and inside zone 2 (30-70) (Figure 8).

CONCLUSION

In conclusion, the estimates of scattering Q suggest that two zones with anomalous Q values are observed in the southeastern Tennessee seismic zone. Zone 1 is constituted mainly by a north-east south-west trending subsurface sedimentary basin to the west of CBT and has caused more scattering on waves traveling through it. Zone 2, which is defined by three earthquakes located to the east of CBT, exhibits a low-Q scattering characteristic on the seismic wave. The finite difference simulation of the seismic waves propagation in the hypothetic crustal model can not fully explain the observed phenomena. Three possible reasons may account for the inconsistency: (1) The assumed crustal model is two-dimensional and too simple compared to the real earth, a three-dimensional and more complicated media of heterogeneity; (2) The effect of distance and depth of focus on the initial pulse for different events; and (3) the coda of the observed events contain significant near-surface conversions to surface waves.

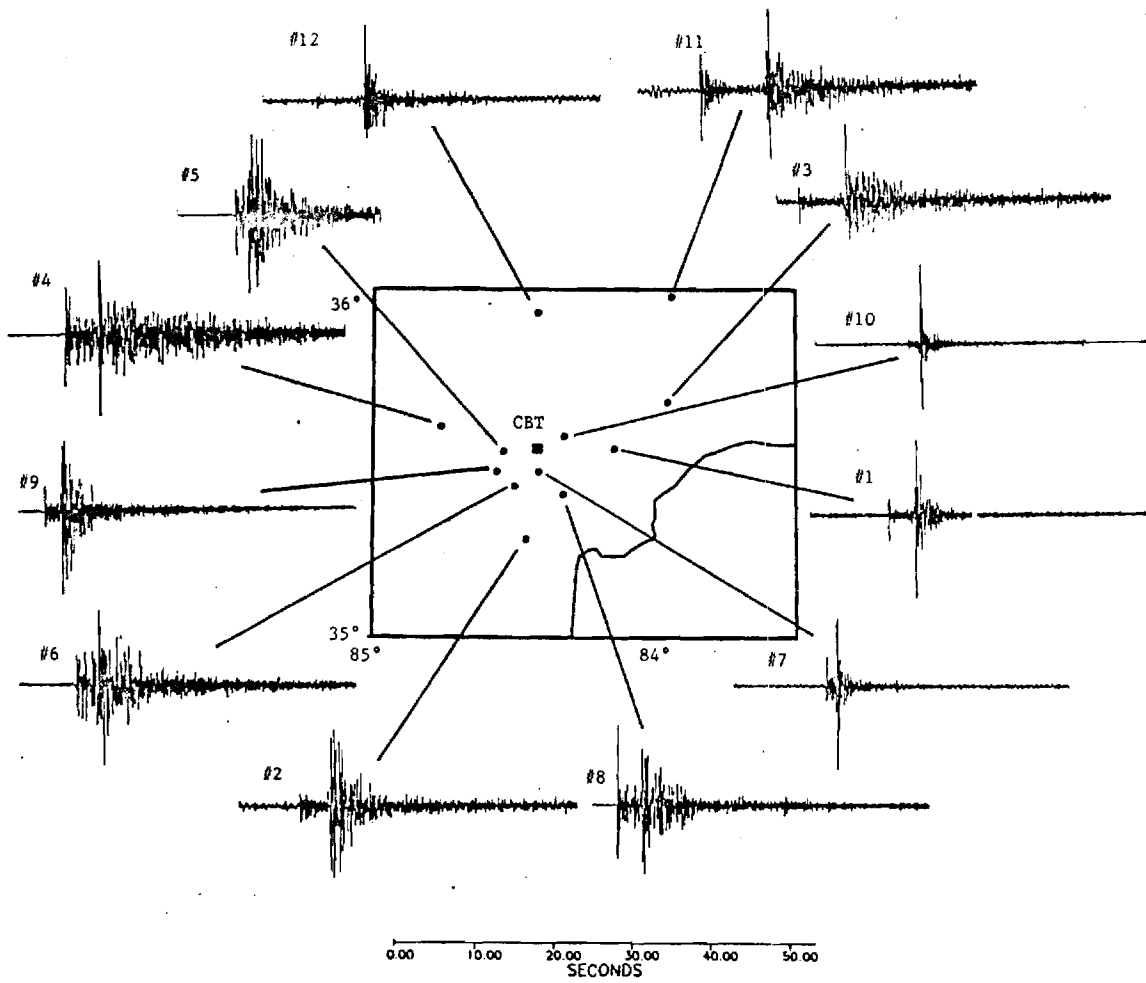


Figure 1. Seismograms recorded at station CBT showing variation in coda with azimuth.

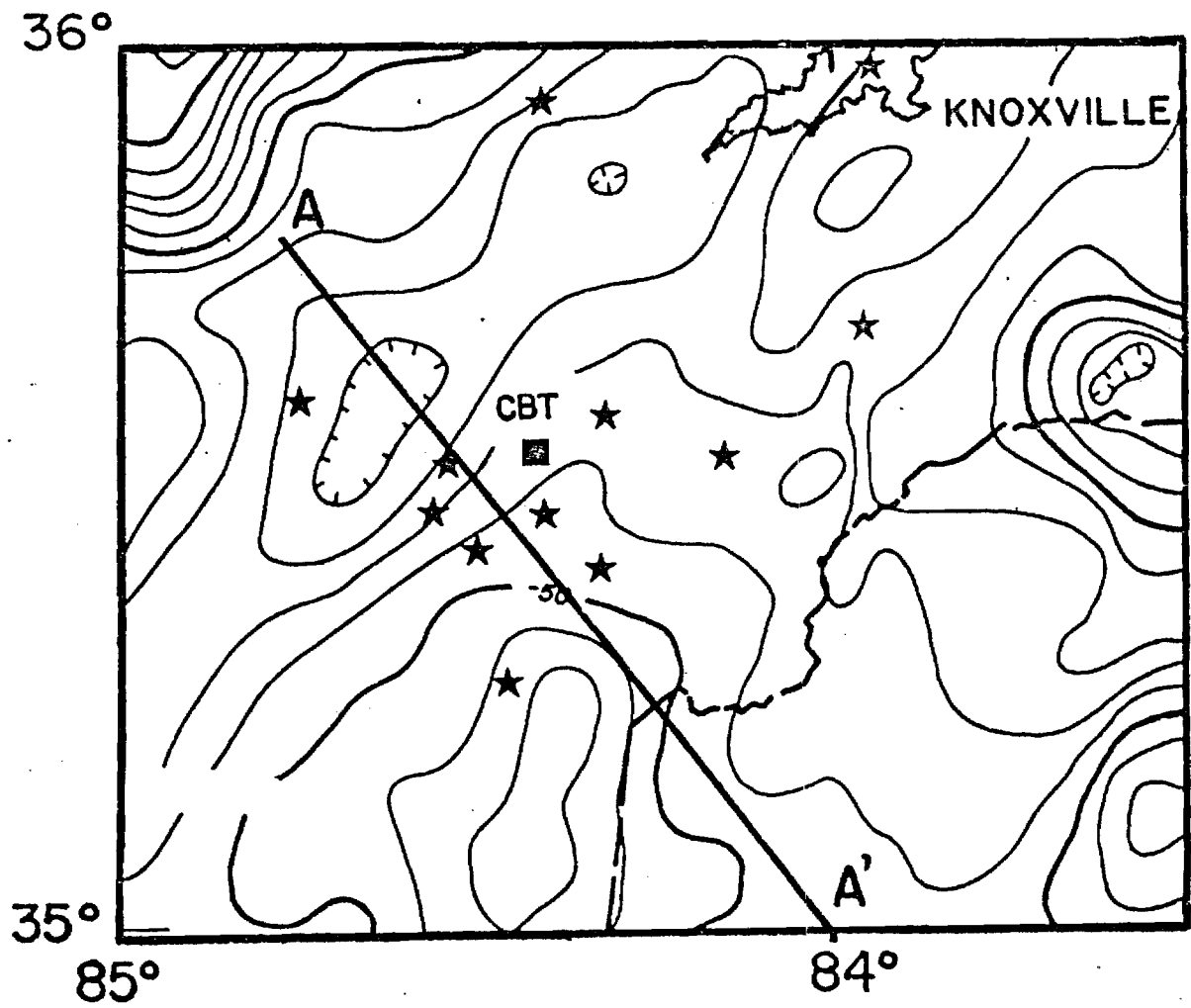


Figure 2. Location of events and Bouguer gravity anomalies near station CBT.

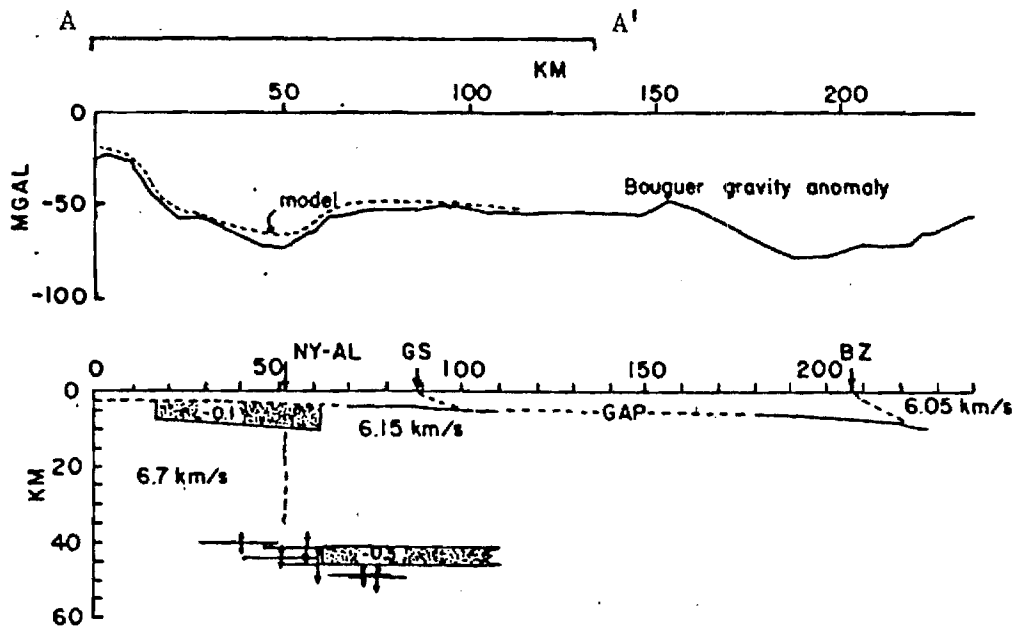


Figure 3. Projection of crustal structure onto northwest trending line (figure 2). The Bouguer anomalies are modeled by two zones of low density. (NY-AL = New York-Alabama Lineament, GS = Great Smoky Fault, and BZ = Brevard Zone).

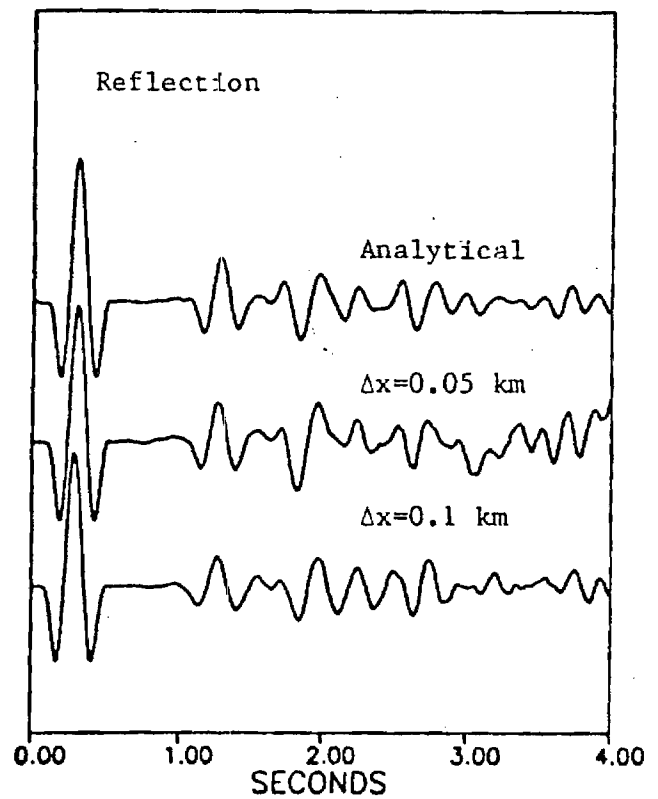
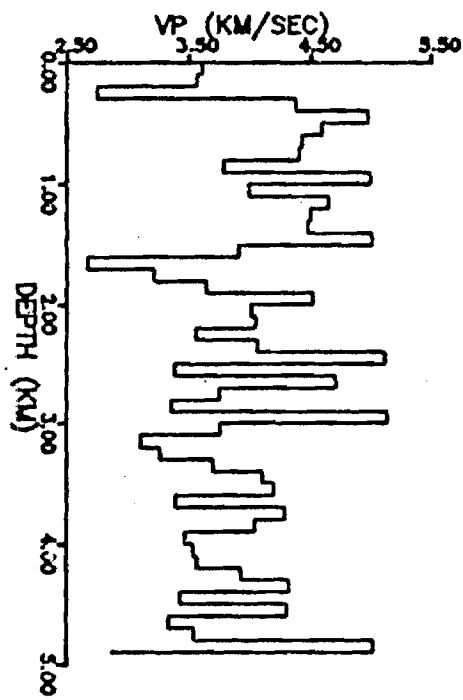


Figure 4. Scattering of an incident P-wave on a layered random velocity zone. The traces compare analytical results with the finite difference synthetic traces.

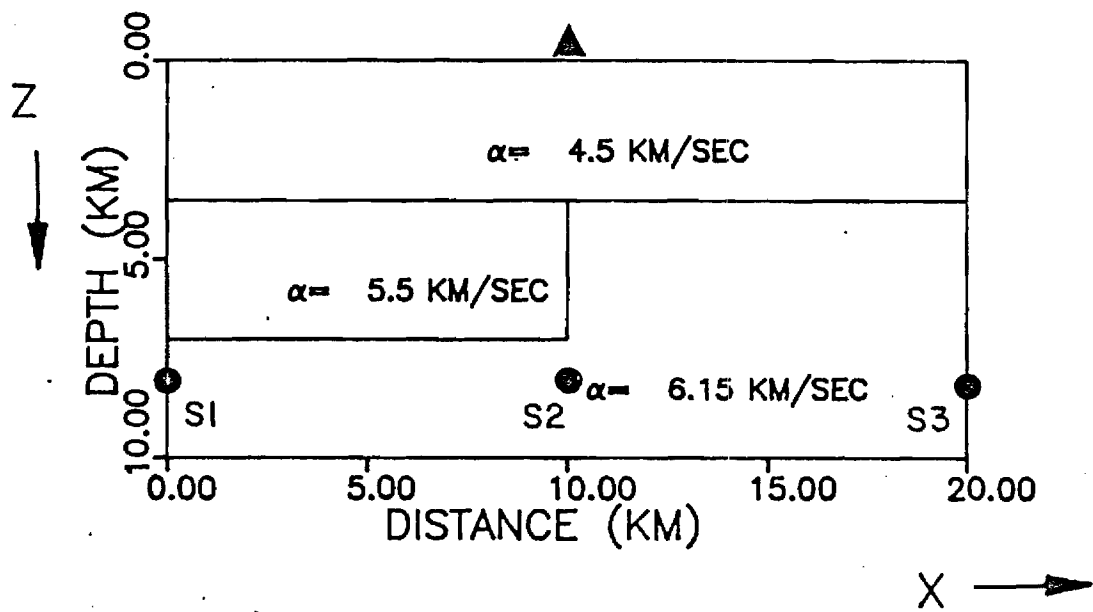


Figure 5. Crustal model used to generate synthetic traces. The S1, S2, and S3 are location of compressional sources.

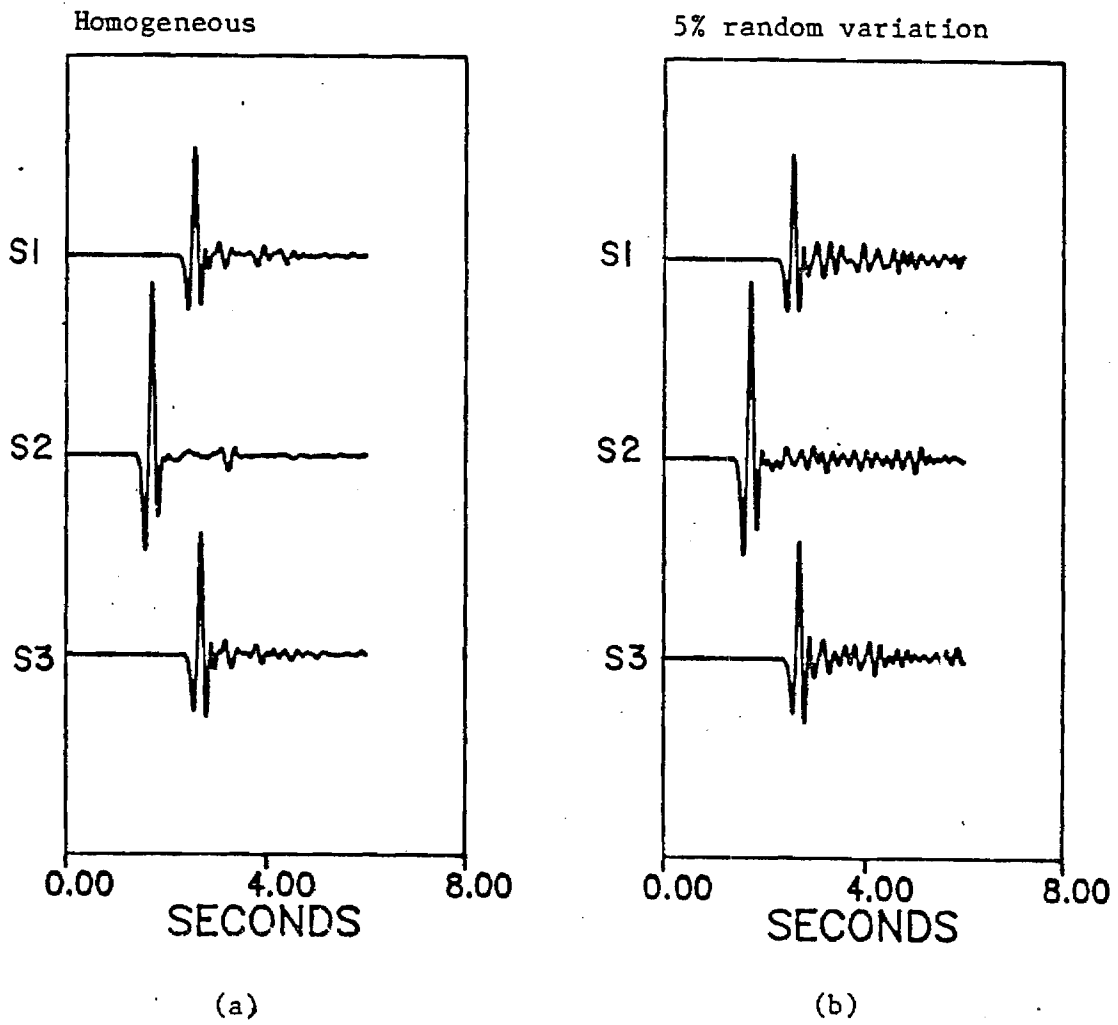


Figure 6. Synthetic traces for homogeneous media and a media with a five percent random perturbation in velocity.

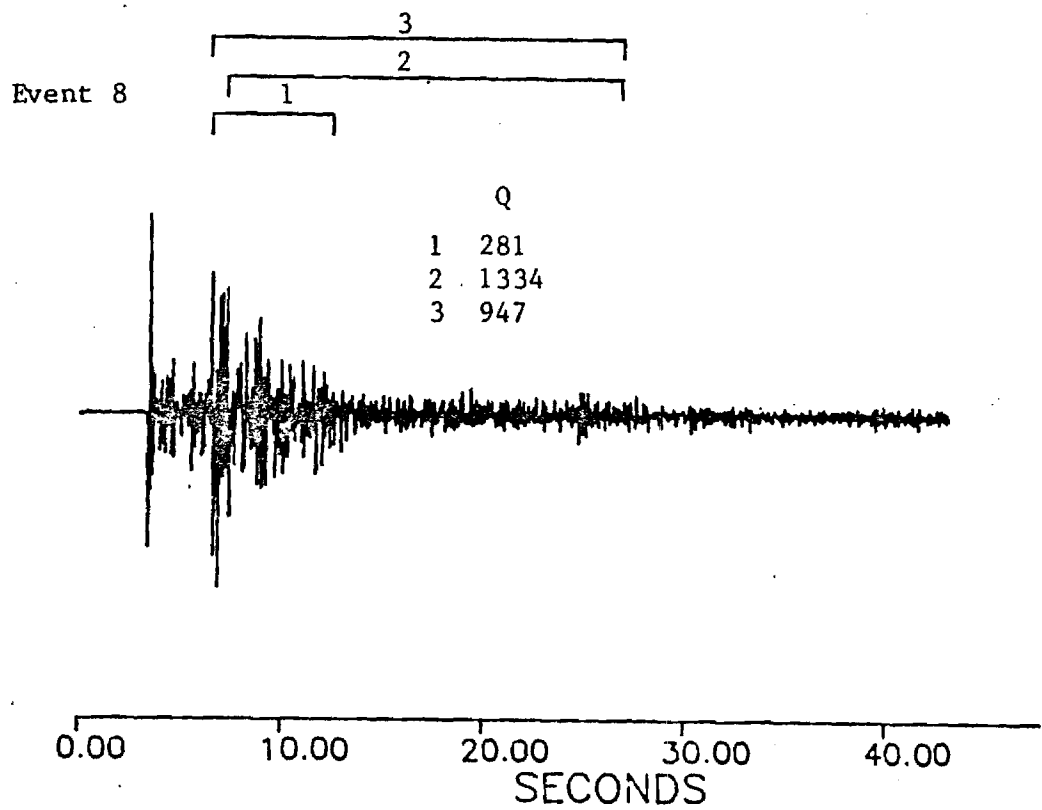


Figure 7. Event 8 showing the variation in Q obtained when examining different portions of the coda.

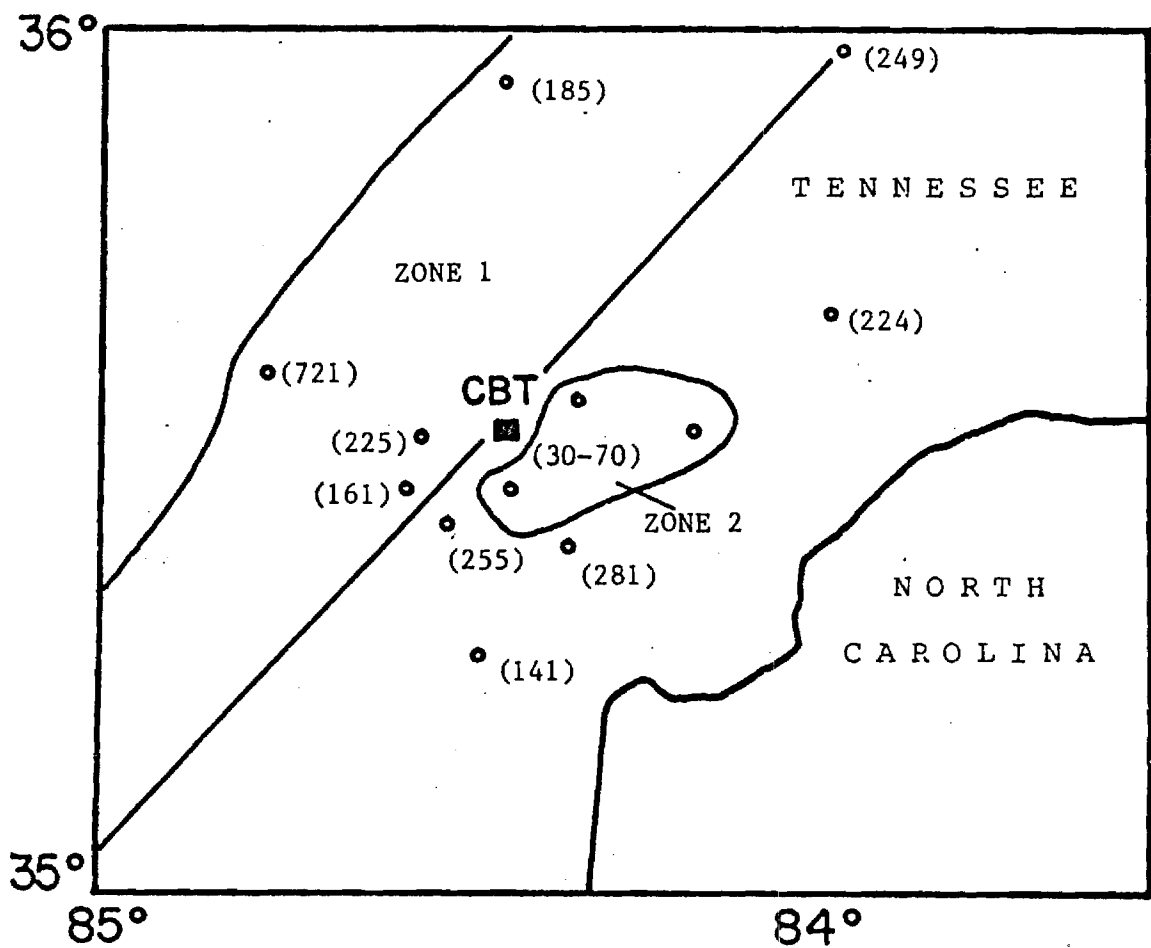


Figure 8. Outline of zone of apparently anomalous Q in southeastern Tennessee.

APPENDIX E

A DISCUSSION OF PRECISION IN HYPOCENTER DETERMINATION

ABSTRACT: The weighting matrix used in earthquake location programs contains important information concerning the uncertainty of an earthquake hypocenter. The off-diagonal elements, which are usually ignored, have significant values when P- and S-wave arrivals are recorded at the same station or when stations are close together. For these arrivals the ray paths are similar and the travel time errors will be strongly correlated. Non-zero off-diagonal elements increase the weights that should be applied to their respective arrivals. In the special case of S- and P-wave arrivals at the same station and small reading errors, the covariance matrix is nearly singular and the resulting weighting matrix can make the origin time computation virtually independent of the location. Where seismic data are too sparse to estimate the elements of the covariance matrix, the elements may be estimated from an autocorrelation function of travel time residuals along near by refraction lines or inferred indirectly from the autocorrelation of Bouguer anomalies. Use of the properly formulated weighting matrix yields estimates of location errors which are directly dependent on the local distribution of the stations and epicenter and the velocity model. Such estimates will be independent of travel time residual usually used to compute precision. The near-singularity of the weighting matrix for P- and S-wave arrivals at the same station suggests an alternate computation method whereby the location equations containing S and P waves at each station can be transformed to isolate the computation of the origin time from the computation of the hypocenter.

INTRODUCTION

The determination of earthquake hypocenters in the earth's crust is made complicated by the unavoidable noise in seismic data and the destabilizing attributes of the crustal velocity model. In an ideal case each source-receiver path has a unique perturbation and one could have a "perfect velocity model" and all errors would be reading errors only. In the absence of a perfect velocity model, there is information in the statistics of velocity perturbations and their correlation. Little can be done to change the destabilizing attributes of the crustal velocity model except to improve the accuracy and detail of its representation. Although the location algorithms, their precision and ability to handle noisy data, have been discussed extensively (Aki and Richards, 1980; Lee and Stewart, 1981; Buland, 1986), a consensus on the treatment of errors has not evolved (Boyd and Snoke, 1984).

Methods for estimating the accuracy of hypocenters generally assume that the deviation of individual observations from those predicted by the velocity model are uncorrelated and follow a normal statistical distribution or at least are statistically predictable. Also, the accuracy of the location can be computed by submitting the solution to travel time perturbations which are made random in proportion to the uncertainty of the observations (Everndon, 1969). An assumption that the travel time residuals are uncorrelated simplifies the use of a matrix consisting of the covariances of observations as a weighting matrix for normalizing the data relative to the certainty of

the observations (Wiggins, 1972). However, for local seismic arrays where stations are sited in the same geologic unit or for location techniques that combine the use of P and S phases at the same station, the assumption that travel time residuals related to the velocity structure are uncorrelated is inappropriate.

The objective of this paper is to discuss the significance of the correlation of travel time residuals in determining accuracy and precision of earthquake locations and suggest that the off-diagonal elements of the weighting matrix can be computed using observed measures of covariance. In the special case where both P and S waves are observed at the same station, a transformation of the location equations can be used to virtually isolate the origin time computation from the hypocenter computation. In more general cases, the diagonalization of the covariance matrix will achieve the same result in a statistically rigorous format. In this study, an attempt will be made to improve the understanding of errors and uncertainty in location by recasting the location problem in terms of contributions evident in the covariance function of the residual travel times.

THEORY FOR THE CONCEPTUAL MODEL

The Gauss-Newton formulism for hypocenter determination, usually attributed to Giger (1910), is based on a minimization of the L_2 norm of the differences between observed and theoretical travel times. The equations for location are established by assuming that the observed arrival time O'_i for the i th observed phase will satisfy a crustal velocity model which allows computation of a theoretical travel time T'_i given a trial location vector $X' = (t', x', y', z')$. The t' is the trial origin time and (x', y', z') is the coordinate of the trial hypocenter. A correction vector $dP = (dt, dx, dy, dz)$ is defined by the first order terms of the Taylor expansion of the travel time such that for the i th phase

$$O'_i = T'_i(t', x', y', z') + \left[\frac{\partial T'_i}{\partial t}, \frac{\partial T'_i}{\partial x}, \frac{\partial T'_i}{\partial y}, \frac{\partial T'_i}{\partial z} \right] (dt, dx, dy, dz)^T \quad (1)$$

The higher order terms in the Taylor expansion are truncated since they are unneeded in the iterative solution for the location vector. The correction vector dP for each step in the iteration can then be obtained from the simultaneous solution of the equations relating the arrival times of all phases to the derivatives of the travel times. The vector dP is used to correct the initial trial location vector and the solution is recomputed at the new trial location vector until the difference between the observed data O' and the theoretical times T' at the corrected location vector are minimized in the least squares sense.

The set of simultaneous equations which are of course inconsistent in general and are to be solved only in the least squares sense can be written conveniently in matrix notation:

$$(O' - T')^T = A' dP^T = e'^T \quad (2)$$

where $(O' - T') = (O'_1 - T'_1, O'_2 - T'_2, \dots)$

$$\text{and } A' = \begin{vmatrix} \frac{\partial T'_1}{\partial t} & \frac{\partial T'_1}{\partial x} & \frac{\partial T'_1}{\partial y} & \frac{\partial T'_1}{\partial z} \\ \frac{\partial T'_2}{\partial t} & \frac{\partial T'_2}{\partial x} & \dots & \dots \\ \dots & \dots & \dots & \dots \\ \dots & \dots & \dots & \text{etc.} \end{vmatrix}$$

The matrix A' is the Jacobian matrix consisting of the derivatives of the theoretical travel times.

The justification for using the least-squares solution as a sensible estimator rests ultimately on the assumption of uncorrelated observations and homogeneity of variance of the observations (Gauss-Markov theorem; see Rao (1965)). Wiggins (1972) has used an estimate of the variances of the observations to weight them in inverse proportion to their uncertainty (standard deviation). This has the effect of producing approximately homogeneous variances, but it ignores correlations between observations, i.e., assumes that the covariance matrix is diagonal. This is the issue we wish to address.

The elements of the covariance matrix S of the observations O'_i are,

$$S_{ij} = \text{Cov}(O'_i, O'_j). \quad (3)$$

These are usually estimated using residual travel times from many samples (events). More will be said about this later. In matrix terms:

$$S = E[(O' - T')^T (O' - T')]. \quad (4)$$

The i and j refer to the propagation path from the j th hypocenter to the i th station. The propagation path is observed many times to compute the estimated value. The weighting matrix is defined as the inverse square root of S , the covariance matrix of the observed errors. Unlike Wiggins (1972), in this derivation a problem variance is not defined from the residual travel times and used to normalize the covariance matrix. Instead the location uncertainty will be based on a consideration of the variance of the observations.

At this point in the derivation most developments assume that the covariance matrix is diagonal, thus simplifying computation of the inverse square root. Two significant problems are associated with the acceptance of a normalized diagonal weighting matrix. First, the error covariance matrix can have large off-diagonal elements when both the compressional and shear waves at the same station are included or when stations are close together and their travel paths experience similar velocity structures. Second, when there are few stations the problem variance computed from the travel time residuals may

underestimate the uncertainty of the solution for the location. The uncertainty in the computed location represents the precision associated with the particular combination of errors and station locations for one event. Boyd and Snoke (1984) have discussed the various techniques used to evaluate uncertainty in currently used computer programs. The non-diagonal weighting matrix is the subject of this paper.

We shall now show the correct transformation to produce uncorrelated, homogeneous variance variables when S is not assumed to be diagonal. Assume S is non-singular. Then, there exist an orthogonal matrix M and a diagonal matrix D with positive diagonal entries (the eigenvalues of S) such that $M^T S M = D$ (principal axis theorem). Thus:

$$S = M D M^T = M D^{1/2} (M D^{1/2})^T = F F^T, \quad (5)$$

where $F = M D^{1/2}$.

Then transform the equations (2) above as follows:

$$F^{-1} (O' - T')^T = F^{-1} A' d P^T,$$

$$\text{or} \quad (O - T)^T = A d P^T \quad (6)$$

$$\text{where} \quad (O - T)^T = F^{-1} (O' - T')^T$$

$$\text{and} \quad A = F^{-1} A'.$$

Now observe that the entries in $O - T$ are uncorrelated and have variance one; that is, their covariance matrix is the identity:

$$\begin{aligned} E[(O - T)^T (O - T)] &= F^{-1} E[(O' - T')^T (O' - T')] F^{-T} \\ &= F^{-1} S F^{-T} = I. \end{aligned} \quad (7)$$

Thus to estimate $d P^T$, one should find the least-squares solution for the transformed equations (6).

When S is diagonal, the factor matrix F is just the square root of S , so multiplying by F^{-1} is equivalent to dividing the entries in $(O' - T')$ by their standard deviations in this case. Thus our procedure generalizes that of Wiggins to the case of a non-diagonal S . One way of looking at this is that in transforming by $F^{-1} = D^{-1/2} M^T$, the rotation M^T produces uncorrelated variables and the $D^{-1/2}$ part produces homogeneity of variance; it is the M^T part that seems to have been previously ignored.

This also has implications for the precision of the location parameter estimates, of course. Since dP^T is the least-squares solution to $(O-T)^T = AdP^T$ and $(O-T)$ has uncorrelated entries of variance one, it is a standard result of least-squares theory (see Rao, 1965) that the covariance matrix of dP^T is:

$$E[dP^T dP] = (A^T A)^{-1}. \quad (8)$$

In terms of the original untransformed data:

$$(A^T A)^{-1} = (A^T T_F^{-1} T_F^{-1} A)^{-1} = (A^T T_S^{-1} A)^{-1}, \quad (9)$$

so the correct covariance matrix S of the observations must be used in order to correctly assess the precision of the estimates of the location parameters. Assuming S to be diagonal when it is not could be very misleading in estimating the precision of the solution.

THE S MATRIX

The usual method of determining the diagonal elements of the S matrix is by examining travel time residuals in the location of many earthquakes (Boyd and Snoke, 1984). The event solution is assumed to be equivalent to the true solution and the residuals and errors are assumed to be equivalent. The residuals will underestimate errors since they are a measure of solution precision and not accuracy. With few points to establish a reasonable estimate of the true solution, the precision can be significantly better than the accuracy. In this paper an independent estimate of S is proposed and the observed residuals are used as a measure of consistency with the estimated values and as a tool to identify large errors such as improperly picked phases.

The random and uncorrelated errors depend on the resolution of the recording medium, the technique for reading phases, and timing precision at individual stations. Improperly identified phases usually generate anomalously large errors that can be identified and removed, or minimized by numerical methods such as uniform reduction error analysis (Buland, 1986). Correlated errors are dependent on measurable deviations of the earth's velocity structure from the velocity model. For stations close together, the ray paths experience similar travel time perturbations. An increase in station separation will generally decrease the correlation of the travel time residuals from a single event. Knowledge of the spatial relation among residuals, the autocorrelation function, can be used in the S matrix to improve the measurement of the precision of event locations. In most situations with sparse data, a reliable covariance of observations between stations can not be computed. However, alternate data sources are available to estimate the autocorrelation function and the autocorrelation function can serve as a statistical estimate of the covariance for the S matrix.

Because stations are stationary and finite, it is useful to compute station delay times. Travel time residuals along a seismic refraction line can be used to estimate the autocorrelation function of travel time residuals,

provided that the origin times of individual shots do not contribute significantly to the uncertainties of the arrival time. The autocorrelation function of these residuals along a refraction line approximate a one-directional slice of the two-dimensional autocorrelation function. Hence, if the assymetry of the autocorrelation function is negligible, the covariance of residuals at two nearby stations for a single event can be computed approximately with the autocorrelation function of residual travel times along refraction lines. For the purpose of computing the autocorrelation function, travel times obtained from a single source measured as a function of distance are equivalent to travel times measured at a single station from many sources. The only restriction is that the similarity of the propagation path be preserved for stations or sources close together. Figure 1 shows travel time data from two refraction lines, one in southeastern Tennessee where the source was a mine near Ductown, Tennessee, and the second in the Piedmont of Georgia and South Carolina where the sources were rock quarries. The autocorrelation functions for these refraction lines have correlation distances of 5 km or less.

A two-dimensional autocorrelation function would be more appropriate for earthquake location studies where the earthquakes occur throughout an area. As a first approximation, the two-dimensional autocorrelation function may be assumed to be radially symmetric. However, most geologic structures are two dimensional and correlation distances may be different parallel and perpendicular to the structure. Travel time residuals at station CBT for earthquakes in southeastern Tennessee are shown in Figure 2. The positive residuals (i.e. delayed arrivals) are consistent with the interpretation of the local negative Bouguer Anomaly as caused by low-velocity rocks (a sedimentary basin ?) in the shallow crust. An estimate of the radially symmetric autocorrelation function (Figure 2b), however, decays rapidly indicating a correlation distance of less than five kilometers and a negative correlation in the distance range of 10 to 50 km. The cause of the negative correlation is apparent in the regional pattern of positive and negative residuals. The scatter in the residuals which explain the short correlation distance is probably related to the influence of the depth on the ray path, a few anomalously large travel time residuals, and the uncertainty in the computed hypocenter parameters. A similar pattern is observed for mean residuals projected along a profile directed N 40° W, perpendicular to the basement structure (Figure 2c,d). Controlled sources or a single event recorded on a denser seismic net would be needed to develop a better estimate of the autocorrelation function.

A strong correlation between Bouguer gravity anomalies and the time term delays observed in southern New Mexico (Olsen et al., 1986) suggests that the travel time autocorrelation function may also be approximated by the autocorrelation function of the gravity field. They concluded that the strong correlation suggested that the cause was the same and that deep or lateral velocity anomalies and density anomalies are derived from the same structure. A typical autocorrelation function for the Bouguer gravity anomaly is given in Figure 3 and is converted to travel time anomalies by a ratio of delay time to gravity anomaly in Olsen et al. (1986). The value of the autocorrelation function at the lag distance between two seismic recording stations would be an appropriate value to use to compute the elements of the S matrix. The advantages of gravity data in computing the autocorrelation function are its

availability and higher signal to noise ratio. The higher signal to noise ratio may also explain the fact that the correlation distance, which is about 10 km, for gravity data, is greater than the apparent correlation distance in the travel time residuals. For gravity data, Goad et al. (1984) also observed correlation distances, predominantly in the range of 8 to 11 km. In the southeastern United States, Long (1974) computed autocorrelation half widths, for gravity data, of 10 to 25 km.

In the special case of observations of P- and S-wave arrivals at the same station, the correlation is definitely not small; in fact, it approaches one as the variance of the reading errors approaches 0. A heuristic argument may be presented to determine the covariance. Variations in Poisson's ratio may be assumed to be of second order and insignificant. The P and S waves follow very similar paths and the perturbations of the travel times will be proportional and related through Poisson's ratio by the equation

$$\left(e_s = \frac{(2-2\sigma)}{(1-2\sigma)} e_p \right) \quad (10)$$

The contribution of the reading errors must be combined with the variance related to the velocity model. The covariance matrix for a pair of P and S phases thus takes the form taking $\sigma = 0.25$ for a concrete example,

$$\begin{vmatrix} (s_p^2 + s_r^2) & (3s_p^2) \\ (3s_p^2) & (3s_s^2 + s_r^2) \end{vmatrix}$$

where s_p^2 is the variance of the P-wave travel time, s_r^2 is the variance of the reading errors (assumed independent and homogeneous for P and S waves), and $3s_p^2 = s_s^2$, the variance of the S-wave travel time. The extension to multiple stations is straight forward. The S matrix approaches singularity as the ratio of the variance of the reading errors s_r^2 to the variance related to the velocity model approach zero. Reading errors and the minor variations in Poisson's ratio prevent the S matrix from becoming singular. The covariance of a P- and S-wave arrival pair can be significantly larger than the uncorrelated reading errors, and hence, the elements of the inverse of the S matrix could be significantly larger than would be implied by the diagonal elements alone. In this case the use of the complete weighting matrix will increase the weight that is applied to stations with both P and S wave arrivals. The complete S matrix can be defined by the autocorrelation function, the covariance of P and S phases at the same station, and reading errors.

In case of a near-perfect linear relation between P- and S-wave arrival times at the same station (i.e., s_r^2 above nearly equal to zero and Poisson's ratio holds exactly), then we shall show that the origin time computation

should be carried out separately from the location computation, with nearly zero variance in the estimate of dt. Still using $\sigma = 0.25$ for our example, the eigenvectors for the 2x2 matrix above approach $(\sqrt{3}, -1)/2$ and $(1, \sqrt{3})/2$, and the eigenvalues are approximately s_r^2 and $4s_p^2 + s_r^2$. Then the transformation of the equations discussed above, considering only these two observations, is:

$$\begin{array}{c}
 \left| \begin{array}{cc} 1/s_r & 0 \\ 0 & 1/\sqrt{(4s_p^2 + s_r^2)} \end{array} \right| \left| \begin{array}{cc} \sqrt{3}/2 & -1/2 \\ 1/2 & \sqrt{3}/2 \end{array} \right| \left| \begin{array}{c} P - T_P \\ S - T_S \end{array} \right| \\
 \\
 - \left| \begin{array}{cc} 1/s_r & \\ 0 & 1/\sqrt{(4s_p^2 + s_r^2)} \end{array} \right| \left| \begin{array}{cc} \sqrt{3}/2 & -1/2 \\ 1/2 & \sqrt{3}/2 \end{array} \right| \left| \begin{array}{cc} \frac{dT_P}{dt} & \frac{dT_P}{dx} \\ \frac{dT_S}{dt} & \frac{dT_S}{dx} \end{array} \right| \left| \begin{array}{c} dt \\ dx \\ dy \\ dz \end{array} \right| \\
 \\
 - \left| \begin{array}{cccc} (\sqrt{3}-1)/2s_r & 0 & 0 & 0 \\ \cdot & \cdot & \cdot & \cdot \\ \cdot & \cdot & \cdot & \cdot \\ \cdot & \cdot & \cdot & \cdot \end{array} \right| \left| \begin{array}{c} dt \\ dx \\ dy \\ dz \end{array} \right|
 \end{array}$$

Note this decouples the computation of dt, and puts very large weight for the least-squares computation on the first residual of the transformed equations since s_r is very small. The first line is equivalent to the familiar relation between S-P time and P-wave travel time or to the use of a Wadati plot to compute origin time. With the addition of pairs of S- and P-wave arrivals from other stations, the origin time and location computations can be separated. If, however, at some stations the P or S phase is unreadable, the origin time and location computations will be slightly coupled through the minimization of the errors associated with the unpaired arrivals. It is suggested that this additional reduction in the mean square error is an unneeded artifact of the location process and that the origin time should be computed only from the pairs of S-P times when available. The single phases may be reintroduced in the location computation. A consideration of the weights also suggests that this is practically what happens anyway, when the covariance matrix is properly factored into the weighting matrix. The larger weights associated with the near-singularity of S as above will virtually isolate the origin time computation.

EXAMPLE

Four stations from the Georgia Tech Net in southeastern Tennessee are used to illustrate the significance of the difference in uncertainty estimated from a properly formulated weight matrix versus the traditional estimate from residual arrival times. The stations, shown in Figure 4, were used to locate a small event occurring on January 8, 1986. The epicenter is near the center of the array and thus it avoids most of the difficulties associated with a non-ideal station distribution. The results of two solutions are shown in Table I. The first presents the actual data and the second presents a fictitious event at the same hypocenter, but with very small residual errors. The uncertainty estimates for generation of the S matrix in both cases were based on an autocorrelation distance of $a = 10$ km, a P-wave variance of $c = 0.02$ and the empirical covariance function for separation r given by $C*(1+(r/a)^2)$ (after Goad et al., 1984). In this example the weights along the diagonal are increased by 10 percent by including the off-diagonal elements. The error ellipses computed from the uncertainty estimates and a properly formulated S matrix are the same for both events. The error ellipses based on residuals are significantly smaller and proportional to the mean residual.

SUMMARY AND CONCLUSIONS

The weighting matrix, which has been largely ignored in location programs, contains important information concerning the error estimate and weighting of arrivals for earthquake hypocenters. The off-diagonal elements have significant values for P- and S-wave arrivals at the same station and at stations close together. These off-diagonal elements increase the weights applied to their respective arrivals. In the special case of S- and P-wave arrivals at the same station, the weights can be large enough to make the origin time and location virtually independent of the single arrivals from isolated stations. Alternately, the location equations containing S and P waves at each station can be transformed to isolate the origin time computation from the hypocenter computations. Where data are inadequate to estimate the elements of the covariance matrix, the elements may be estimated from an autocorrelation function of travel time residuals along refraction lines or from gravity data. Use of the properly formulated weighting matrix yields consistent estimates of location errors which are independent of the precision implied by station residuals. In most cases the inclusion of off diagonal elements improves the precision and accuracy of location estimates.

ACKNOWLEDGMENTS

This research was supported by the Nuclear Regulatory Commission Contract NRC-04-85-122.

REFERENCES

- Aki, K. and P. Richards (1980). Quantitative Seismology: Theory and Methods, Vol-2, W. H. Freeman Co., San Francisco.

- Boyd, T. M. and J. A. Snoke (1984). Error estimates in some commonly used earthquake location programs, Earthquake Notes, Vol. 55, No. 2,3-6.
- Buland, Ray. (1986). Uniform Reduction Error Analysis, Bull. Seism. Soc. Am., Vol. 76, 217-230.
- Evernden, J. F. (1969). Precision of epicenters obtained by small numbers of world-wide stations, Bull. Seism. Soc. Am., Vol. 59, 1365-1398.
- Geiger, L. (1910). Herdbestimmung bei Erdbeben aus den Ankunftszeiten, K. Gesell. Wiss. Goett., Vol. 4, 331-349.
- Goad, Clyde C., C. Christian Tscherning, and M. Miranda Chin (1984). Gravity Empirical Covariance Values for the Continental United States, Journal of Geophysical Research, Vol. 89, No. B9, pp 7962-7968.
- Lee W. H. K. and S. W. Stewart (1981). Principles and Applications of Microearthquake Networks, Academic Press, New York.
- Long, L. T. (1974). Bouguer gravity anomalies of Georgia, in Symposium on the Petroleum Geology of the Georgia Coastal Plain, Bulletin 87, Georgia Geological Survey, Atlanta, Georgia, 141-166.
- Olsen, K. H., L. W. Braile, J. N. Stewart, C. R. Dundt, G. R. Keller, L. A. Ankeny, J. J. Wolff (1986). Jemez Mountains Volcanic Field, New Mexico: Time term interpretation of the CARDEX Seismic Experiment and Comparison with Bouguer Gravity. Journal of Geophysical Research, Vol. 91, No. B6, pp 6175-6187.
- Rao, C.R., (1965). Linear Statistical Inference and its Applications, John Wiley and Sons, New York.
- Wiggins, R. A. (1972). The general linear inverse problem: Implication of surface waves and free oscillations for earth structure, Reviews of Geophysics and Space Physics, Vol. 10, 251-285.

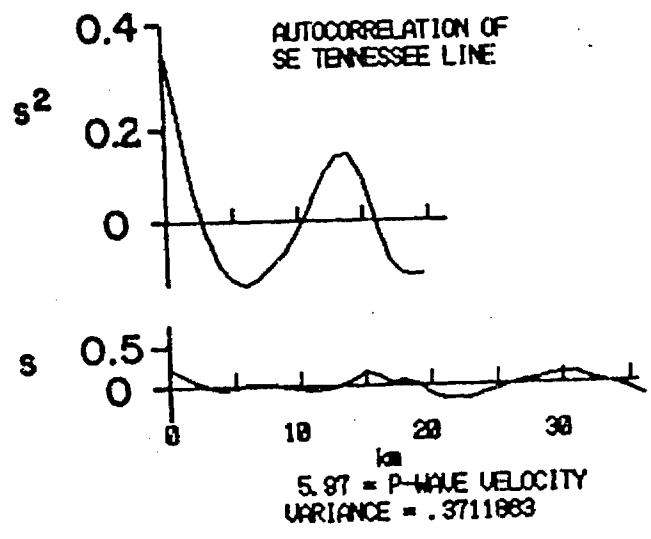
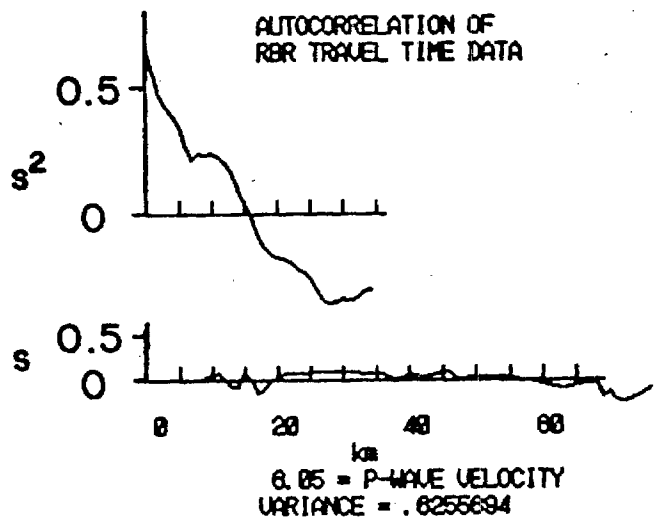
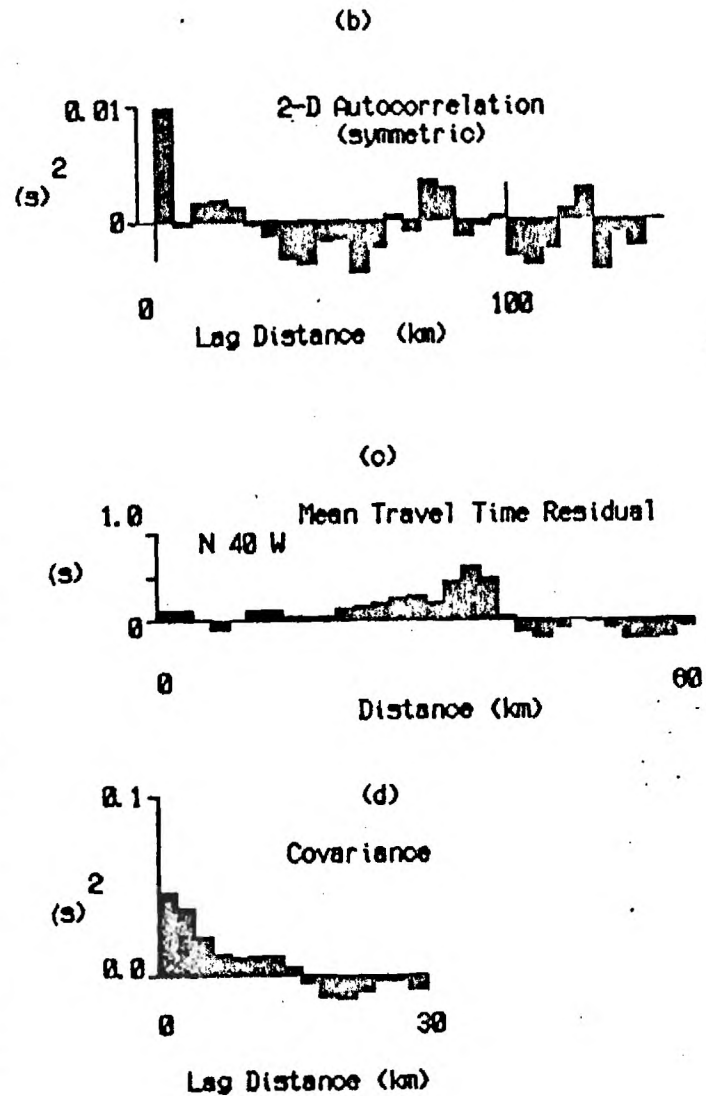
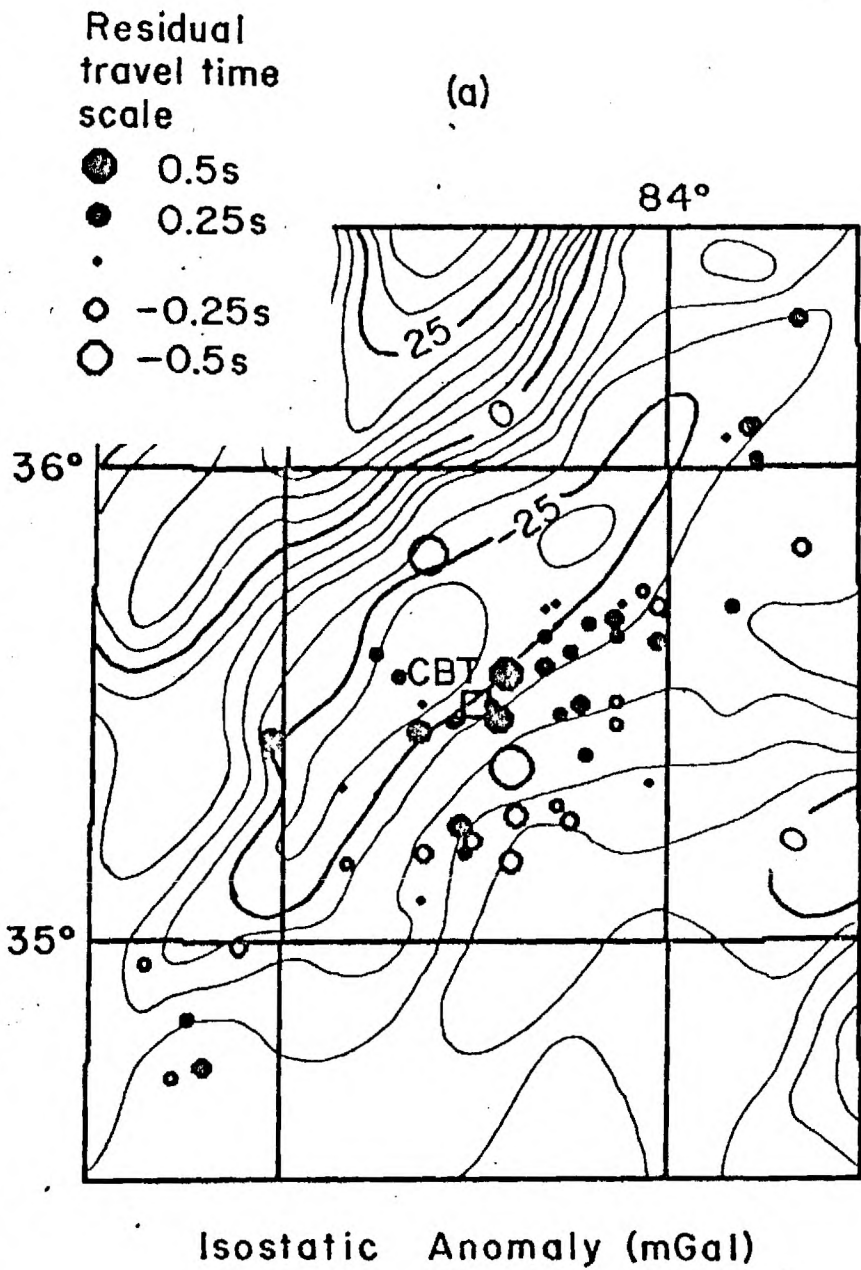


Figure 1. Autocorrelation functions for two seismic refraction lines. The reduced travel time curves are shown below. The reduced velocity for the RBR data was 6.05 km/s and is typical of crystalline Piedmont rocks in Georgia and South Carolina. The southeastern Tennessee data has a reduced velocity of 5.95 km/s and represents Blue Ridge metasediments.

Figure 2. Analysis of travel time residuals for earthquakes recorded at station CBT. a) epicenter map showing the magnitude of the travel time residuals superimposed on isostatic gravity anomalies. b) autocorrelation function of travel time residuals assuming radial symmetry. c) projection of residuals onto a line perpendicular to the strike of the basement structures. d) one dimensional autocorrelation function for projection in c.



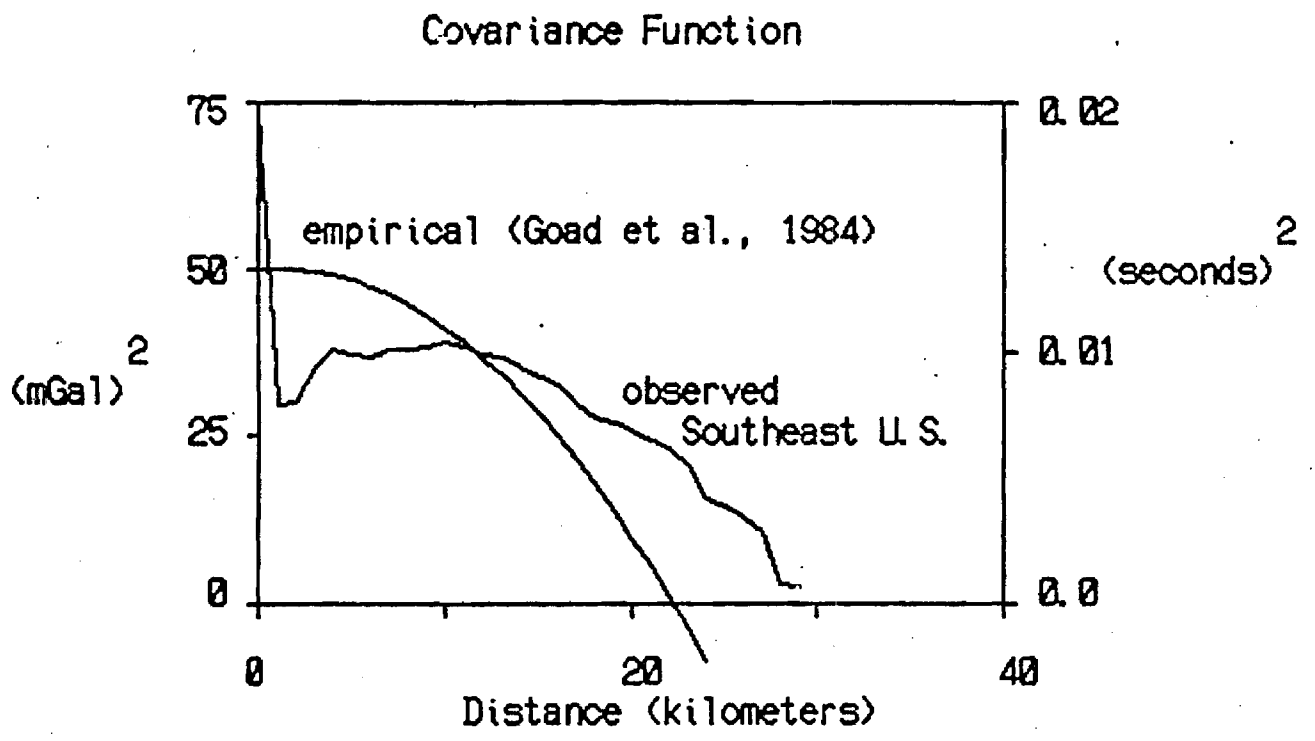


Figure 3. Autocorrelation function from gravity data and its conversion to equivalent travel time residuals using the relation from Olsen et al., (1986).

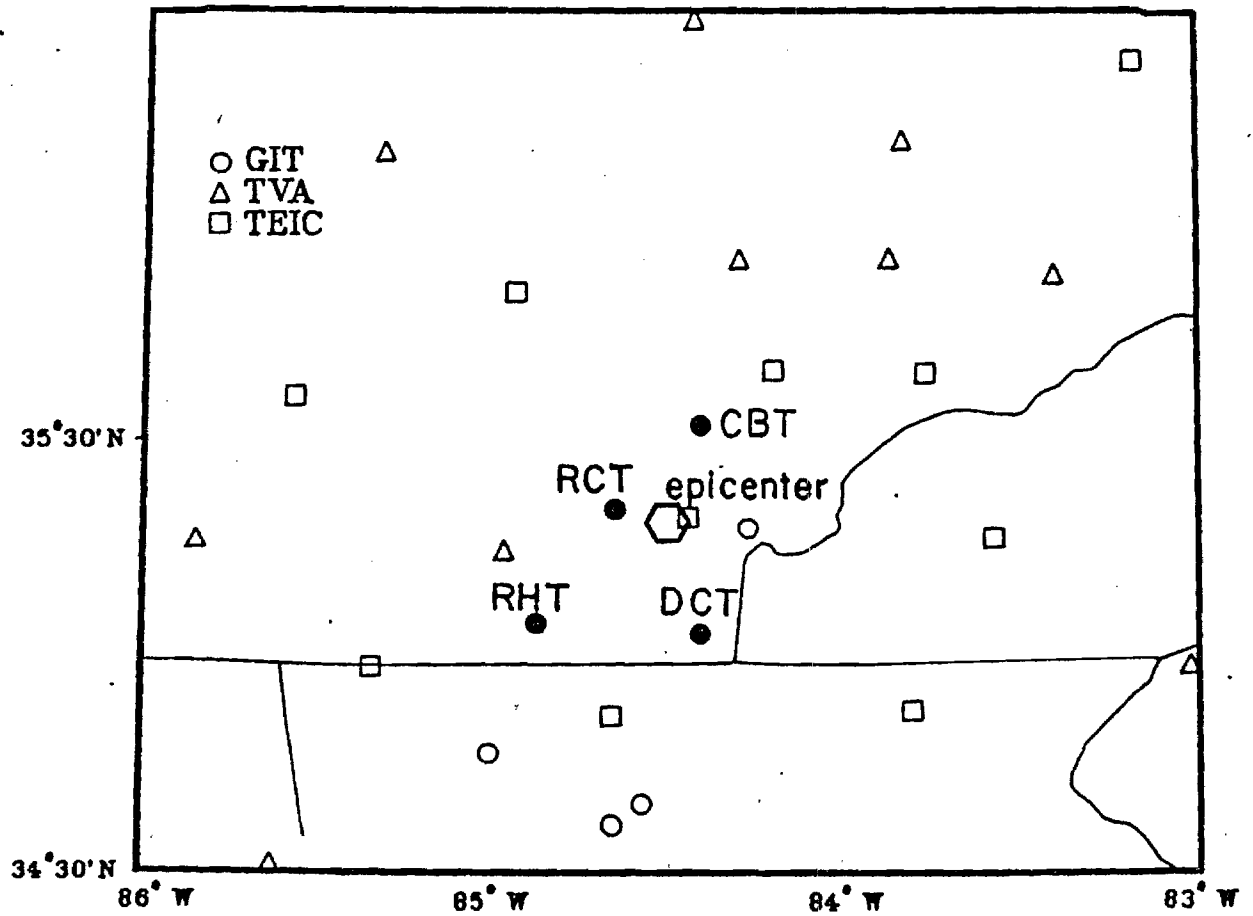


Figure 4. Stations (solid circles) and epicenter (hexagon) for the event of January 8, 1986.

TABLE I Data from event of January 8, 1986

Station	Phase	Weight	Actual Data		Fictitious Data	
			Time(s)	Residual	Time(s)	Residual
RCT	P	0.2	43.8	0.263	43.442	-0.017
RCT	S	0.4	46.0	-0.114	46.000	0.020
CBT	P	0.2	44.2	-0.194	44.430	-0.006
CBT	S	0.4	47.7	0.102	47.700	0.029
DCT	P	0.2	46.3	0.117	46.120	-0.015
DCT	S	0.4	50.5	-0.197	50.647	0.032
RHT	P	0.2	48.0	-0.067	48.000	0.032
RHT	S	0.4	53.5	-0.460	53.738	-0.052

	Actual Data	Fictitious Data
Origin Time(s)	7:10:40.0167	7:10:40.0152 Greenwich Time
Latitude (degrees)	35.3544 N	35.3515 N
Longitude (degrees)	84.4960 W	84.5011 W
Depth (km)	15.43	15.24

Error Ellipse	Principle Axes (km)	Direction Cosines		
		E	N	Z
for Actual Data:	1.39	0.15	-0.15	0.98
	0.36	0.97	0.22	-0.12
	0.55	0.19	-0.96	-0.18
for Fictitious Data:	0.18	0.15	-0.16	0.98
	0.05	0.97	0.22	-0.11
	0.07	0.20	-0.96	-0.19
for Covariance Data: (same for actual and fictitious data)	3.43	0.14	-0.22	0.96
	1.13	0.97	0.24	-0.09
	1.67	0.21	-0.94	-0.25

Covariance Matrix

0.080	0.069	0.004	0.007	0.002	0.004	0.003	0.005
0.069	0.280	0.007	0.012	0.004	0.007	0.005	0.009
0.004	0.007	0.080	0.069	0.001	0.002	0.001	0.002
0.007	0.012	0.069	0.280	0.002	0.004	0.002	0.003
0.002	0.004	0.001	0.002	0.080	0.069	0.002	0.004
0.004	0.007	0.002	0.004	0.069	0.280	0.004	0.006
0.003	0.005	0.001	0.002	0.002	0.004	0.080	0.069
0.005	0.009	0.002	0.003	0.004	0.006	0.069	0.280

Weighting Matrix

3.937	-0.658	-0.045	-0.030	-0.027	-0.019	-0.033	-0.022
-0.658	2.029	-0.030	-0.024	-0.019	-0.015	-0.022	-0.018
-0.045	-0.030	3.936	-0.659	-0.014	-0.010	-0.008	-0.006
-0.030	-0.024	-0.659	2.028	-0.010	-0.008	-0.006	-0.005
-0.027	-0.019	-0.014	-0.010	3.935	-0.659	-0.024	-0.017
-0.019	-0.015	-0.010	-0.008	-0.659	2.028	-0.017	-0.013
-0.033	-0.022	-0.008	-0.006	-0.024	-0.017	3.935	-0.659
-0.022	-0.018	-0.006	-0.005	-0.017	-0.013	-0.659	2.028

The test program was written in BASIC for Personal Computers

6-33-621

NUREG/

GEORGIA/ALABAMA REGIONAL SEISMOGRAPHIC NETWORK

Annual Report
July 1, 1987 -- June 30, 1988

Prepared by L. T. Long

Georgia Institute of Technology

Prepared for

U. S. Nuclear Regulatory Commission

NUREG/

GEORGIA/ALABAMA REGIONAL SEISMOGRAPHIC NETWORK

Annual Report
July 1, 1987 -- June 30, 1988

Manuscript Completed
Date Published:

Prepared by L. T. Long
Georgia Institute of Technology

School of Earth and Atmospheric Sciences
Georgia Institute of Technology
Atlanta, Georgia 30332

Prepared for
Division of Engineering
Office of Nuclear Regulatory Research
U. S. Nuclear Regulatory Commission
Washington, D.C. 20555

Under Contract No. NRC 04-85-122

EXECUTIVE SUMMARY AND ABSTRACT

OBJECTIVE:

The objective of this study is to contribute data and analyses conducive to the development of criteria for establishing earthquake hazard potential in the southeastern United States.

TASKS:

The first task is to install and maintain the Georgia/Alabama seismic network. The seismic network consists of about 21 stations in Alabama, Georgia, and adjoining regions of southeastern Tennessee and South Carolina. The seismic net includes three three-component short period stations and operates completely on solar power.

The second task is to monitor the seismic activity in southeastern Tennessee, northern Alabama, and Georgia. The data are to be used in appropriate topical studies.

RESULTS:

Four topical studies achieved notable conclusions or were completed during the reporting period of July 1987 to June 1988. The principal conclusions for these four topical studies are summarized below and presented in detail in the Appendices. In addition, we examined the rate of seismicity through time in southeastern Tennessee. A review of the historical seismicity of southeastern Tennessee suggests that the period of 1970 through 1988 was anomalously more active than before 1970. The greatest uncertainty relates to the uniformity of coverage and detection. If this period is indeed more active, then it represents a unique stress release event that would satisfy the model for major intraplate earthquakes proposed by Long (1988).

First motion data and SV/P amplitude ratios were used to determine 36 single event and two composite focal mechanism solutions for earthquakes in southeastern Tennessee. The dominant focal mechanism is strike slip; however, the focal mechanisms exhibited components of reverse and normal fault movement. Estimates of solution confidence suggest that the variation in focal mechanism is significant.

Coda Q is determined by the integrated effects of crustal parameters in the ellipsoidal volume of crust with the recording station and hypocenter as foci. Zones of anomalous crust will influence the computation of coda Q differently for different station and hypocenter pairs. We have linearized the relation between the measured apparent coda Q and an assumed constant coda Q for discrete zones of crust. Inversion of coda Q data near station CBT suggests an anomalously low coda Q region ($Q=50$) in a 300 kilometer region northeast of station CBT.

Fracture density was mapped in an area of induced seismicity in the Clarks Hill Reservoir area in sufficient detail to allow contouring of the

data. These contours suggest that areas of higher joint spacing correspond to zones of induced seismicity. The rock type typically described as granite gneiss has shown a spatial correlation with reservoir induced seismicity in this and other seismic reservoirs. Earthquakes tend to occur where jointing is sparse and the rock is strong. In contrast, seismic activity is not often observed in foliated schists and altered mafic rocks, in which stress may be released through creep or failure along the many foliations and fractures.

Earthquakes in the Lake Sinclair Reservoir area were relocated using a technique in which the origin time was computed independent of the location. The location residuals improved substantially with a velocity model which includes an abnormally high (6.6 km/s) crustal velocity at 2.0 km depth. The relocated activity suggests clustering of seismicity in five distinct zones.

TABLE OF CONTENTS

	page
Executive Summary and Abstract.....	iii
Table of Contents.....	v
List of Figures.....	vi
List of Tables.....	ix
Georgia/Alabama regional Seismographic Network.....	1
Objectives.....	1
Summary of Results and Findings.....	2
Network maintenance and seismic monitoring.....	2
Graphical representation of operational status.....	3
Plans for next year.....	3
Abstracts of Presentations.....	4
Results of topical studies.....	8
Appendix A. Pattern of Earthquake Focal Mechanisms in southeastern Tennessee.....	17
Appendix B. A technique for the inversion of Coda Q.....	49
Appendix C. Fracture intensity and Reservoir Induced Seismicity.....	57
Appendix D. Relocation of Earthquakes in the Lake Sinclair Reservoir Area.....	77

LIST OF FIGURES

	page
Figure 1. Distribution of seismic stations recorded during the period of 1 July, 1987 to 30 June, 1988.....	10
Figure 2. Frequency of occurrence of events with magnitude greater than three. The number of events is for ten year periods in southeastern Tennessee.....	11
Figure 3. Frequency of occurrence of events with magnitude greater than four. The number of events is for ten year periods in southeastern Tennessee.....	12
Figure 4. Strain release in ten year increments for recorded seismicity in southeastern Tennessee.....	13
Figure 5. Energy release in ten year increments for southeastern Tennessee computed from magnitude.....	14
Figure 6. Graphical representation of the operational status of the Georgia/Alabama Seismographic Network.....	15
 Appendix A	
Figure 1. Published focal mechanism solutions for southeastern Tennessee (see Table I for reference numbers.....)	31
Figure 2. Composite plot of seismic refraction velocities in the southeastern United States showing the relation of velocity with depth.....	32
Figure 3. Relation between random probability factor and maximum azimuthal gap.....	33
Figure 4. Relation between variance of polarity observations and probabilities of a correct reading.....	34
Figure 5. Distribution of the random probability factor for all earthquakes.....	35
Figure 6. Relation between random probability factor for small and large numbers of stations.....	36
Figure 7a. Significance for all events for polarity data.....	37
Figure 7b. Significance for all events for SV/P amplitude ratios.....	38
Figure 7c. Significance for polarity and SV/P amplitude ratios.....	39
Figure 8. Location of earthquakes in southeastern Tennessee. Solid dots are events which have focal mechanism solutions.....	40

List of Figures (continued)

Figure 9a-d.	Focal mechanism solutions.....	41
Figure 9e-h.	Focal mechanism solutions.....	42
Figure 9i-k.	Focal mechanism solutions.....	43
Figure 10.	Dip of the null-axis in the central zone. This is a measure of strike-slip motions.....	44
Figure 11.	Difference between the dip of the tension axis and pressure axis. A value of -90 corresponds to a pure reverse fault. A value of +90 corresponds to a pure normal fault.....	45
Appendix B		
Figure 1.	Seismograms recorded at station CBT showing variation in character of coda decay and their location relative to CBT.	53
Figure 2.	Data for preliminary analysis. (a) Comparison of anomalous area and ellipses of influence, and (b) locations of stations and events used.....	54
Figure 3.	Apparent Coda Q versus percent contribution of anomalous area in the ellipse of influence.....	55
Appendix C		
Figure 1.	Location map for area of joint measurements in the Clarks Hill Reservoir. Geology abstracted from Griffin (1973).....	69
Figure 2.	Outline of the study area showing station locations and joint directions. Small crosses are the epicenters of earthquakes from Dunbar (1977). Origin is 33.925 N, 82.625 W.....	70
Figure 3.	Joint pole plot for station ch28 showing dominant joint set for the Clarks Hill Reservoir.....	71
Figure 4.	Average fracture intensity plot of observation points.....	72
Figure 5.	Autocorrelation of the trimean intensity data at separation distances of 0.5 and 0.25 km. Heavy line is autocorrelation function for the gridded data.....	73
Figure 6.	Contoured map of the trimean fracture intensity. The crosses indicate locations of epicenters.....	74
Figure 7.	Contoured map of Rock Quality. The crosses indicate locations of epicenters.....	75

List of Figures (continued).

Appendix D

Figure 1.	Historical Seismicity of Central Georgia (after Long, 1982).....	84
Figure 2.	Locations of events in the Lake Sinclair and Lake Oconee Areas (from Allison, 1980).....	85
Figure 3.	Typical traces of Lake Sinclair events.....	86
Figure 4.	The 189 relocated epicenters of the Lake Sinclair and Lake Oconee areas. Dashed circles identify clusters A through E.....	87
Figure 5.	P-wave travel-time residuals for stations ETG and WDG plotted versus azimuth.....	88
Figure 6.	P-wave travel-time residuals for stations REG and GBG plotted versus azimuth.....	89
Figure 7.	Mean P-wave residuals from a constant velocity model for cluster A events that were recorded on four stations.....	90
Figure 8.	Mean P-wave residuals for a two-layer model for cluster A events that were recorded on four stations.....	91
Figure 9.	Bouguer Map of the Lake Sinclair area and Lake Oconee area (after O'Nour, 1982).....	92
Figure 10.	Reduced P-wave travel times for a two-layered model plotted versus station distance and a velocity model for the Lake Sinclair and Lake Oconee areas.....	93
Figure 11.	Epicenters for the Lake Sinclair and Lake Oconee areas using the two-layer velocity Model.....	94

LIST OF TABLES

page

Appendix A

Table I. Location parameters and focal mechanisms of southeastern Tennessee earthquakes.....	46
Table II.....	46
Table III.....	47
Table IV.....	48
Table V.....	48

GEORGIA/ALABAMA REGIONAL SEISMOGRAPHIC NETWORK

Objectives

The objective of this study is to contribute data and analyses conducive to the development of criteria for establishing earthquake hazard potential in the southeastern United States. The main tasks are to install and maintain a seismic network and monitor the seismic activity in eastern Tennessee, northern Alabama, and Georgia. The data are to be contributed to the southeastern U. S. regional bulletin. Also, available information will be used in appropriate topical studies.

- * Specific objectives for network maintenance and seismic monitoring are as follows:
- * Install or provide about 16 short-period seismograph stations deployed in Tennessee, Alabama, and Georgia. This network is to be operated with a maximum of 5 percent downtime.
- * Obtain and/or reaffirm use permits and telemetry service to convey the data to a central recording point.
- * Provide all seismic phase readings and hypocenter locations to the Southeast U. S. Seismographic Network Bulletin.
- * Provide a recording medium with on-line digital recording at the Central Recording Facility.
- * Report any significant earthquake within the study region to the Nuclear Regulatory Commission within 24 hours.
- * Relocate and/or establish new seismograph stations as it becomes necessary after approval of the Nuclear Regulatory Commission.

Objectives for topical studies are as follows:

- * Study the spatial and temporal distributions, including earthquake recurrence rates, of seismicity and relate them to structural features.
- * Identify parameters that influence seismic processes within the network area and use these in defining seismogenic/tectonic provinces.
- * Study crustal and upper mantle velocity structure in the United States based on the current data from the network.
- * Study the magnitudes of historic events using magnitude-felt area relationships and obtain the magnitude-frequency relationships.
- * Evaluate the relative significance of results obtained in each of the above analyses as they impact the determination of seismic hazards.

Summary of Results and Findings

Network maintenance and seismic monitoring

During the period of 1 July, 1987, to 30 June, 1988, the Georgia/Alabama regional Seismic Net consisted of 21 stations located as shown in Figure 1. The Clarks Hill Reservoir Area and the area of Lake Richard B. Russell were monitored by four stations. The State of Georgia is monitored by five additional stations. Seven stations are located in Alabama and five in southeastern Tennessee. The Alabama, Tennessee and northwest Georgia stations constitute coverage for the termination of the southern Appalachian seismic zone. Most of the time during July and August was consumed by trips to replace or fix field systems damaged by thunder storms. The efforts to replace or fix field systems damaged by thunder storms continues to require a significant portion of the work time during the summer quarter. Station CH6 will be taken down to allow lumbering on the station site during the winter months.

All stations in the Georgia/Alabama Regional Seismographic Network are monitored by a digital acquisition system. Triggered events are saved to disk and, if appropriate, saved on tape for later study. The digital system recorded the entire record of the Alaskan Earthquake and most smaller local events. The large Virginia mine collapse was recorded. A magnitude 2.7 event was detected near Knoxville. The Alabama quake was recorded in its entirety by the digital system. Two significant local events were recorded during December. One near our station TLT in southeastern Tennessee and the other in a swarm in the Richard B. Russell Reservoir, marking the first significant induced seismicity by that reservoir. Later, one additional small event was detected in the Richard B. Russell Reservoir area, suggesting continued reservoir induced seismicity.

With the cooperation of mine operators in Alabama, a digital event recorder in the area of recent large mine bumps is obtaining data on local events for the period of September, 1987 through mid-December, 1987. However, the expected Alabama mine collapse event caused only a swarm of activity that reached a peak March 20. We have a set of digital 3-component records of the swarm. The Alabama mine monitoring indicated an increase in activity at the time the longwall was in line with the previous large mine collapses.

One interesting aspect of the historical seismicity in southeastern Tennessee is the apparent increase in seismicity in the last 20 years. During this year an effort was made to test the stationarity of the seismicity by examination of the historical record. The study included a reevaluation of the ATL WWSSN records of southeastern Tennessee earthquakes to develop consistency in magnitudes. Reported felt area, duration magnitude and local body wave magnitudes were examined and recomputed where appropriate. Some minor adjustments in recently computed magnitudes were made; however, most historical events, before 1960, have magnitudes based on intensity data and no significant discrepancies were found. The resulting catalog was then used to compute strain release, energy release and event frequency in ten year increments.

Figure 2 shows frequency of occurrence of magnitude greater than three events and Figure 3 shows frequency of occurrence of magnitude greater than

four events. In both cases a dominant peak appears in the 1955 decade. The last 20 to 40 years are greater than the previous years. Figure 4 gives the strain release, which also shows a minor peak in 1955, but is dominated by the influence of the many small events reported in the last decade. The strain release mimics the number of magnitude greater than two events, which are susceptible to gaps in detection. The energy release, Figure 5, also shows an increase in the 1955 to present time span. Unfortunately, the normal tests for completeness do not work when testing for variations in activity with time. Two observations suggest that the recent increase is valid. First the magnitude four and larger events show a distance increase. These would be expected to be detected at least for the last 100 years. Second, the rate of seismicity from historical data in western North Carolina is greater than in the recent monitored data, suggesting that such events would have been noted and a change in activity is possible.

A review of the historical seismicity of southeastern Tennessee suggests that the period of 1970 through 1988 was anomalously more active than before 1970. The greatest uncertainty relates to the uniformity of coverage and detection. If this period is indeed more active, then it represents a unique stress release event that would satisfy the model for major intraplate earthquakes proposed by Long (1988).

Graphical representation of the operational status of the network

The high level of station down time in the late spring was caused by heavy thunder storm activity and lightening damage. The graphical representation of the operational status of the network is given in the form of the daily log of recording and is given in figure 6.

Plans for next year

Digital data accumulating for the southeastern Tennessee area is showing evidence of a highly variable coda Q. Plans for next year include the development of an inversion technique for coda Q in southeastern Tennessee. The first step will be the development of a computational model to generate synthetic coda.

The studies of seismicity and crustal structure in southeastern Tennessee have lead to the development of a theory for major intraplate earthquakes. The data from southeastern Tennessee will be examined for consistency with this model. In particular, we will look for evidence in coda Q and focal mechanisms.

Focal mechanisms will be compared to computed estimates of stress surrounding a weak zone in a plate in order to evaluate the consistency of focal mechanisms in southeastern Tennessee with a model for major earthquakes.

The rate of attenuation of Lg phase in Alabama will be examined for possible comparison with intensity data. Because earthquake data are sparse, the attenuation study will use blast data.

The Rg waves recorded from the many blasts in Alabama will be used to solve for the shallow crustal structure.

Abstracts of Presentations

The following are abstracts of talks which were made possible by data and research related to the Georgia/Alabama seismographic network.

A STUDY OF THE DISTRIBUTION OF FOCAL MECHANISM SOLUTIONS OF EARTHQUAKES IN SOUTHEASTERN TENNESSEE.

ZELT, K.-H. and LONG, L. T., School of Geophysical Sciences, Georgia Institute of Technology, Atlanta, Georgia 30332-0340.

The infrequent occurrence of earthquakes in the southeastern United States and sparse seismic station coverage limits the number and distribution of first motions and SV/P amplitude ratios available for the determination of focal mechanism solutions. Subsequently, only solutions from large MD > 3.0 earthquakes are well constrained. For most of the smaller events, the sparse coverage of the focal sphere introduces ambiguity to the focal mechanism. Consequently, the certainty of determining a local stress field or a deviation from the regional stress field is limited. In southeastern Tennessee, the pattern of seismicity is diffused and cannot be associated with a distinct single fault. The majority of large events (MD > 3.0) occur near the center of southeastern Tennessee activity and have a strike-slip mechanism with predominantly north-south striking nodal planes. Outside the central zone, smaller events which may be recorded on only a few stations show a spatial distribution of normal or reverse components in the predominant strike-slip component. A statistical treatment of the distribution of first motions on the focal sphere is used to establish a measure of confidence for the focal mechanism solution of the smaller events in southeastern Tennessee and to establish the validity of the special distribution of normal and reverse components.

Presented at the American Geophysical Union, Spring Meeting, Baltimore, Maryland, May 16, 1988.

A MECHANISM FOR MAJOR INTRAPLATE EARTHQUAKES

LONG, L.T., School of Geophysical Sciences, Georgia Institute of Technology, Atlanta, GA 30332.

The seismicity associated with a major intraplate earthquake is proposed to be a transient phenomenon triggered by a perturbation in the fluid and thermal regime of the lower crust. A major intraplate earthquake has a magnitude greater than 6, and a fault rupture of crustal dimensions; 20 km or greater. Regional plate stress provides the energy, and a perturbation in the fluid content, which decreases crustal strength, determines the location. The timing of a major earthquake and the characteristics of associated seismicity may be described by a sequence of five phases in the perturbation of crustal

strength. The five phases are: (1) initiation, (2) strength corrosion, (3) stress concentration, (4) failure, and (5) crustal healing. (1) A major intraplate earthquake is initiated by the underplating at Moho depths of a portion of the continental crust. (2) A corrosion in crustal strength follows the upward migration of fluids from the area of recent underplating. (3) As a weakened central zone deforms in response to tectonic plate stress, stresses are concentrated in the surrounding rigid crust. (4) A major earthquake occurs when the stress surrounding the weakened core exceeds the crustal strength, either because the concentrated stresses are anomalously high or because the dispersing fluids have spread beyond the core. (5) The final phase in the occurrence of a major intraplate earthquake is extended aftershock activity concentrated on the fault plane of the main event. The occurrence of a major intraplate earthquake as described above releases the strain energy in a perturbed area. Additional major events would not occur there again until the strength has recovered sufficiently for a repeat of the cycle.

Presented at the American Geophysical Union, Spring Meeting, Baltimore, Maryland, May 16, 1988.

PARADIGM FOR MAJOR INTRAPLATE EARTHQUAKES

LONG, L. T., Georgia Institute of Technology, School of Geophysical Sciences, Atlanta, Georgia, 30332.

Let us discard the traditional paradigms of continental seismicity. Let us assume, instead, that the seismicity associated with a major (magnitude 6 or larger) intraplate earthquake is a transient phenomenon triggered by a perturbation in the fluid and thermal regime of the lower crust. Regional plate stress may still provide the energy, but instead of high stress triggering an event, let us assume a decrease in crustal strength in the vicinity of the major earthquake. The timing of a major earthquake and the characteristics of the associated seismicity may be described by a sequence of five phases: (1) initiation, (2) strength corrosion, (3) stress concentration, (4) failure, and (5) crustal healing. (1) A major intraplate earthquake is initiated by the under-plating at Moho depths of a portion of the continental crust. (2) A corrosion in crustal strength follows the upward migration of fluids from the area of recent underplating. (3) As a weakened central zone deforms in response to tectonic plate stress, stresses are concentrated in the surrounding rigid crust. (4) A major earthquake occurs when the stress surrounding the weakened core exceeds the crustal strength, either because the concentrated stresses are anomalously high or because the dispersing fluids have spread beyond the core. (5) The final phase in the occurrence of a major intraplate earthquake is extended aftershock activity which is concentrated on the fault plane of the main event. The occurrence of a major intraplate earthquake as described above releases the strain energy in a perturbed area. Additional major events would not occur there again until the strength has recovered sufficiently for a repeat of the cycle.

Presented at the National Workshop on Seismogenesis in the Eastern United States, University of Illinois at Urbana-Champaign, Urbana, Illinois, April 12, 1988.

ZONES OF INDUCED SEISMICITY DEFINED BY ROCK QUALITY

SORLIEN, C. C., LONG, L. T., Georgia Institute of Technology, Atlanta, Georgia, 30332, and SCHMITT, T. J., Georgia Geologic Survey, 19 Dr. Martin Luther Dr., Atlanta, Georgia 30334.

Preliminary measurements of fracture density and rock quality have shown a relation with reservoir induced seismicity. Fracture density maps have been made at Clarks Hill Reservoir. The results show that areas of higher joint spacing correspond to zones of induced seismicity. Also, in other reservoirs, the rock type typically described as granite gneiss has shown a spatial correlation with reservoir induced seismicity. In reservoir induced seismicity, earthquakes occur by failure on pre-existing joints. Hypocentral depths of these earthquakes are typically less than 1 km, and it has been demonstrated that fracture density is not strongly dependent on depth in the first km. Therefore quantitative surface measurements of rock quality (which includes fracture density) can be extrapolated to the zone of induced earthquake nucleation. In contrast, stress may be released through creep on (foliated) schists and altered mafic rocks, explaining the lack of seismicity in those rock types. A complementary measurement of slickenside data can usually be collected on the same outcrops. Very fine scratches, and fresh slickensides in saprolite are both assumed to be related to the recent stress field. The striation data is then inverted for the local and regional stress field at time of movement. In this manner, rock quality measurements can be used to predict susceptibility to induced or natural shallow seismicity, so that important facilities can be properly sited and engineered.

Presented at the Association of Engineering Geologists, 30th Annual Meeting, Atlanta, Georgia, October 8-13, 1987.

FOCAL MECHANISM SOLUTIONS FOR NORTH GEORGIA AND SOUTHEASTERN TENNESSEE EARTHQUAKES (1982-1987).

ZELT, K.-H., and LONG, L. T., School of Geophysical Sciences, Georgia Institute of Technology, Atlanta, GA 30332-0340.

Seventy-one earthquakes recorded on the Georgia Tech Seismic Network and adjacent stations operated by the Tennessee Valley Authority and the Tennessee Earthquake Information Center were investigated to determine focal mechanism solutions. These events occurred during the period between January 1982 and December 1986 and have epicenters in North Georgia and southeastern Tennessee. First motion data and SV/P amplitude ratios were used to determine 36 single event and two composite focal mechanism solutions. The composite solutions were determined using data of two earthquakes. The solutions include four previously published focal mechanism solutions (Teague et al., 1984). The duration magnitude ranged from 0.7 to 3.8. Focal mechanism solutions of nine events could not be restricted to a unique domain. Including both unique and multiple domain solutions the results are divided into three categories of focal mechanism solutions: Twenty-two strike-slip, nine reverse and 18 normal. Twenty of the 38 earthquakes have data coverage over all four quadrants, 17 over three quadrants and one focal mechanism solution was determined from data coverage over two quadrants. The average depth of earthquakes investi-

gated equals 17.68 kilometers. The percent of the nodal planes that strike north-south is 59, 44.5, 27.7 and for those that strike northwest 41, 55.5, 61 for strike-slip, reverse and normal focal mechanism solutions respectively, The strike-slip, reverse and normal focal mechanism solutions have average depths of 18.4, 15.3 and 17.9 kilometers respectively.

Published as [(abs.) Seism. Res. Lettrs., Vol. 58, No. 4, 1987, p. 106]

Presented at the 59th Annual Meeting Eastern Section, Seismological Society of America, St. Louis University, St. Louis, Missouri, October 7-9, 1987.

A FINITE DIFFERENCE STUDY OF THE EFFECT OF AN OVERTHRUST ON THE PROPAGATION OF SEISMIC WAVES.

LIOW, J.-S. and LONG, L.T., School of Geophysical Sciences, Georgia Institute of Technology, Atlanta, GA 30332

A two-dimensional finite difference technique was developed to study the effect of an overthrust on the propagation of seismic waves. The structural model consists of a 3.5 km thick sedimentary layer over a crystalline basement. The P-wave velocity of the sedimentary layer and the basement are 4.5 km/s and 6.15 km/s respectively. A wedge-shaped overthrust zone with P-wave velocity of 6.05 km/s replaces part of the sedimentary layer on one side of the model. Synthetic seismograms are generated for a compressional line source at depths of 0.5 km and 7.0 km. The amplitude variation with distance of different phases are compared for waves traveling from the opposite direction. For a source at shallow depth, the existence of the high-velocity overthrust zone causes a more rapid decay of the amplitude of the direct wave. However, the overthrust zone does not affect the P and S reflections from the bottom of the sediments and the Rayleigh waves as strongly as it affects the direct wave. The amplitude of the secondary phases increase on traveling from the overthrust zone into the sediments. For the deeper source, the existence of the overthrust zone does not significantly affect the amplitude decay of either the direct wave or the other phases. For the deep source underneath the overthrust zone, the amplitude of the direct wave observed in the sediments within a short distance from the edge of the overthrust zone is enlarged by a factor of three. Also, more scattered phases are observed in the sediments.

Published as [(abs.) Seism. Res. Lettrs., Vol, 58, No. 4, 1987, p. 100]

Presented at the 59th Annual Meeting, Eastern Section, Seismological Society of America, St. Louis University, St. Louis, Missouri, October 7-9, 1987.

A TECHNIQUE FOR THE INVERSION OF CODA Q

LONG, L. T., LIOW, J.-S., School of Geophysical Sciences, Georgia Institute of Technology, Atlanta, Georgia 30332 and JONES, F. B., Georgia Southwestern, Department of Physics, Americus, Georgia 31709

Digital data from station CBT in southeastern Tennessee provide estimates of

coda Q with variations which depend on the direction to the earthquake. We interpreted this azimuthal variation to indicate a spatial variation of the properties of the crust that determine coda Q. Coda Q is a phenomenological parameter characterizing coda decay and it is determined by the integrated effects of crustal parameters in the ellipsoidal volume of crust with the recording station and hypocenter as foci. Zones of anomalous crust will influence the computation of coda Q differently for different station and hypocenter pairs. Through a sequence of approximations, we have linearized the relation between the measured apparent coda Q and an assumed constant coda Q for discrete zones of crust. Inversion of coda Q data from regional stations in the southeastern United States suggests a reduction in coda Q as one nears the coastal plane, consistent with the results of Singh and Herrmann (1983). Inversion of coda Q data near station CBT suggests an anomalously low coda Q region (Q=38) in a 300 square kilometer region northeast of station CBT.

Published as [(abs.) Seis. Res. Lettrs., Vol. 58, No. 4, 1987, p. 101]

Presented at the 59th Annual Meeting, Eastern Section, Seismological Society of America, St. Louis University, St. Louis, Missouri, October 7-9, 1987.

A Master's thesis by Jeff Ogilvie was completed on the generation of seismic coda and on the inversion of seismic coda for structure in the earth's crust.

Results of topical studies

Four topical studies achieved notable conclusions or were completed during the reporting period of July 1986 to June 1987. The principal conclusions are summarized below and presented in detail in Appendices A-D.

Appendix A summarizes the results of focal mechanism studies. First motion data and SV/P amplitude ratios were used to determine 36 single event and two composite focal mechanism solutions for earthquakes in southeastern Tennessee. The dominant focal mechanism is strike slip; however, the focal mechanisms exhibited components of reverse and normal fault movement. Estimates of solution confidence suggest that the variation in focal mechanism is significant. The unique and new approach of this analysis, which includes improved hypocentral precision, is the use of statistical parameters to quantify the confidence level of focal mechanism solutions. The confidence levels allow a rational comparison of focal mechanism solutions of differing quality with models of stress in the crust. For an individual event the distribution of first motions was quantified by the random probability factor, a measure of randomness of the distribution of take-off points. The quality of first motions was quantified by confidence levels which were assigned by the interpreter to each reading and which were adjusted by a consideration of adjacent points. The quality of the fit of the focal mechanism solution was quantified by a confidence measure which was computed for the fit of the data to a focal mechanism solution by using a Chi-Square distribution test developed specifically for polarity data.

Appendix B describes the initial development of a technique to find regional variations in Coda Q. Coda Q is determined by the integrated effects of crustal parameters in the ellipsoidal volume of crust with the recording station and hypocenter as foci. Zones of anomalous crust will influence the computation of coda Q differently for different station and hypocenter pairs. We have linearized the relation between the measured apparent coda Q and an assumed constant coda Q for discrete zones of crust. Inversion of coda Q data near station CBT suggests an anomalously low coda Q region ($Q=50$) in a 300 kilometer region northeast of station CBT.

Appendix C gives the results of the analysis of field data on joint systems obtained in the seismic zone of the Clarks Hill Reservoir. Fracture density was mapped in an area of induced seismicity in the Clarks Hill Reservoir area in sufficient detail to allow contouring of the data. These contours suggest that areas of higher joint spacing correspond to zones of induced seismicity. The rock type typically described as granite gneiss has shown a spatial correlation with reservoir induced seismicity in this and other seismic reservoirs. Earthquakes tend to occur where jointing is sparse and the rock is strong. In contrast, seismic activity is not often observed in foliated schists and altered mafic rocks, in which stress may be released through creep or failure along the many foliations and fractures.

Appendix D gives the results of relocating earthquakes in the Lake Sinclair Area. Earthquakes in the Lake Sinclair Reservoir area were relocated using a technique in which the origin time was computed independent of the location. The location residuals improved substantially with a velocity model which includes an abnormally high (6.6 km/s) crustal velocity at 2.0 km depth. The relocated activity suggests clustering of seismicity in five distinct zones.

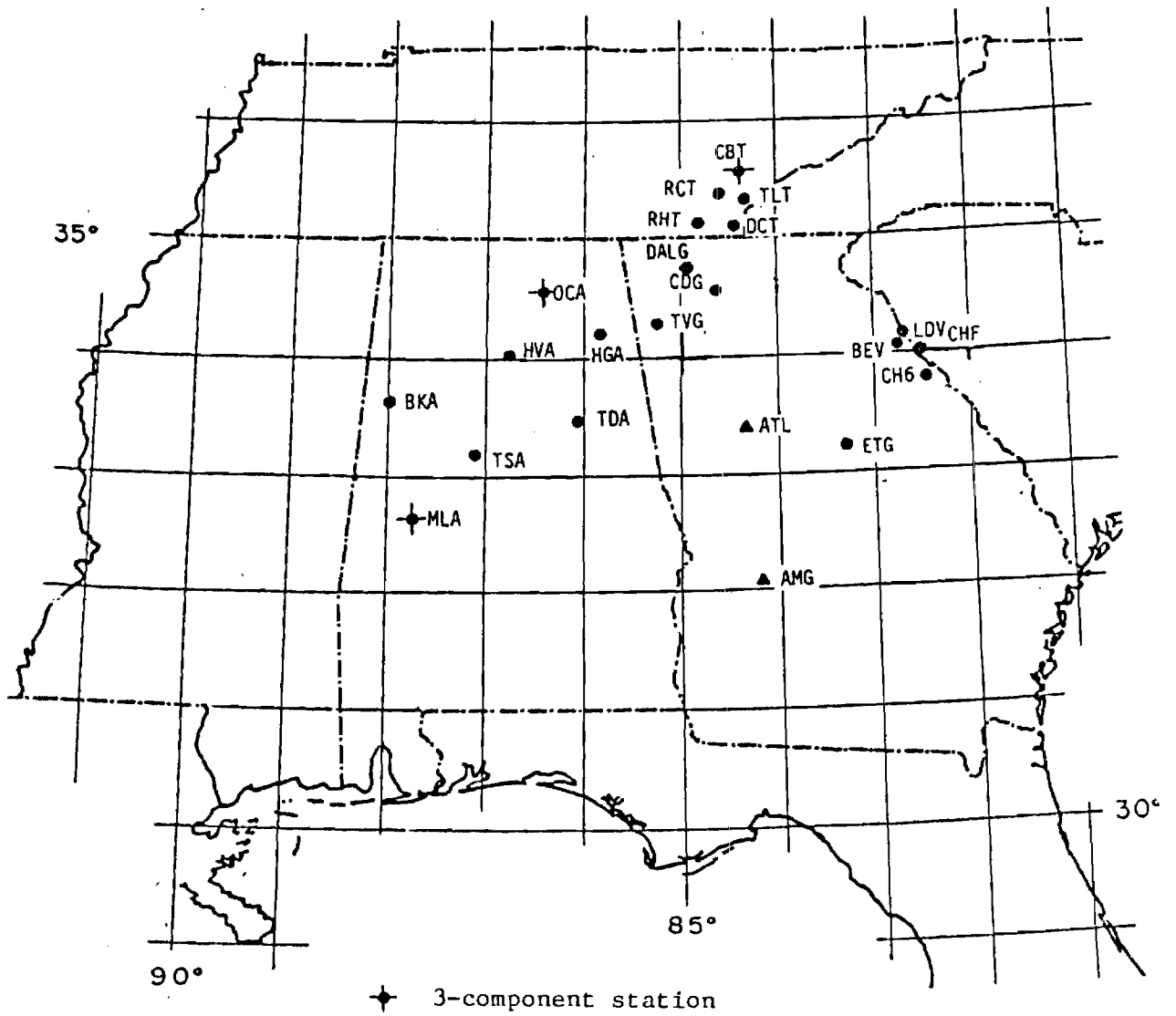


Figure 1. Distribution of seismic stations recorded during the period of 1 July, 1987 to 30 June, 1988.

MAGNITUDE ≥ 3

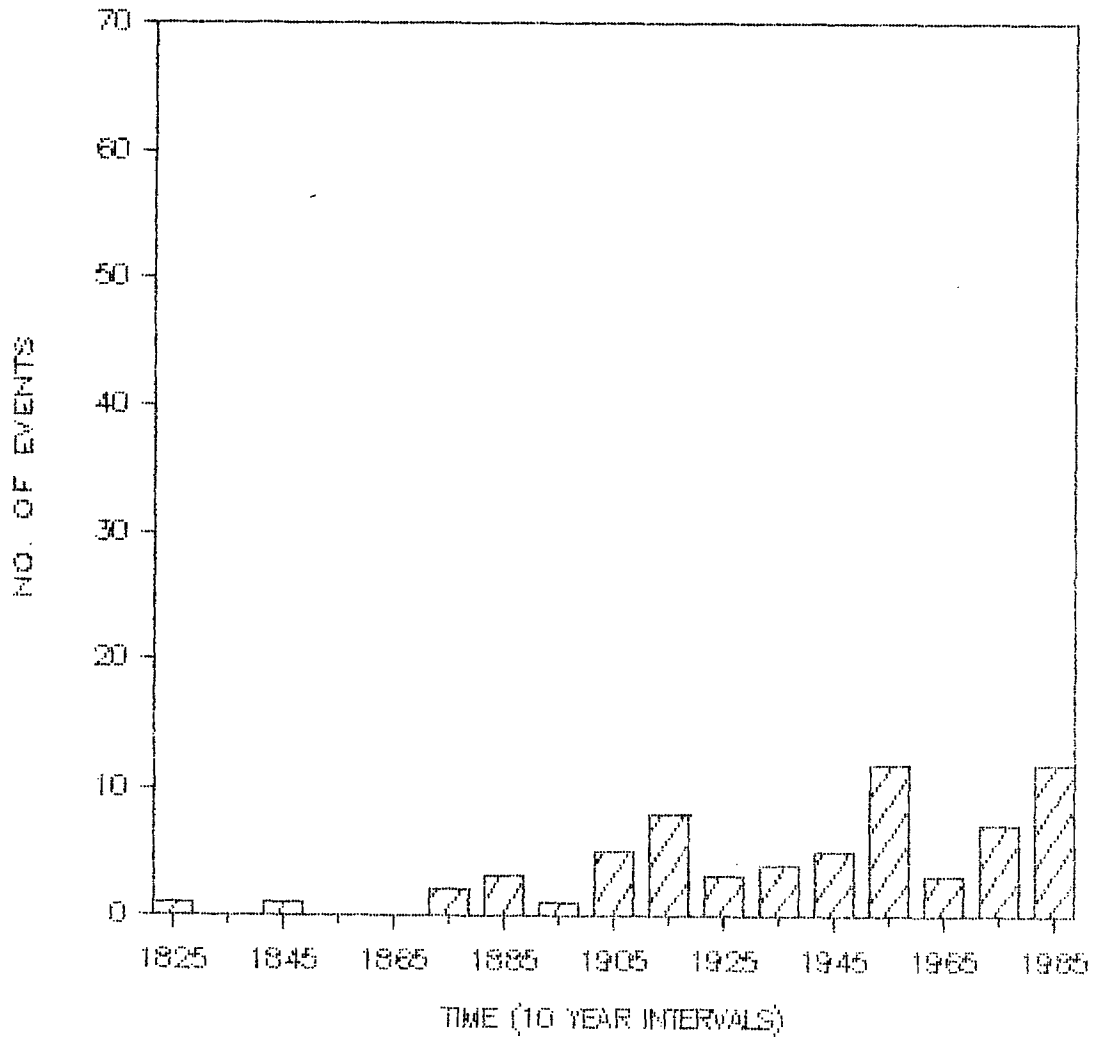


Figure 2. Frequency of occurrence of events with magnitude greater than three. The number of events is for ten year periods in southeastern Tennessee.

MAGNITUDE ≥ 4

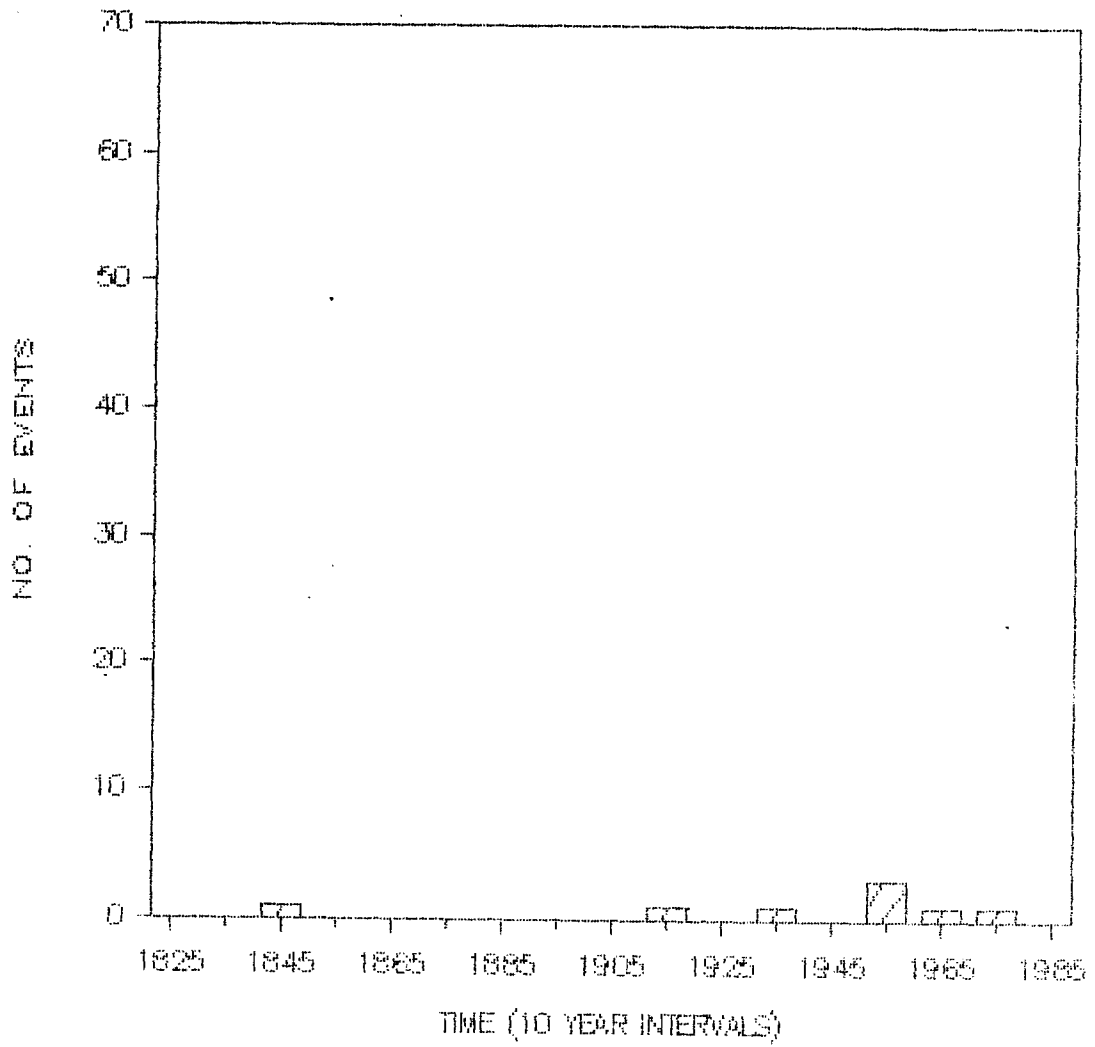


Figure 3. Frequency of occurrence of events with magnitude greater than four. The number of events is for ten year periods in southeastern Tennessee.

STRAIN RELEASE

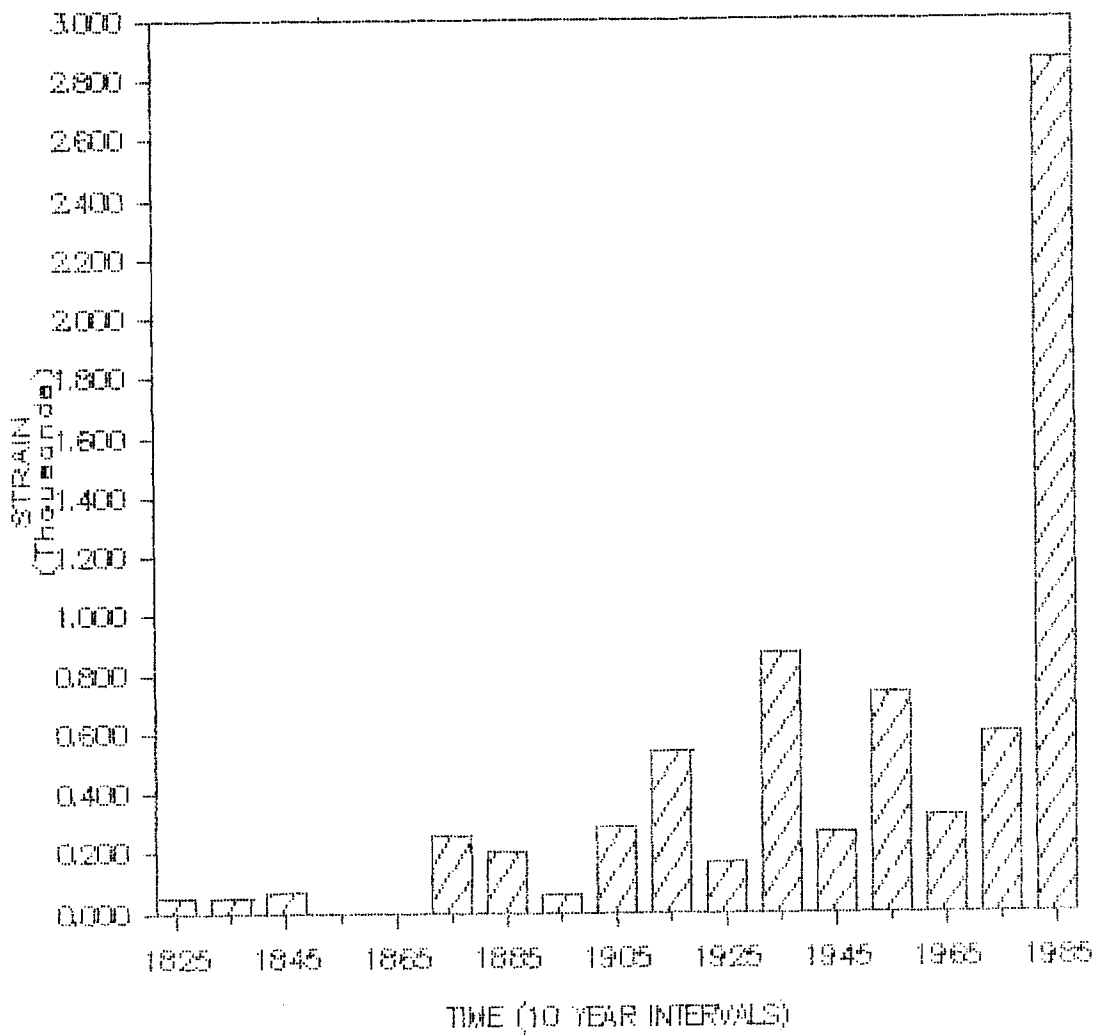


Figure 4. Strain release in ten year increments for recorded seismicity in southeastern Tennessee.

ENERGY RELEASE

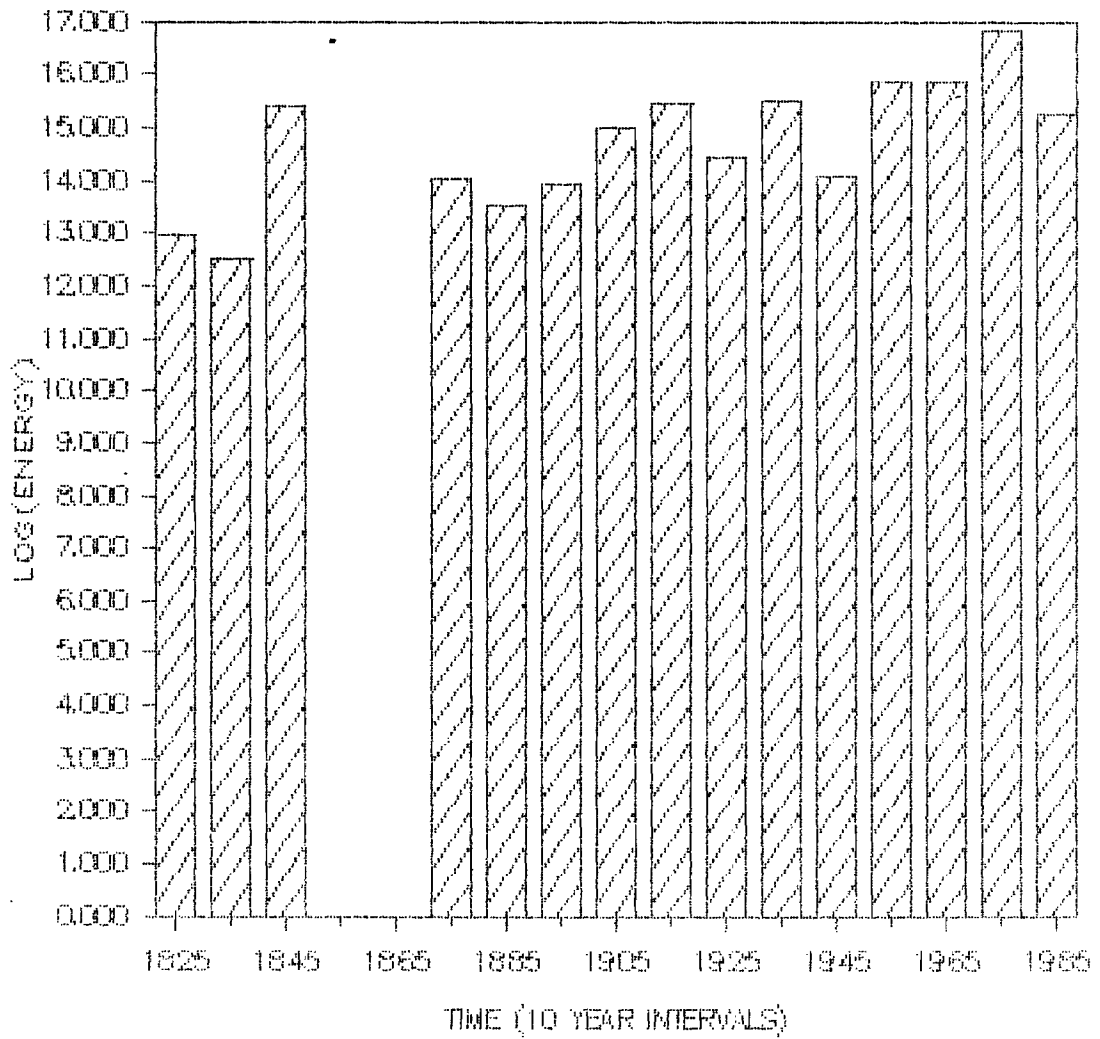


Figure 5. Energy release in ten year increments for southeastern Tennessee computed from magnitude.

Sta.	JUL-SEP	OCT-DEC	JAN-MAR	APR-JUN

ALABAMA				
OCAZ	XXXXXXXX-----	-----	-----	-----
OCAN	XXXXXXXX-----	-----	-----	-----
OCAE	XXXXXXXX-----	-----	-----	-----
HGA	-----XXX---	----X-		-----X-
HVA	XXXXXXXX--X-X	XXXXX--XXXXX	XXXXXXXXXXXXX--	--XXXX-----
TDA	-----X--	-----	-----	-----X
TSA	XXX-XX--XX-	XXXX-----	-----	-X-----
BKA	-----X--XXX	-----	-----	-XXXX-----
MLAZ	-----XXX	-----	---X-	-----
MLAN	-----XXX	-----	---X-	-----
MLAE	-----XXX	-----	---X-	-----

SOUTHEASTERN TENNESSEE				
CBTZ	-----XX-	-----	-----	-----
CBTN	-----XX-	-----	-----	-----
CBTE	-----XX-	-----	-----	-----
RCT	-----	XX-----	-----	-----X
RHT	-----XXXX	XX-----	-----	-----
TLT	XXXXXXXXXX-XXX	-----XXX	XXX-X-	-----
DCT	-----XX-	-----	-----	-----X

GEORGIA				
TVG	-XX-----	-----	-----XXX-	--XXXXXXXXXX
DALG	X-----X	-----	-X-----	XXXXXXXXXX-X
CDG	-----XXXX	-----	-----	-----
ATL	-X-XXXX-	-----	--XX-----	X----XX---
ETG	XX-XX--XXXX	-X-XXXX-	-----	-----
CH6	-XXXXXXXXXXXXX	XXXXXX----	XXXXXXXXXXXXXXX	XXXXXXXXXXXXX
CHF	XXXXXXXXXXXXX	XX-----XXX	XX-XXXXXXXXXXXXX	-XXXXXXXXXXXXX
LDV	X-X-XXXXXXXXXX	XXX-XX-	-----	-X----XXXXX
BEV	XXXXX-	-----	--XXX-	-----XXXXX

"-" = Station Operating
X = Station Down

Figure 6. Graphical representation of the operational status of the Georgia/Alabama Seismographic Network.

APPENDIX A

Pattern of Earthquake Focal Mechanisms
in Southeastern Tennessee

APPENDIX A

PATTERN OF EARTHQUAKE FOCAL MECHANISMS IN SOUTHEASTERN TENNESSEE

Karl-Heinz Zelt and Leland T. Long

ABSTRACT: In southeastern Tennessee earthquakes are located in a diffused pattern and cannot be associated with a single distinct linear structure. We have extended the data set of 14 published focal mechanism solutions for the period of 1977 to 1984 with 43 focal mechanism solutions for the period 1982 to 1987. In this study earthquake locations were computed by a method that uses the S-P times to isolate the origin time computation from the location computation. A statistical treatment of the distribution of first motions on the focal sphere is used to establish a measure of confidence for the focal mechanism solution of the smaller events in southeastern Tennessee. The majority of events with magnitude greater than three occur near the center of southeastern Tennessee activity and have a strike-slip mechanism with predominantly north striking nodal planes. Outside the central zone, smaller events which may be recorded on only a few stations show a spatial distribution of normal or reverse components in the predominant strike-slip component. The validity of the spatial distribution is investigated using a statistical treatment as a measure of confidence in each focal mechanism solution.

INTRODUCTION

As of 1985, earthquake focal mechanism solutions had been published for 14 earthquakes in southeastern Tennessee and northern Georgia (see Table 1 for published focal mechanism solutions). The Maryville, Tennessee, earthquake of 30 November 1973 provided the first estimate of the principle stress directions; however, the results were ambiguous. Bollinger *et al.* (1976) with regional P-wave first motions determined two equally possible solutions: normal faulting on either a northeast or a southeast striking nodal plane or reverse faulting with northwest striking nodal planes. First motion data obtained during the aftershock survey suggested a strike-slip or horizontal thrust motion incompatible with the solution for the main shock. Herrmann (1979) using surface waves obtained a solution with predominantly strike-slip faulting on north-northeast or east-southeast striking nodal planes for the Maryville event. Guinn (1980) and Guinn and Long (1977) introduced the concept of domains of valid P, T and B axes as a means of evaluating focal mechanism solutions in cases of limited data. The domains of valid principle axes for first motions for the 30 November 1973 Maryville earthquake contained both focal mechanism solutions published by Bollinger *et al.* (1976). In condition, Guinn (1980) found domains of valid P, T and B axes suggesting reverse fault movement with northwest striking nodal planes for both the 4 February 1976 Conasauga, and the 27 July 1977 Englewood, Tennessee, earthquake. Reinbold and Cornwell (1983) using first motion data determined a composite solution suggesting strike-slip fault motion with a north-northeast and a nominally east striking nodal plane for the Greenback, Tennessee, earthquakes on 24 September 1982.

The first analysis of focal mechanisms from data recorded through 1983 by a regional network installed in 1980 (Teague, 1984) found 11 single event and 11 composite focal mechanism solutions. The Teague *et al.* (1986) analysis used the technique of Guinn and Long (1977) as extended by Tzeng (1982) to include both first motions and SV/P amplitude ratios and as rewritten in program FOCMEC by Snoke *et al.* (1984). The dominant focal mechanism solution obtained by Teague *et al.* (1986) was strike-slip with north or east striking nodal planes. Many of Teague's (1984) results are based on data sets of less than 10 points and thus the domains of valid principle axes can be large. Johnston *et al.* (1985) extended the focal mechanisms from the seismic network data through 1984 to include a focal mechanism solution for the 14 February 1984 earthquake occurring north of Knoxville near Mascot, Tennessee. This well-constrained solution was strike-slip on a north or east striking nodal plane. The focal mechanism solutions are shown in Figure 1.

The total of 14 published focal mechanism solutions did not suggest that a single type of focal mechanism would apply to all southeastern Tennessee and northern Georgia earthquakes; however, for all of the 14 solutions the principle compressive stress direction strikes northeast. Focal mechanism solutions range from pure strike-slip to events with large components of reverse or normal fault movement (see Figure 1). Nine of the 14 solutions were composite solutions because the single events had usable arrivals at less than 10 stations which were distributed so as to require additional data from nearby events to limit the size of the domains of valid principle axes. In addition to sparse data, uncertainty in depth of focus could contribute to the uncertainty in direction of the principle axes. Johnston *et al.* (1985) discussed the issue of hypocentral depth for earthquakes in southeastern Tennessee and concluded that the most critical factor in depth determination is distance to the nearest recording station. They found that only 57 percent of 101 events satisfied this criteria for reliable depth computation. Eight of the 14 events for which focal mechanisms were presented satisfied the criteria for reliable depth estimate.

In this study we present 43 new or reinterpreted focal mechanism solutions. Within the central seismic zone (see inset, Figure 1), the number of focal mechanism solutions is increased from 10 to 24, allowing interpretation of the spatial distribution of focal mechanisms. The earthquakes were located using a velocity gradient model (Propp, 1985) and a fixed origin time (Long *et al.*, 1986). The gradient velocity model and fixed origin time provides a ± 5 kilometer confidence in the depths of earthquakes in southeastern Tennessee and northern Georgia with the existing seismic array. The individual focal mechanism data sets were evaluated for randomness of distribution on the focal sphere. This unique test was used to qualify the sampling of the focal sphere as determined by the location of seismic monitoring stations and the hypocenter of the event. Each first motion reading was assigned a confidence value expressing the estimated probability that the reading is correct. This confidence value was then adjusted, according to the distribution of polarities of adjacent data points. Focal mechanism solutions were then found using the adjusted or conditional probability values as a measure of consistency with a possible solution. A centroid solution is obtained from the domain of valid principle axes at a given confidence level. This centroid solution is then used to compute a Chi-Square estimate of confidence in the focal mechanism.

RELOCATION OF EARTHQUAKES

The linear dependence of origin time and depth is a well known problem in using P-wave data to locate earthquakes recorded at a few unevenly distributed stations. In this study, earthquake locations were computed by a method that uses the S-P times to isolate the origin time computation from the location computation. The method requires only a constant Poisson's ratio. The origin time is first fixed on the basis of the S-P times. Anomalous readings are corrected in the process and the epicenter is found by the traditional iterative least squares method of Geiger (1910). Then the epicenter is held constant and the depth is found by the iterative least squares method. The epicenter and depth are obtained alternately until convergence to a solution is achieved. The distributed method has two advantages; first, computation of the origin time, epicenter and depth are uncoupled, and second, separate weights can be used for epicenter and depth computations (Liow *et al.*, 1985). A weighting scheme which combines the reading accuracy and the scatter in the P- and S-wave arrivals in the Southern Appalachian area is taken into consideration while finding the epicenter and depth. An additional distance weight is incorporated into the weights for the depth computation since only stations within a distance comparable to the focal depth can realistically constrain the depth (Johnston *et al.*, 1985).

A gradient velocity crustal model is used in order to compute the theoretical travel times. Recent seismic refraction data (Propes, 1985) indicate that one gradient velocity model will satisfy variations in apparent velocity observed in the granitic crust of the southeastern United States. The model simultaneously satisfies the observed 6.05 km/s P-wave velocity of the Georgia Piedmont, the 6.14 km/s velocity of central Alabama and a 6.2 km/s velocity observed for the 10 kilometer deep North Georgia earthquake of October 9, 1984 (Long *et al.*, 1986). Figure 2 compares the observed crustal refraction velocities and velocity gradients as a function of depth. The data suggest that the crust can be modelled by a constant velocity gradient from 5.95 km/s at the surface to 6.3 km/s at 15 kilometer depth. A velocity of 6.7 km/s could exist below 15 kilometer. Velocity structure below 20 km is not needed for the relocation of these events. The greatest variation in velocity exists near the surface and can be related to variations from mafic to sedimentary structural units. A 6.5 km/s rock unit could exist in the remnants of a rift zone in eastern Tennessee centered north-northeast of the central active zone. The Paleozoic sediments in Tennessee and Alabama for simplicity were assumed to satisfy a velocity gradient from 5.5 km/s to 5.7 km/s in the top two kilometers. However, the sediments in some areas may extend to depths of 6 km and in other areas the velocity could be as low as 4.5 km/s. An area of 6 by 7 kilometers in a zone northwest of seismic station CBT provided measurable velocity delays of 0.1 to 0.2 seconds (Tie, 1986) which were corrected for in the relocation of all events.

STATISTICAL EVALUATION OF FOCAL MECHANISMS

Focal mechanism solutions generally assume a random distribution of data coverage over the focal sphere. Non-random distributions can affect the solution. For the distribution of first motion readings and their amplitudes the focal sphere is a continuous function. The pattern of available

observation on the focal sphere are dependent on the location of seismicity and terrain available for installation of seismic stations. Subsequently, the distribution of points is dependent on many factors and neither uniform nor random. Although the occurrence of a non-random distribution can be demonstrated, the significance of differences in the pattern of two or more populations is hard to evaluate. The distance between nearest neighbors, first used by Dice (1952), measures the departure from randomness. Clark and Evans (1954) used the distance between nearest neighbors to define randomness as a spatial concept, providing the possibility of searching for randomness in sub-populations or smaller areas of interest. The distance between nearest neighbors is applied in this study. If

$$R_A = \frac{\sum_{n=1}^n r_n}{N} \quad (1)$$

where R_A = mean of the series of distances to nearest neighbor

r_n = distance to nearest neighbor

N = total number of points

and

$$R_E = \frac{1}{\sqrt{2\rho}} \quad (2)$$

where R_E = mean distance to the nearest neighbor expected in an infinity large random distribution of density ρ

ρ = density (points/ km²)

then

$$R = \frac{R_A}{R_E} \quad (3)$$

is a measure of the degree to which the observed distribution departs from random expectation with respect to the distance to the nearest neighbor. Subsequently, for a random distribution, $R = 1$, for a maximum aggregation $R = 0$, where all the data occupy the same locus and for a perfectly uniform data set $R = 2.1491$, where all the data are equidistant from each other. The random probability factor can be interpreted as a measure of expected deviation from randomness. For instance, for a R value of 0.5, on the average, the nearest neighbors are half as far apart as expected under conditions of randomness. Figure 3 shows the direct correspondence between the random probability factor and the conventional measure of station coverage, the maximum azimuthal gap. It can be seen that as the maximum azimuthal gap decreases and the data trends towards maximum aggregation, the

value of the random probability factor trends towards zero. Also, the maximum azimuthal gap increases with increasing random probability factor. Data sets with no regularity in azimuthal spacing tend to have one or two large (greater than 90 degrees) azimuthal gaps and their associated random probability factor values are scattered.

Each individual data point in this study was assigned a confidence value following the criteria listed in Table 2. In addition, these user-assigned confidence values are modified by a conditional probability based on consistency with neighboring points. For each data point, the nearest data are tested for similarity of polarity, resulting in a lower adjusted probability if data of different polarity are nearby, a higher adjusted probability value if data nearby is of the same polarity and a constant value if no data are nearby. In the case of an obvious inconsistency of a low user confidence value surrounded by first motions of opposite polarity, the confidence value can be changed to a value less than 0.5 (random) by this consistency test. Nearest neighbors are determined by searching a circular area with a 10 degree radius around the point tested. If no points are found within this area, the radius is increased by 10 degrees. Beyond a circular radius of 30 degrees the data point tested is considered independent and no adjustments to the confidence value is made.

Focal mechanism solutions are found using the search technique on the focal sphere and using cumulative probability as criteria for valid solutions instead of the number of correct points as used by Guinn and Long (1977), Tzeng (1982) and Snoke (1984). The computational details using cumulative probability to determine a focal mechanism solution area s follows. All assigned probabilities of the polarity data are changed so that all polarities are considered compressive. The mean probability for both polarities and SV/P amplitude ratios is used as a threshold value. If a polarity fits the stress axes orientation tested then a cumulative probability value is incremented by the polarity's probability value. If the cumulative value for all p9olarity data is greater than the threshold value a solution has been found. the SV/P amplitude ratios the probability value is the measure of deviation from the theoretical SV/P amplitude ratio value and a separate cumulative probability value is found. If both the polarity and the SV/P amplitude ratio threshold value is exceeded a valid solution has been found.

Once the domain of the pressure and the tension axes are known, the centroid solution is found and the distribution of data points is evaluated with respect to that solution using the Chi-Square test (Sachs, 1982). The Chi-Square distribution is expressed as (Sachs, 1982, page 139, equation 1.130)

$$\chi^2 = (n-1) \frac{s^2}{\sigma^2} \tag{4}$$

where s^2 - variance of random sample data set

σ^2 - variance of parent data set (theoretical)

By definition,

$$s^2 = \frac{1}{(n-1)} \Sigma(x_i - \mu)^2 \quad (5)$$

where x_i = probability values

μ = mean of probabilities

The probability data are adjusted to provide only two distinct cases for evaluation; -1, compressive or -1, dilatational. Therefore the mean of observed polarities from the estimates of conditional probability is the probability value, if compressive, multiplied by n cases minus the probability value, if dilatational, multiplied by n cases and this value divided by n cases, or

$$\mu = \frac{x_i n - (1-x_i)n}{n} = 2x_i - 1 \quad (6)$$

Assuming that each probability value was derived from a large number of readings

$$s^2 = \frac{1}{(n-1)} (\rho_1^2 + \dots + \rho_i^2 + \dots + \rho_n^2) \quad (7)$$

where $\rho_i^2 = \frac{1}{k} \Sigma(x_i - \mu)^2$

$$= \frac{1}{k} (kx_i(1-\mu)^2 + k(1-x_i)(-1-\mu)^2)$$

$$= 4(1-x_i)x_i$$

Thus, $s^2 = \frac{1}{(n-1)} \Sigma 4(1-x_i)x_i \quad (8)$

For the parent distribution

$$\sigma^s = \frac{1}{(n-1)} \sum (x_i - \mu)^2$$

$$= \frac{1}{(n-1)} \sum (\pm 1 - \mu)^2 = \frac{n}{(n-1)} \quad (9)$$

as $\mu = 0$ for all four quadrants. Therefore

$$\chi^2 = \frac{(n-1)}{n} \sum 4(1-x_i)x_i \quad (10)$$

To take care of adjusted probabilities less than random, i.e. < 0.5 ,

$$\rho_i^2 = 2 - 4(1-x_i)x_i \quad (11)$$

The complete function ρ^2 is plotted in Figure 4. Confidence levels for a focal mechanism solution are read from a χ^2 distribution table (Sachs, 1982, p. 140).

RESULTS

The distribution of the random probability factor for the earthquake data set (see Figure 5) indicates that the individual data sets are all nearly random, as the distribution is centered around $R=1$. The distribution of the random probability factor is dependent on the number of data points per data set. Large data sets have lower values of R or maximum aggregation, whereas smaller data sets show more uniformity. This is indicated in Figure 6. The random probability factor also shows no dependence on duration magnitude of the events. Earthquakes greater or smaller than duration magnitude 2.75 show a broad range of values of R , centered around $R=1$. For all determined values of R , see Table 3.

The Chi-Square distributions were transformed to significance (or confidence values) using statistical tables (Sachs, 1982). The resulting values are listed in Table 3. Confidence values were determined for polarity data, SV/P amplitude ratio data and all data separately. The results are shown in Figure 7a through 7c. In each of these figures, the data are further separated into earthquakes greater or less than duration magnitude 2.75. The confidence values are not different when comparing small and large magnitude earthquakes for all three cases. In general, confidence values range from 0.4 to 0.99, with the majority between 0.75 and 0.99. Also, confidence values are higher for polarity data only compared to SV/P amplitude ratio data only. Confidence values show no correlation with the number of data points per data set. For both data points greater or less than 10, the range of confidence values is from about 0.5 to 0.99.

We examined 77 events between January 1982 and August 1987 to determine focal mechanism solutions. The directions of first motions and SV/P amplitude

ratios were used to determine 41 single event and two composite focal mechanism solutions for earthquakes in southeastern Tennessee and northern Georgia. The composite solutions were determined using data of two earthquakes. The solutions include reinterpretation of four of the 11 single event focal mechanisms determined by Teague et al. (1986). All four events have consistent P-axis trends when compared with Teague et al.,'s (1984) results, which are all strike-slip solutions. Only one result is different in that our data analysis also allows a normal component. These events were detected by all three major seismic networks in the southeastern Tennessee area (Georgia Tech Seismic Network, Tennessee Valley Authority Seismic Network and the Center for Earthquake Research and Information Seismic Network) between 1982 and 1987. The dates, epicenter location, duration magnitude, depth and origin time are listed in Table 3. Figure 8 shows the location of the earthquakes and their depths along a northeast profile.

The 43 solutions can be divided into three categories which are listed in Table 4. Twentyfour solutions could be considered pure strike-slip, six strike-slip with a normal or reverse component, six normal, two normal with strike-slip component and five reverse with strike-slip component. The average depth for all events is 16.9 ± 4.8 kilometers. The average depth for strike-slip fault earthquakes is 17.3 ± 4.6 kilometers. The normal fault earthquakes and reverse fault earthquakes had similar average depths of 15.9 ± 5.7 kilometers and 15.7 ± 3.1 kilometers respectively.

Pure strike-slip solutions are confined to three distinct areas: A central zone between 84.2W and 84.5W and 35.5N and 35.8N, a zone at Knoxville and a southern zone in northern Georgia (Long et al., 1986, and Zelt and Long, 1987). Earthquakes with normal and reverse components generally surround areas of strike-slip mechanisms.

The focal mechanism solutions were divided into different categories of quality. Each statistical parameter was divided into four quality categories, as shown in Table 5. The quality of a solution thus is ultimately derived from 12 different categories, the highest quality solution being defined by a (S1, R1, P1) quality combination and the lowest quality solution by a (S4, R4, P4) quality combination.

Figures 9a through 9k show our focal mechanism solutions. Their statistical qualifications in the form of the random probability factor, number of data points and significance are listed in Table 3. Each diagram shows the polarity readings, domains of the pressure, tension and null axes and the nodal planes of the central solution. Each of the solutions has its distinct character with respect to the performed statistical analysis.

Figure 9a shows a solution where $R = 0.982$, the number of data points = 35 and the significance value equals 0.99. Figure 9b shows a solution where $R = 1.09$, the number of data points = 16 and the significance value equals 0.96. The statistics indicate near-random, equally distributed data sets and therefore solutions of (S1, R1, P1) quality. Every statistical parameter evaluated provides a measure of confidence in the solution. Lack of data in one or two quadrants can result in non-random values of R and near-random (random equals 0.5) significance. Examples of this case are seen in Figure 9c and 9d, where the values of the random probability factor are 1.273 and 0.702

respectively. The solutions of Figure 9c and 9d are of (S2, R2, P2) quality. Figure 9e shows a solution where 11 out of 22 data points are SV/P amplitude ratios. In general, user assigned probabilities are lower for SV/P amplitude ratios than for polarities (see Table 3). Although the value of $R = 1.005$ (near random) the significance value is only 0.78 because of the abundance of SV/P amplitude ratios in the data set. The result is only a (S3, R1, P1) quality. Figure 9f and 9g are examples of focal mechanism solutions that are not strike-slip but rather normal and normal with a large strike-slip component respectively. The statistics for the solution of Figure 9f (Significance = 0.78, $R = 0.918$, number of data points = 13) and the solution of Figure 9g (Significance = 0.67, $R = 1.241$, number of data points = 14) indicate qualities of (S3, R1, P2) and (S4, R2, P2) respectively. This shows that focal mechanism solutions other than strike-slip with north striking nodal planes are possible solutions for southeastern Tennessee and northern Georgia earthquakes as some of the determined qualities are high, but such solutions may be ambiguous. Figure 9h shows a strike-slip solution found in southeastern Tennessee for 9 events. The nodal planes here trend northwest or northeast. The number of data points available for this solution equals only 8 and their distribution makes this a low quality solution of (S3, R2, P3). Figures 9i through 9k show more focal mechanism solutions of non-strike-slip character. The first two shows normal fault plane solutions, whereas the third shows a reverse fault plane solution with a strike-slip component. Significance values for all three events are rather low ($S = 0.68, 0.53$ and 0.66), resulting in qualities of (S4, R3, P3), (S4, R1, P2) and (S4, R1, P2).

Significance values and other statistical results show that not just strike-slip solutions are valid for southeastern Tennessee and northern Georgia, but that solutions with large normal and reverse components are acceptable.

Pure strike-slip solutions are confined to three distinct areas: A central zone between $84.2W$ and $84.5W$ and $35.5N$ and $35.8N$, a zone at Knoxville and a southern zone in northern Georgia (Long et al., 1986, and Zelt and Long, 1987). Earthquakes with normal and reverse components generally surround areas of strike-slip mechanism.

The focal mechanism solutions of the central zone of seismicity were used to investigate a possible regional pattern of characteristic stress release in earthquakes. Figure 10 shows a contoured map of the dip of the null-axis for the central seismic zone in southeastern Tennessee. Three distinct areas of near-vertical dip, corresponding to strike-slip regions are apparent. First, a central region centered at $35.55N$ and $84.35W$, second a region towards the east and third a region in the northwest of the study area. The central region is of greatest interest, because it is surrounded by regions of low B-axis dips, thus regions of normal and reverse components.

The following method was used to determine which of the low B-axis dip regions corresponds to a normal or a reverse fault component region. The dip of the tension axis was subtracted from the dip of the pressure axis for each solution. This results in a range of values from -90 to $+90$, where -90 corresponds to a pure reverse fault and $+90$ to a pure normal fault. Values close to zero correspond to strike-slip fault solutions. Figure 11 shows the result of this evaluation. All three non-strike-slip areas can still be

distinguished, but only the southwestern and southeastern zones surrounding the central zone show a large normal component. The northeastern zone is broken up into zones of either normal or reverse character.

DISCUSSION AND CONCLUSION

The random probability factor and significance values for each of the earthquake polarity and SV/P amplitude ratio data sets indicate no distinct difference in quality between small and large magnitude earthquakes. Both small and large magnitude earthquakes can have random and non-random R values and low and high significance values. It is important to note that a large magnitude earthquake ($M_D > 2.75$) usually has a large and well distributed data set (more than 15 data points), which in turn has significance values greater than 0.9 and near-random R values. Events with magnitudes less than 2.75 can have a large data set resulting in a near-random R and a high confidence value, but most of the time the data set is small, resulting especially in lower confidence values. A well-determined focal mechanism solution can therefore be classified as one with a data set consisting of more than 15 data points, near-random R and a significance value greater than 0.9. Throughout the examined data set the strike-slip solutions with north trending nodal planes exemplify this classification. Strike-slip solutions with normal or reverse components, considered anomalous focal mechanism solutions also exemplify this classification. Fifteen anomalous focal mechanism solutions indicate confidence values of less than 0.85 (see Table 3), R values not close to one and have data sets of less than 10 points. The results indicate that the statistical analysis provides an additional tool in the standard focal mechanism analysis (Guinn and Long, 1977; Tzeng, 1982; and Snoke *et al.*, 1984) and is a measure of confidence in each solution. The statistics enhance the interpretation of the stress regime in southeastern Tennessee and northern Georgia. Good results were obtained for solutions other than strike-slip solutions with north trending nodal planes. The anomalous seismic zone hypothesis can therefore not be discounted.

Three major areas where strike-slip mechanisms dominate in southeastern Tennessee have been delineated. They are the northern Georgia seismic zone, the Knoxville seismic zone and a central seismic zone centered around Madisonville. These three areas are also the zones of largest seismic activity, as can be seen in Figure 16 where all 296 relocated events within the southeastern United States that occurred between 1982 to 1987 are shown. The central seismic zone is surrounded by areas where focal mechanisms with normal or reverse components dominate. These areas gave less seismic activity. The northern Georgia seismic zone is connected with the central seismic zone by two seismic lineations trending northeast (see Figure 8). The mean depth of strike-slip events indicates that they generally occur at greater depths than the surrounding reverse or normal events.

The central zone corresponds to an area near a proposed Precambrian rift zone (McKeown, 1978). Shear wave reflections from the Moho (Liow and Long, 1985) and the time-term analysis of refraction data (Long and Liow, 1986) suggests a 5 to 10 kilometer deeper Moho in this zone when compared with the surrounding areas of southeastern Tennessee. A thickening of the crust is consistent with the regional gravity gradient (Winester, 1984). The average depth of strike-slip fault earthquakes in this zone of 17.29 kilometers

correlates with deeper Moho because the depth is deeper than the average depth of the surrounding events. This may suggest that the brittle ductile transition zone (BDT) is deeper in the central zone of seismicity. Bollinger et al. (1985) already have described a difference in depth of the BDT when comparing the Piedmont area with southeastern Tennessee. A further zoning of the BDT therefore is possible. The seismicity of the central zone has also been related to a possible zone of weakness in the lower crust (Long, 1988), where fluid injection from the upper mantle may be a further mechanism for seismicity in southeastern Tennessee and northern Georgia. The zone is also the area of greatest seismic activity in southeastern Tennessee.

Earthquakes with normal or reverse fault components generally surround the central zone of seismicity. Some of these events are located on the southern edge of the central seismic zone, which correlates to a northwest trending seismic boundary (see Figure 16). The nodal planes determined for these events strike north-northwest to northwest. McKeown (1978) relates different types of focal mechanisms in a region to the complex system of geologic discontinuities due to mafic intrusives which in turn could be responsible for local changes in the level of stress. Mareschall and Kuang (1986) have found high enough levels of stress due to topographic loading to accommodate seismicity in southeastern Tennessee and northern Georgia.

Long (1988) correlates the strike-slip focal mechanism solutions of the central zone with the surrounding normal or reverse focal mechanism solutions. Zones of weakness could explain areas of high density seismicity and the majority of strike-slip mechanisms within. Earthquakes with normal or reverse components could be explained by stress release on the edges of such a zone. Such events would subsequently be shallower as has been determined here. The two linear seismic features connecting the North Georgia seismic zone with the central seismic zone are similar to features described by Long's (1988) proposed model for major intraplate continental earthquakes.

In summary, the density of focal mechanism solutions for southeastern Tennessee and northern Georgia has been increased by 43 new or revised focal mechanism solutions. A statistical measure has been introduced to provide a measure of confidence in each solution. The derived spatial distribution of focal mechanism solutions indicates zones where strike-slip mechanisms dominate and surrounding zones of focal mechanism solutions with large normal or reverse components. The spatial distribution provides new speculation on the origin of seismicity in the southeastern Appalachian area and makes it clear that focal mechanism studies in this area should continue. Also, seismic modelling of the stress regime would be a future step in providing answers to the seismic origin of earthquakes in southeastern Tennessee and northern Georgia.

REFERENCES

- Bollinger, G.A., C.J. Langer and S.T. Harding, April 1976. The Eastern Tennessee Earthquake Sequence of October through December, 1973, BSSA, Vol. 66, No. 2., pp. 525-547.
- Bollinger, G.A., M.C. Chapman, M.S. Sibol and J.K. Costian, 1985. An analysis of earthquake focal depths in the southeastern U.S., Geophysical Research Letters, Vol. 12, No. 11, pp. 785-788.

- Clark, P.J. and F.C. Evans, 1954. Distance to Nearest Neighbor as a measure of spatial relationships in populations, Ecology, Vol. 35, No. 4, pp. 445-453.
- Dice, L.R., 1952. Measure of the spacing between individuals within a population, Contrib. Lab. Vert. Biol. Univ. Mich., 55, p. 1-23.
- Geiger, L., 1910. Herdbestimmung bei Erdbeben aus den Ankunftszeiten, K. Gesell. Wiss. Goettingen, 4, pp. 331-349.
- Guinn, S.A. and L.T. Long, 1977. A computer method for determination of valid focal mechanism solutions using P-wave first motions applied to southeastern United States earthquakes, Abstract, Earthquake Notes, Vol. 48, No. 3., p. 16.
- Guinn, S.A., June 1980. Earthquake Focal Mechanisms in the Southeastern United States, NUREG/CR-1503.
- Herrmann, R.G., July 1979. Surface wave focal mechanisms for Eastern North American Earthquakes with Tectonic Implications, Journal of Geophysical Research, Vol. 84, No. B7, pp. 3543-3552.
- Johnston, A.C., D.J. Reinbold and S.I. Brewer, 1985. Seismotectonics of the Southern Appalachians, BSSA, Vol. 75, pp. 291-312.
- Liow, J.-S, An Tie, L.T. Long, 1985. Earthquake Location: A Consideration of independent computation of origin time, epicenter and depth, Abstract, Earthquake Notes, Vol. 56, No. 3, p. 77.
- Liow, J.-S and L.T. Long, 1985. Analysis of reflections from the base of the crust in southeastern Tennessee, in Summary Report for contract GSA-80-3053. Geological Survey of Alabama; A Study of Seismicity and Earthquake hazard in northern Alabama and adjacent parts of Tennessee and Georgia, Georgia Institute of Technology, School of Geophysical Sciences, Atlanta, GA 30332, 16 pp.
- Long, L.T. and J.-S. Liow, 1986. Crustal Thickness, velocity structure, and the isostatic response function in the southern Appalachians, in Reflection Seismology: The Continental Crust, Geodynamics Series, Vol. 14, AGU, pp. 215-222.
- Long, L.T., J.-S. Liow, An Tie and K.-H Zelt, May 1986. Seismicity and Crustal Structure in southeastern Tennessee, Abstract, EOS Transactions, AGU, Vol. 67, No. 16, p. 314.
- Long, L.T., K.-H. Zelt, J.-S Liow, R.P. Propes, J. Shand, D. Reinbold and B. Schechter, July-September 1986. The North Georgia Earthquake of October 9, 1984, Earthquake Notes, Vol. 57, No. 3. ESSA, pp. 77-82.
- Long, L.T., 1988. A Mechanism for Major Intraplate Earthquakes, Abstract. EOS, Transactions, AGU, Vol. 69, No. 16, p. 402.

- Mareschal, J.C. and Jian Kuang, 1986. Intraplate Stresses and Seismicity: The role of topography and density heterogeneities, Tectonophysics, Vol. 132, pp. 153-162.
- McKeown, F.A., 1978. Hypothesis: Many earthquakes in the central and southeastern United States are casually related to mafic intrusive bodies, Jour. Research U.S. Geol. Survey, Vol. 6, No. 1, pp. 41-50.
- Propes, R.L., 1985. Crustal Velocity variation in the Southern Appalachians, Thesis, Master of science, School of Geophysical Sciences, Georgia Institute of Technology, Atlanta, GA 30332.
- Reinhold, D. and J. Cornwell, March 1983. The Greenback, Tennessee Earthquakes of 24 September 1982 and their tectonic associations, TEIC Special Report No. 9, Tennessee Earthquake Information Center, Memphis State University.
- Sachs, L., 1982. Applied Statistics, A Handbook of Techniques, Springer Verlag, pp. 139-141.
- Snoke, J.A., J.W. Munsey, A.G. Teague and G.A. Bollinger, 1984. A Program for Focal Mechanism Determination by Combined use of Polarity and SV/P Amplitude Ratio Data, Abstract, Earthquake Notes, Vol. 55, No. 3, p. 15.
- Teague, A.G., December 1984. Focal Mechanisms for Eastern Tennessee Earthquakes, 1981-1983, Master's Thesis, Virginia Polytechnic Institute and State University, Dept. of Geological Sciences, pp. 161.
- Teague, A.G., G.A. Bollinger and A.C. Johnston, February 1986. Focal Mechanism Analyses for Eastern tennessee Earthquakes (1981-1983), BSSA, Vol. 76, No. 1, pp. 95-109.
- Tie, An, J.-S, Liow and L.T. Long, 1986. Study of traveltime residuals at seismic stations in the southeastern Tennessee area, SEUSSN Report No. 18, pp. 73-77.
- Tzeng, W.S., 1982. Investigation of SV to P Wave Amplitude Ratio for Determining Focal Mechanism, Thesis, Master of Science, School of Geophysical Sciences, Georgia Institute of Technology, Atlanta, GA 30332.

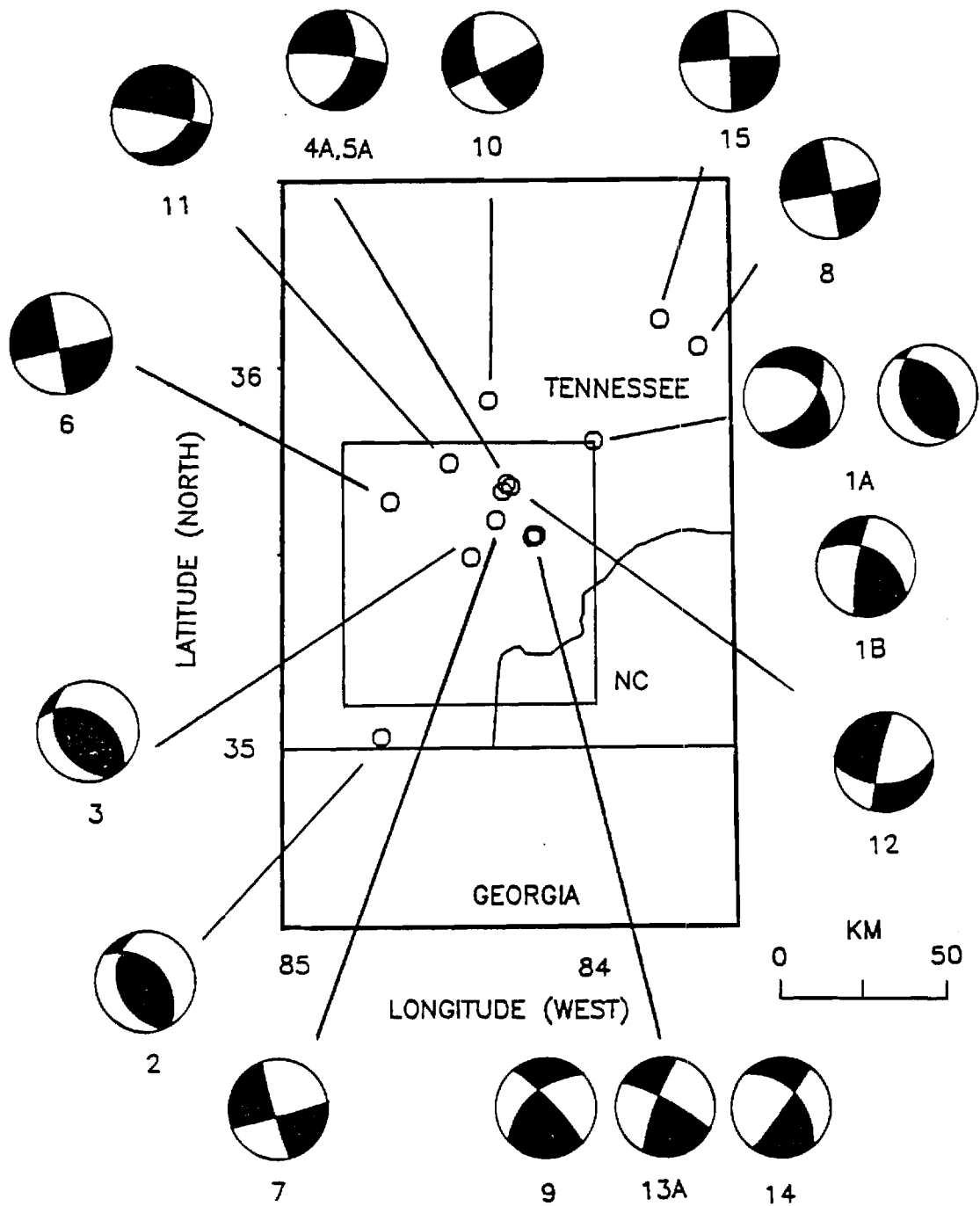


Figure 1. Published focal mechanism solutions for southeastern Tennessee (see Table I for reference numbers).

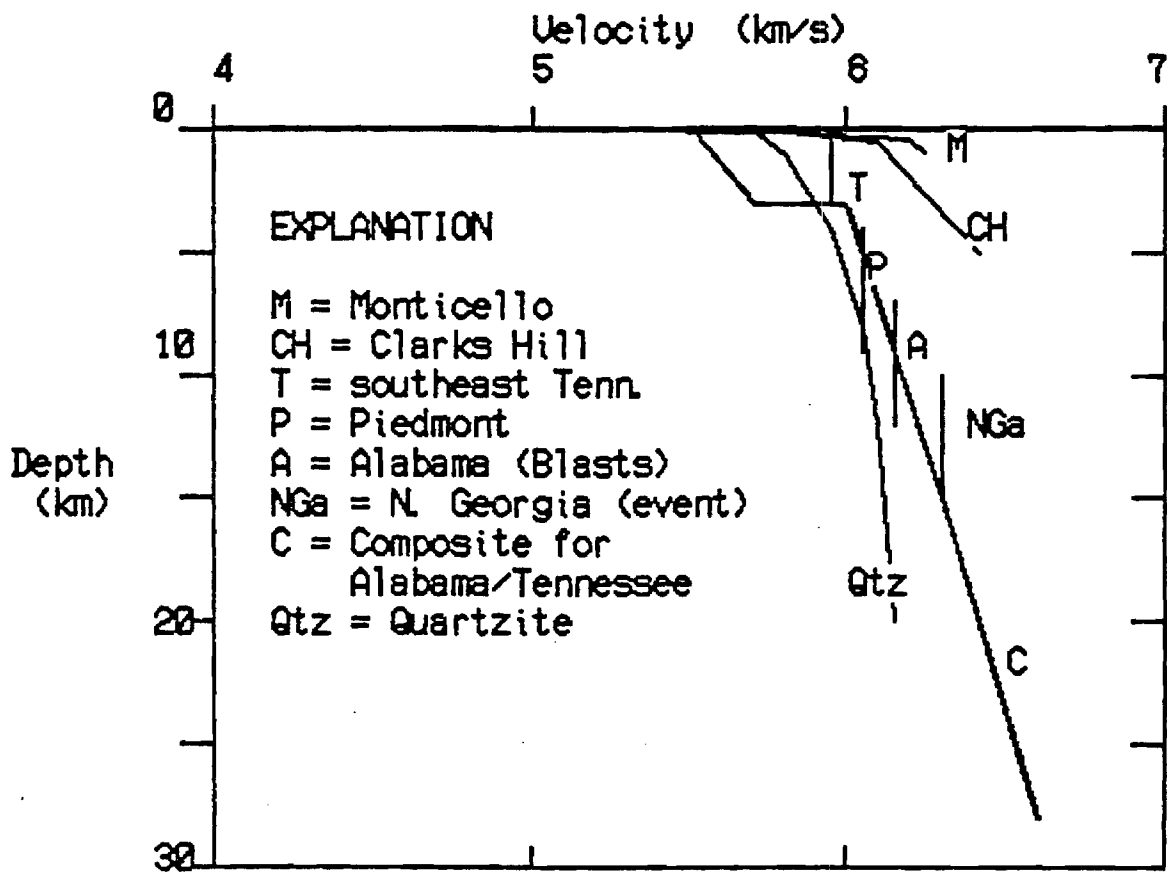


Figure 2. Composite plot of seismic refraction velocities in the southeastern United States showing the relation of velocity with depth.

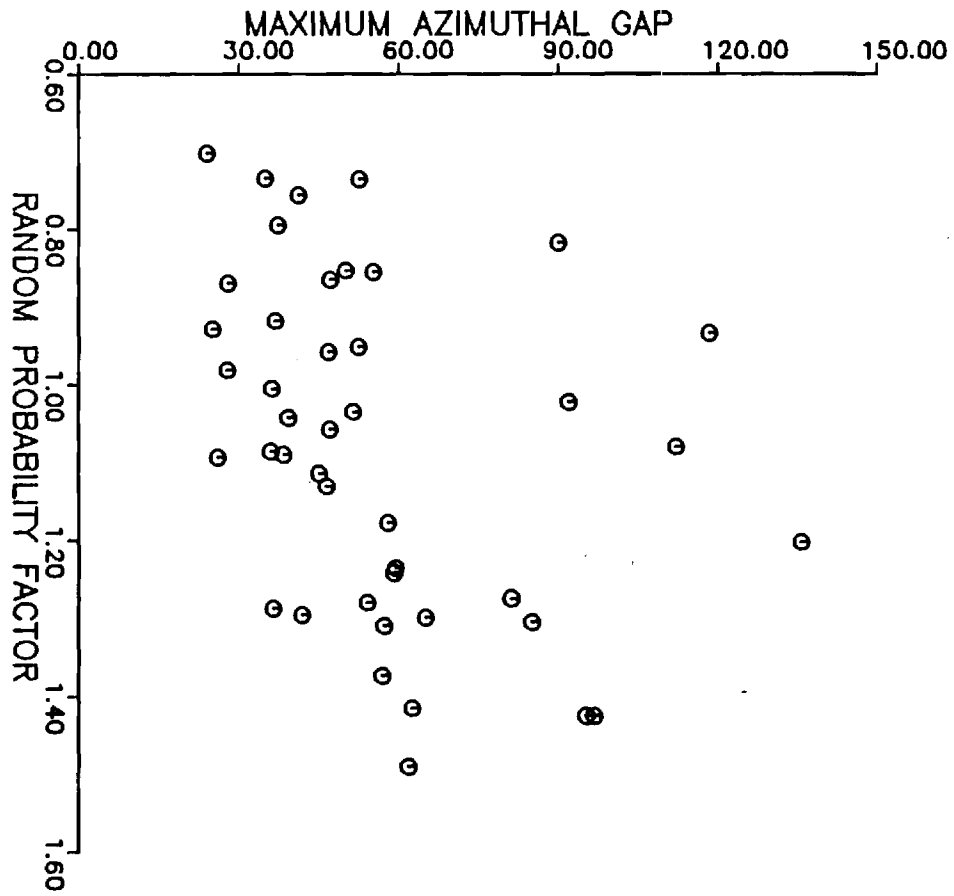


Figure 3. Relation between random probability factor and maximum azimuthal gap.

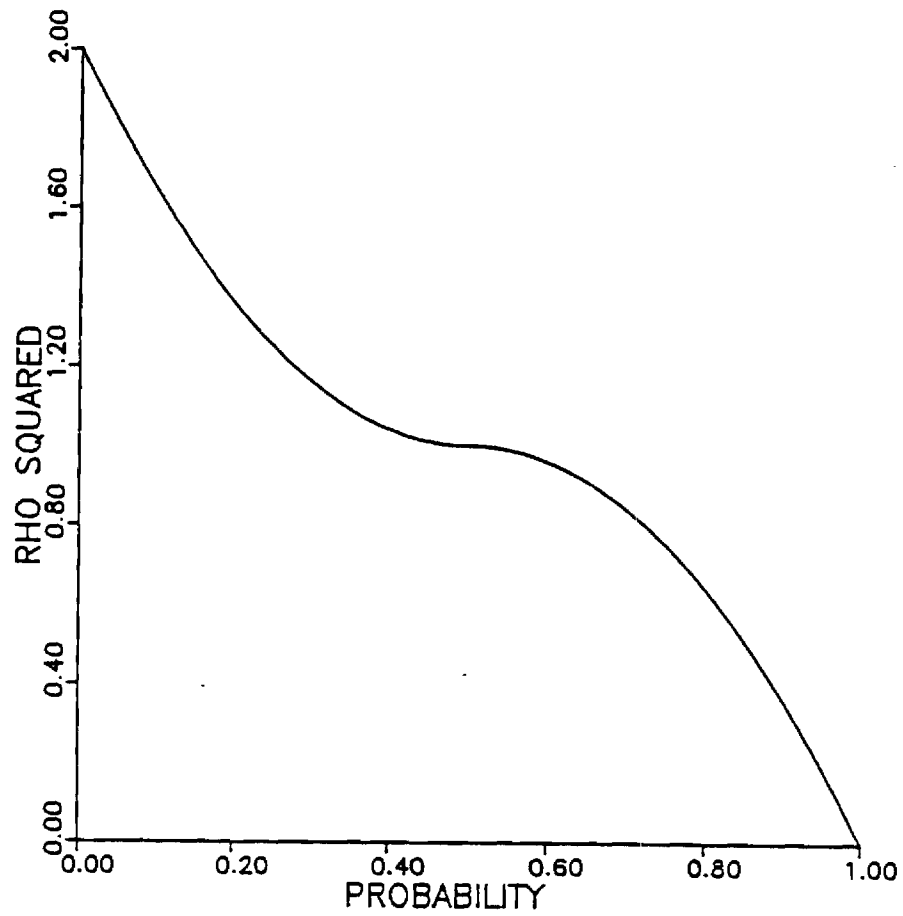


Figure 4. Relation between variance of polarity observations and probabilities of a correct reading.

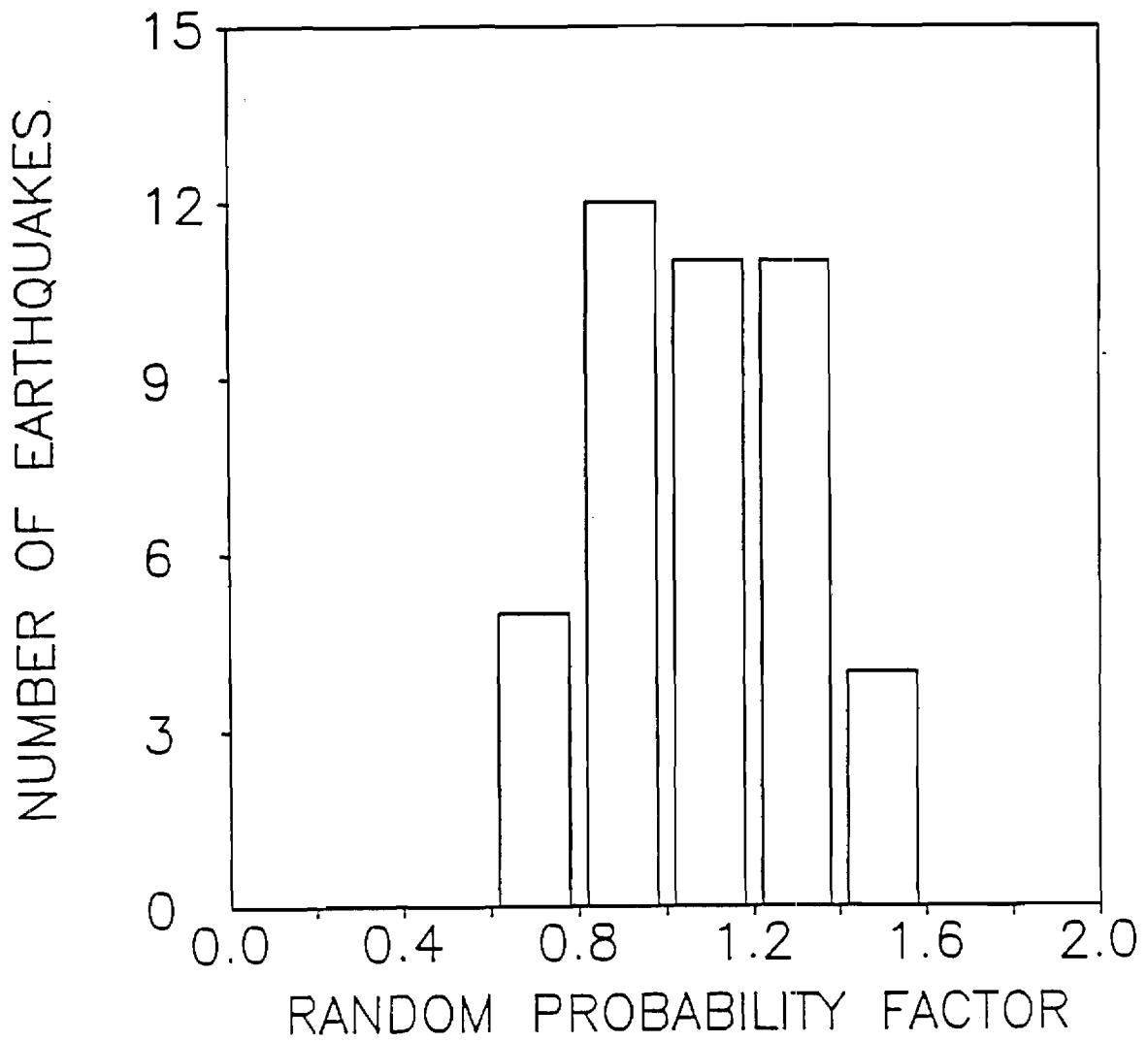


Figure 5. Distribution of the random probability factor for all earthquakes.

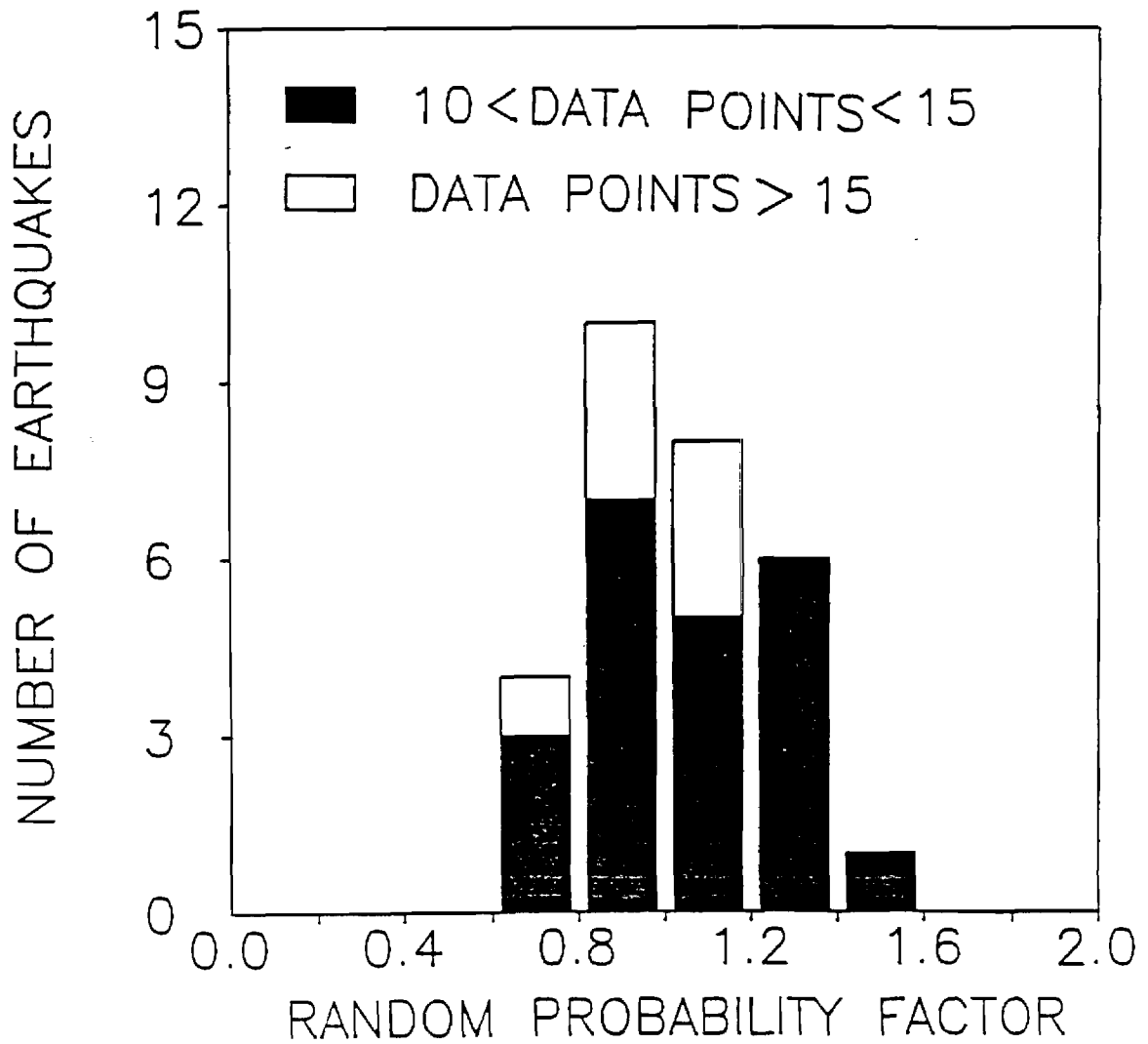


Figure 6. Relation between random probability factor for small and large numbers of stations.

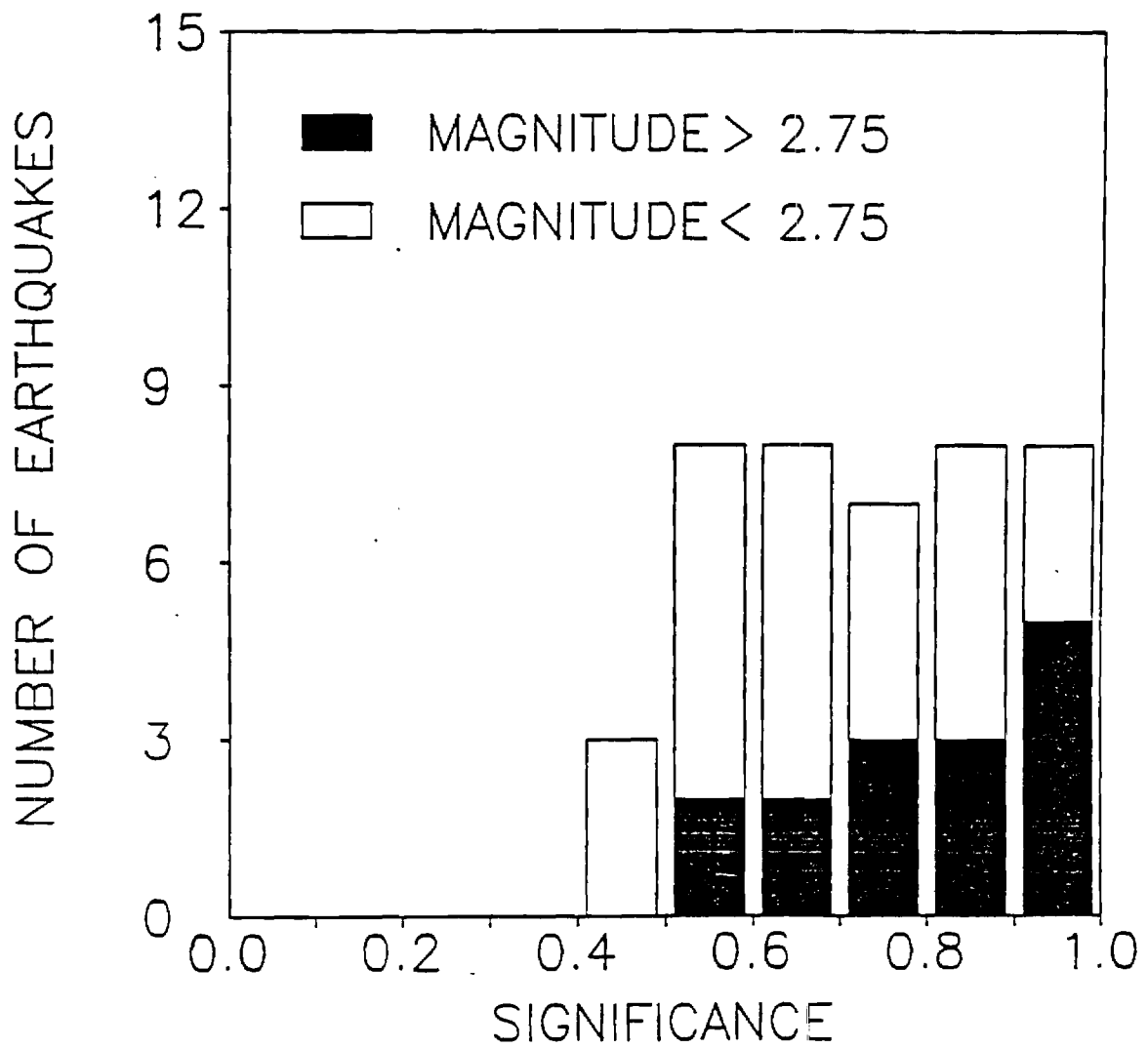


Figure 7a. Significance for all events for polarity data.

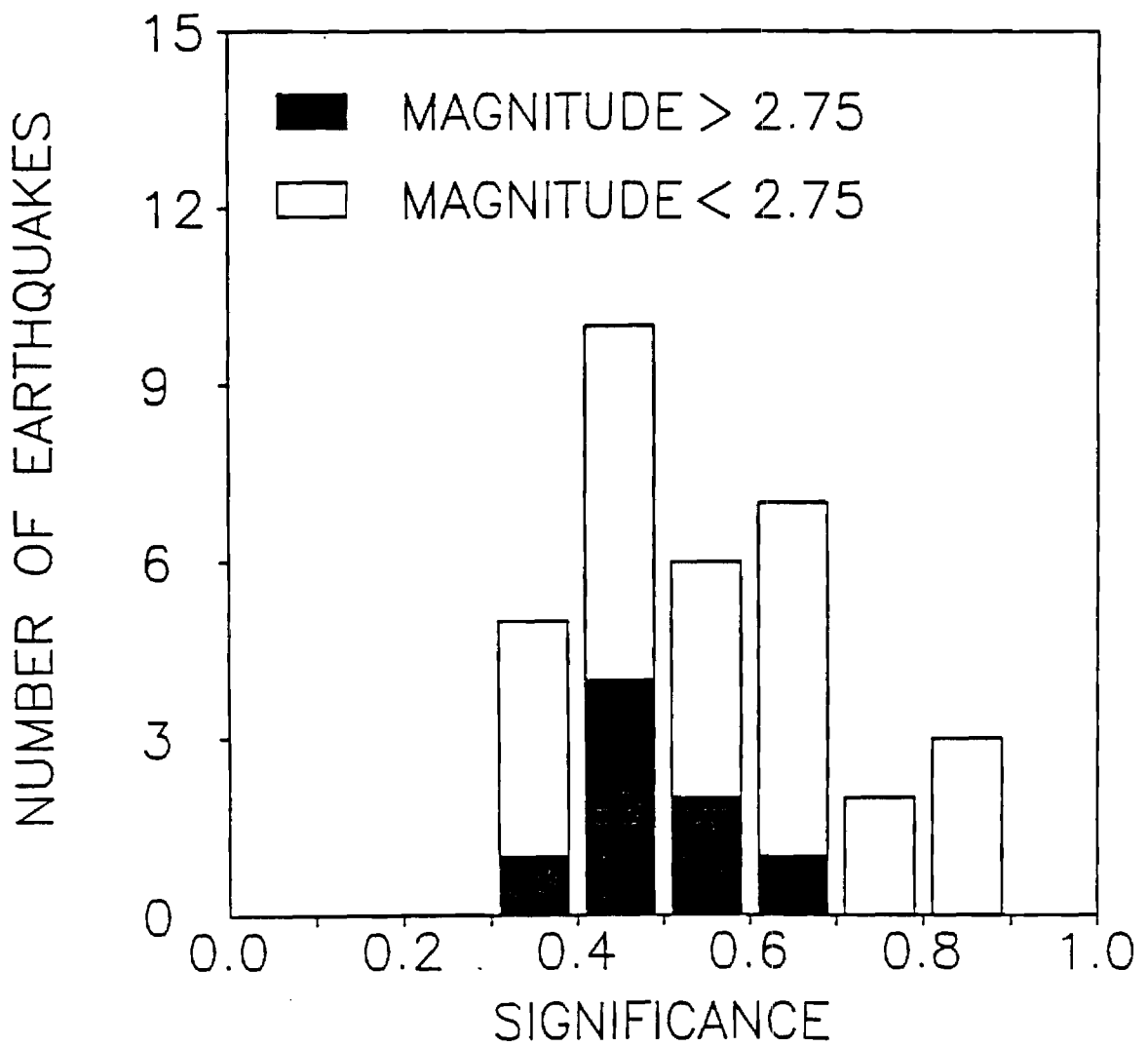


Figure 7b. Significance for all events for SV/P amplitude ratios.

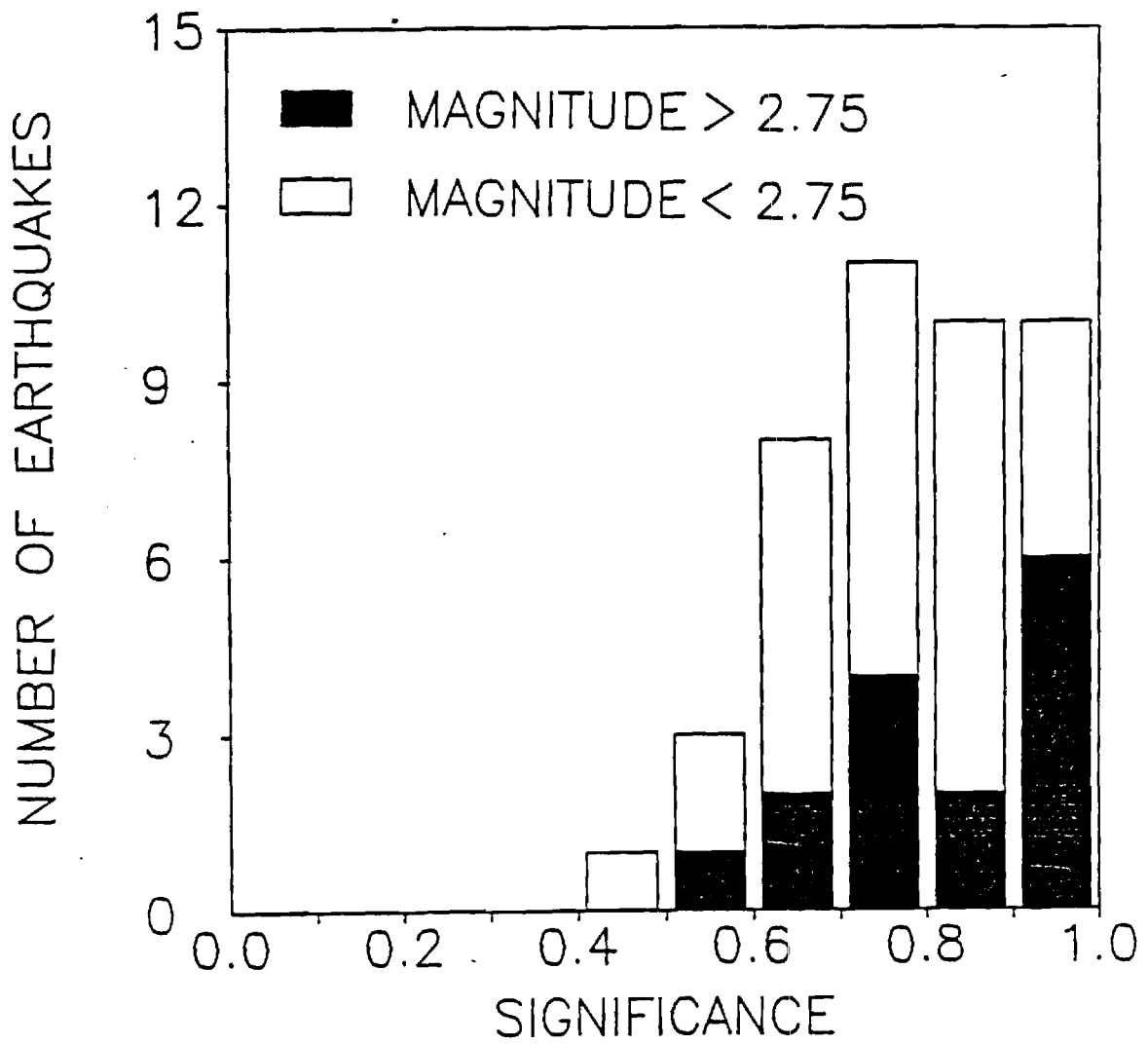


Figure 7c. Significance for polarity and SV/P amplitude ratios.

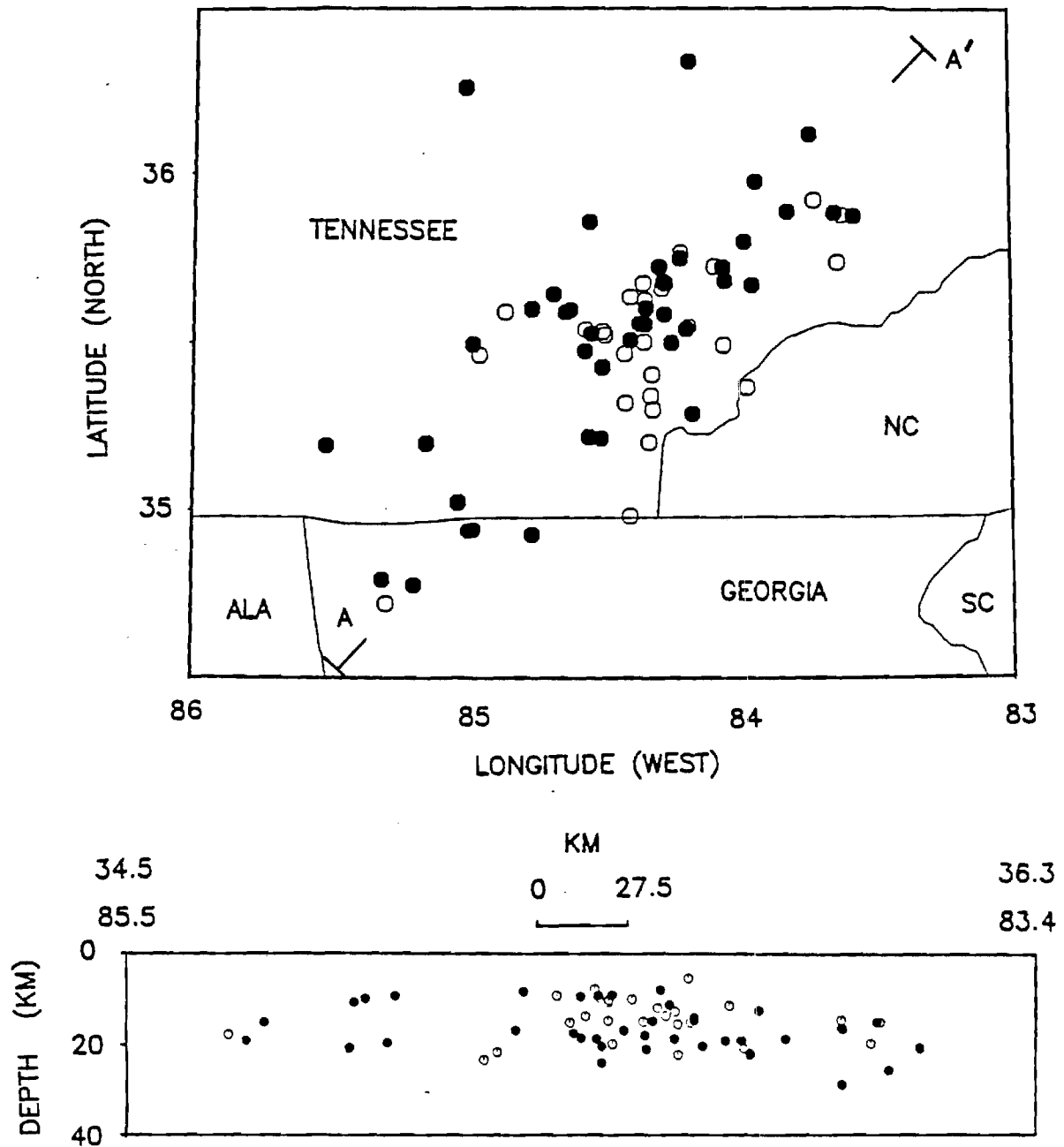
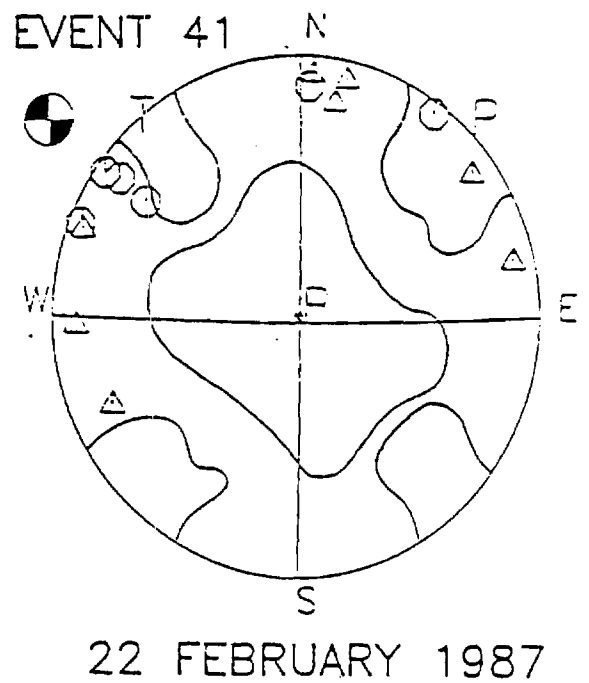
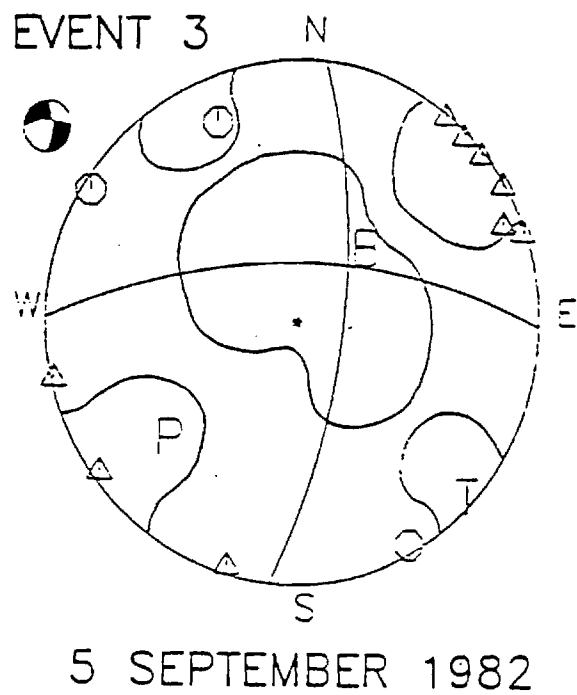
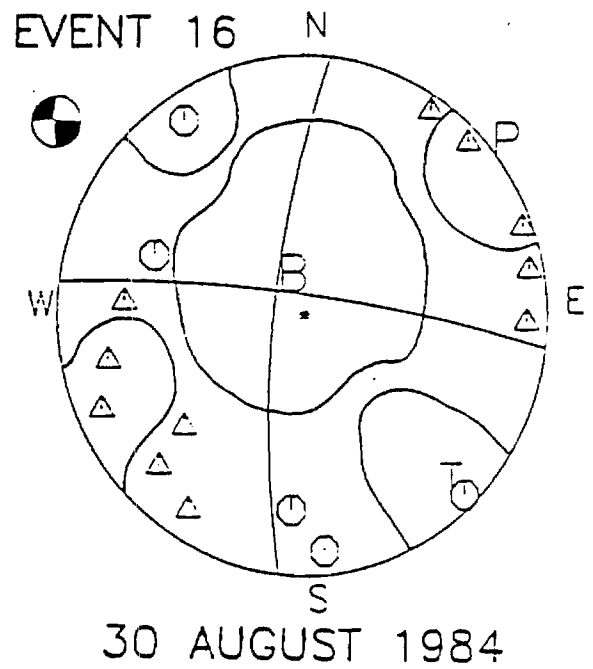
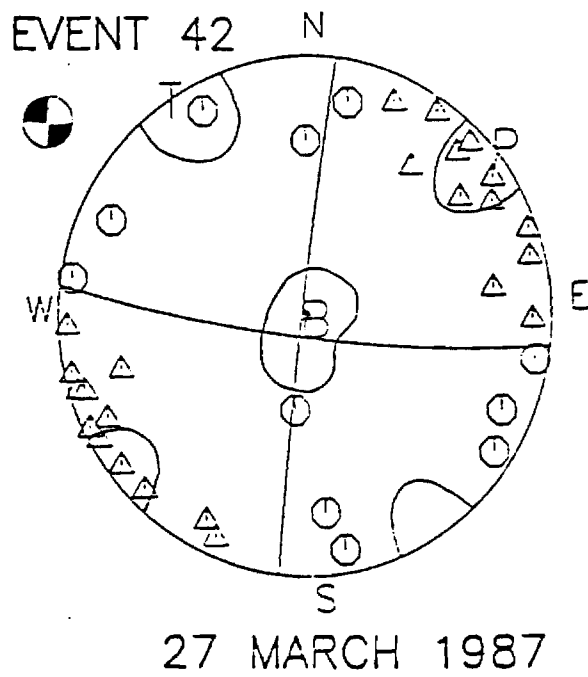
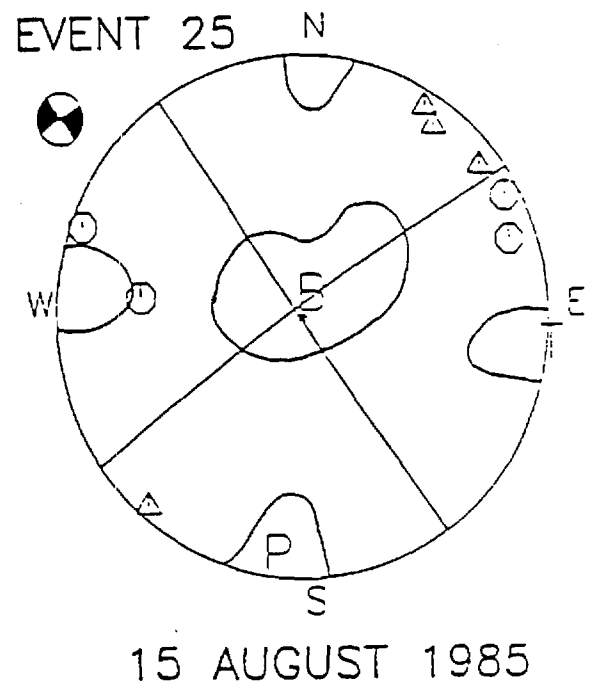
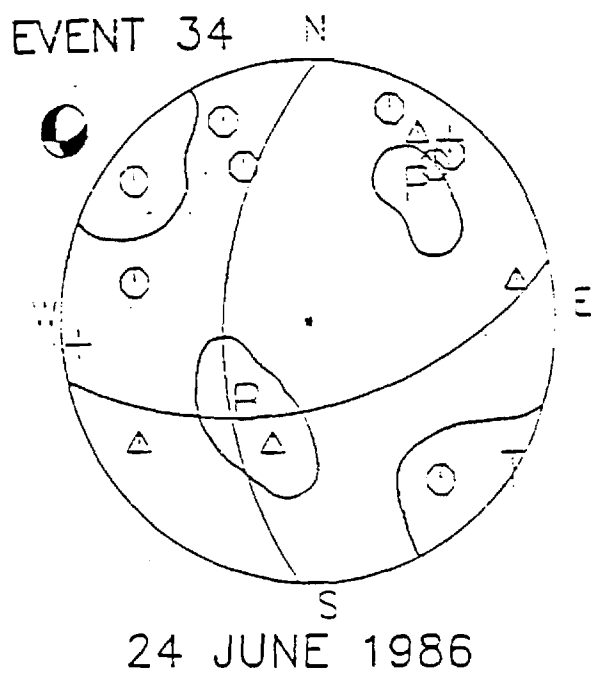
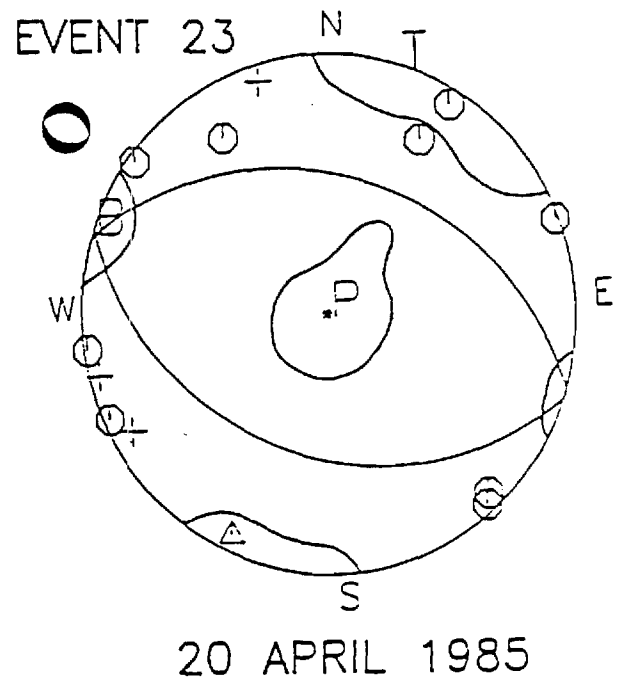
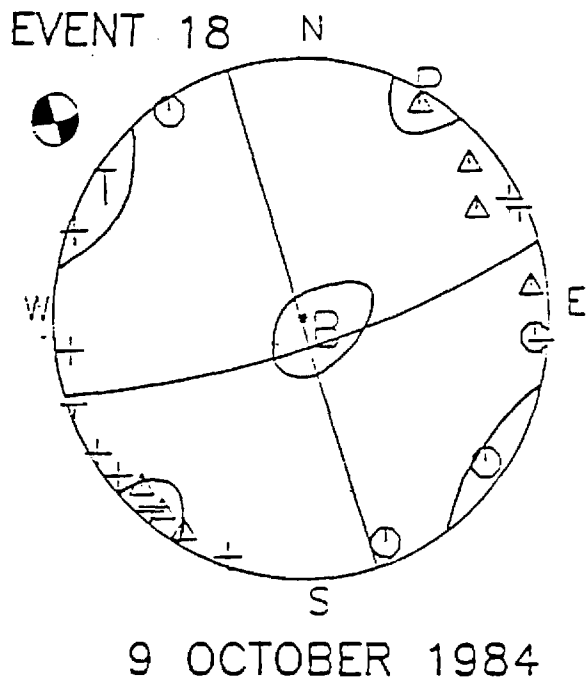


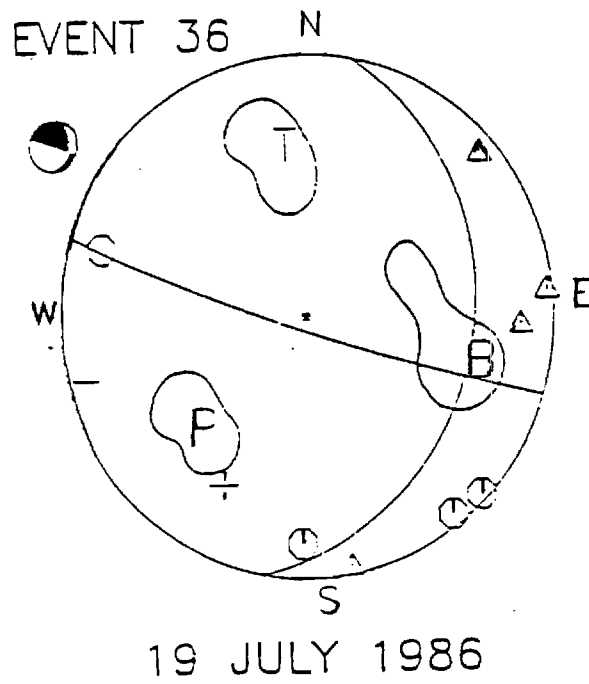
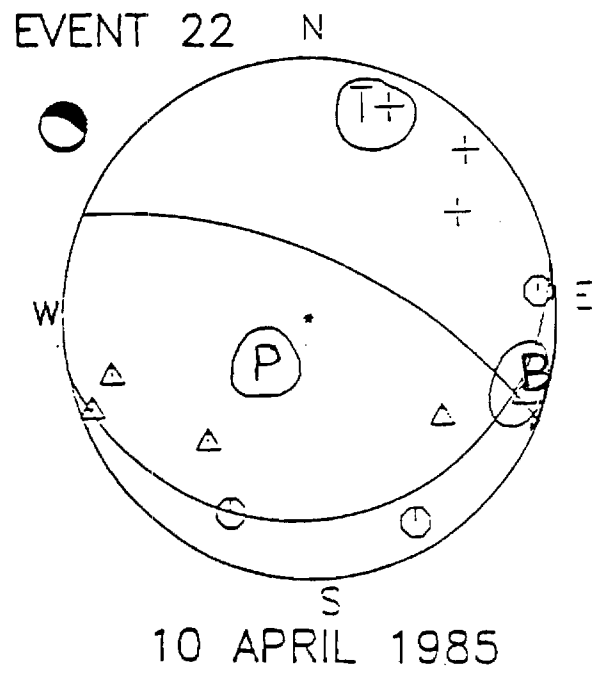
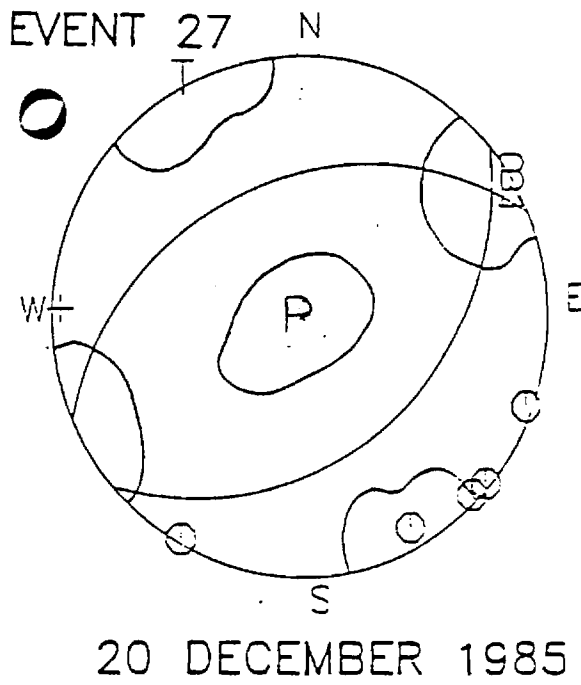
Figure 8. Location of earthquakes in southeastern Tennessee. Solid dots are events which have focal mechanism solutions.



Figures 9a-d. Focal mechanism solutions.



Figures 9e-h. Focal mechanism solutions.



Figures 9i-k. Focal mechanism solutions.

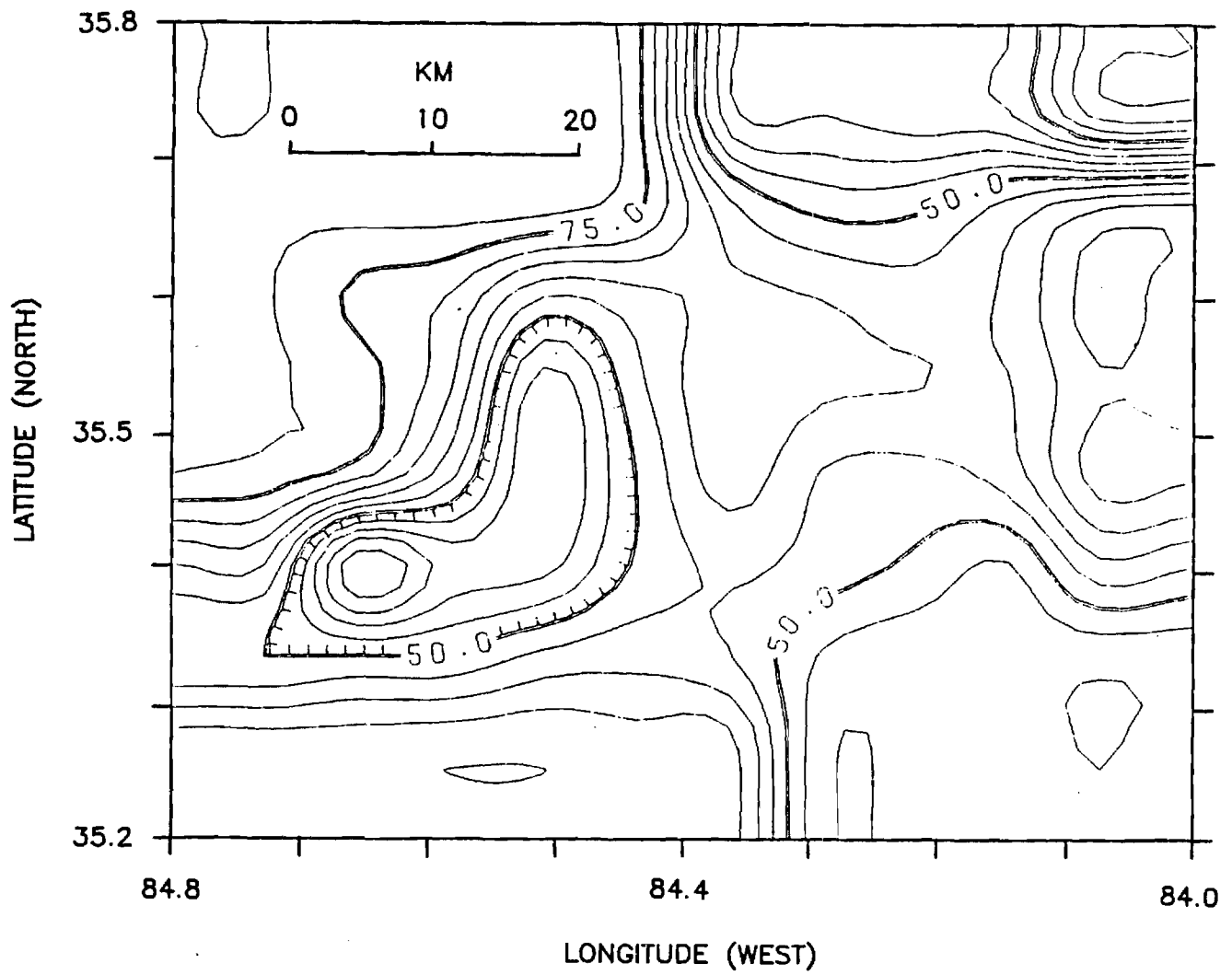


Figure 10. Dip of the null-axis in the central zone. This is a measure of strike-slip motions.

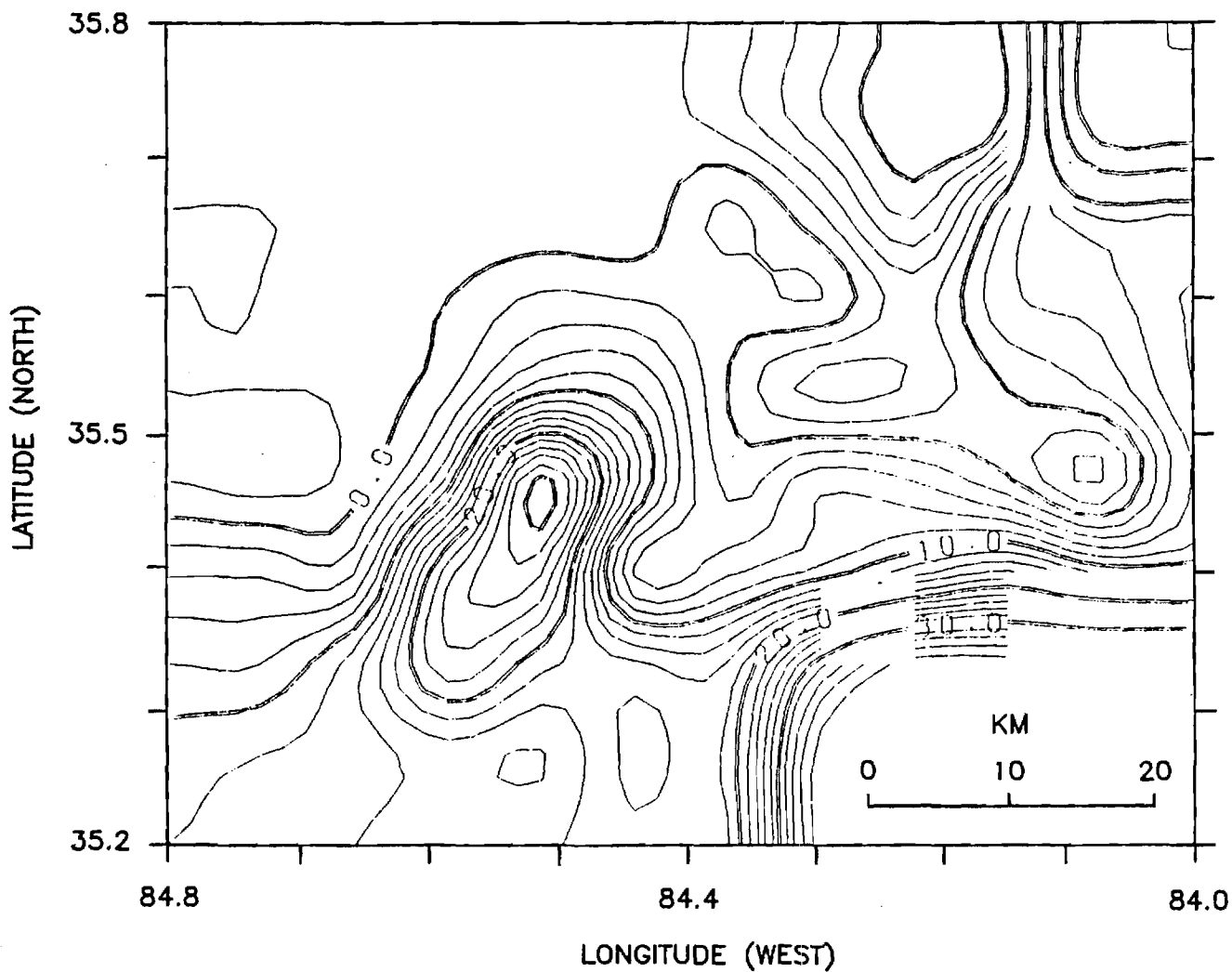


Figure 11. Difference between the dip of the tension axis and pressure axis. A value of -90 corresponds to a pure reverse fault. A value of +90 corresponds to a pure normal fault.

TABLE I.

No.	REFERENCE	DATE	M_D	DEPTH (KM)	EPICENTER
1a	Bollinger et al. (1976)	731130	4.6	3.0	35.799N, 83.962W
1b	Herrmann (1979)	731130	4.6	13.0	35.8N, 84.0W
1c	Guinn (1980)	731130	4.6	3.0	35.799N, 83.962W
2		760204	3.1	4.0	35.01N, 84.67W
3		770727	3.5	4.5	35.49N, 84.37W
4a	Reinbold and Cornwell (1983)	820924	3.2	14.0	35.678N, 84.236W
5a			3.5	10.0	35.686N, 84.250W
6	Teague 1984 and Teague et al. (1986)	811125	2.9	12.67	35.639N, 84.638W
4b		820924	3.2	10.0	35.678N, 84.236W
5b			3.5	14.0	35.686N, 84.250W
7		830118	2.3	8.22	35.589N, 84.287W
8		830127	3.1	18.29	36.052N, 83.608W
9		830405	2.0	12.89	35.542N, 84.166W
10		830516	1.9	16.36	35.916N, 84.311W
11		830525	1.6	17.8	35.741N, 84.441W
12		830526	2.5	3.3	35.666N, 84.264W
13a		830708	3.4	9.25	35.545N, 84.156W
14		830715	2.7	15.8	35.550N, 84.162W
4c	Johnston et al. (1985)	820924	3.4	14.0	35.678N, 84.236W
5c			3.5	10.0	35.686N, 84.250W
13b		830708	3.4	9.7	35.548N, 84.153W
15		840214	3.8	9.8	36.125N, 83.737W

TABLE II.

DATA TYPE	CONFIDENCE VALUE
Polarities:	
Incident, digital and developeorder	1.00
Incident, analog	0.85
Emergent, but readable	0.70
Emergent and random (not usable)	0.50
SV/P amplitude ratios:	
Incident, non-clipped	1.00
Emergent, non-clipped	0.70
Clipped and random (not usable)	0.50

TABLE III. Earthquake locations and focal mechanisms.

Date YrMoDa	Origin Time	Lat. North	Long. West	Dur. Mag.	Depth km	# of pts.	Sig.	Tension Pressure		Null		P-T		
								az.	dip	az.	dip	az.	dip	
820130	12:39	35.80	83.94	2.8	18.8	9	0.76	38	47	221	43	130	1	-4
820224	12:10	35.72	84.29	1.3	20.4	8	0.69	189	7	283	27	86	62	20
820905	10:11	35.21	84.51	3.2	8.4	12	0.86	138	2	229	24	44	66	22
820924	21:57	35.68	84.24	3.2	14.0	12	0.78	161	25	257	14	14	61	-11
821214	06:35	35.29	84.17	2.4	9.1	11	0.81	312	8	51	47	215	42	39
821215	02:27	35.75	84.22	2.1	19.2	9	0.65	252	57	13	18	112	26	-39
830118	05:09	35.58	84.27	2.3	11.2	11	0.71	335	49	71	6	166	40	-43
830129	18:08	36.12	83.74	2.1	20.7	10	0.91	322	31	220	20	102	52	-11
830304	14:03	35.60	84.34	2.3	8.0	7	0.71	53	20	150	17	277	63	-3
830316	09:13	35.22	84.55	2.6	16.9	6	0.71	327	8	234	16	83	72	8
830405	03:17	35.54	84.19	2.1	18.8	7	0.96	176	16	266	3	6	74	-13
830526	12:30	35.67	84.27	2.5	14.6	12	0.88	146	4	54	19	247	71	15
831016	22:02	35.86	84.55	2.5	19.8	12	0.84	348	24	82	9	191	64	-15
840207	06:32	35.65	84.64	1.8	20.4	7	0.71	19	2	289	1	172	88	-1
840525	10:15	35.60	84.62	2.0	24.1	11	0.87	319	34	110	53	219	14	19
840830	16:26	35.55	84.35	3.1	21.1	16	0.96	142	12	59	3	315	78	-9
840830	16:41	35.55	84.35	2.4	18.0	7	0.99	331	7	239	16	84	72	9
841009	11:54	34.77	85.19	3.5	15.0	22	0.78	298	6	29	7	168	81	1
841107	09:31	35.59	84.64	2.0	18.7	14	0.71	308	40	199	21	88	43	-19
850309	14:29	35.03	85.03	2.5	9.7	12	0.68	8	6	277	8	134	80	2
850312	13:04	35.87	83.57	2.0	25.6	12	0.82	311	7	218	16	64	72	9
850410	10:53	35.72	84.06	2.3	22.0	11	0.53	14	24	226	62	110	13	38
850420	04:21	35.48	84.56	2.5	9.4	13	0.78	20	1	151	89	290	1	88
850712	18:20	35.20	85.15	3.0	19.6	10	0.60	123	17	216	9	333	71	-8
850815	17:31	35.67	83.95	1.8	12.5	8	0.78	100	3	190	2	314	86	-1
850924	00:01	35.68	84.05	1.7	19.1	9	0.88	140	10	233	16	19	71	6
851220	15:15	34.93	84.76	2.9	9.3	7	0.68	329	0	236	81	59	9	81
860107	01:26	35.60	84.76	3.1	17.5	24	0.95	107	11	198	4	308	78	-7
860127	06:44	35.88	83.65	2.6	15.0	11	0.83	289	8	21	17	175	71	9
860419	07:40	35.19	85.51	3.0	21.0	27	0.91	183	9	280	35	81	53	26
860423	07:18	34.79	85.30	1.8	19.1	8	0.60	120	2	24	70	211	20	68
860519	23:46	35.53	84.54	2.6	9.7	14	0.67	284	11	16	15	159	71	4
860602	07:46	35.43	84.50	2.5	18.6	14	0.87	132	32	31	17	277	53	-15
860624	19:22	35.98	83.94	2.8	28.8	14	0.67	131	1	40	41	222	49	40
860711	14:26	34.93	84.99	3.8	20.7	30	0.98	329	18	60	3	159	72	-15
860719	12:31	34.94	84.97	1.9	10.6	10	0.66	349	40	226	32	112	33	-8
860807	12:36	35.49	84.54	2.5	14.9	11	0.49	285	15	25	32	174	54	17
860819	20:51	36.26	85.01	2.9	20.0	13	0.73	112	20	244	62	15	19	42
861115	12:08	35.88	83.82	2.0	16.4	9	0.70	172	2	81	7	278	83	5
870112	18:56	35.50	84.25	2.1	14.8	9	0.85	320	23	121	65	227	7	42
870222	10:35	36.39	84.21	2.8	19.0	14	0.81	314	2	44	1	161	88	-1
870327	01:26	35.60	84.76	3.9	17.5	35	0.99	323	4	53	6	199	83	2
870901	23:02	35.51	84.40	3.2	16.9	17	0.99	304	20	41	18	170	63	-2

The significance measure is based on the number of points, the distribution of data points, quality of first motions and SV/P ratios, and a Chi-square estimate of goodness of-fit.

TABLE IV.

CATEGORY	FOCAL MECHANISM SOLUTION	LIMITS OF P- AND T- AXES (DEGREES)
1	Strike-slip Strike-slip with normal or reverse component	Dip < 25 Degrees $25 \leq \text{Dip} \leq 45$
2	Normal Normal with strike-slip component	Dip of P-axis > 60 $45 \leq \text{Dip of P-axis} \leq 60$
3	Reverse Reverse with strike-slip component	Dip of T-axis > 60 $45 \leq \text{Dip of T-axis} \leq 60$

TABLE V.

SIGNIFICANCE	Q	R	Q	NO. OF POINTS	Q
≥ 0.9	S1	$0.8 \leq R \leq 1.2$	R1	$P \geq 15$	P1
$.8 \leq S < .9$	S2	$0.8 > R > 1.2$	R2	$15 > P \geq 10$	P2
$.7 \leq S < .8$	S3	$0.6 > R > 1.4$	R3	$10 > P \geq 5$	P3
< 0.7	S4	$0.4 > R > 1.6$	R4	$P < 5$	P4

APPENDIX B

A Technique for the Inversion of Coda Q

APPENDIX B

A TECHNIQUE FOR THE INVERSION OF CODA Q

Leland T. Long Jeih-San Liow and Frank B. Jones

ABSTRACT: Digital data from station CBT in southeastern Tennessee provide estimates of coda Q with variations which depend on the direction to the earthquake. We interpreted this azimuthal variation to indicate a spatial variation of the properties of the crust that determine coda Q. Coda Q is a phenomenological parameter characterizing coda decay and it is determined by the integrated effects of crustal parameters in the ellipsoidal volume of crust with the recording station and hypocenter as foci. Zones of anomalous crust will influence the computation of coda Q differently for different station and hypocenter pairs. Through a sequence of approximations, we have linearized the relation between the measured apparent coda Q and an assumed constant coda Q for discrete zones of crust. Inversion of coda Q data from regional stations in the southeastern United States suggests a reduction in coda Q as one nears the coastal plane. Inversion of coda Q data near station CBT suggests an anomalously low coda Q region ($Q=38$) in a 300 square kilometer region northeast of station CBT.

INTRODUCTION

The wavelets that make up a seismic coda are affected by the size, shape, and distribution of scatterers and by intrinsic attenuation. In a coda, the combined influence of intrinsic attenuation and scattering are difficult to separate. Hence, coda Q, as measured from the rate of decay of the coda, should with objectivity be treated as a phenomenological parameter characterizing coda decay.

We have observed significant variations in the shape of the shear wave coda in records from our station CBT in southeastern Tennessee. Figure 1 shows some of these records and the epicenters for these events. In particular, note the rapid decay for events northeast of CBT and the slow decay of the coda for events to the northwest.

We use coda Q in this study only as a phenomenological parameter to characterize this variation in coda decay. The assumptions invoked in the derivation of equations used to give numerical values to coda Q will change the values of coda Q, although relative differences in coda Q will generally remain the same. We leave the interpretation of Q for later studies.

Coda Q is of particular interest because low Q values have been associated with greater rates of occurrence of large events in China and in the western US. In those studies, the spatial variation of coda Q was inferred from estimates of Q for a distribution of single station average values. Alternately, for single events the coda Q could be assigned to the midpoint of the line connecting the epicenter and station. In this analysis we consider the possibility of using coda Q as measured at an array of stations for an array of epicenters to determine the spatial variation of coda Q in the crust. Hence, we are attempting to attain a higher resolution of coda Q than is currently possible with single station techniques.

THEORY

One can not do justice to the multiplicity of mechanisms in scattering and attenuation with this abbreviated derivation. For a single arrival that traverses media of varying Q , the cumulative attenuation ($1/Q$) is the sum of the effects of attenuation in each segment. The resulting equations are intuitively correct for one dimension. The extension to three dimensional scattering and attenuation is not straight forward, but the relation can be shown to be approximately correct.

Fundamental to showing this result is the assumption that coda Q calculated from increasingly longer lengths of the coda are representative of increasingly larger "ellipsoidal" volumes of the crust. It would be natural to generalize the analysis to a crust divided into many segments, but in this presentation we consider only acknowledged regional provinces or a single anomalous zone.

First we assume that the amplitude in the coda is given by,

$$A(t) = A_0(t) \exp[-\pi ft/Q] \quad (1)$$

where f = frequency, t = time from origin, $A(t)$ = amplitude in the coda at time t , $A_0(t)$ = geometrical attenuation of the original amplitude and Q = attenuation coefficient that describes the decay with time.

We next consider the energy density for the path to the j th scatterer in a single scattering model for individual scatterers to be,

$$dn_j \exp[-2\pi ft/Q]$$

and the attenuation is expressed as an integral over the path,

$$t/Q = \int (1/Q) dt.$$

The integral is converted to a discrete summation by approximating the crust as discrete zones of constant coda Q . Combining the two expressions above gives,

$$\sum_j dn_j \exp[-2\pi f \sum_i T_{ij}/Q_i] \quad (2)$$

where T_{ij} = the fraction of time within the zone of Q_i along the path to the j th scatterer. The next step is to expand exponent in Taylor series and interchange order of summation. This requires one assume a uniform distribution of scatters. From geometrical arguments, we note that only a fraction (P_i) of the arrivals will pass through the i th crustal block. This allows in a first approximation, that the P_i are the percent of the energy at time t ,

$$\begin{aligned} & \sum_j dn_j + \sum_i -\pi f/Q_i \sum_j dn_j T_{ij} \\ & \sum_j dn_j T_{ij} \approx [A_0(t)]^2 P_i \end{aligned} \quad (3)$$

The expansions are undone in a similar reverse procedure to show that $1/Q$ is approximately the sum of P_i/Q_i , or that,

$$1/Q \approx \sum P_i/Q_i \quad (4)$$

Equation (4) is a linear relation between observed coda Q and the percent of area "volume" that is assigned an unknown value Q_i .

RESULTS

We can present results for two inversions for Q . The first a study of regional events in the southeastern United States; the second a study of an anomalous area in southeastern Tennessee.

In the regional southeastern United States study, we utilized physiographic provinces: Atlantic Coastal Plane, Piedmont, Folded Appalachians, Interior Lowland Plateau and the Gulf Coastal Plane. The events ranged in location from South Carolina to New Madrid, MO. The data used were recorded on stations equivalent to WWSSN short period records. Q for the interior Lowland Plateau exceeded 700. The Gulf Coastal Plane gave values of 250. In-between values were obtained for the Folded Appalachians and the Piedmont, about 425. The Atlantic Coastal Plane Q of 388 was slightly less than average.

In the study for southeastern Tennessee we used data from four stations and about 50 records of earthquakes. Figure 2b shows the epicenters and stations used. The area considered for computation of anomalous Q is shown shaded in Figure 2a and was based on seismicity and travel time residuals. This area was then used to define the area or volume of the ellipse that optimized the influence of the anomalous zone and, hence, the length of coda for computation of coda Q . Figure 2a shows a set of ellipses for station CBT. Note the variation in area of influence that allows use of such data in a linear inversion technique. The inversion in this case gave a coda Q in excesses of 1000 for the surrounding area, and a value of 4000 was assigned to the regional area based on measurements of extended lengths of coda. A least squares estimate of Q for the anomalous zone gives $Q = 38$ with a range from 10 to 100 at one standard deviation.

Figure 3 shows the fit of the data to theoretical curves for various values of anomalous Q , with a fixed regional Q of 4000. The scatter may be related to a number of factors:

- 1) inappropriate choice for boundaries of anomalous zone,
- 2) expected uncertainty in measurement of coda decay,
- 3) choice of 2 or 3 dimensional models for scattering,
- 4) existence of other anomalous zones , and 5) multiple versus single scattering contributions.

In any case, a definite trend exists in this data and that trend is consistent with a zone of anomalous crust in southeastern Tennessee. This technique, with appropriate refinements and tests, will be capable of defining coda Q in relatively small areas of the crust.

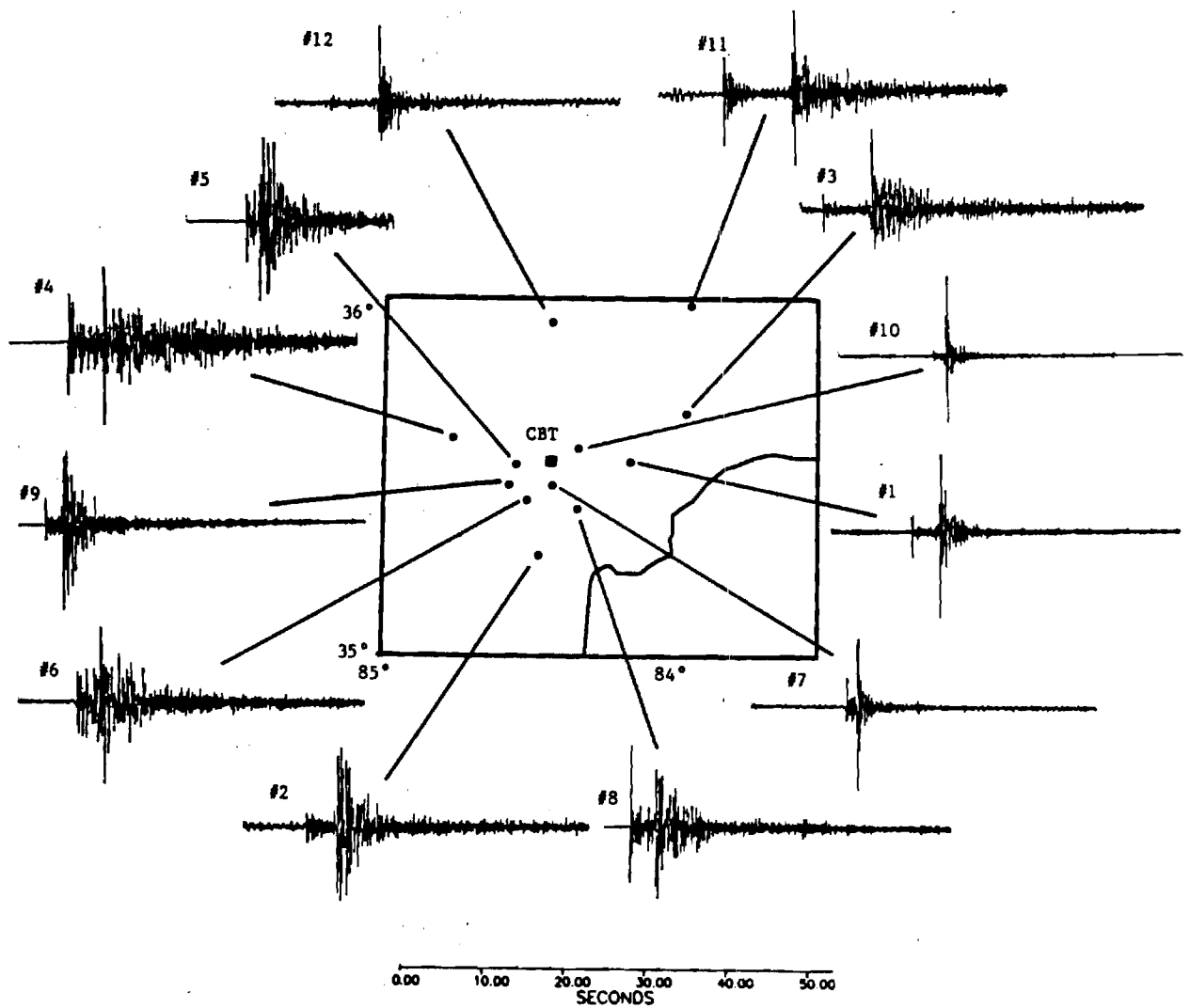


Figure 1. Seismograms recorded at station CBT showing variation in character of coda decay and their location relative to CBT.

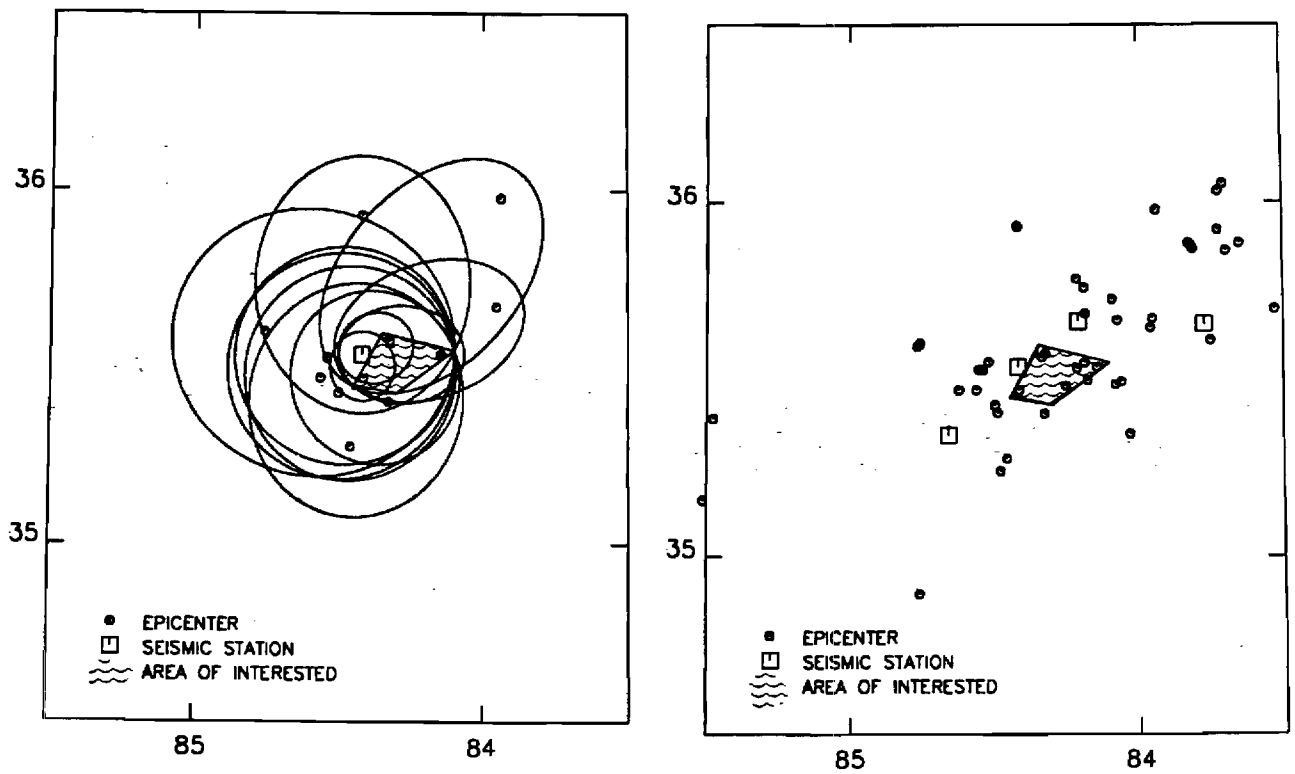


Figure 2. Data for preliminary analysis. (a) Comparison of anomalous area and ellipses of influence, and (b) locations of stations and events used.

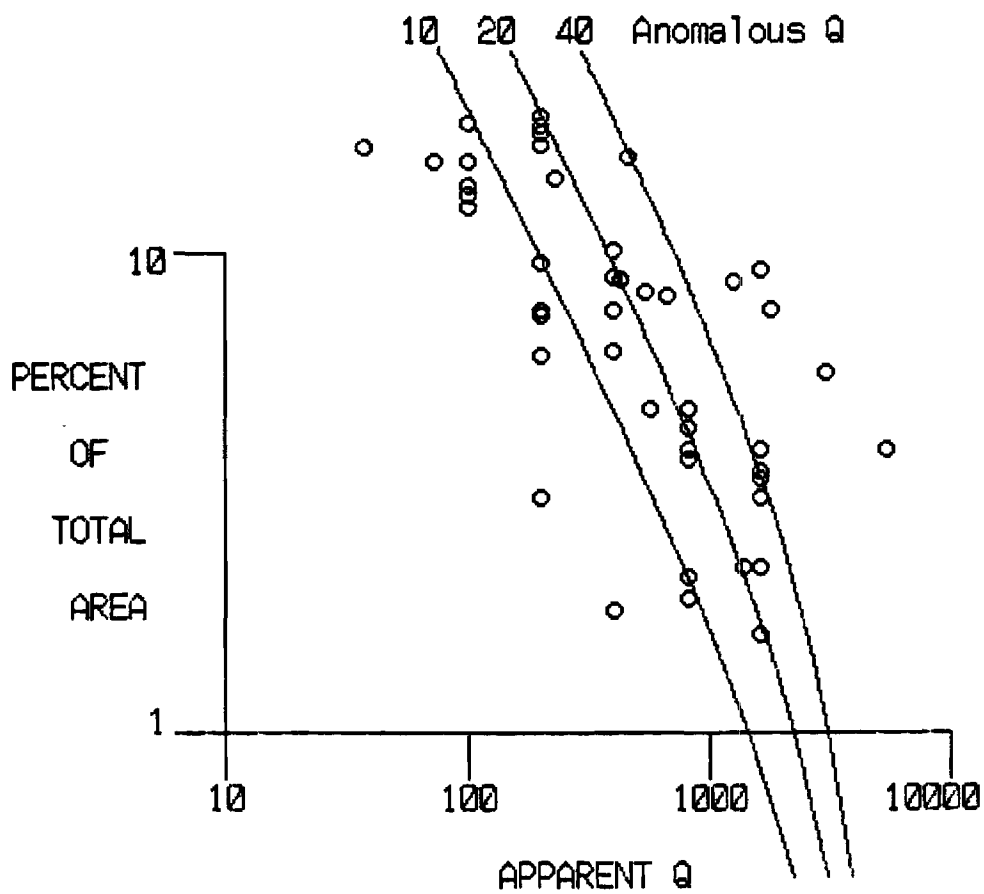


Figure 3. Apparent Coda Q versus percent contribution of anomalous area in the ellipse of influence.

APPENDIX C

Fracture Intensity and Reservoir Induced Seismicity

APPENDIX C

FRACTURE INTENSITY AND RESERVOIR INDUCED SEISMICITY

Leland T. Long, Christopher C. Sorlien and Thomas J. Schmitt

ABSTRACT: Detailed field measurements of fractures and joints were taken near the epicentral zone of the August 2, 1974, magnitude 4.3 earthquake in the Clarks Hill Reservoir (now Lake Strom Thurmond). Zones of anomalous fracture intensity are consistent over distances of a kilometer and an observation spacing of 0.5 to 1.0 km will allow contouring of fracture intensity. The joint intensity varied systematically in the study area. The area of induced earthquakes was concentrated along the edge of a zone of low fracture intensity and high rock quality. Hypocentral depths of earthquakes which are attributed to movement on shallow joints are typically less than 1 km, and within this depth range the fracture intensity does not significantly decrease or vary. Quantitative surface measurements of rock quality (which includes fracture intensity) can be extrapolated to the depths of nucleation of these induced earthquakes. In contrast, stress may be released through creep on (foliated) schists and altered mafic rocks, explaining the lack of seismicity in zones of high fracture intensity and low rock quality. The association of granite gneiss and high rock quality measurements can be used to predict susceptibility to induced or natural shallow seismicity.

INTRODUCTION

Earthquakes in the Piedmont Province of Georgia and South Carolina have unique properties that distinguish them from events in many other seismic areas of the continental interior. These properties are their near surface to 2.0 km depth of focus (Dunbar, 1977; Fogle et al., 1976; Talwani, 1977;), their swarm-type occurrence and associated high b values (Long, 1974; Talwani et al., 1979; Johnson, 1984), their cubic high-frequency spectral decay (Marion and Long, 1980), their association with reservoirs and water loading (Talwani, 1976; Costain et al, 1987; Jones et al, 1986), and the similarity between joint directions and focal mechanism solutions (Guinn, 1980). Taken singly or in concert, these properties of Piedmont earthquakes have been interpreted as supporting an association between Piedmont seismicity and shallow joints or fractures.

In a study of the geology of the area of induced seismicity around Monticello Reservoir, Secor, et al. (1982) observed numerous diversely oriented small fractures and lithological inhomogeneities in the Winnsboro complex, and speculated that these control the diffuse induced seismicity. Although the association between seismicity and jointing or small fractures has been established on the basis of depths of focus, source spectral properties, and a comparison of focal mechanisms with joint plane patterns in the Southern Piedmont, the details of the style of jointing and its correlation with seismicity have not previously been investigated. This study was undertaken to discover how joints and fractures are related to induced seismicity and, hopefully, to suggest ways in which rock quality may be used to asses a potential for induced seismicity. The objective of this paper is to present our systematic examination of joints and fractures in an area of induced seismicity.

THE STUDY AREA

The study area is a rectangle of 6 by 12 km which covers the epicentral zone of the August 2, 1974, M_L 4.3 earthquake (Fogle et al, 1974). Portable seismographs were deployed immediately following the 1974 event (Talwani et al., 1975) in an aftershock survey. Additional intermittent monitoring in the aftershock zone (Bridges, 1975; Guinn, 1977) and continuous monitoring by a regional network (Long et al., 1976) has defined the distribution of epicenters. The aftershocks and study area are located in the upper reaches of the Storm Thurmond Reservoir (figure 1). The aftershocks were not restricted to a single fault plane, but instead were scattered over 7 km^2 area centered 1.5 km northeast of the Savannah River channel. The depth-of-focus of aftershocks to the 1974 earthquake were computed by Talwani (1976) to range from 0.5 to 2.5 km. A relocation using a revised velocity model on an independent set of 81 aftershocks showed that most are above 1 km (Dunbar, 1977). The relocated events had a hypocentral precision of better than 200 meters both horizontally and vertically. The 1974 event and its aftershock sequence was not the first occurrence of seismicity in the Storm Thurmond Reservoir area, with notable events in 1969 (Long 1971) and an intensity VI earthquake felt near Lincolnton, Georgia, in 1875 (Long, 1984).

The geology of the study area is complex, (Griffin, 1973; Hatcher, 1987) consisting of metamorphic lithologies which have been migmatized and intruded by granite. The major contacts strike northeast parallel to the Charlotte belt structures in which they reside. An advantage of the study area is the availability of rock exposures along the shoreline of the Storm Thurmond Reservoir and in adjacent streams. The rocks in these exposures were sufficiently intact to allow joint spacing measurements and most were easily accessible from the reservoir or roads.

ANALYSIS AND FIELD METHODS

Well defined cracks or fractures pervade the near-surface crystalline rocks of the Piedmont province. We refer to these cracks or fractures as joints if the slippage of one block against the other can not be determined or is very slight. The average separation of joints in a joint set may be difficult to quantify because the joint spacing and distribution may display great variety which (among other factors) depends on rock type. The trimean joint intensity was proposed (Wheeler and Dixen, 1980) as a means of quantifying rock strength properties based on field measurements and as a means of minimizing the effects of extreme values of joint spacing. The intensity of a joint set has the dimensions of surface area of joints per cubic meter with units of inverse meters. The trimean estimator of joint spacing was used in this study to compute the trimean intensity, and effectively minimize the effects of extreme values in the separation of joints. The trimean spacing is calculated for each joint set by adding the first and third quartiles to twice the median spacing and dividing by 4 (Wheeler and Dixon, 1980). Trimean intensity then uses trimean spacing in the same way as average spacing is used in average intensity calculations, and is considered a statistically robust estimator of joint intensity.

A proper choice of statistical measures for joint spacing is not well established. The use of average spacing or trimean spacing assumes a distri-

bution of spacings about some mean or median value. In field observations, the distribution of joint spacings can be highly irregular, with variations from almost uniformly spaced joints to highly bunched joints with many small spacings and a few large spacings.

An alternate statistical technique for quantifying joints is to find their fractal dimension. Many related natural systems, such as rock permeability (Wong, 1988) or the roughness of joint and fault surfaces (Scholz and Aviles, 1986), satisfy self similar (fractal) models. In this evaluation we considered that the distribution of joint spacings would satisfy the relation,

$$N = A \left[\frac{L}{r} \right]^{dr} \quad (1)$$

where N is the number of joints spacings of length greater than or equal to r in a total length (outcrop length) L. The A is a constant of approximate value one that represents the difference between the measured L and its statistical estimate. The fractal dimension is dr and is computed from a least squares estimate of the slope of Log(N) versus Log(L)-Log(r). For those sites that satisfied a self similar distribution, the fractal dimension has the advantage of being the most robust statistical parameter. A disadvantage is that the relation between fractal dimension and rock quality is unknown.

Fracture intensity and fractal dimension determinations require measurements of the attitudes of joint sets and spacings between individual joints. A study of the spatial variation of joint intensity requires a relatively uniform distribution of rock exposures. The shoreline and tributaries of the reservoir provided nearly continuous rock exposure except where limited by the area covered by the lake and by deeply weathered saprolite in the higher elevations northeast of the epicentral zone. Where possible in the study area, rock outcrops were examined at a separation of no more than 2 km. More dense observations were taken along the shore line and where possible in the epicentral zone. Along the lake shore, a minimum of 1 km spacing was maintained, and for 20 stations in the epicentral area, separations of 100 to 500 m were achieved. In the northeast sector, saprolite and rock exposures were limited to stream beds where the saprolite was fresh enough to preserve exposed joint surfaces. The shores of the reservoir provide nearly continuous saprolite or unweathered rock outcrops. Most stream outcrops were from 1 to 5 square meters, and had to be reached on foot. The precision of map coordinate measurement was 0.01 minute or approximately 20 m. Hence, stations located on distinct physiographic features such as points of land by the lake were located to within 20 meters. Those few stations on streams or unmapped roads, which were devoid of easily identified landmarks, allowed a precision that was about 50 meters. No corrections were made for magnetic deviation in location or in fracture attitude measurements, since the magnetic deviation of the study area was less than 1 degree, which is less than the precision of the measurements.

The primary goal of the field study was to obtain fracture spacing measurements distributed uniformly over the study area for the major joint sets. The criteria for the degree of variation of attitude within one set was

dependent on ability to accurately measure the perpendicular spacing measurement. Joints that intersect might be separated into two sets, while the same range of attitudes might fit in one set if attitudes vary smoothly across an outcrop. Usually a variation of 20 degrees about a mean is permitted within one set for both strike and dip, unless there are two distinct sets of parallel joints within that range. The average strike and dip of each joint set was divided into six groups based on azimuth and dip. The classification allowed independent examination of distinct joint sets and a comparison of them with rock quality, average intensity, trimean intensity, and fractil dimension.

Where attitude measurements were limited, usually a few attitudes could be measured to allow correction of joint spacings to the perpendicular. For 75 percent of the measuring locations, the outcrop allowed spacing to be measured perpendicular to the joint surface for each joint set. The resulting data set includes over 4000 spacing measurements. In vertical outcrops, usually only a few spacings of horizontal joints could be measured. Few sub-horizontal joints could be found in the horizontal outcrops.

FRACTURE AND ROCK QUALITY MEASUREMENTS

The fracture or joint intensity for a rock volume was determined by adding the intensities of each joint set. To minimize the effects of extreme values, the trimean measure of intensity was adopted. Trimean fracture intensity was computed directly from the inverse of the trimean spacing, where trimean spacing is the weighted average of the first quartile, the third quartile, and the median (Wheeler and Dixon, 1980) according to the equation:

$$I = \frac{1}{n} \sum_{i=1}^n I(i)$$

where $I(i) = 4/(S_1 + S_3 + 2S_2)$

for the *i*th joint set and,

S_1 - first quartile,
 S_2 - median spacing
 and S_3 - third quartile.

Fracture intensity can be used directly in the calculation of rock quality by using the system described by Barton et al. (1974). This system uses six parameters to describe the rock mass quality, *Q*. The parameters used in this study include; the number of joint sets (*J_{sn}*), the roughness, flatness, and continuity of the joint surface (*J_{rn}*), alterations of the joint surface (*J_{an}*), and the rock quality designation (*RQD*) computed from the fracture intensity. The ratio of the joint water reduction factor to the stress reduction factor in this study was taken as one to be compatible with near-surface conditions. Hence, in this study, rock mass quality *Q* was computed from,

$$Q = (RQD/J_{sn})(J_{rn}/J_{an})$$

where $RQD = 115 - 3.3I$, and where J_{sn} , J_{rn} , and J_{an} were estimated according to the scales presented in Barton et al. (1974). In this study, all subplanar open cracks were measured. Because Barton et al. (1974) considers only systematic through-going joints, the data needed to be adjusted. This was accomplished by use of high (1.5 to 2.5) joint roughness numbers for discontinuous, uneven, or extremely fine cracks. Since the surface rocks measured in this study varied from fine, discontinuous cracks to open, mineralized systematic joints, these four parameters serve as a correction for the variability in importance of the fractures in different types of rock. In this study of the variation in rock quality, Q should be a better measure of rock strength than fracture intensity.

Because the size and quality of the outcrops varied widely, a supplemental weighting for the data based on outcrop size and degree of weathering was developed. Although most features were evident in the unweighted data (Figure 4), the weighting of the data helped identify the erratic data of poor quality.

Rock types within five kilometers of inlet A (Figure 2) were in order of predominance, coarse grain granite, coarse and fine grain gray granite gneiss, layered and folded or contorted gneiss, and red clay saprolite derived from mica schist. Mafic dikes with an average thickness of one meter intrude these rocks. Ten stations had more than 25 percent of the measurements in pegmatite dikes or quartz veins, and two stations were entirely in quartzite. Three stations and three stream substations were in unweathered rock. Generally, joints would cut across granite, granite-gneiss, and gneiss equally when present in the same outcrop, but weathering of the gneiss or very coarse grain granite can form a surface crust that obscures fine fractures. These rocks dominate the immediate epicentral region, as well as the area across the lake to the southwest. Therefore, in this study area variations in joint intensity should be determined by factors other than rock type. Outcrops of highly decomposed mica schist that might be expected to fracture with a different intensity under identical conditions are found outside the study area. At stations where mica schist was found in the study area, systematic joints cross both rock types, but are much less noticeable in the mica schist. Stations where a red clay saprolite was found were not used in the trimean data and are given very low weights. The preferential appearance of unfractured rock in outcrops due to its resistance to weathering was considered as a potential source of bias. Although this could influence isolated outcrops, the continuous exposure of rocks along the reservoir shoreline provided data independent of rock hardness. In contrast, thin quartz veins or pegmatite dikes have either more fracturing or more easily recognizable fracturing than the country rock. Outcrops with thin quartz veins or pegmatite dikes generally have lower joint intensities. Although no adjustment for rock type was made, the spatial weighting of the large numbers of stations tend to smooth out local effects.

OBSERVATIONS OF JOINT SETS

The SE and NE striking near-vertical joints occur systematically throughout the Clarks Hill study area (Figure 2). Stream courses near inlet A are controlled by the SE and NE joint sets. The most planar and parallel joint set strikes SE between 110 and 140 degrees azimuth and the less important

strikes NE between 40 and 60 degrees azimuth (Figure 3). Bell (1973) has also shown NE and SE lineaments in the topography in the southern part of the study area, and the same trends in joint orientations. Bevis and Gilbert (1984) describe pervasive NE and SE striking conjugate joint sets in the southeastern United States. The regional nature of the major joint sets make it improbable that they are purely a near surface phenomena. The SE joint set is probably the oldest, as other sets abut against them and dikes are intruded parallel to the SE set in some outcrops. Generally, the SE set terminates against the NE set. The SE striking set is easily recognized because the joints that make up the set are very continuous, planar, and parallel. At CH37 this set has a 5 mm mineral coating, implying that they were more under tension than other orientations at the time of mineralization. In some cases subhorizontal microfaults offset vertical joints, while in others the subhorizontal surfaces of joints terminate against other joints. In both cases the subhorizontal joint surfaces are more recent, and may be related to unloading. Observations immediately after the 1974 event in this area revealed flaking or chipping of a crust that forms during weathering of some granitoid outcrops. This effect was not noticed during the 1987 study. Chipping is taken to represent surface movement on joints during the 1974-1975 activity.

RESULTS

For purposes of contouring the data, the value at each point in an evenly spaced distribution of points was estimated by a normalized weighted average determined from the product of the size and quality weight with the inverse of the square of the distance from measured outcrops. A 0.5 km spacing was used in this study and only outcrops within a radius of 1 km were considered in the weighted average. The weighted average smooths the local variations in fracturing and suppresses spurious values associated with smaller outcrops and lower quality rocks.

The raw data show scatter (Figure 4) and to evaluate the appropriateness of the data for contouring we computed its autocorrelation function (Figure 5). The variance of the trimean intensities is 18, but the non-random or correlated portion of this is about 12 suggesting an uncertainty of ± 2.3 and a spatial variance of 3.4. The autocorrelation distance is about 1.5 km. An autocorrelation distance of 1.5 km suggests that a data separation of 0.5 to 1.0 km would be sufficient to define the anomalies in this study area. The uncertainty of 2.3 suggests that a contour interval of 5 would be appropriate for this data. The gridded data have the same spatial variance of 12; however, the process of gridding has extended the autocorrelation distance to 2.0 to 2.5 km. The extension of the autocorrelation distance was influenced by the smoothing effects of areas of sparse data on the fringes of the study area, whereas the gridding process would retain the details of the densely sampled central area.

The trimean fracture intensity (Figure 6) shows areas of high and low intensity which generally follow the reservoir. Some of the low fracture intensities adjacent to high fracture intensity are related to the condition or size of the outcrops. The assigned weights for these stations were effective in suppressing the influence of the low quality and smaller outcrops in generating the concurred versions of the data. Some of the variability on a scale of less than 500 m is real and related to lithology or small scale

fracture zones or areas where different fracture sets cross. Examination of the data in its gridded format assumes that the variations on a scale of 10's of meters are not as important to the stress level that can be supported by the rock as are the variations on a scale of kilometers. We consider bulk strength on a scale of kilometers more important than local rock strength.

The contoured values of rock quality (Figure 7) show a large area to the east of the aftershock zone where fracture intensity is very low and rock quality high. A belt of more highly fractured rock extends to the west-north-west. The aftershocks of the August 2, 1974, earthquake occurred along the steep gradient in joint intensity separating the low intensity zone from the high-intensity zone. Low fracture intensities are also found to the south-east, but are based on sparse (two) data points with low weights. These two sites were also more highly weathered and the crusted boulders could have obscured some fractures. Outcrop condition was not a problem in half of the 14 outcrops that showed low fracture intensity near the epicentral zone. The contours of high fracture intensity tended to be elongated parallel to the SE striking fracture set. With the rock quality, (figure 7) a SE striking zone of low rock quality determination values follows the channel of the Savannah River in the reservoir. Rock quality, which uses average intensity, has slightly different contours than the trimean intensity. Where outcrops permit evaluation of Jrn and Jan, and if these evaluations are consistent, rock quality is a better indicator of rock strength. An example of the effect on rock quality occurs at stations CH47 and CH65, where intense but fine and sometimes discontinuous joints were measured. A Jrn of 2.0 caused the rock quality to be double what it would have been if the joints had been open, through, and systematic.

The trimean data (Figure 6) excluded the near-horizontal joint systems, because they are difficult to measure in many of the horizontal and flat outcrops. Since the data requirements were more severe for the trimean computation, these measures should be less dependent of outcrop quality. Generally, trimean intensities were about 25 percent higher than average intensities. This is explained by the suppression of a few large joint spacings by the trimean computation method. Station 4.1 was an example of the influence of widely varying joint spacing on joint intensity estimates. The trimean joint intensity will emphasize the weakest zones of the rock.

DISCUSSION

A key element in associating joint patterns with induced seismicity is verifying that the surface expression of joints extends to the focal depth of the earthquakes. Seeberger and Zoback (1982) showed that in 8 wells near the San Andreas fault in California, the fracture intensity is not dependent on depth in the upper 250 meters. Zoback and Hickman (1982) showed that intensity is only slightly dependent on depth for the upper 1100 meters near Monticello reservoir in the Piedmont of South Carolina. The geology of the Monticello area and the Strom Thurmond Reservoir area are similar and hence the joint intensity likewise in the study area would not be expected to vary significantly with depth. In contrast, the joint intensity of the subhorizontal joints may vary significantly with depth since the subhorizontal joints may have formed relatively recently in a compressive near-surface stress field. Schaeffer (1988) has reviewed evidence for joint intensity variations

with depth in the vicinity of the Bad Creek project, South Carolina, and found little variations in intensity to the 1000 m depths comparable to the hypocentral depths of the induced seismicity.

Although the lithology is variable in the study area, the discontinuities tend to strike NE and dip steeply, and much of the variation is between granitoid rocks of assumed similar rheology. The fact that the major trend in rock quality contours (Figure 7) trends SE, while the strike of most lithologic units is NE, suggests that regional fracture sets, and not lithology, most affects fracturing.

STATE OF STRESS

Focal mechanisms of the aftershocks of the McCormick earthquake were not consistent, with individual aftershocks often showing focal mechanisms that differed from previous events (Guinn, 1980). These include a low angle thrust for the main quake; EW striking sinistral faults, SE striking normal and dextral faulting, and low angle thrusting for aftershocks. A mixture of focal mechanism solutions and stress directions have been observed at other reservoirs in the S. Carolina Piedmont (Zoback and Hickman, 1982; Haimson and Zoback, 1984). Talwani (1977) reports that focal mechanism solutions favor a maximum horizontal compressive stress axis oriented NW at Lake Jocassee, while nearby hydraulic fracturing (Haimson, 1975) show it to be NE. The horizontal stress levels are typically high in the crystalline Piedmont rocks. Stress inferred in wells in Virginia (Rundle et al, 1985), and at Monticello Reservoir in South Carolina (Zoback and Hickman, 1982), show that the rock is near failure.

Reservoir induced seismicity is generally hypothesized to be related to the release of elastic stress due to loading, and to the increase in pore pressure reducing effective stress (Simpson and Narasimhan, 1986). Marion and Long (1978) suggest a process of pressure solution and mineral alteration weakening joints until failure occurs. Near the surface, the residual stress may be related to the formation of tension joints. These release residual horizontal stress (Price, 1966). The release of horizontal stress would contribute to a variable stress field related to fracture intensity. Highly fractured areas would be under a lower stress field, one more favorable to normal faulting than adjacent unfractured regions of low intensity or high rock quality. Hence, as suggested in this paper, rock quality may control the availability of stress for reservoir induced earthquake.

CONCLUSIONS

Aftershocks of the 1974 McCormick South Carolina earthquake near Clarks Hill Reservoir are spatially related to the border between relatively unfractured rock to the southeast and intensely fractured rock to the northwest. Seismicity occurred in areas of gneiss and granite, and not in mica schist, which is assumed not rigid enough to accumulate high stresses. The region of lightly fractured high quality rock will not deform at the same rate as intensely fractured rock, and so higher than average stresses were concentrated along the margin. Rock strength is lower in highly fractured areas, and so with a homogeneous stress field failure will occur there. Thus the largest shallow earthquakes should take place on pre-existing fractures in otherwise high quality rock.

Pressure solution along joints, or alteration of feldspars will weaken the strength of a fracture and accelerate the time of failure. Major through-going faults are not required in this model, although ancient faulting may influence fracture intensity. The dominant orthogonal joints are continuous enough to form fracture zones that could transmit hydraulic pressure pulses or be permeable, especially if in an orientation under tension in the current stress field, or if they were rebroken in the main quake. A combination of long term alteration in joints, yearly spring rises in lake level, rapid rise after heavy rainfall, and possibly infiltration of rain directly into joints could affect the timing of aftershocks here. The low recent level of seismicity means that most of the excess stress along the unfractured rock margin was released.

We conclude that induced earthquakes are unlikely to occur in unfractured crystalline rock, and unlikely to occur in the middle of a large area of low rock quality or otherwise weak rock. Therefore areas of intense fracturing in rigid rock adjacent to unfractured rock should be avoided in the siting of facilities that might be damaged by shallow focus local magnitude 4 to 5 earthquakes.

REFERENCES

- Angelier, J. and P. Mechler, 1977. Sur une methode graphique de recherche des contraintes principales egalement utilisable en tectonique et en seismologie: la methode des diedres droits, Bull. Soc. Geol. France, No. 6, 1309-1318.
- Angelier, J., 1979. Determination of the mean principal stresses for a given fault population, Tectonophysics, 56, T17-T26.
- Barton, N., Lien, R. and J. Lunde, 1974. Engineering classification of rock masses for the design of tunnel support, Rock Mechanics, 6, p. 189-236.
- Bell, H., III, 1973. Some results of geochemical sampling in McCormick county, South Carolina, Geological Survey Bulletin 1376.
- Costain, J.K., G.A. Bollinger and J.A. Speer, 1986. Hydroseismicity: A hypothesis for intraplate seismicity near passive rifted margins, Earthquake Notes, 57, 13.
- Costain, J.K., G.A. Bollinger and J.A. Speer, 1987. Hydroseismicity: a hypothesis for the role of water in the generation of intraplate seismicity, Seism. Res. Lett., 58, 41-64.
- Costain, J.K., G.A. Bollinger and J.A. Speer, 1987. Hydroseismicity: a hypothesis for the role of water in the generation of intraplate seismicity, Geology, 15, 618-621.
- Dunbar, D.M., 1977. A seismic velocity model of the Clarks Hill Reservoir area, Master Thesis, Georgia Institute of Technology, Atlanta, GA, 59 pp.

- Fogle, G.H., R.M. White, A.F. Benson, L.T. Long and G.F. Sowers, 1976. Reservoir induced seismicity at Lake Jocassee, northwestern South Carolina, Law Engineering Testing Co., Marietta, Georgia.
- Griffin, V.S., Jr., 1973. Geology of the Old Pickens Quadrangle, South Carolina, Publication MS-18, div. of Geology, S.C., State Development Board, Columbia, S. C., 54pp.
- Guinn, S.A., 1980. Earthquake focal mechanisms in the southeastern United States, Nureg/Cr-1503, 150 p.
- Haimson, B.D., 1975. Hydrofracturing stress measurements, Bad Creek Pumped Storage project, Report for Duke Power Company, 19pp.
- Haimson, B.C. and M.D. Zoback, 1978. A new look at the hydrofracturing stress measurements near the Monticello Reservoir, S. Carolina, EOS (Am. Geophys. Union Trans.), 65, No. 16, 278.
- Hatcher, R.D., Jr., 1987. Tectonics of the southern and central Appalachian internides, Annual Reviews of Earth and Planetary Sciences, v. 15, p. 337-362.
- Johnson, A.P., 1984. The Twiggs County earthquake swarm, Master Thesis, Georgia Institute of Technology, Atlanta, GA 125 pp.
- Jones, Frank B., L.T. Long, M.C. Chapman and K.-H. Zelt, 1985. Columbus, Georgia, earthquakes of October 31, 1982, Earthquake Notes, 56, No. 2, 55-61.
- Long, L.T., 1974. Earthquake sequences and b values in the southeast United States, Bull. Seism. Soc. Am., 64, 267-273.
- Long, L.T., 1976. Short-period surface wave attenuation and intensities in the Georgia-South Carolina Piedmont Province, Earthquake Notes, 47, 3-11.
- Long, L.T., 1979. The Carolina Slate Belt-Evidence of a continental rift zone, Geology, 7, 180-184.
- Long, L.T., 1982. Seismicity of Georgia, in Arden, D.D., Beck, B.F., and Morrow. Petroleum geology of the southeastern Coastal Plain, Americus, Georgia, March 5-6, 1979: Atlanta, Georgia Geologic Survey Information Circular 53, 202-210.
- Marion, G.E., and L.T. Long, 1980. Microearthquake spectra in the southeastern United States, Bull. Seism. Soc. Am., 79, 1037-1054.
- Price, N.J., 1966. Fault and Joint Development, Pergamon Press, London.
- Rundle, T.A., M.M. Singh and C.H. Baker, 1985. In situ stress measurements in the earth's crust in the eastern United States, final report, Engineers International, Inc., prepared for U.S. Nuclear Regulatory Commission, 75 pp.

- Scholz, C.H. and C.A. Aviles, 1986. The fractal geometry of faults and faulting, in Earthquake Source Mechanics, (eds. S. Das, J. Boatwright, and C. H. Scholz) Geophysical Monograph 37, American Geophysical Union, Washington, D.C. 147-155.
- Secor Jr., D.T., L.S. Peck, D. Pitcher, D. Powell, D. Simpson, W. Smith and A. Snoke, 1982. Geology of the area of induced seismic activity at Monticello Reservoir, South Carolina, J. Geophys. Res., 87, B8, 6945-6957.
- Seeberger, D.A., and Zoback, M.D., 1982. The distribution of natural fractures and joints at depth in crystalline rock, J. Geophys. Res., 87, 5517-5534.
- Simpson, D.W. and T.N. Narashimhan, 1986. Reservoir-induced earthquakes and the hydraulic properties of the shallow crust, (Abs.) EOS, Trans. Am. Geophys. Un., 67, 242.
- Talwani, P., 1976. Earthquakes associated with the Clark Hill reservoir, South Carolina - A case of induced seismicity, Engineering Geology, 10, 239- 253.
- Talwani, P., 1977. Stress distribution near Lake Jocassee, South Carolina, Pageoph, 115, 275-281.
- Talwani, P., D. Stevenson, D. Amick and J. Chiang, 1979. An earthquake swarm at Lake Keowee, South Carolina, Bull. Seism. Soc. Am., 69, 825-841.
- Wheeler, R.L. and J.M. Dixon, 1980. Intensity of systematic joints: Methods and application, Geology, v. 8, 230-233.
- Wong, Po-zen, 1988. The statistical physics of sedimentary rock, Physics Today, v 41, no. 12, 24-32.
- Zoback, M.D. and S. Hickman, 1982. In situ study of the physical mechanisms controlling induced seismicity at Monticello Reservoir, South Carolina, J. Geophys. Res., 87, B8, 6959-6974.

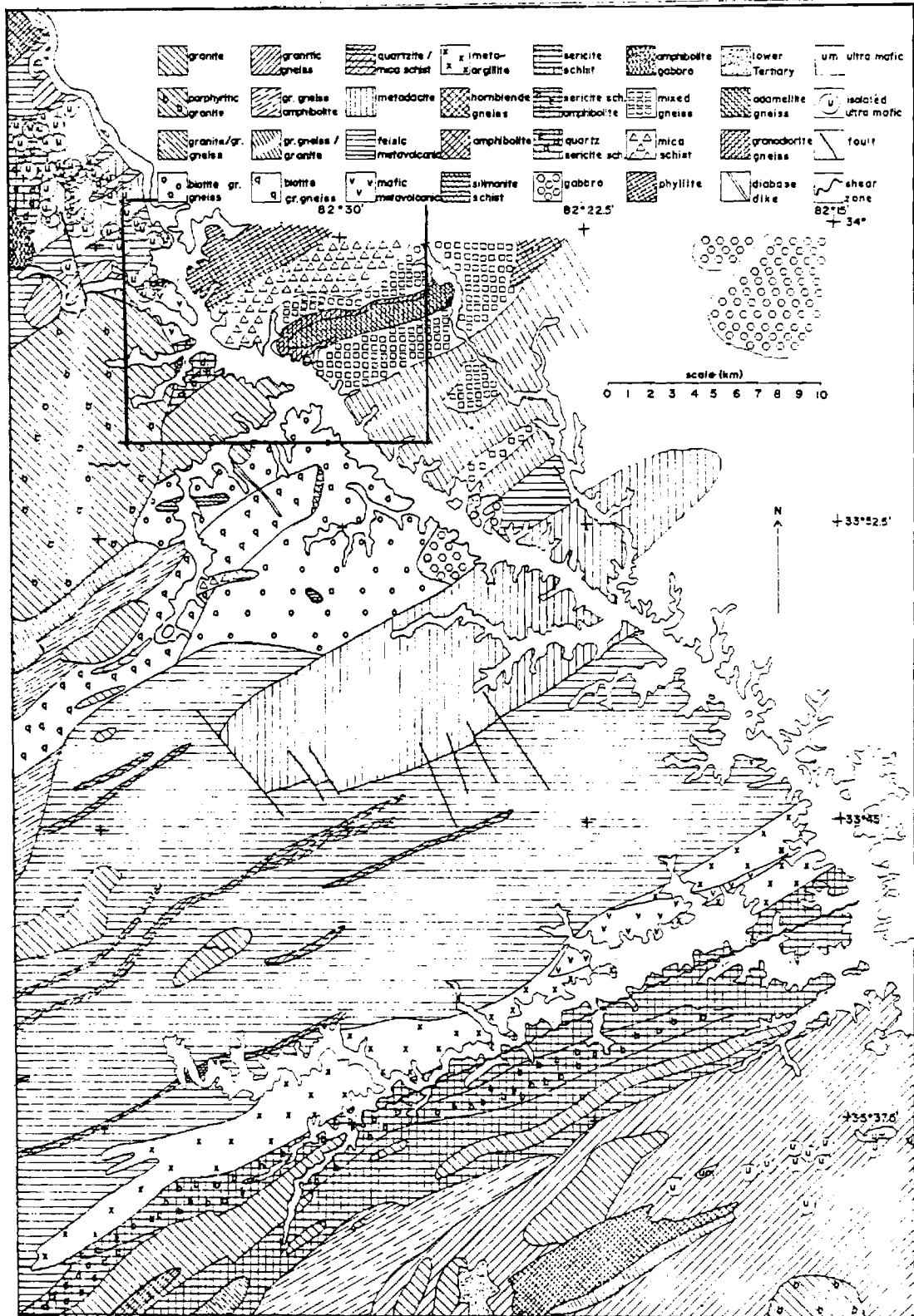


Figure 1. Location map for area of joint measurements in the Clarks Hill Reservoir. Geology abstracted from Griffin (1973).

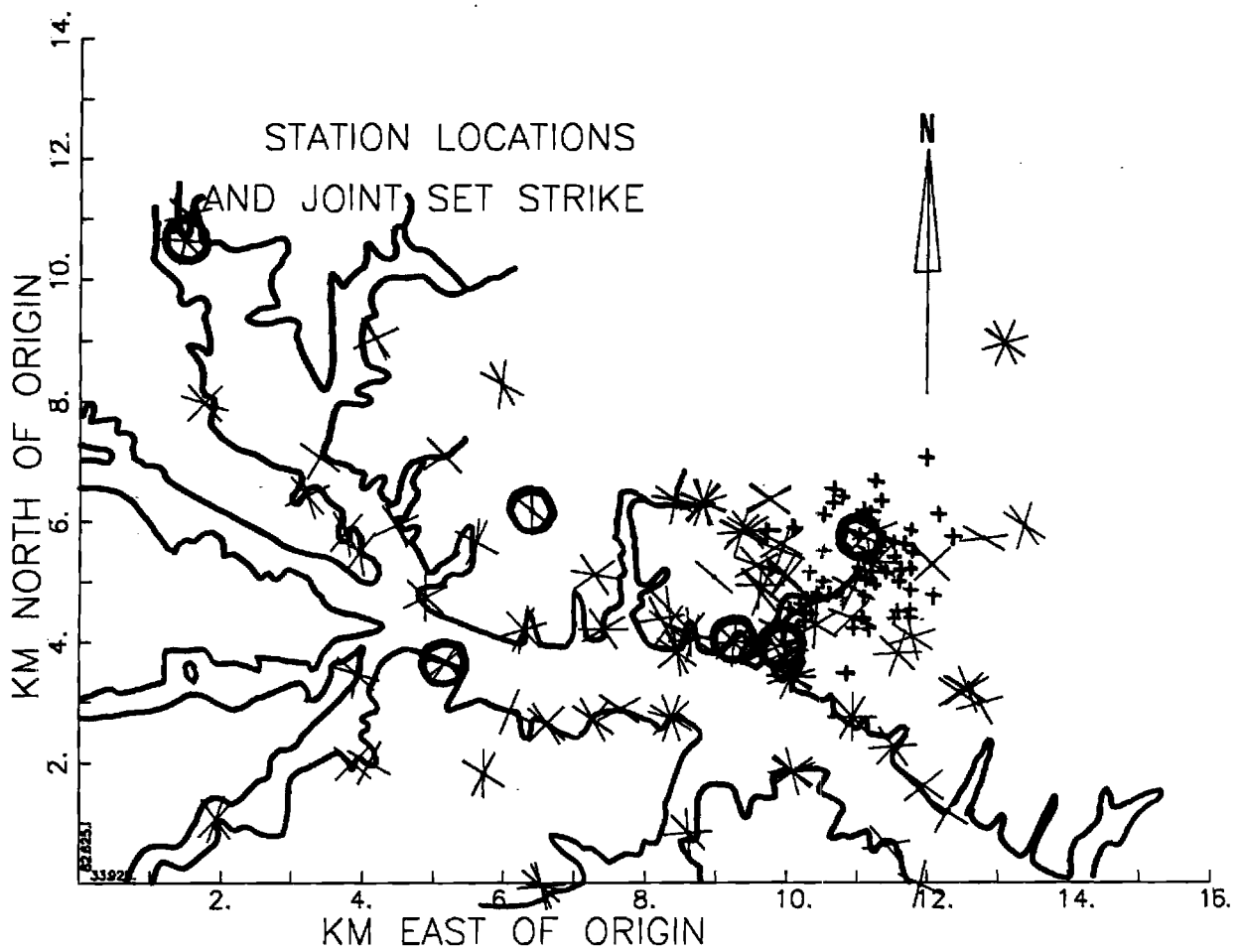


Figure 2. Outline of the study area showing station locations and joint directions. Small crosses are the epicenters of earthquakes from Dunbar (1977). Origin is 33.925 N, 82.625 W.

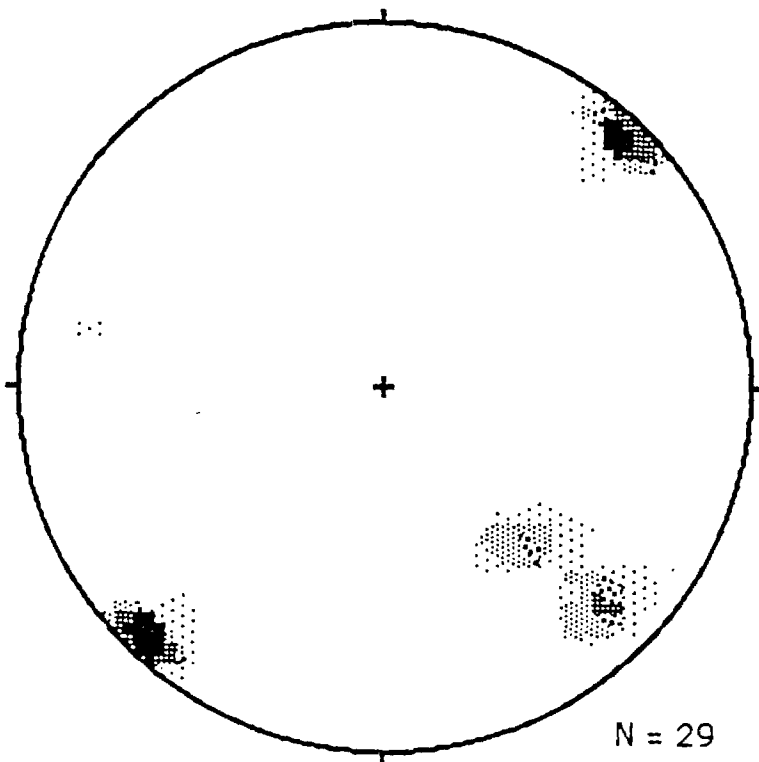
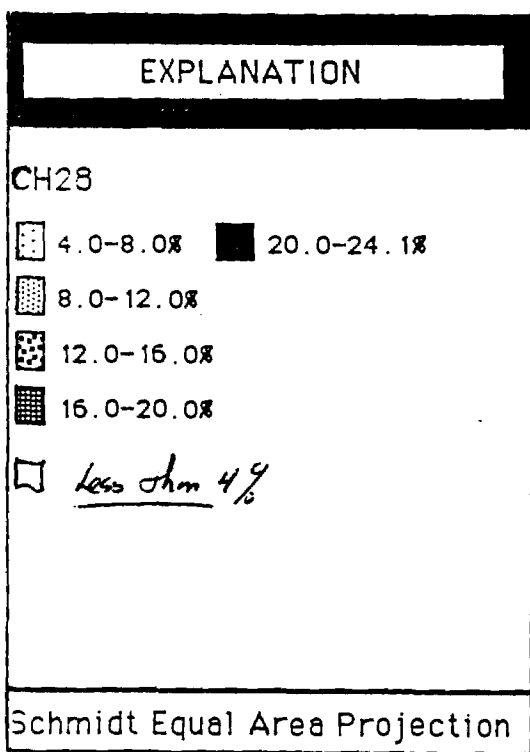


Figure 3. Joint pole plot for station ch28 showing dominant joint set for the Clarks Hill Reservoir.

AUTOCORRELATION OF TRIMEAN INTENSITY
SETS DIPPING MORE THAN 45

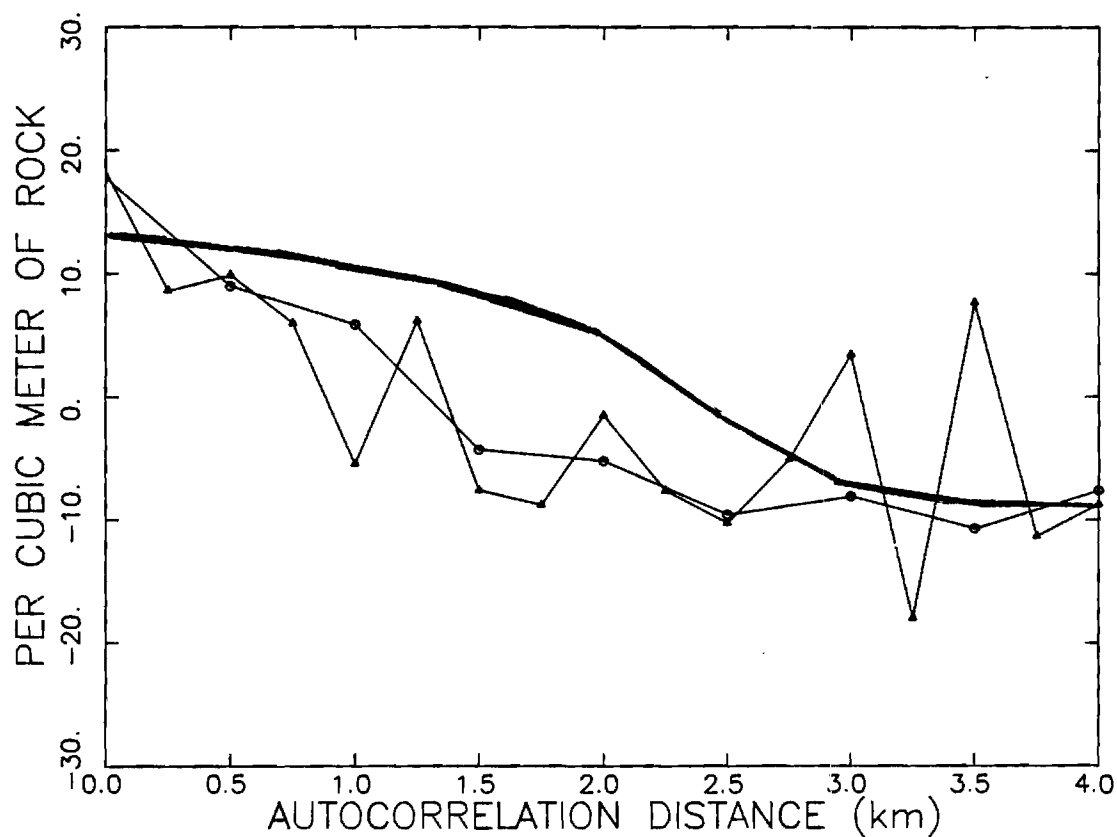


Figure 5. Autocorrelation of the trimean intensity data at separation distances of 0.5 and 0.25 km. Heavy line is autocorrelation function for the gridded data.

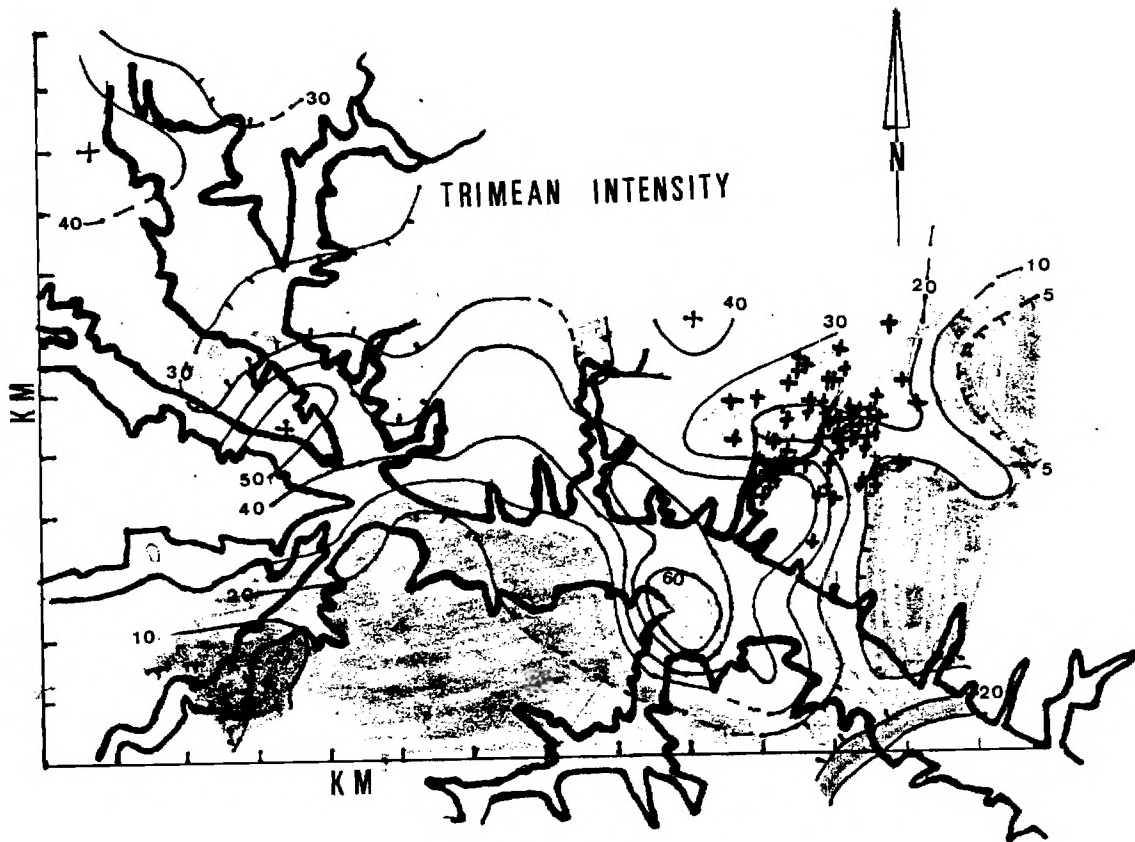


Figure 6. Contoured map of the trimean fracture intensity. The crosses indicate locations of epicenters.

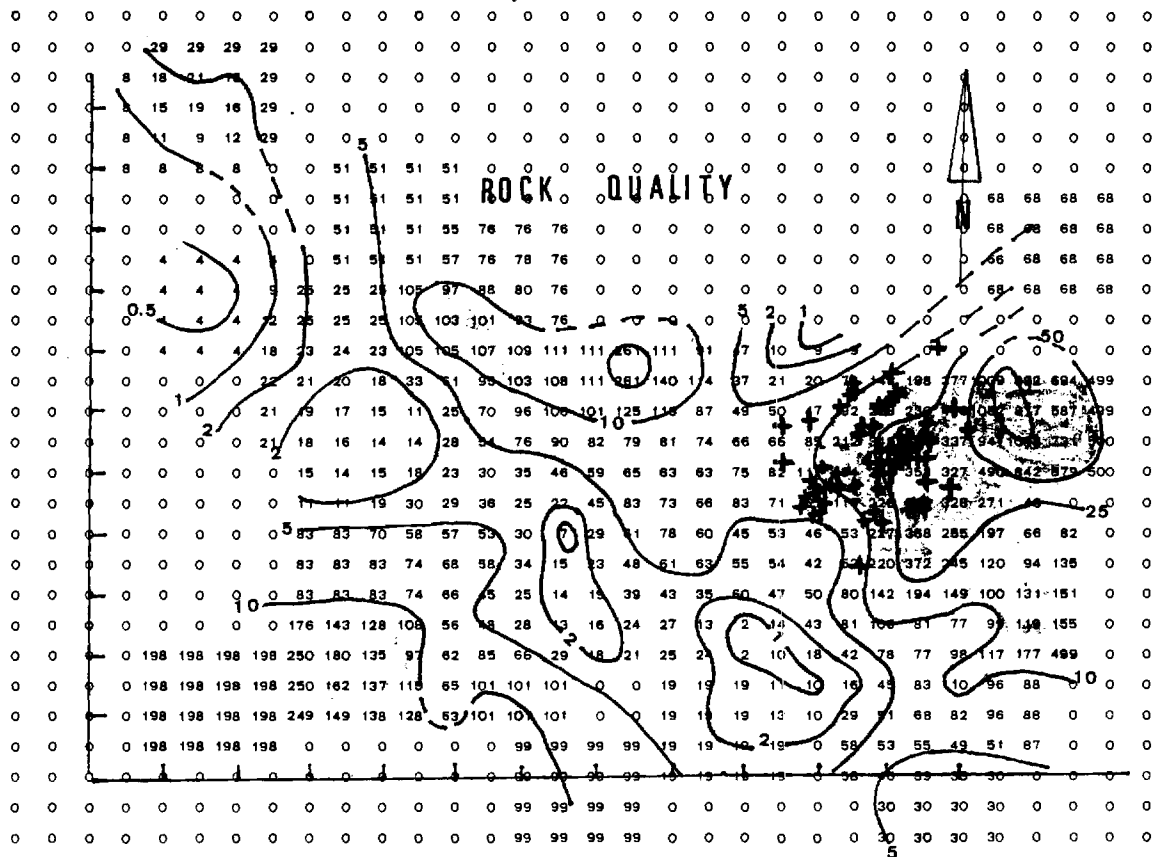


Figure 7. Contoured map of Rock Quality. The crosses indicate locations of epicenters.

APPENDIX D

Relocation of Earthquakes in the Lake Sinclair Reservoir Area

APPENDIX D

RELOCATION OF EARTHQUAKES IN THE LAKE SINCLAIR RESERVOIR AREA

Wilbur Edward Radford, Jr, and Leland T. Long

ABSTRACT: One hundred and eighty-nine earthquakes in the Lake Sinclair and Lake Oconee areas of central Georgia were located. The epicenters were computed with a technique designed to reduce reading error and inconsistency in the data by separating the origin time computation from the epicenter computation. The small separations among stations did not allow computation of focal depths. With respect to previous locations, the epicenters exhibited significant reduction of scatter and defined four distinct clusters of events in the Lake Sinclair area. The area of the average error ellipse for the relocations was 0.10 square kilometers. The clusters are centered on or near the body of Lake Sinclair. The travel-time residuals for the relocated epicenters were increasingly negative for stations greater than 20 km distant from the epicenters. A two-layered velocity model was developed to explain the travel times for stations at distances greater than 20 km. The Model consists of the observed 6.0 km/s surface layer of thickness of 2.37 km above a layer with a P-wave velocity of 6.6 km/s. Shear wave velocities were determined from Poisson's relation. The two-layered model reduced the area of the average error ellipse for the relocations from 0.11 km² to 0.10 km².

INTRODUCTION

The seismicity of central Georgia is contained within a circle of radius 75 km centered on Milledgeville, Georgia (see Figure 1). The seismicity is moderate and includes historic events as large as 4.9 m_bLg. The larger historical earthquakes have been documented by Allison (1980). The impoundment of Lake Sinclair in the 1950's and the continued sporadic seismicity in central Georgia, along with occurrences of reservoir-induced seismicity at the Jocassee and Monticello reservoirs in South Carolina, raised the possibility that the Lake Sinclair seismicity is reservoir-induced and increased concern that the new reservoir, Lake Oconee, would induce significant activity. Because of this concern, the seismicity was closely monitored during the impoundment of Lake Oconee by Wallace Dam in 1977.

The impoundment of Lake Oconee by Wallace Dam was followed by only a few small events and significant reservoir-induced seismicity was not triggered. Natural seismicity before the lake was impounded consisted of the historical events and one prefilling event of magnitude 1.4. A post-filling swarm of earthquakes with magnitudes between -0.3 and 0.8 occurred in May 1980. The swarm showed no single outstanding event and did not precede a larger event as in the usual case of earthquake swarms near Lake Sinclair. Most of the events in the Lake Oconee swarm occurred in a tight spatial cluster. The majority of the seismicity in central Georgia occurs in the Lake Sinclair area (LSA). Spatial distribution of the epicenters with respect to Lake Sinclair and the characteristics of LSA swarms suggests possible reservoir-induced seismicity. However, the existence of significant pre-impoundment earthquakes suggests a natural explanation for seismicity.

The epicenters of Lake Sinclair events occur in clusters (Allison, 1980); however, scatter in those clusters does not allow the identification of sub-clusters or alignments within the clusters. The events were recorded on analog pen-and-ink recorders. A few were recorded on analog tape. The arrivals and phases were picked by different persons. As a result, considerable inconsistency may exist in the P and S arrival times. Such variations in precision could account for much of the scatter in the epicentral distribution. Also, the local velocity model was determined for the Lake Oconee Area (LOA) where the station-to-epicenter distance ranged from ten to twenty kilometers. This velocity model may cause problems with the location of the Lake Sinclair events because the velocity model was not defined for distances greater than twenty kilometers. The object of this study has been to reduce the scatter in the data by relocating the events. The possible inconsistency in the reading has been minimized by reevaluating all phases. Events occurring after Allison's (1980) study have been added to the catalog. Consistency in readings have been further checked by separating the origin time computation from the epicenter computation. A reduction of scatter would reveal clusters or other patterns that might suggest possible causes of the seismicity in this area. The re-evaluation of the velocity model would aid in understanding geologic units in the crust.

WALLACE DAM NETWORK AND SEISMIC RECORDING

Earthquakes for this study occurred in the Lake Sinclair and Lake Oconee areas between longitudes 82.8° and 83.6°W and latitudes 32.9° and 33.5°N (see Figure 2). The earthquakes were recorded by the Wallace Dam Seismic Network (WDN) which became operational in June 1977 under a commission from the Georgia Power Company. Although the network was implemented in order to monitor the Lake Oconee area, the network also provided coverage for Lake Sinclair through the addition of station ETG (see Figure 2) under a commission from the Nuclear Regulatory Commission. The detection threshold for the Lake Sinclair and Lake Oconee areas was magnitude -0.3.

From June 1977 through May 5, 1980, 167 events were recorded by the Wallace Dam Network. Of these, 135 were located in the Lake Sinclair area. These earthquakes made up the data base that was used in the initial report of the monitoring by the Wallace Dam Network (Allison, 1980). The majority of the seismic activity occurred in the Lake Sinclair area. The Lake Sinclair seismicity has two major concentrations of events. The largest of these is centered at 33.24°N, 83.29°W and contains the majority of all recorded events. The uncertainty in the locations makes it impossible to determine clusters on a smaller scale within the two major concentrations of events. One of the goals of this study is to reduce the epicentral uncertainty in order to better define the areas of concentrations of these events.

The arrival times for Allison's (1980) locations came directly from the WDN log books. These books were maintained by different graduate students over a period of four years and the interpretation and recording of the data could vary systematically. This introduces the uncertainty of inconsistent precision in the P- and S-wave arrivals used in the locations. P and S arrivals from a microearthquake can be picked to a precision of ± 0.1 seconds when the event is recorded at 1 mm/s as on ink and paper recorders. Figure 3 shows typical LSA events that were recorded with ink on paper. The traces vary from

having strong, clear P and S arrivals to having barely discernible arrivals. Different individuals may have different interpretations on the latter. To guarantee consistency in this study, all the records were reevaluated and a magnifying lens was used to facilitate a 0.1 s precision. The resulting P and S arrivals for 189 events were used for the relocations in this study. The 189 events include most of Allison's (1980) events and 22 previously unlocated events.

RELOCATION TECHNIQUE

The previous locations were found using an iterative, least-squares error minimization based on the method introduced by Geiger (1910). The

algorithm solves a set of equations of the form:

$$b' = A'dp \quad (1)$$

where for n observations, A' is the $n \times 4$ matrix of the partial derivatives with respect to T (origin time), x (longitude), y (latitude), and z (depth) of the travel times from a trial hypocenter, b' is the n -length vector of observed minus theoretical travel times for individual phases and dp is the four-dimensional vector representing a correction in time, latitude, longitude and depth of the trial hypocenter. The problem is to find $dp = (dT, dx, dy, dz)$ such that the length of $A'dp - b'$ is minimized (Boyd and Snoke, 1984) in the least-squares sense.

For a closely spaced network such as the WDN, influence of the variation in velocity within various geologic units is assumed to contribute the same uncertainty at each station. However, events that have both P and S phases recorded at the same station would be expected to exhibit a correlation between the residuals and have a correlation between the standard deviations of the residuals. In this study, the correlation of the P- and S-wave residuals is used to develop an alternate method for separating the origin time computation from the hypocenter computation. In this method, the seismograms that have readable P and S arrivals are separated from observations that have only one readable arrival in order to compute the origin time. This origin time is then fixed and we solve for the parameters of the epicenter by using all the observations. With the reading precision of 0.1 seconds, the origin times are typically precise to less than 0.2 seconds. Because the distances were short and velocity anomalies were lacking in the area, origin times in error by more than 0.2 seconds are considered mispicked phases. The assumed mispicked traces were re-examined and origin times were recomputed. This was repeated until the best possible picks were obtained for the P and S arrivals. As a result of this quality control in identifying phases, the standard deviation of the origin time is generally less than 0.2 s.

RELOCATIONS

The initial velocity model used for relocations in this study was the same as that used by Allison (1980). The P-wave velocity of 6.0 km/s and the S-wave velocity of 3.43 km/s were determined in a refraction survey completed for the Lake Oconee area by Allison (1980). Records from smoked-paper seismographs deployed before the implementation of the WDN indicated shallow events

(Allison, 1980). Thus, the depth for each relocation was constrained to 0.5 km.

The distribution of the relocated epicenters suggests five clusters designated A through E in Figure 4. Clusters A, B, and C were the main concern of this study. Scatter has been reduced by relocation most significantly in Cluster A. This reduction allowed part of this cluster to be separated as another cluster (d) centered approximately 6 km southwest. Felt reports from recent events give epicenters between these clusters. Because this data set represents only four years of seismic coverage out of twenty three years of suspected reservoir-induced seismic activity in central Georgia, clusters A and D may be part of a larger cluster. The relocated epicenters of cluster B are more concentrated near the center of the cluster than they were prior to relocation.

The most notable difference generated by relocation is the shifting of certain epicenters from the main cluster to a cluster near the westernmost branch of Lake Sinclair. It was discovered while reexamining the original records that these events were located using only arrivals from station ETG and REG. This fact, along with the geometry of the locations of these stations, allowed solutions for epicenters in cluster A or in cluster C. The travel-time data alone provide insufficient criteria to distinguish the correct epicenters. To establish correct epicenters, all events in this category were relocated again. Because location are determined by a least-squares minimum in residual travel times, certain combinations of stations and locations may possess multiple minima. In the case of cluster A, the location process will find the minimum closest to the initial guess. Therefore, events in this category were relocated using first guesses corresponding to each cluster. Most of these events remained in cluster A. The records of the remaining events were reexamined for evidence for arrivals at stations WDG and GBG. The phases at these two stations were weak compared to events definitely located in clusters A or D. The weakness of the signals was interpreted to mean that the sources of these events were located at a greater distance from the recording station than from both stations ETG and REG. Thus, these events were relocated in cluster on the basis of signal amplitude. The dimensions of cluster C are poorly defined and the cluster is not dense.

VELOCITY ANALYSIS

With the origin time computation removed from the epicenter computation, the errors associated with the epicenters were small. Considering only latitude and longitude, the average error ellipse for events that had P and S phases recorded on three or more stations is 0.11 square kilometers compared to error ellipses of 1.15 square kilometers prior to relocation. The residuals for the P arrivals are plotted versus azimuth in Figures 5 and 6. The mean residuals are consistent with the reading error of 0.1 s for each station. Thus, no obvious corrections would be expected to m=improve the arrival times. It is interesting to note, however, that the averages of the residuals shown in Figure 5 for stations ETG and WDG are slightly positive while the averages of the residuals shown in Figure 6 for stations REG and GBG are slightly negative. Since the majority of the LSA events are located in cluster A, one can consider that stations REG and GBG are greater than 25 km from the cluster while stations ETG and WDG are less than 25 km from the cluster.

This suggests that the crustal velocities used in the relocations may be too large for the close-in stations and too small for the distant stations.

The original velocity survey (Allison, 1980) was obtained for distances of only up to 20 km. The mean P residuals for cluster A events that were recorded on all four stations are plotted versus station distance in Figure 7. The residuals become increasingly negative beyond 20 km. Because the residuals were computed with a constant velocity of 6.0 km/s, the increasingly negative residuals for stations beyond 20 km indicate that a velocity of 6.6 km/s would be necessary beyond 20 km to obtain a zero residual. Because the mean P residuals are essentially constant for stations ETG and WDG and drop off rapidly for stations REG and GBG, a two-layered model was adopted for this study. The 6.0 km/s velocity of the near-surface layer was defined by Allison's (1980) refraction survey. The slope of the mean P-wave residual arrival times for the three more distant stations define a velocity of 6.6 km/s \pm 0.2 and a zero-distance intercept of 0.2 seconds. Figure 8 shows the resulting mean P residuals for a relocation of all events using the two-layered model. This model reduced the area of the average error ellipse from 0.11 square kilometers for the half-space model to 0.10 square kilometers for the two-layer model computed from events of cluster A recorded on 4 stations.

Figure 9 shows a detailed Bouguer map of the LSA (O'Nour, 1982). The positive anomalies exceeding +20 mGals and sharp gradients (near REG and GBG) indicate that shallow, mafic rocks underlie much of the LSA. For a crossover distance of 20 km, the two-layered model gives a high-velocity medium at 2.4 km depth. A velocity of 6.6 km/s as indicated by Figure 7 would be consistent with the hypothesis that the area is underlain by a fragment of high velocity (oceanic ?) crust as shown in Figure 10. The reduced travel-time plot for the two-layered model is also shown in Figure 10. Relocations using a two-layer velocity model are shown in Figure 11. Cluster A is slightly tighter and the Lake Sinclair clusters are shifted 2 to 3 km southward. The improvement in the epicentral distribution is more evident for events of magnitude greater than 0.7. One should note the further separation of cluster D from cluster A and the tightening of cluster D.

DISCUSSION AND CONCLUSIONS

The efforts of this study can be divided into four major results. First, the events of the Lake Sinclair area have been systematically reviewed for accuracy and consistency. Second, the scatter of the epicenters has been reduced relative to those based on the original data. This reduction has allowed the identification of four distinct clusters in the Lake Sinclair area; however, the reduced scatter did not reveal any evidence in the form of linear trends that would suggest an active fault. Third, the epicenters are close to the lake suggesting that fluid penetration, related to the reservoir, is a factor in the triggering of these earthquakes. The historical pre-reservoir events suggest a natural cause. Hence, the cause of this seismicity may be a combination of reservoir-induced seismicity and release of natural stresses. Fourth, the seismic arrival times were used to develop a velocity model for the Lake Sinclair area. The model consists of two layers, a shallow 6.0 km/s layer and a 6.6 km/s half-space below 2.4 km. Gravity data also suggest the presence of dense material at shallow depths under much of the Lake Sinclair and Lake Oconee areas.

REFERENCES

- Allison, J.D., 1980. Seismicity of the Central Georgia Seismic Zone, Master's Thesis, Georgia Institute of Technology, Atlanta, GA 30332.
- Boyd, T.M. and J.A. Snoke, 1984. Error estimates in some commonly used earthquake location programs, Earthquake Notes, 55, 3-6.
- Geiger, L, 1910. Herdbestimmung bei Erbeben aus den Arnkunftszeiten, K. Geseau. Wiss. Gott., 4, 331-349.
- Long, L.T., 1982. Seismicity of Georgia, in Arden, D.D, Beck, B.F., and Morrow, E., eds., Proceedings of the second Symposium on the Geology of the southeastern Coastal Plain, Americus, Georgia, March 5-6, 1976: Atlanta, Georgia Geologic Survey Information Circular 53, pp. 202-210.
- O'Nour, I.M., 1982. Gravity Anomalies in Central Georgia. Master's Thesis, Georgia Institute of Technology, Atlanta, GA 30332.

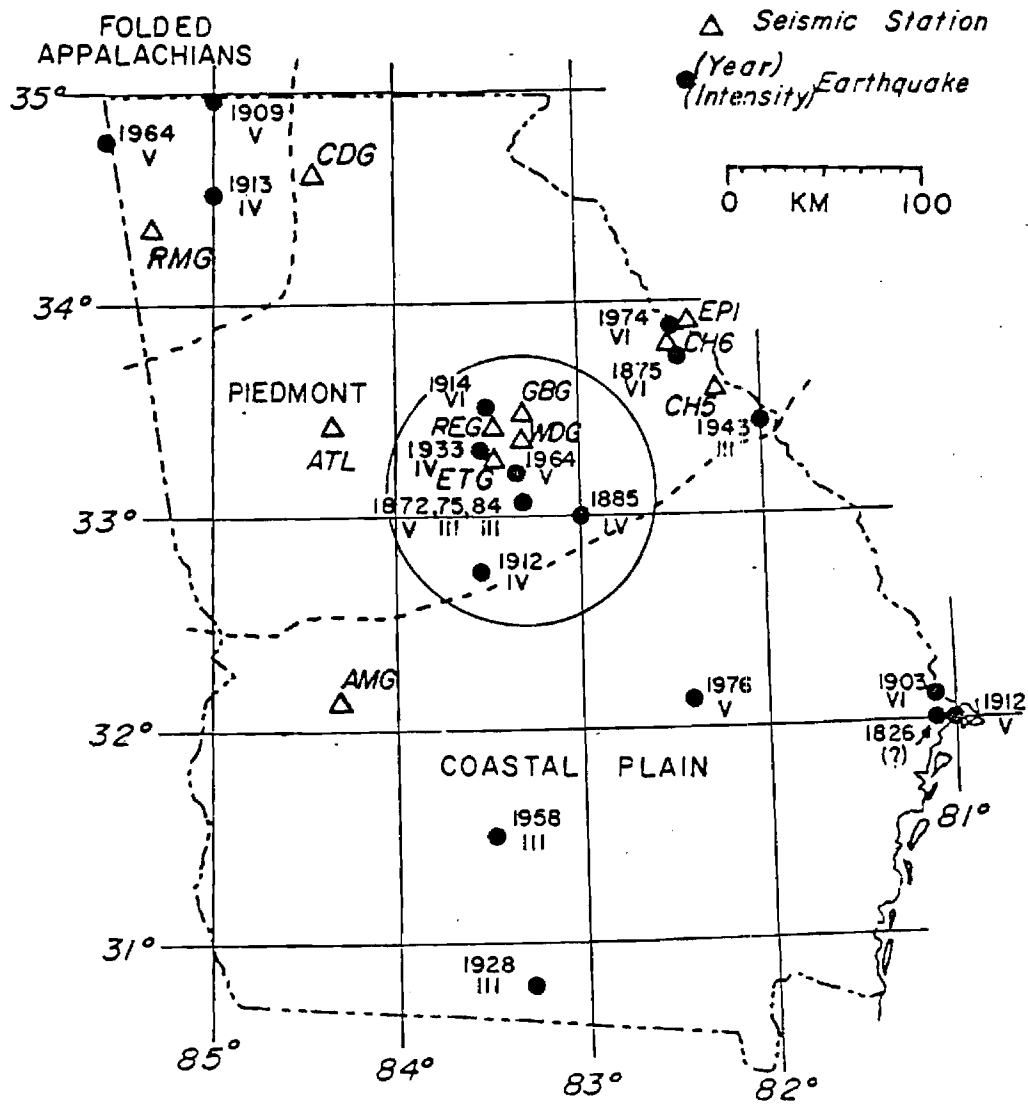


Figure 1. Historical Seismicity of Central Georgia (after Long, 1982).

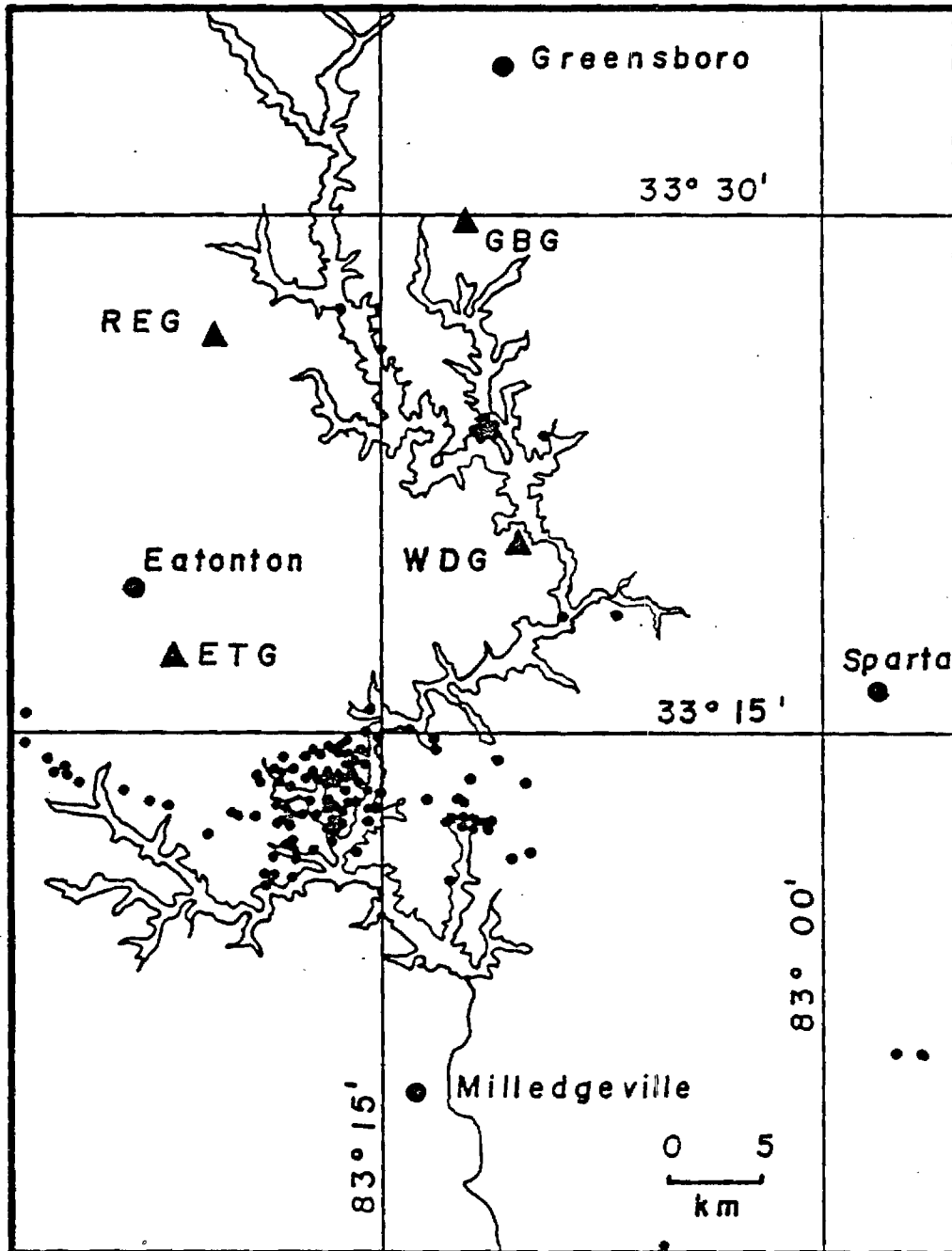


Figure 2. Locations of events in the Lake Sinclair and Lake Oconee Areas (from Allison, 1980).

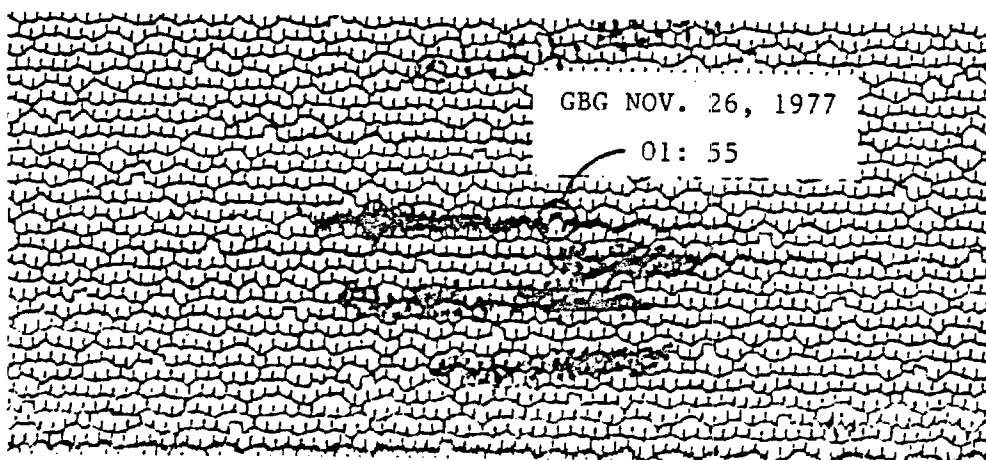
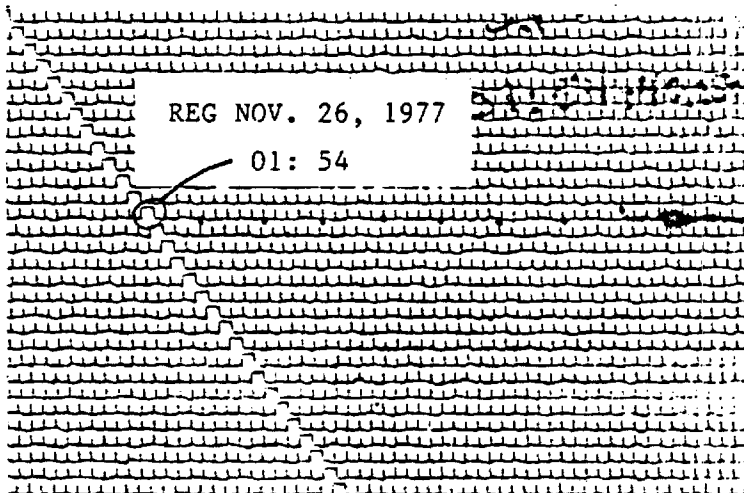
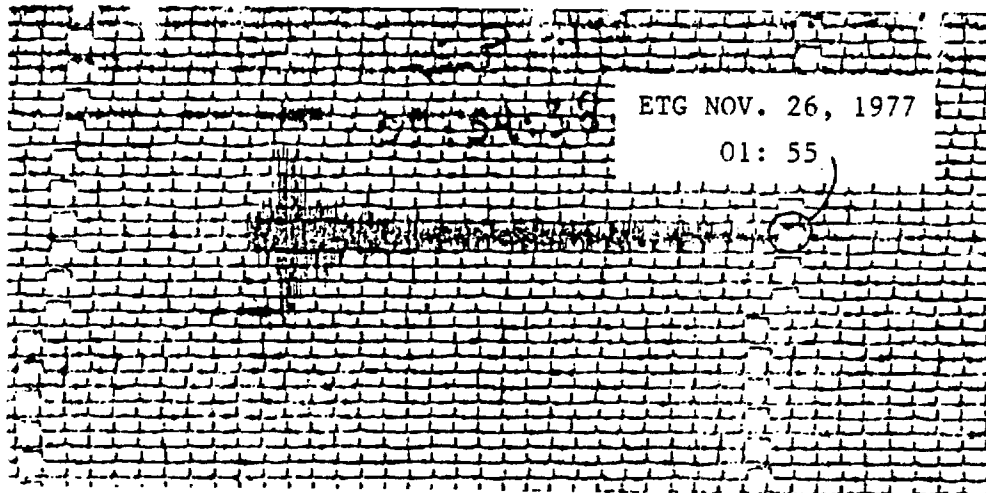


Figure 3. Typical traces of Lake Sinclair events.

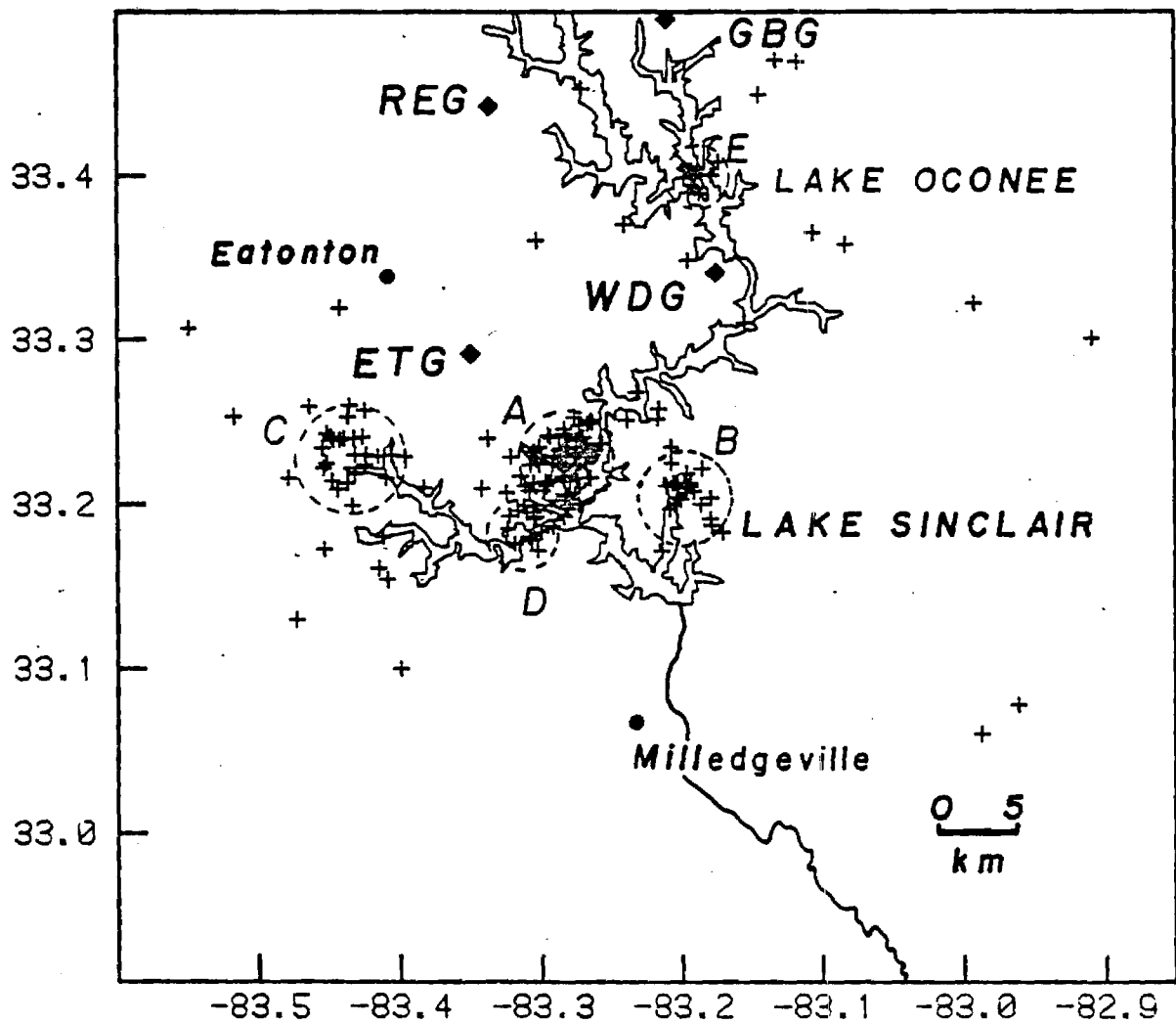


Figure 4. The 189 relocated epicenters of the Lake Sinclair and Lake Oconee areas. Dashed circles identify clusters A through E.

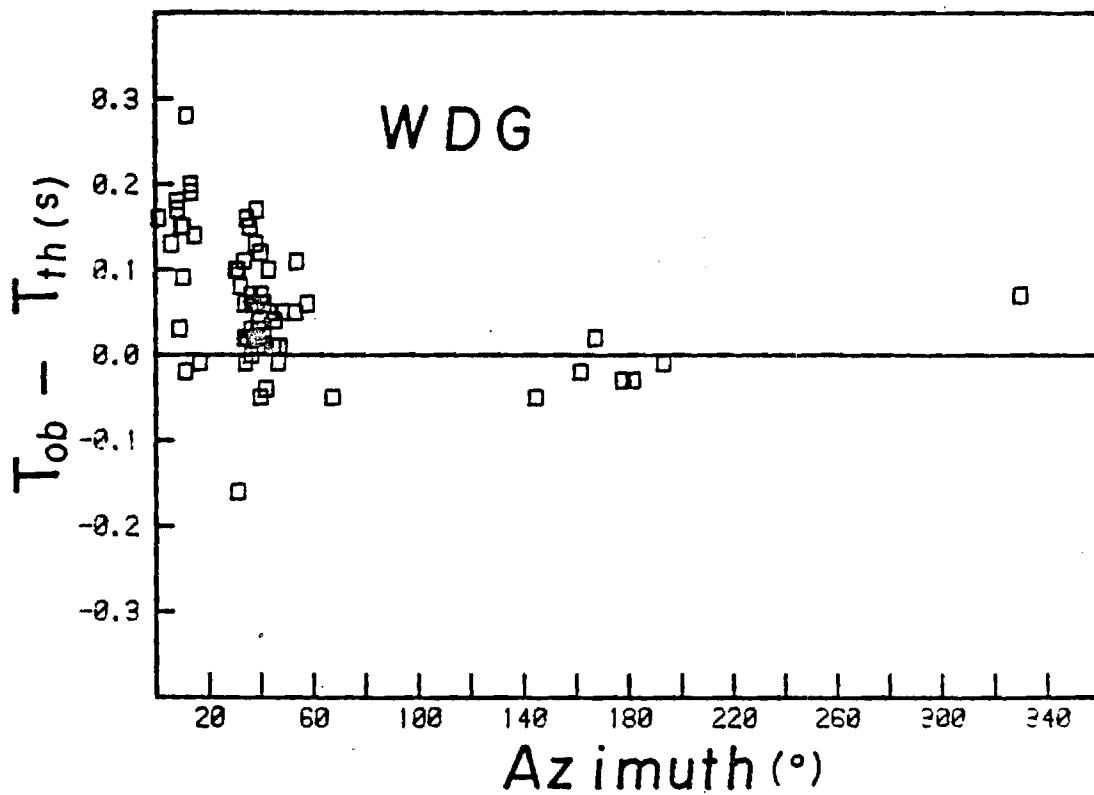
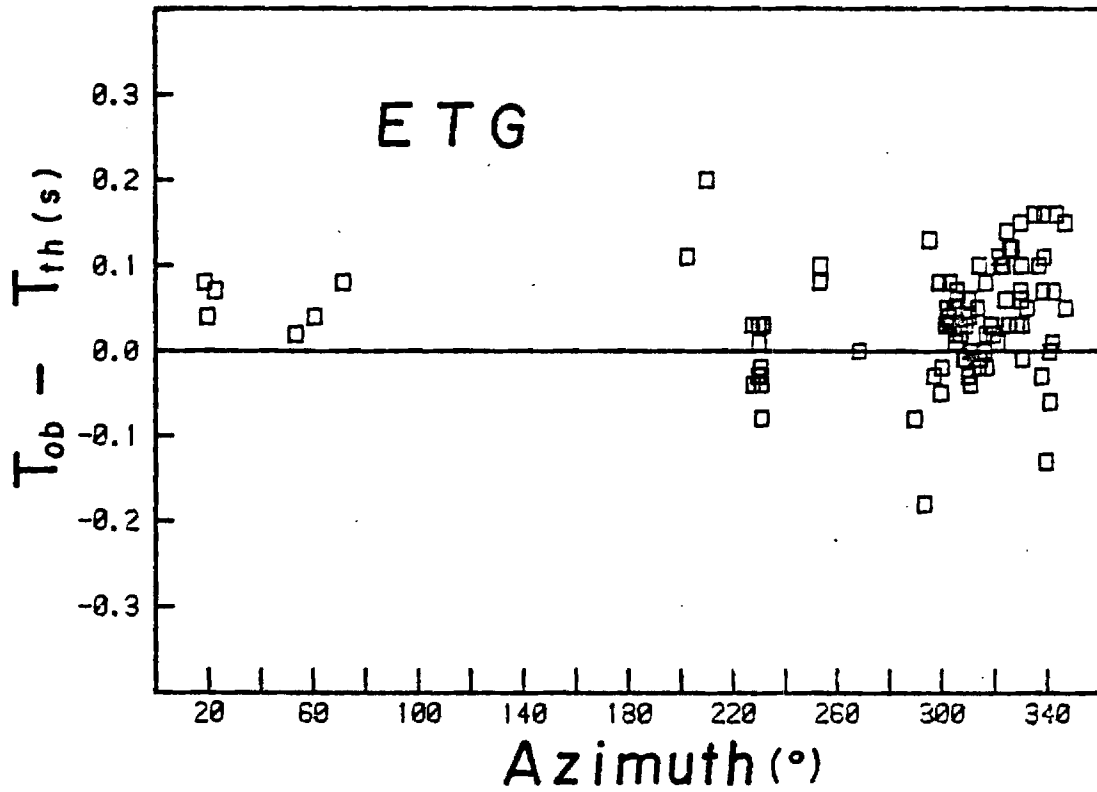


Figure 5. P-wave travel-time residuals for stations ETG and WDG plotted versus azimuth.

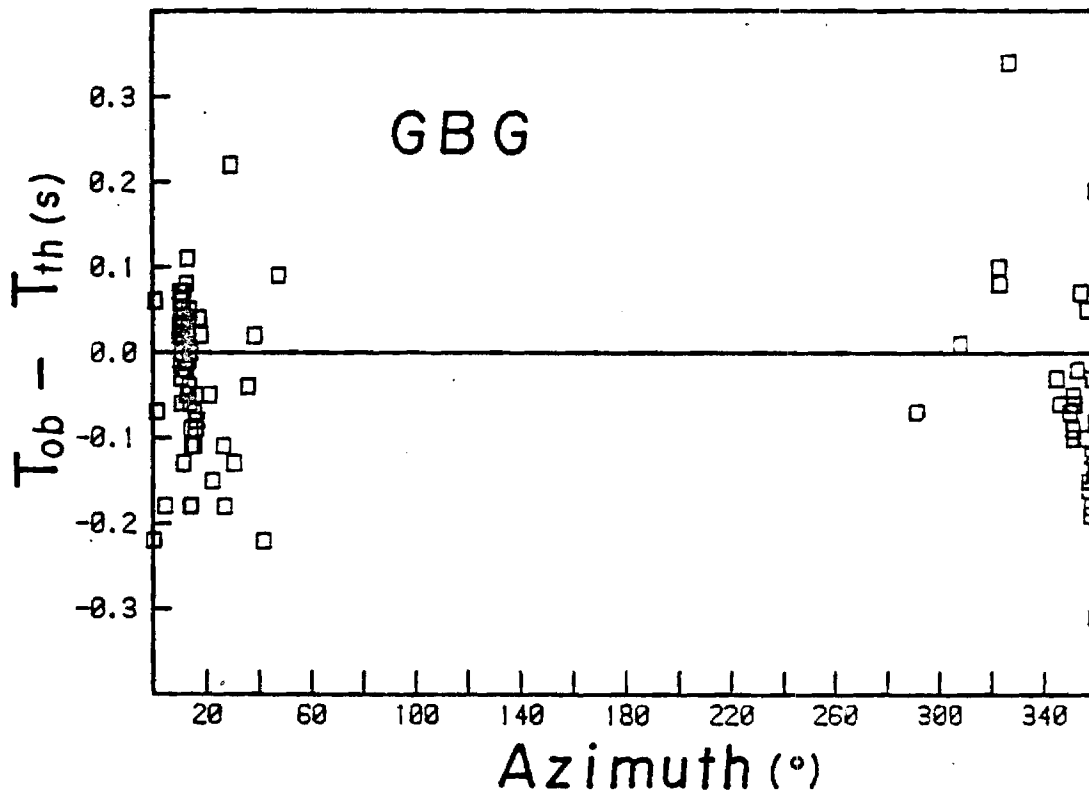
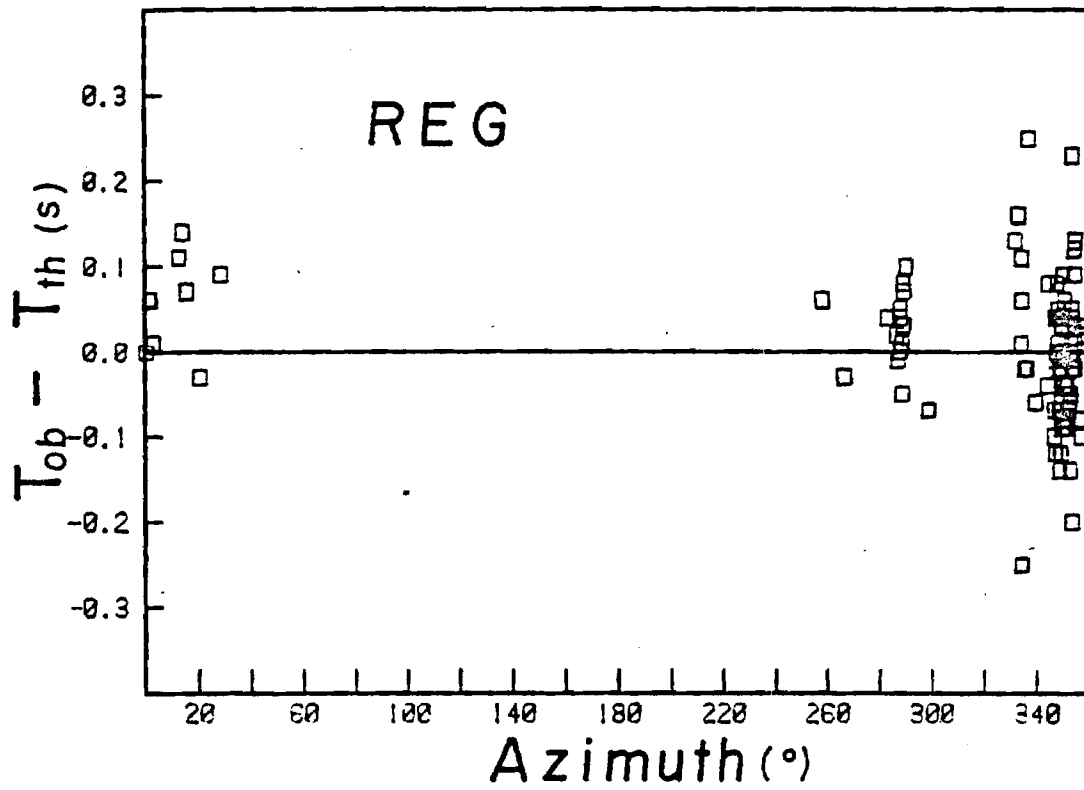


Figure 6. P-wave travel-time residuals for stations REG and GBG plotted versus azimuth.

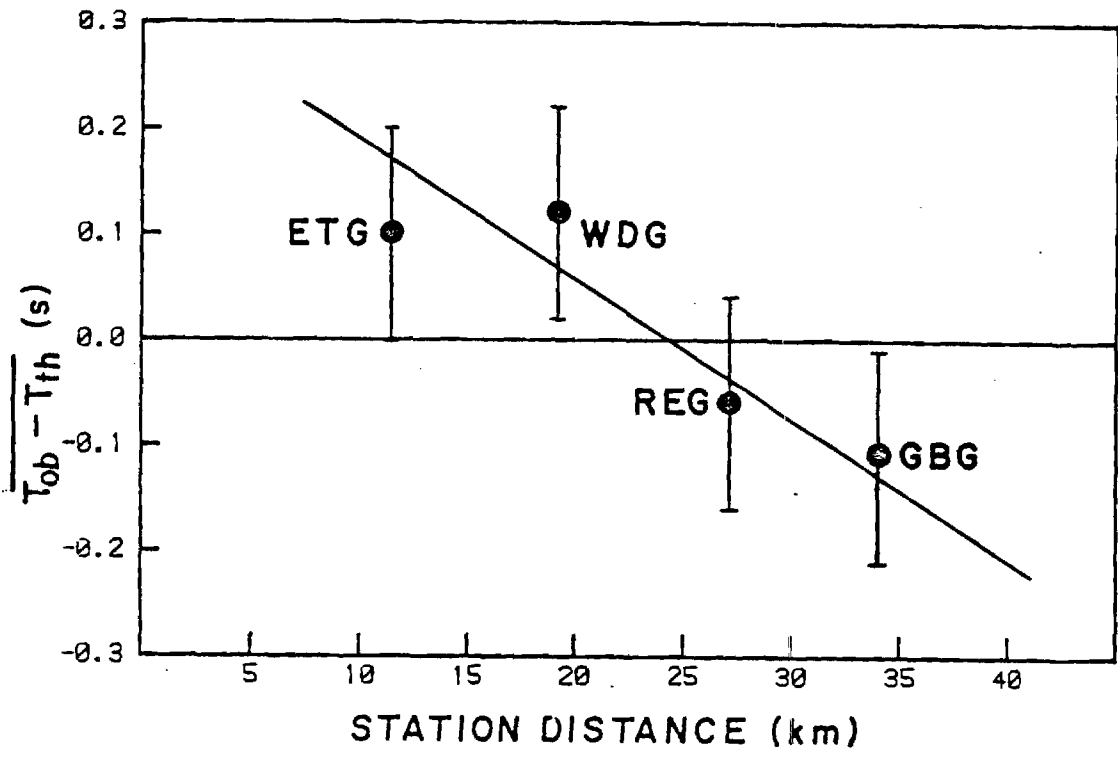


Figure 7. Mean P-wave residuals from a constant velocity model for cluster A events that were recorded on four stations.

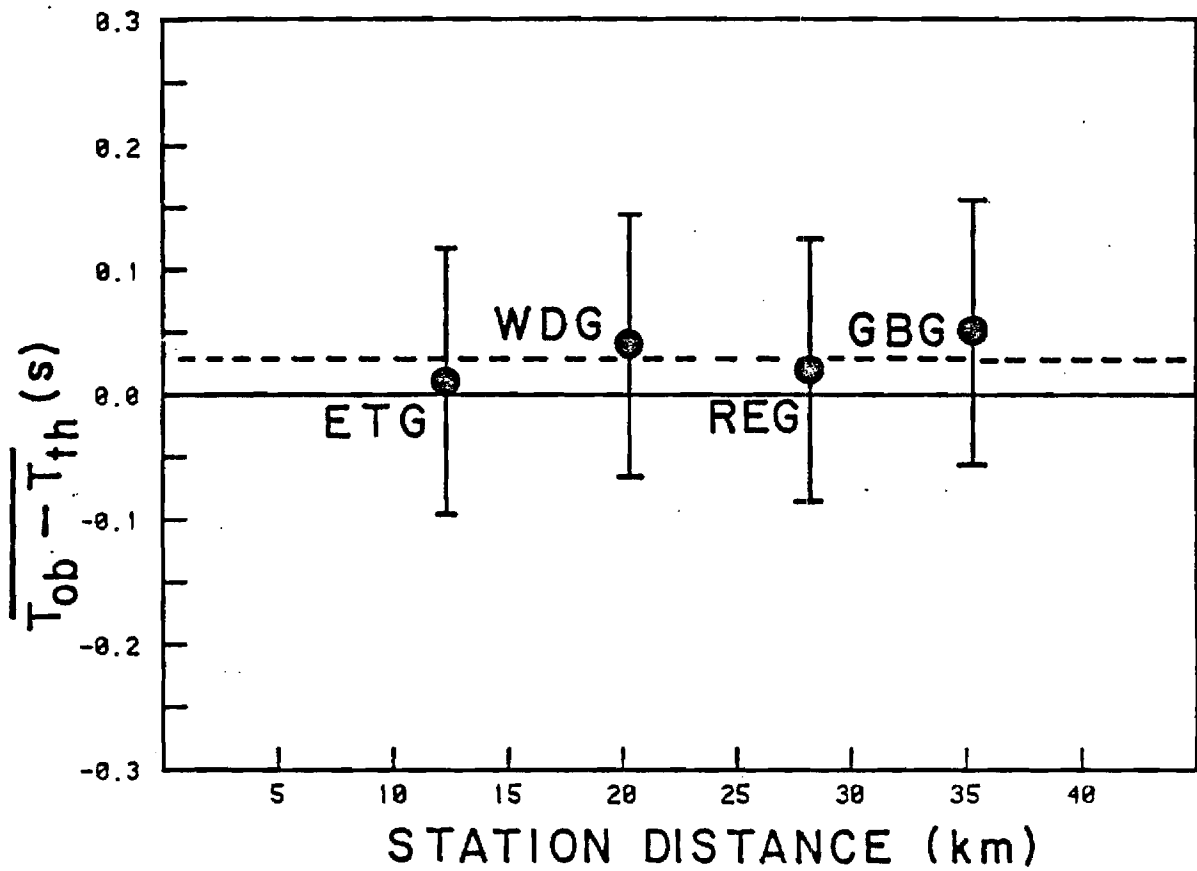


Figure 8. Mean P-wave residuals for a two-layer model for cluster A events that were recorded on four stations.

SIMPLE BOUGUER GRAVITY
MAP OF CENTRAL GEORGIA

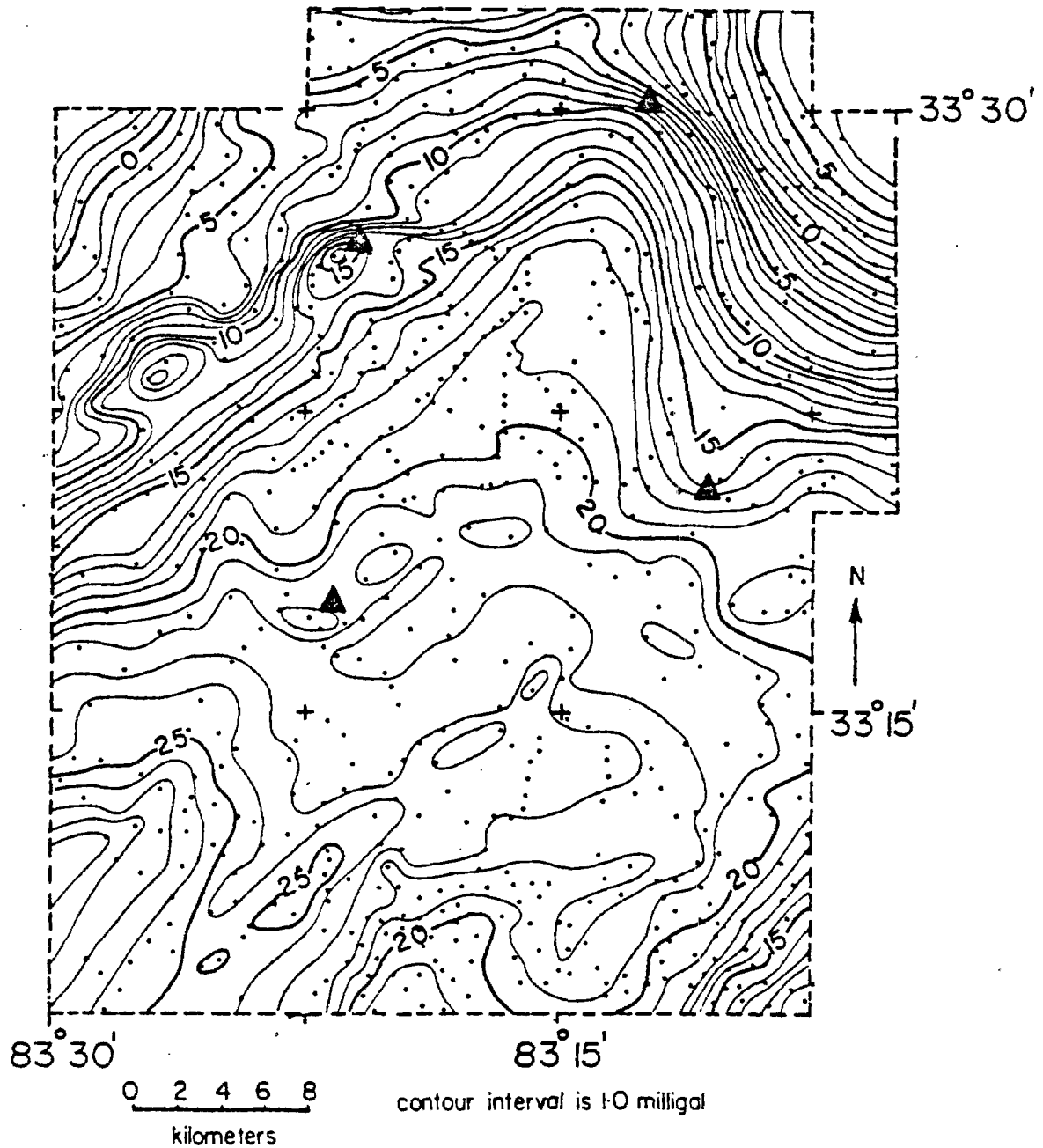


Figure 9. Bouguer Map of the Lake Sinclair area and Lake Oconee area (after O'Nour, 1982).

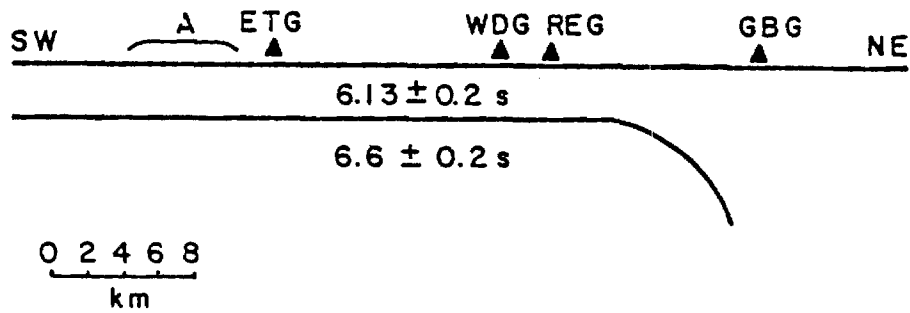
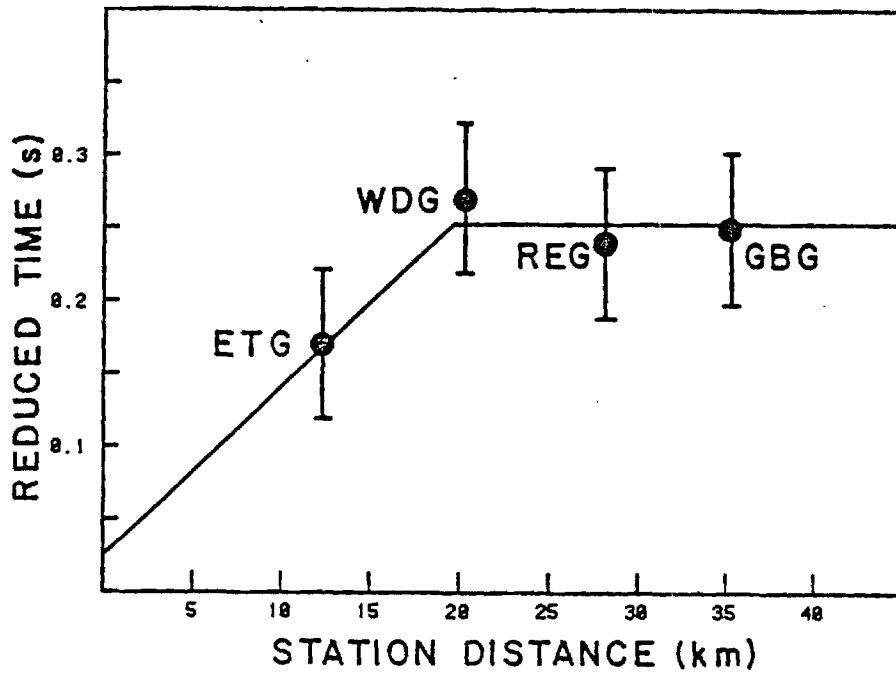


Figure 10. Reduced P-wave travel times for a two-layered model plotted versus station distance and a velocity model for the Lake Sinclair and Lake Oconee areas.

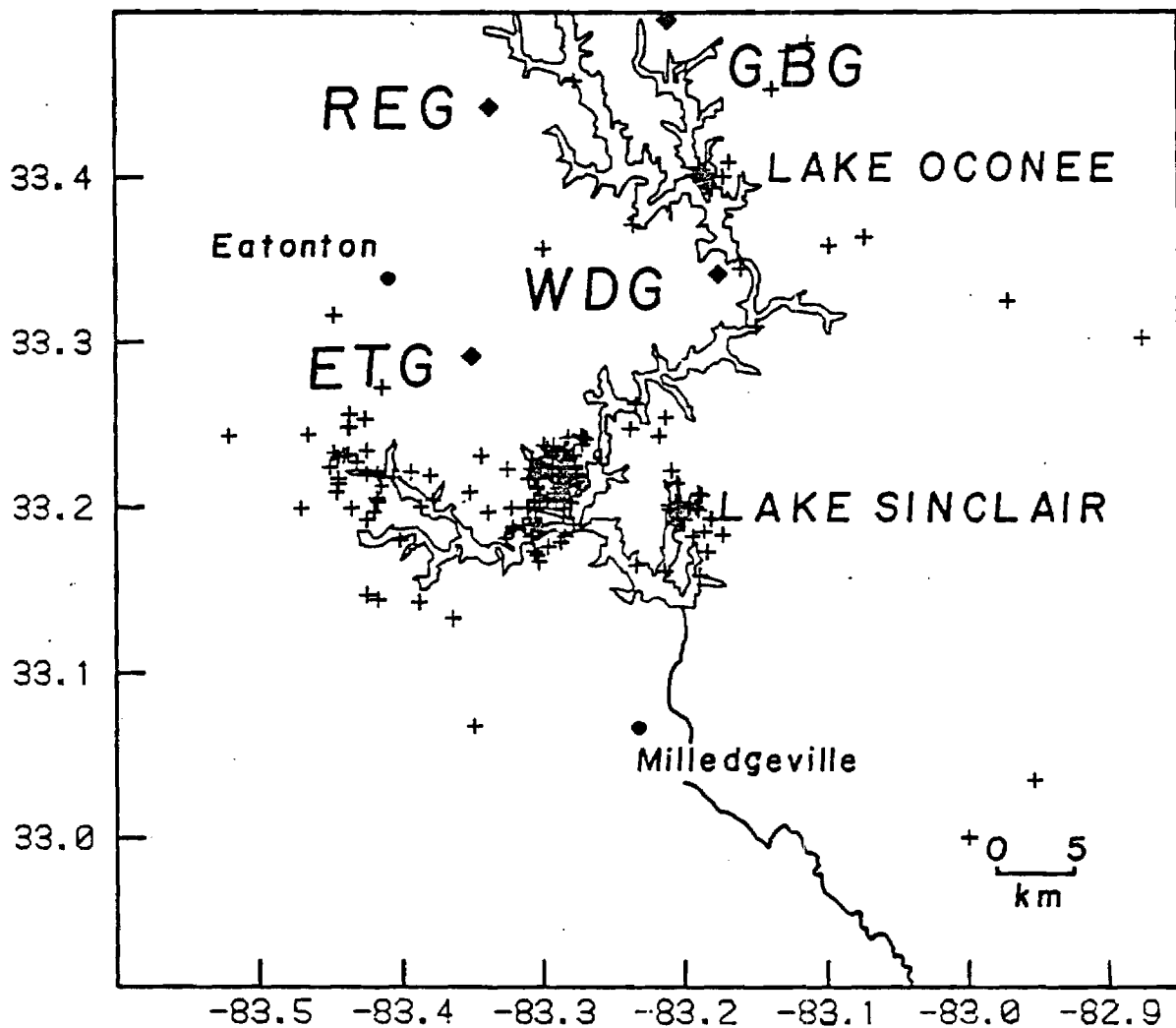


Figure 11. Epicenters for the Lake Sinclair and Lake Oconee areas using the two-layer velocity Model.

G-35-651

NUREG/

=====

GEORGIA/ALABAMA REGIONAL SEISMOGRAPHIC NETWORK

Final Report
July 1, 1988 -- July 31, 1989

=====

Prepared by L. T. Long

Georgia Institute of Technology

Prepared for
U. S. Nuclear Regulatory
Commission

NUREG/

=====

GEORGIA/ALABAMA REGIONAL SEISMOGRAPHIC NETWORK

Final Report
July 1, 1988 -- July 31, 1989

=====

Manuscript Completed: July 4, 1990
Date Published:

Prepared by L. T. Long
Georgia Institute of Technology

School of Earth and Atmospheric Sciences
Georgia Institute of Technology
Atlanta, Georgia 30332

Prepared for
Division of Engineering
Office of Nuclear Regulatory Research
U. S. Nuclear Regulatory Commission
Washington, D.C. 20555
Under Contract No. NRC 04-85-122

EXECUTIVE SUMMARY AND ABSTRACT

OBJECTIVE:

The objective of this study is to contribute data and analyses conducive to the development of criteria for establishing earthquake hazard potential in the southeastern United States.

TASKS:

The first task is to install and maintain the Georgia/Alabama Regional Seismographic Network. The seismic network consists of about 21 stations in Alabama, Georgia, and adjoining regions of southeastern Tennessee and South Carolina. The seismic net includes three three-component short period stations and operates completely on solar power.

The second task is to monitor the seismic activity in the southeastern Tennessee, northern Alabama, and Georgia. The data are to be used in appropriate topical studies.

RESULTS:

The Georgia/Alabama regional Seismographic Network has enhanced the study of seismicity in the southeastern United States in three general ways.

(1) Perhaps most important, studies made possible by the Georgia/Alabama Regional Seismographic Network have led to the development of a theory to explain major intraplate earthquakes. The model for major intraplate earthquakes shows how tectonic plate stress is converted or concentrated for release in major intraplate earthquakes. The process starts by a perturbation of the fluid regime of the lower crust and a subsequent weakening of the stress channel, the mid-crustal zone of high strength subject to forces at plate boundaries. The weakening causes a deformation in a central core and a concentration of the stress on the boundary of this core. Further weakening at the edge of the core can lead to a major earthquake. Following a major earthquake, the area remains active in an extended aftershock sequence. The mechanism is explained in Long (1988) and is given in this report.

A paper on the relation between major earthquakes and the brittle-ductile transition draws heavily on data from southeastern Tennessee. There is a strong implication in the analyses and data from this study that a major earthquake has

occurred (or could occur) in the southeastern Tennessee seismic zone. The existence of nuclear power plants within a radius of 400 km from southeastern Tennessee conveys a need for careful monitoring of the seismicity of southeastern Tennessee.

(2) The network data have been routinely made available to the community and published in the SEUSSN Bulletin.

(3) Topical studies at Georgia Tech have used the network data as a basis for numerous observational studies and for comparison with theoretical exercises. Topical studies include: (1) an investigation of a strata collapse behind a longwall in an Alabama coal mine, (2) a study of reservoir induced events in the Richard B. Russell reservoir showing correlation of the events with the Middleton-Loundesville Fault Zone, and (3) focal mechanisms in southeastern Tennessee showing a pattern of stress orientation consistent with a weak zone in a stressed crust as the cause of the southeastern Tennessee seismicity.

TABLE OF CONTENTS

	<u>page</u>
Executive Summary and Abstract	iii
Table of Contents	v
List of Figures	vi
List of Tables.....	ix
Georgia/Alabama Regional Seismographic Network	1
Objectives.....	1
Summary of Results and Findings	2
Network maintenance and seismic monitoring	2
Graphical representation of operational status	2
Plans for next year.....	2
Abstracts of Presentations	4
Results of topical Studies	11
Appendix A. Modeling the seismic P coda as the response of a discrete-scatterer medium ...	17
Appendix B. A model for major intraplate continental earthquakes	67
Appendix C. A local weakening of the brittle-ductile transition can explain some intraplate seismic zones.....	83

LIST OF FIGURES

	<u>page</u>
Figure 1. Seismic stations maintained or monitored	15
Figure 2. Graphical representation of station coverage.....	16
 Appendix A	
Figure 1. Relation among scattering angle, emergent angle and location of source, scatterer, and receiver	49
Figure 2. Source wavelet.....	50
Figure 3. System response of Georgia Tech seismic network	51.
Figure 4. Scatterer based polar coordinate system	52
Figure 5. Coordinate system used to determine polarization of the scattered S wave	53
Figure 6. Radiation patterns for granite scatterer embedded in sandstone host	54
Figure 7. Radiation patterns for basalt scatterer embedded in sandstone host	55
Figure 8. Scattered responses for granite scatterer in sandstone host	56
Figure 9. Combined response for attenuation and scattering	57
Figure 10. One-scatterer model and synthetic seismogram	58
Figure 11. Alabama blast model	59
Figure 12. Comparison of observed blast, emergent onset, with synthetic seismograms	60
Figure 13. Comparison of observed blast, impulsive onset, with synthetic seismograms	61
Figure 14. Schematic model for horizontal layer of scatterers	62
Figure 15. Model and synthetic seismogram for horizontal layer of scatterers	63

Figure 16. Earthquake model	64
Figure 17. Synthetic seismograms generated using earthquake model	65
Figure 18. P-wave codas of earthquakes recorded in Tennessee	66
Figure 19. Synthetic seismograms generated using earthquake model	66

Appendix B

Figure 1. Illustration of the five phases of a major intraplate earthquake	80
Figure 2. Pattern of seismicity and focal mechanisms for south- eastern Tennessee; a possible example of phase 3. Pattern of seismicity for New Madrid; a possible example for phase 5	81

Appendix C

Figure 1. Seismicity of southeastern Tennessee	102
Figure 2. Focal mechanism solutions and epicenters in the central zone	103
Figure 3. Dip of the B axis of the focal mechanism solution for the central zone	104
Figure 4. Difference between the dip of the tension axis and the dip of the pressure axis	105
Figure 5. Model for a single circular zone of weakening in a horizontal crustal plate	106
Figure 6. Stress surrounding a weak circular zone in a horizontal crustal plate	107
Figure 7. Deviatoric stresses surrounding a weak zone in a hori- zontal crustal plate	108
Figure 8. Dilatation surrounding a weak zone in a horizontal crustal plate	109
Figure 9. Deviatoric stress for two circular zones of weakened crust aligned parallel to the applied stress	110
Figure 10. Deviatoric stress for two circular zones of weakened crust aligned perpendicular to the applied stress..	111

Figure 11. Deviatoric stress for two circular zones of weakened crust aligned at 45 degrees to the direction of applied stress	112
Figure 12. Geologic model for a vertical profile across a zone of weakness in the crust	113
Figure 13. Deviatoric stress in a vertical section across a zone of weakness in the crust	114
Figure 14. Model for focal mechanisms surrounding a zone of weakness in the lower crust	115

LIST OF TABLES

Appendix A		
Table 1.	Properties for typical geologic materials	48
Appendix B		
Table 1.	Conventional Paradigms and Alternates	71
Appendix C		
Table 1.	Earthquake locations and focal mechanisms	101

GEORGIA/ALABAMA REGIONAL SEISMOGRAPHIC NETWORK

Objectives

The objective of this study is to contribute data and analyses conducive to the development of criteria for establishing earthquake hazard potential in the southeastern United States. The main tasks are to install and maintain a seismic network and monitor the seismic activity in eastern Tennessee, northern Alabama, and Georgia. The data are to be contributed to the southeastern U. S. regional bulletin. Also, available information will be used in appropriate topical studies.

Specific objectives for network maintenance and seismic monitoring are as follows:

- * Install or provide about 16 short-period seismograph stations deployed in Tennessee, Alabama, and Georgia. This network is to be operated with a maximum of 5 percent downtime.
- * Obtain and/or reaffirm use permits and telemetry service to convey the data to a central recording point.
- * Provide all seismic phase readings and hypocenter locations to the Southeast U. S. Seismographic Network Bulletin.
- * Provide a recording medium with on-line digital recording at the Central Recording Facility.
- * Report any significant earthquake within the study region to the Nuclear Regulatory Commission within 24 hours.
- * Relocate and/or establish new seismograph stations as it becomes necessary after approval of the Nuclear Regulatory Commission.

Objectives for topical studies are as follows:

- * Study the spatial and temporal distributions, including earthquake recurrence rates, of seismicity and relate them to structural features.
- * Identify parameters that influence seismic processes within the network area and use these in defining seismogenic/tectonic provinces.
- * Study crustal and upper mantle velocity structure in the United States based on the current data from the network.

* Study the magnitudes of historic events using magnitude-felt area relationships and obtain the magnitude-frequency relationships.

* Evaluate the relative significance of results obtained in each of the above analyses as they impact the determination of seismic hazards.

Summary of Results and Findings

Network maintenance and seismic monitoring

During the period of 1 July, 1988, to 31 July, 1989, the Georgia/Alabama Regional Seismic Net consisted of 18 stations located as shown in figure 1. The Clarks Hill Reservoir Area and the area of Lake Richard B. Russell were monitored by three stations. The state of Georgia is monitored by three additional stations. Seven stations are located in Alabama and five in southeastern Tennessee. The Alabama, Tennessee and northwest Georgia stations constitute coverage for the termination of the Southern Appalachian seismic zone. During June 1989 a complete calibration of the stations was completed.

Problems were encountered with field stations. Repair has been slowed by the need to train new electronics assistants and the decrease in number of student assistants. Station CH6 is out due to lumbering activity. The phone line service provided by Georgia Power was terminated and station TVG will be down until alternatives are found. To alleviate the difficulties in closing down the net, and to allow completion of the reports, an unfunded extension has been requested.

Graphical representation of the operational status of the network

The high level of station down time in the late spring was caused by heavy thunder storm activity and lightning damage. The graphical representation of the operational status of the network is given in the form of the daily log of recording and is given in figure 2.

Plans for next year

During the one year extension, the contract will provide only communication costs for the network, time to complete some of the topical studies, and time to phase down the size of the network. Repair and maintenance will be absorbed by Georgia Tech to the extent possible. The seismic net will continue to be recorded. As station fail, they will be taken off line. Georgia Tech will strive to maintain a net in Georgia for which communication facilities are available.

Many of the topical studies were these topics under investigation by master's degree and Ph.D. students. Such students often need more time to develop background materials and capabilities and they do not feel constrained by contract deadlines. The unfunded continuation will allow the students these that are nearing completion to be recognized as contributing to the project. Topics of these theses include:

(1) The inversion of short period surface waves in Alabama is a Master's thesis topic for Argun Kocaoglu. The study will use the Rg phase, which is well recorded from the many mining related events in central Alabama. The group velocity for each path will be computed from spectral amplitude versus group velocity plots generated by using a maximum entropy spectral estimator. These group velocities will be used in a tomographic determination of the group velocity in selected blocks. After solving for the group velocity in each block, the structure for the block will be obtained by inversion of the computed group velocity. The method can resolve structures to a depth of 2.5 km.

(2) The frequency dependence of amplitude decay in the shear or Lg waves in Alabama will be the Master's thesis topic of David Chen. Approximately 25 events recorded at a minimum of 3 stations will be chosen for spectral analyses of the shear or Lg arrival. The distance range of the recording in Alabama is 25 to 150 km, with some events recorded at 250 km in southeastern Tennessee. Estimates of spectral amplitude from 0.5 Hz to 32 Hz in 6 dB increments were obtained from blasts digitized since system calibration in June 1989. A least squares reduction for attenuation rates will include station corrections and equivalent source amplitude as a function of frequency.

(3) The modeling of seismic coda is the Ph.D. topic of Mitch Craig and the results of this study are presented in Appendix A. The model is essential for developing an inverse technique for computing the spatial distribution of scattering intensity and attenuation.

(4) Gravity data could provide a constraint on seismic velocity determination because a general relation exists between velocity and density. Joint inversion of gravity anomalies and seismic travel time residuals for crustal structure would be one way to utilize this constraint.

Abstracts of Presentations

The following are abstracts of talks which were made possible by data and research related to the Georgia/Alabama Regional Seismographic Network.

ATTENUATION OF THE LG WAVE IN NORTHERN ALABAMA

DEMERE, Judy and LONG, L.T., School of Geophysical Sciences, Georgia Institute of Technology, Atlanta, GA 30332

ABSTRACT: The maximum sustained amplitudes of the Lg phase were measured on 76 seismograms from 16 Alabama mining related events recorded on seven stations of the Georgia/Alabama Seismographic Network. Distances ranged from 30 to 300 km in the area covering the terminus of the Southern Appalachians in northern Alabama. Station corrections, S_c , were incorporated in the least squares reduction for event magnitudes using a magnitude equation in the form ($m_b = B + C \text{ Log}(\text{Dist.}) + S_c$). Stations MLA, in the thick Coastal Plane, and OCA, in the Appalachian Plateau, were consistently lower in amplitude and required positive corrections. The constant C for Alabama was 1.2, which suggests greater attenuation than implied by the 0.9 value for C in Nuttli's magnitude equation for the Central United States. By assuming an Airy phase decay rate proportional to $D^{-1/3}(\text{Sin}(D))^{-1/2}$ the rate of decay suggests an average value of $Q=800$.

A Talk presented at the Eastern Section, Seismological Society of America Meeting, October 1989.

DETERMINISTIC MODELING AND INVERSION OF THE P-WAVE CODA

CRAIG, M.S., LONG, C.F., and TIE, A. School of Geophysical Sciences, Georgia Institute of Technology, Atlanta, GA 30332

ABSTRACT: The P- and S-wave coda from earthquakes in southeastern Tennessee exhibit different degrees of scattering. In order to model zones of anomalous scattering and to model the frequency dependence of the scatterers, we assume that each scatterer is a sphere and compute the effects of propagation on each scattered wavelet. Thus, the seismic coda is modeled as a superposition of wavelets scattered from spherical heterogeneities embedded in a three-dimensional elastic medium. The scattered waves for an incident P-wave are determined for wavelengths as short as 1/3 the radius of the sphere using Bessel functions up to order 15. This provides P and SV responses as a function of scattering angle and wavelength for the material contrasts used to calculate the effects of scattering. Absorptive attenuation and scatterer response are combined in the frequency domain and minimum phase is determined by spectral factorization. These spectral responses are calculated for each

raypath, corrected for geometric spreading and free-surface effects, time-shifted according to the length of the travel path and superimposed to obtain the complete coda. The inverse method combines coda information from a group of seismograms recorded by a regional network. Since each arrival in a coda corresponds to a raypath from source to scatterer to receiver, the arrival time constrains the scatterer to lie on a shell which encloses the source and receiver. Areas intercepted by the shell are assigned weights depending on the energy density of the coda at the corresponding time and the properties of the propagation path. By stacking data from several earthquakes and stations, the principal scatterers can be resolved as points where many of the heavily weighted shells intersect.

A Talk presented at the Eastern Section, Seismological Society of America Meeting, October 1989.

THE SEISMIC CODA AS A RESULT OF SCATTERED BODY WAVES: MODELING AND INVERSE METHODS

CRAIG, M., and L.T. LONG, School of Geophysical Sciences, Georgia Institute of Technology, Atlanta GA 30332

ABSTRACT: The seismic coda is modeled as a series of wavelets scattered from spherical heterogeneities embedded in a three-dimensional elastic medium. Using this scattering model, synthetic seismograms are prepared for source and receiver locations which correspond to those of several digitally-recorded events. Both earthquakes and explosions are modeled, using oriented double-couple and spherically symmetric sources, respectively. Geometric spreading, absorptive and scattering attenuation, the free-surface effect, and instrument response are taken into account. Singly-scattered arrivals are obtained individually by calculating response and lapse time corresponding to each scatterer in the medium. This is done independently for P- and S-waves. The individual contributions are then superimposed to obtain the complete coda. The agreement between synthetic and observed seismograms is quite good in several cases.

The locations and relative contributions of the principal scatterers in a region can be determined by an inverse method which utilizes the scattering model of the seismic coda. The method combines coda information from a group of seismograms recorded by a regional network. Since each arrival in a coda corresponds to a raypath from source to scatterer to receiver, the arrival time constrains the scatterer to lie on a shell which encloses the source and receiver. In the case of a constant-velocity medium this shell is ellipsoidal with foci at the source and receiver. Areas intercepted by the shell are assigned appropriate weights depending on the energy density of the coda

and a propagation factor which includes geometrical and absorptive attenuation and normalized source amplitude. Energy density is preferred over instantaneous amplitude as a measure of coda strength because of the lesser time precision needed. By stacking data from several earthquakes and stations, the principal scatterers can be resolved as the points where many of the heavily weighted shells intersect. The resulting scatterer distribution is tested by using it as a model to generate synthetic seismograms for several combinations of source and receiver locations. This technique makes no assumption of horizontal layering and may prove more appropriate than conventional reflection or direct-raypath tomographic methods in regions where there is strong and heterogeneous scattering.

Presented at the IASPEI meeting, September 1, 1989, Turkey

A LOCAL SHALLOWING OF THE BRITTLE-DUCTILE TRANSITION CAN EXPLAIN SOME INTRAPLATE SEISMIC ZONES

LONG, L. T. and K.-H. ZELT, School of Geophysical Sciences, Georgia Institute of Technology, Atlanta GA 30332

ABSTRACT: A local decrease in the strength of the crust, which would accompany a shallowing of the brittle-ductile transition, could concentrate crustal deformation through viscous or dislocation creep in response to existing regional plate stress. Two-dimensional finite element models, which include a regional plate stress and various shapes of a local decrease in crustal strength, show concentrations of stress at the brittle-ductile transition surrounding the local decrease in strength. The deformation and stress of the model suggest that strike slip faulting should dominate in the central local area of decrease in crustal strength. Outside the central area, the deformation of the crust in the vicinity of the brittle-ductile transition predicts that the dominant strike slip faulting should exhibit components of normal and reverse faulting, and that these components should be more pronounced above the brittle-ductile transition. In southeastern Tennessee the seismicity is diffused over a narrow elliptical zone trending northeast with the greatest concentration of activity near the center. Focal mechanism solutions (43 in total) agree with the predictions of the finite element model within the confidence levels of the solutions. The central zone is characterized by deep strike slip focal mechanisms and events surrounding the central zone exhibit higher proportions of reverse or normal fault movements.

A poster paper displayed at the Symposium on Intraplate Deformation, Neotectonics, Seismicity and the State of Stress in Eastern North America, Montreal, Quebec, Canada, May 17, 1989.

RAYLEIGH-WAVE DISPERSION IN NORTHERN ALABAMA

KOCAOGLU, A. H. and L. T. Long, School of Geophysical Sciences, Georgia Institute of Technology, Atlanta, GA 30332.

ABSTRACT: Surface-wave dispersion analysis in general requires a method by which the spectrum of the non-stationary time sequence (dispersed seismic trace) can be estimated within a window along the trace. When short data segments are used, the spectral resolution of the Fourier transform is quite poor compared to the resolution of maximum entropy spectra. In this study a dispersion analysis of Rayleigh waves in Northern Alabama is carried out by using the maximum entropy spectral estimation method. The dispersion curves are obtained for a number of different raypaths defined by each source-receiver pair used in the analysis. Since the dispersion curve associated with a particular path represents an average along the path, the study area can be divided into regions where individual dispersion characteristics are assumed to be uniform. By employing a linear inversion technique, individual dispersion curves of regions can be calculated to determine the lateral variations of sediment thickness.

A talk presented at the Spring Meeting, American Geophysical Union, Baltimore, Maryland, May 8-12, 1989.

SCATTERER DISTRIBUTION DETERMINED FROM THE SEISMIC CODA

CRAIG, M. S. and L. T. Long, School of Geophysical Sciences, Georgia Institute of Technology, Atlanta GA 30332.

ABSTRACT: An inverse method is presented based on the model in which the seismic coda is composed of a series of wavelets scattered from heterogeneities embedded in an elastic medium. By applying the method to digital earthquake seismograms from a regional network, the relative contributions and locations of the principal scatterers can be determined. Each arrival in a coda corresponds to a raypath from source to scatterer to receiver. The arrival time constrains the scatterer to lie on a shell, which in the case of a constant-velocity medium is ellipsoidal with foci at the source and receiver. Areas intercepted by the shell are assigned appropriate weights depending on the energy density of the coda and a propagation factor which includes geometrical and absorptive attenuation and normalized source amplitude. Energy density is preferred over instantaneous amplitude as a measure of coda strength because of the lesser time precision needed. By stacking data from several earthquakes and stations, the principal scatterers can be resolved as the points where many of the heavily weighted shells intersect. This process is equivalent to a diffraction stack. The scatterer distribution thus determined is tested by using it as a model to

generate synthetic seismograms for several combinations of source and receiver locations. This technique makes no assumption of horizontal layering and appears to be more appropriate than conventional exploration methods in regions where there is strong and heterogeneous scattering.

A talk presented to the Spring Meeting, American Geophysical Union, Baltimore, Maryland, May 8-12, 1989.

A COMPARISON OF TWO TYPES OF SEISMICITY IN THE STABLE CONTINENTAL INTERIOR

LONG, L. T., School of Geophysical Sciences, Georgia Institute of Technology, Atlanta, GA 30332.

ABSTRACT: Earthquakes with hypocenters near the brittle-ductile transition in the stable continental interior occur only in a few active seismic areas, such as southeastern Tennessee (SET). In contrast, earthquakes such as those in central Georgia (CG), occur typically within the top few kilometers of the crystalline crust and are more widely distributed. In addition to depth, these two earthquake source types are different in most of their other properties. The focal mechanisms from SET are dominantly strike slip with systematic variations about a central zone of active seismicity. Focal mechanisms of CG have scattered orientations which may correlate only with local joint sets. Seismic velocity and attenuation in the crust of SET are anomalously low near the central zone. Changes in these properties unrelated to geologic structure have not been noted in CG. The high-frequency spectral decay is steeper for CG source displacements than for SET. The different properties of these two source types suggest distinct and different causative mechanisms. The CG seismicity is often associated with reservoir impoundment and occurs in response to fluid penetration and weakening of near-surface joint and fracture surfaces. The SET seismicity may be the seismic response to viscous deformation of the lower crust in a local zone of decreased strength at the depths of the brittle-ductile transition. Large events of the CG source type would be limited by the size of the shallow fracture planes, whereas, major intraplate earthquakes could be initiated by the viscous deformation mechanism.

A talk presented to the Annual Meeting, Seismological Society of America, Victoria, British Columbia, April 19-21, 1989.

CRUSTAL STRESS AND FAULTING FROM MAJOR INTRAPLATE CONTINENTAL EARTHQUAKES

LONG, Leland Timothy, School of Geophysical Sciences, Georgia Tech, Atlanta, GA. 30332

ABSTRACT: A new model for major intraplate continental earthquakes is based on a transient perturbation in crustal strength. Regional plate stress provides the driving energy, but the faulting is controlled by crustal weakening in the vicinity of the major event. The weakening is triggered by a disturbance in the hydraulic or thermal properties of the crust. The weak central zone in the lower crust deforms in response to regional plate stress and transfers the stress load to the surrounding competent crust or to the thinned stronger crust above the disturbed zone. Finite element models of the stress field caused by a weak central zone predicts that normal and reverse faulting at the edge of the central weak zone. The central weak zone would exhibit strike slip faulting. At least two distinct patterns of faulting are possible for the major earthquake. One pattern would consist of two near-vertical faults striking parallel to the direction of maximum shear stress of the regional field and extending away from diagonally opposite edges of the central zone. These faults could be connected in the central weak zone by a series of faults. This pattern is exhibited by the New Madrid seismicity. The other pattern would develop when deformation is resisted by a thinned crust above the disturbed zone. The major earthquake would occur on a reverse fault with dimensions comparable to the size of the central weak zone.

A talk presented to the Southeastern Section, Geological Society of America, Annual Meeting, Atlanta, Georgia, April 6-7, 1989.

FOCAL MECHANISMS AND CRUSTAL STRESS IN SOUTHEASTERN TENNESSEE

LONG, L. T., and K.-H. ZELT, School of Geophysical Sciences, Georgia Institute of Technology, Atlanta, Georgia 30332

ABSTRACT: The seismicity of southeastern Tennessee is diffused over a narrow elliptical zone trending northeast with the greatest concentration of activity near the center. We have obtained 43 focal mechanism solutions with confidence levels covering this activity. The central active zone is dominated by strike-slip focal mechanisms. Events surrounding the central zone exhibit higher proportions of reverse or normal fault movements. The inhomogeneous pattern of stress can be modeled by a zone of weak crust at depths of 10 to 30 km. Deformation of this zone by regional plate stress predicts the strike-slip focal mechanisms in the center. Normal and reverse components in the focal mechanisms in the surrounding area corresponding to zones of relative compression or expansion of the crust. The stress models and consistent focal mechanisms support the hypothesis (Long, 1988) that major continental earthquakes are caused by a temporary perturbation of the fluid regime and, hence, strength of the lower crust.

Presented at the Western American Geophysical Union Meeting, San

Francisco, California, Wednesday morning December 7, 1988.

THE MODELING AND INVERSION OF SEISMIC CODA, WITH APPLICATIONS TO SCATTERING IN SOUTHEASTERN TENNESSEE

OGILVIE, J.S., and L. T. Long, School of Geophysical Sciences, Georgia Institute of Technology, Atlanta, GA 30332.

ABSTRACT: Compressional and shear wave coda were modeled by accumulating individual wavelets scattered by many inhomogeneities in the crust. The source wavelet was created by finding the minimum phase wavelet for a typical displacement spectra and adjusting the amplitude for the take-off angle to the scatterer from a double-couple source function. Causal constant Q attenuation and geometrical attenuation were applied for the paths to the scatterer and from the scatterer to the recorder. The spectral response of a sphere was used to create the scattered wavelet from the incident wavelet. At the receiver, the effects of a free surface and instrument response were added. Seismograms generated by this technique were remarkably similar to observed records of earthquakes from southeastern Tennessee, except for events near a suspected anomalous zone. The inversion for scattering coefficients was accomplished by a three-dimensional diffraction stack, in which energy wavelets from each coda were distributed as reflection coefficients among appropriate scatterers. Highly reflecting structures would generate high-energy arrivals in all codas and these structures should appear as large reflection coefficients. The scattering coefficients are strongly dependent on absorptive Q. They suggest that Q is a function of depth (125 at the surface to 400 at 25 km depths for the shear wave) and that anomalous zones exist in southeastern Tennessee.

A talk presented to the Eastern Section, Seismological Society of America, State College, Pennsylvania, October, 12, 1988.

INDUCED SEISMICITY AT THE RICHARD B. RUSSELL RESERVOIR

LONG, L.T., School of Geophysical Sciences, Georgia Institute of Technology, Atlanta GA 31332.

ABSTRACT: On December 12, 1987, at 03:53 UTC (10:53 P.M., EST, December 11, 1987), an earthquake of magnitude 2.3 was felt in Elbert and Hart Counties, Georgia. This and subsequent events marked the first significant reservoir-induced seismicity at the Richard B. Russell Lake. The swarm of earthquakes lasted from December, 1987, to February, 1988. Three of the 33 events were felt. Before impoundment in December, 1983, no natural seismic activity and been observed. Between December, 1983, and December, 1987, 21 earthquakes of magnitude less than one were

identified. The epicenters for the three felt events were near the Middleton-Lowndesville fault zone. No significant water level changes were observed before the swarm of seismicity.

A talk presented to the Eastern Section, Seismological Society of America, State College, Pennsylvania, October, 12, 1988.

Results of topical studies

Many topical studies achieved notable conclusions or were completed during the reporting period of July 1988 to July 1989. The principal conclusions are summarized below. Many of the topical studies will be continued. Significant conclusions that develop later will be reported in the open literature.

The Mechanism of Major Intraplate Earthquakes

Perhaps the most significant development, which was made possible by the Georgia/Alabama Regional Seismographic Network, is the discovery of a theory to explain major intraplate earthquakes. The new model for major intraplate earthquakes shows how tectonic plate stress can be concentrated for release in major intraplate earthquakes. The transient process starts by a perturbation of the fluid regime of the lower crust and a subsequent weakening of the stress channel, the mid-crustal zone of high strength subject to forces at plate boundaries. The weakening causes a deformation in a central core and a concentration of the stress on the boundary of this core. Further weakening at the edge of the core can lead to a major earthquake. Following a major earthquake, the area remains active in an extended aftershock sequence. The mechanism is presented in Appendix B (Long, 1988).

The study of the relation between major earthquakes and the brittle-ductile transition (see Appendix C) draws heavily on data from southeastern Tennessee. The principle investigation in this aspect of understanding the mechanism of major intraplate earthquakes was a Ph.D. dissertation by Karl-Heinz Zelt on focal mechanisms in southeastern Tennessee. A critical aspect of this study was the development of statistical parameters to quantify the quality of the focal mechanism solution. The southeastern Tennessee data were used to show that the spatial variation of focal mechanism solutions in a seismic zone can be used to infer variations in the orientation of the stress field. In particular, in southeastern Tennessee, the observed variations in stress directions fit a model for a weak zone in a crustal plate. There is a strong implication in the analyses and data from this study that a major earthquake has occurred (or could occur) in the southeastern Tennessee seismic zone.

The model and evidence for the model have developed through a sequence of studies and presented in talks. Each has treated a

different aspect of the model and its consequences. Papers on the description of the model (Appendix B) and the relation of the model to spatial variations in focal mechanisms (Appendix C) are presented below. Others will be developed into papers at a later date.

The objective of the paper "Crustal Stress and Faulting by Major Earthquakes" by L.T. Long which was presented at the Southeastern Section, Geological Society of America, was to show how the model for major intraplate earthquakes can explain some faults observed in the continents. The essential elements of the model are the crustal stress channel, intraplate compressive stress, and a perturbation in the strength of the stress channel caused by thermal or fluid mechanisms. The five-phase process of a major event proceeds as described in Appendix B and the stress field for the model is described in Appendix C.

The development of faults in response to the weakening of the crust depends on the extent of penetration of the fluids into the crust. Two characteristic responses can be recognized. The first occurs in the early stages of development of an intraplate seismic zone, when stress is concentrated in the thinned stress channel above the zone of perturbation. Earthquakes would be of thrust type and could range from magnitude 5.5 to 6.8. In this stage the deformation and weakening have not extended to the shallow crust (5 to 10 km) the thinned stress channel fails because it is left supporting the regional stress. The length of the fault would correspond to the size of the zone of lower crustal weakening. An example of this type of response is the Bellair (GA) fault which is about 20 km long curved trace with the up block on the concave side of the arc. The second type is a failure of the entire plate starting at a weakened core. The New Madrid events characterize this response, which develops after the weakness has penetrated the crust. The major zones of failure extend beyond the core and involve the entire crust. The largest magnitude intraplate events would be of this type.

The observation that earthquakes in the southeastern United States can be classified as either shallow events on existing fractures or mid-crustal events associated with potentially major seismic zones was presented in a talk titled "A Comparison of Two Types of Earthquakes". The mechanisms for the generation and release of stress in these two types of earthquakes are different and an understanding of their distinct mechanisms carries significant implications for seismic risk. The shallow events are typical of earthquakes that occur in the Piedmont, including reservoir induced events, and are referred to as Piedmont type earthquakes. They occur principally on existing fractures and are triggered by fluid penetration from the free surface. The fluids, either through chemical erosion or changes in hydrostatic pressure, decrease the shear strength on fractures and release

existing stress in the form of earthquakes. The mid-crustal events occur because plate driving forces are released by developing zones of weakness in the crust. These earthquakes generate new faults in response to the principal direction of plate stress and developing zones of weakness.

The implication of the mechanism for Piedmont type earthquakes is that the stress is limited to residual stress and the size of the fault plane is limited to the upper four to seven kilometers of the crystalline crust. This constrains the maximum magnitude to 5.5 to 5.7 and the exposure to earthquake damage from such events would be moderate, even near the epicenter. The implied seismic risk for the deeper focus crustal earthquakes is much greater. These events gain their energy from a combination of plate driving stress and the development of weak zones by fluids. They occur in response to viscous relaxation of the applied stress and the concentration of stress surrounding the zone of weakness. Their magnitudes are virtually unlimited, but the background activity should allow a prediction of their occurrence.

The concept that "A local weakening of the brittle-ductile transition can explain some intraplate seismic zones" was presented at the symposium on intraplate seismicity in Montreal and is given in detail in Appendix C.

The relation of focal mechanisms to stress in the crust was prepared for the western AGU. Details of this study are presented in Appendix C.

Finite Difference Applications

A Ph.D. dissertation by Jeh-San Liow titled "Finite difference propagation of waves in elastic inhomogeneous media". As an example of the synthetic seismograms, the finite difference computations included a model of southeastern Tennessee crustal structure and a comparison with observed arrivals on the Georgia/Alabama Regional Seismographic Network seismic stations in Tennessee. The high-frequency limit on the synthetic finite difference seismograms was about 2 Hz and the size of the finite difference grid was too small to develop a realistic comparison with observed data without extensive filtering of the seismographs. The finite difference computation will be repeated later when a larger computer is available on an economic basis. The larger run will be designed to place the source at 15 km depth and extend for 40 km with a resolution of 4.0 Hz wavelets.

Reservoir Induced Seismicity

The locations of induced events in the Richard B. Russell

reservoir area lie on (or close) to the Middleton-Lowndesville Fault and its splays. The association of induced seismicity with a mapped fault zone is distinct from the dispersed pattern of the seismicity observed in the Jocassee and Monticello reservoir areas in South Carolina and the seismicity observed to the south in the Clarks Hill Reservoir. However, the limited seismicity associated with the Oconee Reservoir was also concentrated on the Middleton-Lowndesville Fault.

In another possible type of induced seismicity, a swarm of events has been identified as natural near the station DCT in southeastern Tennessee. The swarm started soon after the underground copper mine was abandoned. At this time, we suspect that these events are triggered by the filling of the mine with ground water.

Coda syntheses and inversion

The understanding of the cause of the coda of local earthquakes can be important in understanding local variations in the physical properties of the crust, as well as understanding the amplitude decay of waves from an earthquake. In particular, variations in coda Q were observed in southeastern Tennessee from earthquakes at a variety of depths. A model was developed (Appendix A) that can explain the coda observed in southeastern Tennessee as well as the coda from shallow explosions in central Alabama. These results show that a three dimensional distribution of scatterers is sufficient to explain the variations in seismic coda. The success of the model to generate synthetic coda make this model an appropriate basis for an inversion for local variations in scatterers and attenuation.

Mining events

During March the paper "The Alabama, U.S.A. seismic event and strata collapse of May 7, 1986, by L.T. Long and C. W. Copeland, was accepted for publication in PAGEOPH. Subsequent monitoring in 1989 with a portable digital event recorder identified a swarm of events at the same time as the passage of the longwall past a critical position in the Alabama coal mine. The combination of a critical weak zone and the stresses generated by the longwall mining technique are critical to the triggering of larger seismic events. The data presented in this paper show that events in central Alabama with magnitudes as high as 3.5 can be triggered by mining activity.

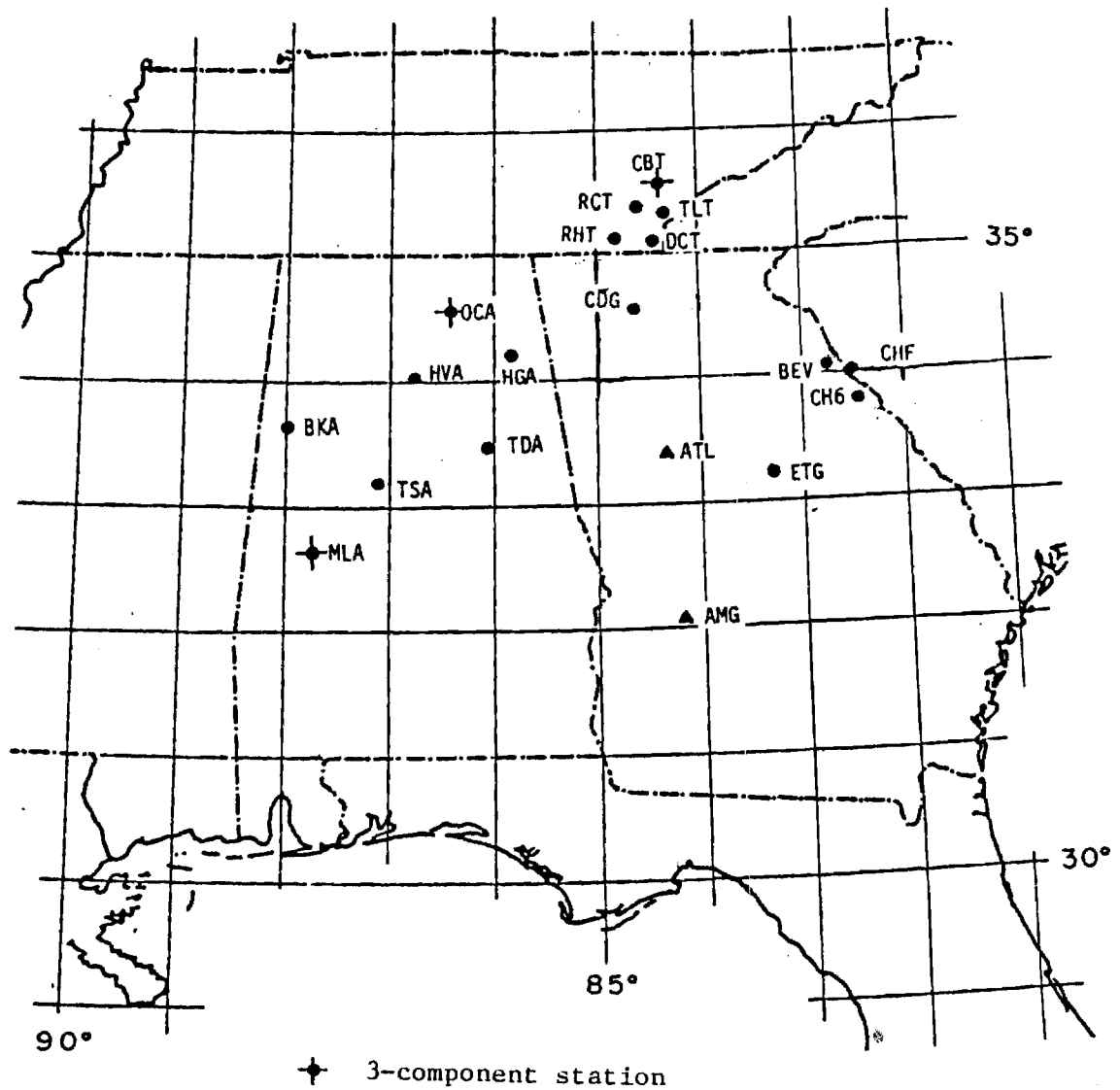


Figure 1. Locations of stations in the Georgia/Alabama Regional Seismographic Network maintained during the period of June 1, 1988, to July 31, 1989.

Network Coverage for 1988-1989

Sta.	JUL-SEP	OCT-DEC	JAN-MAR	APR-JUN
	ALABAMA			*
OCAZ	-----XXXX----	--XXXX-XXXX--	-----XXX	XXXXXXXX-----
OCAN	-----XXXX----	-----X-XXXXX-	-----XXX	XXXXXXXXXX-----
OCAE	-----XXXX----	-----X-XXXXX-	-----XXX	XXXXXXXX-XXXXX
HGA	----XXX-XXXXX	XXXXXXXXXXXXXXXX	XXXXXXXXXXXXXXXX	XXXXXXXX-XXXXX
HVA	----X-----	-----	---XXXX---XXX	XXXXXXXX-XXXXX
TDA	XX--XXXXXXXX-X	XXXXXX-----	-----	XX--XX-XXXXX
TSA	-X--X-----X-	----XX-----	-----	-----XX-----
BKA	----X-----	-----	-----	-XXXXXX-XXXXX
MLAZ	----X-----XXX	X-----XXXX	XXXXXXXXXXXX--	-----XXXX
MLAN	----X-----	-----XXXX	XXXXXXXXXXXX--	-----XXXX
MLAE	----X-----	-----XXXX	XXXXXXXXXXXX--	-----XXXXXXXX
	SOUTHEASTERN TENNESSEE			
CBTZ	-----XXX---	-----X---	-----	-XXXXXXXXXXXXXX
CBTN	-----XXX---	-----X---	-----	-XXXXXXXXXXXXXX
CBTE	-----XXX---	-----X---	-----	-XXXXXXXXXXXXXX
RCT	XXXXXXXXXXXX--	-----XXXX	XXXXXXXXXXXXXX	XXXXX-----XX
RHT	---XXX-----	-----	-----	-----
TLT	----XXXXXX-XX	XXXXXXXXXX--XXX	-----XX	XXXXXXXXXXXXXX
DCT	X-----	-----	-----	-----
	GEORGIA			
TVG	XXXXXXXXXXXXXX	XXXXXXXXXXXXXX		
DALG	XXXXXXXXXXXXXX	XXXXXXXXXXXXXX	XXXXXXXXXXXXXX	XXXXXXXXXXXXXX
CDG	-----XXX---	XXXXXXXXXXXXXX	XXXX-----	-XXXXX-----XX
ATL	-----X-----	-----	-----	-XX-----
ETG	-----	-----XX-XX-	XXXXXXXXXXXXXX	---XX-----
CH6	XXXXXXXXXXXXXX	XXXXXXXXXXXXXX-	-----XXXXX-	XXXXXXXXXXXXXX
CHF	XXXXXXXXXXXXXX	XXXXXXXXXXXXXX	XXXXXXXXXXXXXX-	--XXXXXXXXXXXXXX
LDV	XXXXXXXXXXXXXX	XXXXXXXXXXXXXX	XXXXXXXXXXXXXX	XXXXXXXXXXXXXX
BEV	XXXXXXXXXXXXXX	XXXXXXXXXXXXXX	XXXXXXXXXXXXXX-	-----

"-" = Station Operating
 X = Station Down

Figure 2. Graphical representation of the operational status of the Georgia/Alabama Seismographic Network.

APPENDIX A

Modeling the Seismic P Coda as the Response of a Discrete-
Scatterer Medium

by: M. S. Craig, L. T. Long, and An Tie,
School of Earth and Atmospheric Sciences
Georgia Institute of Technology
Atlanta, GA 30332 USA

In preparation for Proceedings of IASPEI Symposium "Scattering
and Attenuation of Seismic Waves" to be published as a special
issue of Physics of the Earth and Planetary Interiors.

Abstract

The seismic coda can be modeled as a composite of wavelets scattered from spherical heterogeneities embedded in an elastic medium. The exact scattering response of a spherical heterogeneity is calculated for elastic waves using Mie theory. To generate synthetic codas, a P source wavelet is defined for propagation along the ray paths from the hypocenter to the receiver via each scatterer in the model. Only singly-scattered waves are computed. Along the path, the wavelet is adjusted for geometric spreading, intrinsic attenuation, scattering response, the free-surface effect, and instrument response. The source-scatterer-receiver path length is used to determine the appropriate time-shift for the scattered wavelet. Scattered wavelets are obtained individually by calculating the response and lapse time corresponding to each scatterer in the medium. This is done independently for scattered $P - P$ and $P - S$ waves. The individual wavelets are then time-shifted and superimposed to obtain the complete coda. Synthetic codas were able to match the emergent P -wave codas from surface explosions in Alabama and the impulsive P -wave arrivals from earthquakes in southeastern Tennessee.

1 Introduction

The seismic coda, namely the portion of the seismogram that immediately follows the direct arrival, consists of numerous arrivals that cannot be explained completely by a layered-earth. Most workers attribute the unexplained coda energy to the scattering of elastic waves by heterogeneities (Aki, 1969; Sato, 1977a,b; Herraiz and Espinosa, 1987). The complexity of solutions to the wave equation propagation in heterogeneous elastic media has impeded the development of analytical solutions for the seismic coda. Statistical methods have been useful for

describing the general shape of the envelope (Aki and Chouet, 1975). Sato (1977b, 1982, 1984) treated the scatterers as a continuous distribution to be integrated over a volume. The model presented in this work represents the seismic coda by the superposition of singly-scattered wavelets. The model differs from Sato's in that responses in that responses are calculated individually for each scatterer and then summed to form the complete coda. The principal advantage of our model is that the parameters can be varied as a function of position in the host medium.

The scattering of elastic waves has been studied by several workers, but relatively few studies have attempted to account for the angle dependence, or anisotropy, of seismic scattering. Sato (1984) and Snieder (1988) used the Born approximation for a first-order approximation of the scattered wavefield. The exact solution is given by Mie theory (Ying and Truell, 1956) as an infinite series. Tie (1987) used the Mie method to calculate scattered wavefield potentials as a function of ka for a wide range of geologic materials. His work was extended in this thesis by explicitly evaluating the displacement fields and examining their variations as a function of scattering angle, and by implementing the asymptotic forms of the Hankel functions in the solution of the scattered field. The resulting scattering responses were incorporated in our coda modeling scheme, proceeding from the synthesis of an individual scattered wavelet to the generation of a complete coda.

A geologic model is specified by defining host and scatterer materials, and scatterer size and distribution. Path-dependent corrections include geometric spreading, intrinsic attenuation, and the free surface effect. The Mie method is used to determine scatterer responses. All of the above components are combined to produce the scattered wavelet and, finally, many scattered wavelets are superimposed to produce the complete coda. The effects of scatterer properties

and source-receiver geometry on the seismic coda were investigated by generating synthetic seismograms for a range of parameters.

2 The Model

2.1 Overview

Scatterers in this study were approximated by elastic spheres embedded in an elastic crust. The elements of the response due to one scatterer are summarized as follows: A compressional wavelet is propagated from the source to the scatterer, where its energy is scattered in all directions. Part of the energy is scattered towards the receiver in the form of $P-P$ and converted P -to- S wavelets. Source-scatterer and scatterer-receiver pathlengths are calculated and used to correct the wavelet for geometric spreading and intrinsic attenuation. The scattering angle θ (see Figure 1) is required to calculate the amplitudes of the scattered P and S wavelets. The orientation of the plane that contains source, scatterer, and receiver is used to determine the component of scattered S wave polarized in the vertical plane. The emergent angle γ is used to correct P and S_V amplitudes at the free-surface. The path length $r_1 + r_2$ is used to time-shift the scattered P and S wavelets, which are then added together to obtain the complete response for a particular scatterer. In multi-scatterer models, this procedure is repeated for all scatterers within the region of influence associated with the desired coda duration. Each scattered response was added to accumulate the complete coda. The instrument response was applied to the final trace, thus synthetic seismograms may be prepared for a variety of seismometers without having to recalculate the scattered responses.

A more general geologic model containing many scatterers may be specified in terms of scatterer radius and spacing, intrinsic attenuation, and P and S -wave velocity structure. The host material was assumed to have constant P and S -wave

velocity and horizontal layers with constant intrinsic Q . Scatterer radius and spacing were independently specified. The spatial extent, or region of influence, of the model was determined by specifying the duration of coda to be examined. The responses of all scatterers, including the associated path corrections, were calculated and summed to generate the theoretical coda.

2.2 Attenuation and Geometric Spreading

Attenuation of waves along the path from the source to the scatterer and from the scatterer to the receiver was attributed to the combined effects of intrinsic attenuation, Q_i^{-1} , of the host medium and attenuation due to forward scattering, Q_s^{-1} , by the intervening scatterers (Dainty and Toksöz, 1980). Although attenuation was assumed to vary only as a function of depth in the geologic models used to prepare the synthetic seismograms in this paper, depth-dependent attenuation is not a restriction of the coda modeling scheme. Attenuation was calculated for each wavelet according to its travel time T by using

$$A(\omega) = A_0(\omega) \exp\left(-\frac{\omega T}{2Q}\right), \quad (1)$$

where $A_0(\omega)$ is the amplitude at the source, ω is the angular frequency, and Q is the combined effect of Q_s and Q_i . For seismograms of this study, travel-times were calculated for P and S waves, along the path from source to scatterer to receiver, by assuming a constant-velocity medium. The travel times for the scattered P wave, T_P , and the scattered S -wave, T_S , are given by

$$T_P = \frac{(r_1 + r_2)}{\alpha}$$

and

$$T_S = \frac{r_1}{\alpha} + \frac{r_2}{\beta},$$

where r_1 and r_2 (see Fig. 1) are the lengths of the first and second path segments, and α and β are the P - and S -wave velocities, respectively.

Scattering attenuation Q_s and intrinsic attenuation Q_i are difficult to distinguish because they are coupled:

$$\left(\frac{1}{Q_s} + \frac{1}{Q_i} \right)^{-1}$$

Q is often observed to be constant in a given frequency band. However, waves traveling through a strongly scattering medium may suffer greater depletion of high frequencies (Rayleigh, 1896, §296). In the case of a medium with strong scattering and high Q , the high frequencies are shifted to later time in the coda. This effect is manifested as an enrichment of high frequencies in the later portions of seismic codas recorded in southeastern Tennessee and may cause the frequency dependence of $Q = Q_0 f^n$ often observed in spectral studies of L_g wave codas.

Wavelets were corrected for spherical spreading both from the source and the scatterer. The amplitude decay depends on path length and therefore scatterer position but is assumed to be independent of frequency. The correction for geometric spreading along the source to scatterer to receiver path ($r_1 r_2$ in Fig. 1), must account separately for the source to scatterer distance, r_1 , and the scatterer to receiver distance, r_2 . The total attenuation of a wavelet due to geometric spreading along the source-scatterer-receiver path is given, for a constant-velocity approximation, by

$$A(r_1, r_2) = A_0 \frac{a_{\text{src}} a_{\text{scat}}}{r_1 r_2}. \quad (2)$$

A_0 is the initial amplitude (at the source), A is the amplitude at the receiver, and a_{src} and a_{scat} are the radii of source and scatterer. We assumed the medium to have a constant Poisson ratio, thus the P and S waves share the same ray path and have the same geometric spreading correction.

2.3 Source, Free Surface, and Instrument Response

2.4 P-Wave Source

The response of a spherical cavity to a pressure step function (Blake, 1952) was used to model an explosive (*P*-wave) source. Far-field displacement (see Fig. 2) is given by

$$\begin{aligned} s(\tau) &= \frac{C_1 P_0}{r} e^{-C_2 \tau} \sin(\omega_0 \tau) && \text{if } \tau \geq 0, \\ s(\tau) &= 0, && \text{if } \tau < 0, \end{aligned}$$

where $\tau = (t - r/c)$, t = time, r is the distance from the center of the cavity to the observer, c is the velocity of the medium, P_0 = pressure amplitude, and ω_0 is the cavity resonant frequency. C_1 and C_2 are constants that depend on the density and Poisson's ratio of the medium. We initially calculated source amplitude at the surface of the source cavity and later applied geometric spreading corrections according to path length.

The amplitude of a plane wave incident on a free surface depends on the angle of emergence γ (see Fig. 1). The ratio of emergent *P* and *S_v* amplitudes to vertical displacement amplitudes (Ben-Menahem and Singh, 1981, pp. 89-98) were used to convert confined amplitudes to vertical free-surface amplitudes.

The response of a 1.0 Hz seismometer was used as the instrument response of the model. Figure 3 shows the amplitude spectrum, $|R(\omega)|$, of the response to be linear for 1-50 Hz.

3 Scattering Response

3.1 Background

The response of the individual scatterer to an incident plane wave is a unique component of our model. Scatterers were modeled as spherical elastic heterogeneities embedded in an elastic host material. The assumption of sphericity is a first-order approximation that should yield reasonable results for media that contain many scatterers of arbitrary shape and orientation and for non-dimensional wave number $ka \leq 1$. k is wave number, $2\pi/\lambda$, and a is scatterer radius, thus, when $ka = 1$, wavelength λ equals scatterer circumference. Responses for values of ka greater than one are more strongly influenced by higher-order terms, which are required for an accurate solution, but which also lead to resonance effects that are not expected to be sustained by the shapes of scatterers more typically found in the crust.

The range of scatterer radii used in this study was 0.1-1.0 km. The lower bound was based on the resolution of the system, *i.e.* the wavelength of 25 Hz waves that travel with a velocity of 6 km/s. The maximum reliable ka and effective passband of the system determine the upper bound on scatterer size.

Energy scattered from the sphere varies as a function of non-dimensional wavenumber ka , scattering angle θ , and the material contrast between host and scatterer. The problem of determining the scattered wavefield was addressed first by Rayleigh (1896), for scalar (acoustic) waves. He demonstrated that for $ka \ll 1$, *i.e.* wavelengths which are much greater than the size of the scatterer, scattered amplitudes are inversely proportional to the fourth power of wavelength. Mie (1908) extended Rayleigh's work to obtain the general solution which expresses the

scattered vector wave field for all frequencies and the complete range of contrasts between host and scatterer materials. Mie theory has been applied extensively in many of the physical sciences, such as chemistry, meteorology, and astronomy (van de Hulst, 1956). Researchers have only recently considered its applications in elastic materials. Ying and Truell (1956) determined the scattered P and S wave fields that are generated when a P wave impinges upon an elastic sphere embedded in an elastic host medium. Their approach is followed in this work.

3.2 Separation of the Wave Equation

The wave field that is scattered when a wave impinges upon a spherical obstacle is determined by solving the elastic wave equation in spherical coordinates with appropriate boundary conditions. In a homogeneous, isotropic, elastic medium, wave motion is described by

$$\rho \frac{\partial^2 \mathbf{u}}{\partial t^2} = (\lambda + 2\mu) \nabla(\nabla \cdot \mathbf{u}) - \mu \nabla \times (\nabla \times \mathbf{u}), \quad (3)$$

where \mathbf{u} is displacement, ρ is density, and λ and μ are Lamé's elastic constants (see, *e.g.*, Aki and Richards, 1980, p. 68, or Elmore and Heald, 1969, pp. 225-229).

Following Ben-Menahem and Singh (1981, pp. 54-63), \mathbf{u} is found by solving for the radial (P) and transverse (S) components of displacement separately and then combining them for the complete solution. The radial component is represented as the gradient of a potential Φ and the transverse component is represented as the curl of a potential Ψ . By taking the incident wave to be purely P from the negative z direction (Fig. 4), the particle motion of the scattered S -waves is confined to the plane that contains the the source, scatterer and receiver.

The corresponding solution to eq. 3 is

$$\mathbf{u} = \frac{1}{k_\alpha} \nabla \Phi - \frac{1}{k_\beta} \nabla \times \nabla \times (\mathbf{r} \Psi). \quad (4)$$

The two terms represent the radial and transverse (P and S) components, respectively:

$$\mathbf{u} = (\mathbf{u}_r + \mathbf{u}_\theta).$$

3.3 Polarization of the Scattered S Wave

Amplitudes of scattered S waves are calculated in the plane of the source, scatterer, and receiver. In order to synthesize vertical-component seismograms, we need to determine the S_V amplitude, *i.e.* the component of S -wave amplitude that lies in the vertical plane which passes through the scatterer and receiver. This vertical plane and the plane that contains source, scatterer, and receiver intersect along the line that joins scatterer and receiver. The angle between these planes is used to determine the S_V component of the scattered S -wave. In the coordinate system shown in Figure 5, source, scatterer, and receiver are denoted by a , b , and c . Coordinates for longitude, latitude, and depth are given by x , y , and z . The source-scatterer path is represented by

$$\mathbf{r}_1 = (x_b - x_a)\mathbf{i} + (y_b - y_a)\mathbf{j} + (z_b - z_a)\mathbf{k}$$

and the scatterer-receiver path by

$$\mathbf{r}_2 = (x_c - x_b)\mathbf{i} + (y_c - y_b)\mathbf{j} + (z_c - z_b)\mathbf{k}$$

(see Figure 1). The normal to the plane which contains source, scatterer, and receiver is obtained from the cross product of the two path segment vectors,

$\mathbf{r}_3 = \mathbf{r}_1 \times \mathbf{r}_2$. Direction angles of \mathbf{r}_3 are

$$\alpha_3 = \cos^{-1} \left(\frac{r_{3x}}{|\mathbf{r}_3|} \right), \quad \beta_3 = \cos^{-1} \left(\frac{r_{3y}}{|\mathbf{r}_3|} \right), \quad \text{and} \quad \gamma_3 = \cos^{-1} \left(\frac{r_{3z}}{|\mathbf{r}_3|} \right)$$

The normal to the vertical plane which passes through the scatterer and receiver is designated r_4 . Its direction angles are

$$\beta_4 = \tan^{-1} \left(\frac{x_c - x_b}{y_c - y_b} \right), \quad \alpha_4 = 90^\circ - \beta_4, \quad \text{and} \quad \gamma_4 = 90^\circ.$$

The angle between the plane ABC (see Figure 5), which contains the source, scatterer, and receiver, and the vertical plane BCO , which passes through the scatterer and the receiver, is the same as the angle between their normals. The particle motion of the scattered S -wave is confined to the plane ABC and is perpendicular to the raypath \overline{BC} between scatterer and receiver, which is also the line of intersection of the two planes discussed above. Since the amplitude of particle motion is known in the plane ABC , its projection or component in plane BCO can be determined, given the angle between the two planes.

3.4 Scattered Wave Potentials

The potentials Φ and Ψ are needed to evaluate eq. 4. Ying and Truell (1956) and van de Hulst (1957) used the Mie approach to obtain solutions for scattered wavefield potentials. The frequency-domain solution is obtained by writing the potentials Φ and Ψ as spherical basis functions multiplied by undetermined Mie coefficients:

Incident P -wave;

$$\Phi^{\text{inc}} = \sum_{n=0}^{\infty} (-i)^n (2n+1) j_n(k_1 r) P_n(\cos \theta) \quad (5)$$

$$\Psi^{\text{inc}} = 0, \quad (6)$$

Scattered waves:

$$\Phi^{\text{scat}} = \sum_{n=0}^{\infty} (-i)^n A_n h_n(k_1 r) P_n(\cos \theta) \quad (7)$$

$$\Psi^{\text{scat}} = \sum_{n=0}^{\infty} (-i)^n B_n h_n(k_2 r) P_n(\cos \theta), \quad (8)$$

Internal waves:

$$\Phi^{\text{intern}} = \sum_{n=0}^{\infty} (-i)^n C_n j_n(k_3 r) P_n(\cos \theta) \quad (9)$$

$$\Psi^{\text{intern}} = \sum_{n=0}^{\infty} (-i)^n D_n j_n(k_4 r) P_n(\cos \theta). \quad (10)$$

h_n denotes the Hankel functions of the second kind,

$$h_n^{(2)}(kr) = j_n(kr) - in_n(kr),$$

used in the expressions above for outgoing scattered waves. A_n , B_n , C_n and D_n are the Mie coefficients, which must be determined for each order n and each non-dimensional wave number kr . The Bessel functions j_n and h_n are functions of the product, kr , of wave number k and radial distance r . Wave numbers are defined as

$$k_1 = \frac{2\pi f}{\alpha_h}, \quad k_2 = \frac{2\pi f}{\beta_h}, \quad k_3 = \frac{2\pi f}{\alpha_s}, \quad \text{and} \quad k_4 = \frac{2\pi f}{\beta_s} \quad (11)$$

where α and β are the P and S wave velocities in the host material and scatterer, as indicated by subscripts h and s , respectively.

3.5 Boundary Conditions

The boundary conditions at the host-scatterer interface are used to construct a system of equations in terms of the undetermined Mie coefficients A_n and B_n . Since the scatterer is modeled as an elastic heterogeneity embedded in an elastic host material, displacements and stresses are required to be continuous across the host-scatterer interface. The set of equations may be written as

$$u_r^{\text{scat}} - u_r^{\text{intern}} = -u_r^{\text{inc}} \quad (12)$$

$$u_{\theta}^{\text{scat}} - u_{\theta}^{\text{intern}} = -u_{\theta}^{\text{inc}} \quad (13)$$

$$\sigma_{rr}^{\text{scat}} - \sigma_{rr}^{\text{intern}} = -\sigma_{rr}^{\text{inc}} \quad (14)$$

$$\sigma_{r\theta}^{\text{scat}} - \sigma_{r\theta}^{\text{intern}} = -\sigma_{r\theta}^{\text{inc}} \quad (15)$$

evaluated at $r = a$, on the host-scatterer interface (Ying and Truell, 1956). r is the distance from the origin, the center of a spherical scatterer having radius a . u_r and u_{θ} are the radial and tangential components of displacement; σ_{rr} and $\sigma_{r\theta}$ indicate normal and tangential tractions.

The displacements may be written in spherical polar coordinates as

$$u_r = \frac{1}{k_{\alpha}} \frac{\partial \Phi}{\partial r} - \frac{1}{k_{\beta}} \frac{1}{r^2 \sin \theta} \left[\frac{\partial}{\partial \theta} \left(\sin \theta \frac{\partial}{\partial \theta} (r \Psi) \right) \right] \quad (16)$$

$$u_{\theta} = -\frac{1}{k_{\alpha} r} \frac{\partial \Phi}{\partial \theta} + \frac{1}{k_{\beta} r} \frac{\partial}{\partial r} \left(r \frac{\partial \Psi}{\partial \theta} \right) \quad (17)$$

Assuming a linear relation between stress and strain,

$$\sigma_{rr} = (\lambda + 2\mu) \frac{\partial u_r}{\partial r} \quad (18)$$

$$\sigma_{r\theta} = \mu \left(\frac{1}{r} \frac{\partial u_r}{\partial \theta} + \frac{\partial u_{\theta}}{\partial r} \right). \quad (19)$$

3.6 Construction of the Scattering Matrix

In order to write the boundary conditions (equations 12 - 15) in terms of the undetermined Mie coefficients A_n , B_n , C_n , and D_n , the displacements u and stresses σ are expressed in terms of their corresponding potentials Φ and Ψ (equations 5-10). The resulting equations were evaluated by using the differentiation relations among Bessel functions, *e.g.*

$$\frac{d}{dr} f_n(kr) = \frac{1}{r} [n f_n(kr) - kr f_{n+1}(kr)]$$

(Boas, 1966, p. 564) and Legendre's equation expressed in terms of differentiation with respect to θ (Arfken, 1970, p. 542),

$$\frac{1}{\sin \theta} \frac{d}{d\theta} \left(\sin \theta \frac{dP_n(\cos \theta)}{d\theta} \right) + n(\bar{n} + 1)P_n(\cos \theta) = 0. \quad (20)$$

After performing the necessary algebra (see, *e.g.*, Pilant, 1979), the system of equations that correspond to the boundary conditions (12 - 14) may be written as

$$\begin{pmatrix} g_{11} & g_{12} & g_{13} & g_{14} \\ g_{21} & g_{22} & g_{23} & g_{24} \\ g_{31} & g_{32} & g_{33} & g_{34} \\ g_{41} & g_{42} & g_{43} & g_{44} \end{pmatrix} \begin{pmatrix} A_n \\ B_n \\ C_n \\ D_n \end{pmatrix} = \begin{pmatrix} y_1 \\ y_2 \\ y_3 \\ y_4 \end{pmatrix} \quad (21)$$

The elements of the scattering matrix, \mathbf{G} , are listed in Pao and Mao (1963). In general, they are complex. The complex 4×4 system was converted to a real 8×8 before solving (Tie, 1987). In order to determine the scattered wavefield, only A_n and B_n need be calculated.

3.7 Scattered Displacements

With A_n and B_n in hand, the n^{th} -order components of the scattered wave field can be evaluated using

$$u_{r,n}^{\text{scat}}(k_1 r) = \frac{(-i)^n}{r} \left\{ \frac{A_n}{k_1} [n h_n(k_1 r) - k_1 r h_{n+1}(k_1 r)] - n(n+1) B_n h_n(k_2 r) \right\} \times P_n(\cos \theta) \quad (22)$$

$$u_{\theta,n}^{\text{scat}}(k_2 r) = \frac{(-i)^n}{r} \left\{ \frac{A_n}{k_1} h_n(k_1 r) - \frac{B_n}{k_2} [(n+1) h_n(k_2 r) - k_2 r h_{n+1}(k_2 r)] \right\} \times \frac{dP_n(\cos \theta)}{d\theta} \quad (23)$$

In the far field (for large r) equations 4.53 and 4.54 may be approximated by

$$u_{r,n}^{\text{scat}}(k_1 r) \cong -(-i)^n A_n h_{n+1}(k_1 r) P_n(\cos \theta) \quad (24)$$

$$u_{\theta,n}^{\text{scat}}(k_2 r) \cong (-i)^n B_n h_{n+1}(k_2 r) \frac{dP_n(\cos \theta)}{d\theta}. \quad (25)$$

Substitution of the asymptotic form for the Hankel functions,

$$h_n^{(2)}(kr) \sim \frac{i^{n+1}}{kr} e^{-ikr}, \quad (26)$$

produces

$$u_{r,n}^{\text{scat}}(k_1 r) \sim \frac{(-1)^n A_n}{k_1 r} \exp(-ik_1 r) P_n(\cos \theta) \quad (27)$$

$$u_{\theta,n}^{\text{scat}}(k_2 r) \sim \frac{(-1)^{n+1} B_n}{k_2 r} \exp(-ik_2 r) \frac{dP_n(\cos \theta)}{d\theta}. \quad (28)$$

The final scattered displacements are obtained by individually calculating and summing the components of each order n :

$$u_r^{\text{scat}} = \sum_{n=0}^N u_{r,n}^{\text{scat}} \quad \text{and} \quad u_{\theta}^{\text{scat}} = \sum_{n=0}^N u_{\theta,n}^{\text{scat}} \quad (29)$$

u_r and u_{θ} are the scattered P and S -wave displacements, as were to be determined. N is the maximum order of Bessel functions and Legendre polynomials included in the summation. Although the exact solution requires $N = \infty$, in practice, the series may be truncated at $N \approx ka$ without significantly affecting the results (Stenzel, 1938; van de Hulst, 1957).

4 Scattered Radiation Patterns

Scattering responses were calculated for contrasts which approximate granite or basalt scatterers embedded in a sandstone matrix. Elastic properties of the materials are specified in terms of P and S -wave velocities and density in Table 1. Figures 6 and 7 contain a series of radiation patterns, or scattering diagrams, which show the response of the inclusions to an incident plane wave. Each radiation pattern shows the angular variation in displacement amplitudes of scattered waves. An incident P -wave arrives from the left and impinges upon a scatterer indicated by the star, the plot origin. For each value of ka , a pair of radiation patterns are plotted; the top one corresponding to scattered P waves and the bottom to the scattered P -to- S . Since a P -wave source was used, scattered amplitudes are symmetric about the horizontal axis and the angular variation in amplitudes is described completely by the two-dimensional plots; note also that the S -wave response is always zero at $\theta = 0^\circ$ and 180° .

In reviewing the following results, it may be helpful to note that that nondimensional wave number ka is proportional to frequency; $k = 2\pi f/c$. Velocity c of the model is approximately 6 km/s, so $k \approx f$. For ka less than one, the response is relatively weak and the backscattered amplitudes are slightly stronger than those of the forward scattered waves. For ka of 0.4–1.0, the shape of the radiation patterns does not change significantly, but amplitudes grow rapidly as ka increases. At ka greater than one, there are major changes in character. Forward scattering becomes larger than backscattering in both the P and S wavefields as ka increases, but the effect becomes much stronger for the P waves at ka greater than two. Backscattered amplitudes reach their maxima fairly early, roughly between ka of one and two.

The response of the granite scatterer (Fig. 6) was used for most of the simulations that follow. The radiation patterns of the basalt scatterer (Fig. 7) are similar in shape to those of the granite scatterer, their main differences are in amplitude. The P -wave radiation patterns are similar to those prepared by Stenzel (1938), who also used Mie theory to calculate the acoustic wavefield scattered by a rigid sphere. Both the P and $P-S$ radiation patterns determined by us closely resemble those prepared by Wu and Aki (1985) who used the Born approximation to calculate the response of an elastic inclusion in an elastic host. The interested reader may compare our Fig. 7 with their Fig. 16.

Despite the strength of the forward-scattered P -wave at high ka , the backscattered waves tend to dominate the typical seismic coda because they persist for a much greater time (Aki, 1969). For single scattering and a uniform density of scatterers, the dominance of backscattering is explained by comparing the number of scatterers between source and receiver that can be sampled by forward-scattered paths with that sampled by backscattered paths. There is a cutoff time after which there can be no more forward-scattered arrivals, but backscattered waves will be observed until either they become too attenuated to detect or until the limit of the scattering region is reached. Although the amount of forward-scattered S -waves is small compared to that of the P -waves at high ka , the backscattered S -waves have amplitudes on the same order as those of the P for all values of ka considered.

In order to minimize computation time, scattered displacement responses were calculated independently of the synthetic coda computation. Scattered displacements were computed for scattering angles of $\theta = 0 - 180^\circ$ at 15° increments for $0 < ka \leq 2.5$, $\Delta ka = 0.1$, including up to 4th-order spherical functions. During the synthetic coda computation, the response for a particular scatterer size, wave number, and scattering angle was obtained by interpolating between the

previously tabulated values.

5 Scattered Response Spectra

The response spectra of waves scattered from a granite scatterer embedded in sandstone are shown for a series of scattering angles in Figure 8. These responses were calculated up to $ka = 6$ (scatterer circumference equals six times wavelength) and include up to eighth order terms. All of the curves show a very weak response for $ka \ll 1$, which is consistent with Rayleigh scattering and indicates that waves much longer than the size of an obstacle are not scattered. For increasing values of ka that approach one, scattered amplitudes increase rapidly, but reach a maximum at large ka . It is evident, upon comparison of the amplitudes of forward-scattered and backscattered amplitudes, that forward scattering is much stronger than backscattering for ka greater than two. The value of ka at which the maximum response is reached decreases as scattering angle increases. The response curves for backscattering ($\theta = 120^\circ$ and 180°) show that for $ka \gg 1$ the response is modulated and does not appear to converge to a constant value. This is a resonance effect caused by the generation of scattered pulses (see Varadan and Varadan, 1979; Gaunard and Uberall, 1976).

6 Synthesis of the Scattered Wavelet

Synthetic seismograms were generated by calculating the frequency-domain response associated with each scatterer, finding the associated minimum-phase wavelet, and time-shifting the wavelet to its correct position in the coda. The complete coda was obtained by superimposing all scattered wavelets. As an example of the computational method, a synthetic seismogram was calculated for a model which contains only one scatterer. The scattering response u is initially calculated as a function of non-dimensional wavenumber, ka . Velocity and scatterer radius a are used to convert ka to frequency ω so that the scattering response u can be combined with other elements of the model in the frequency domain.

The scattering response and the attenuation operator were combined in the frequency domain. The spectral response of the medium, corrected for geometric spreading and the free-surface effect, is given by

$$|X_{P,S}(\omega)| = \frac{a_{\text{src}} a_{\text{scat}}}{r_1 r_2} F_{P,S}(\gamma) |u_{P,S}(\theta, \omega)| \exp\left(-\frac{\omega T_{P,S}}{2Q}\right). \quad (30)$$

The first factor is the geometric spreading correction, F is the free surface correction, u is the scattering response, and the exponential factor corrects for intrinsic attenuation in the host medium. Vertical bars indicate the amplitude spectrum, or modulus, of a complex spectrum:

$$|X| = \left([\Re(X)]^2 + [\Im(X)]^2\right)^{0.5}$$

The scattering response and attenuation were modeled as having minimum phase. The Hilbert-transform algorithm (Oppenheim and Shafer 1989, pp. 782-789) was used to determine the minimum phase wavelet associated with $|X(\omega)|$, described as follows. First the discrete inverse Fourier transform of the logarithm

of $|X[k]|$ is computed,

$$c[n] = \frac{1}{N} \sum_{k=0}^{N-1} \log |X[k]| \exp \left[\left(\frac{i2\pi}{N} \right) kn \right], \quad (31)$$

where k and n denote frequency and time samples, respectively. Then, the Fourier transform

$$C'[k] = c(0) + 2 \sum_{k=1}^{N-1} c[n] \exp \left[\left(\frac{-i2\pi}{N} \right) kn \right], \quad (32)$$

is exponentiated and inverse Fourier transformed,

$$x[n] = \frac{1}{N} \sum_{k=0}^{N-1} \exp [C'[k]] \exp \left[\left(\frac{+i2\pi}{N} \right) kn \right], \quad (33)$$

to yield the minimum phase wavelet, $x[n]$. Claerbout's (1976, p. 62) subroutine was used to execute this algorithm.

Figure 9 shows sample moduli $|X_P(\omega)|$ and $|X_S(\omega)|$ and the wavelets, $x_P(\tau)$ and $x_S(\tau)$, which were obtained by finding and inverse Fourier-transforming the minimum-phase spectra associated with $|X_P(\omega)|$ and $|X_S(\omega)|$.

7 Superposition of Scattered Wavelets

The travel-times for for P -to- P and converted P -to- S waves along paths from source to scatterer to receiver, T_P and T_S , are used to position the scattered wavelets in the synthetic coda. Time measured from the onset of the scattered wavelet is given by $\tau = t - T$, where t is the time after source initiation. In a simple one-scatterer model, scattered P and S wavelets are time-shifted and combined with the direct wave in a single time-trace as

$$y(t) = x_0 + x_P(t - T_P) + x_S(t - T_S). \quad (34)$$

where x_0 , x_P , and x_S are the direct, scattered P , and scattered S wavelets, respectively. In a medium containing many scatterers, they can be iteratively in-

corporated in a single time trace as

$$y(t) = x_0(t) + \sum_{n=1}^N x_{P,n}(t - T_{P,n}) + x_{S,n}(t - T_{S,n}), \quad (35)$$

where $x_{P,n}$ and $x_{S,n}$ are the P and S responses of the n^{th} of N scatterers in the medium. $T_{P,n}$ and $T_{S,n}$ are the travel times from source to receiver via the n^{th} scatterer.

8 Convolution of Source and Instrument Response with the Coda

The contributions of a spherically-symmetric explosive source and instrument response are the same for all scatterers. Their incorporation may be postponed until the end and applied in a single operation on the entire coda, rather than individually for each scattered wavelet. The combined response of the source and instrument is convolved with the coda trace in the time domain. The convolution of the combined source and instrument response with the coda to generate the synthetic seismogram completes the computation. Figure 10 illustrates the synthetic seismogram generated for a one-scatterer case, it consists of a direct wave, scattered P , and scattered S wavelet.

9 Synthetic Codas

Synthetic codas were generated for models using several sets of parameters. Results are compared with observed seismograms of blasts in Alabama and earthquakes in Tennessee. Our models consisted of a 50 km thick crust with several hundred scatterers spaced 5 km apart (Figure 11). Scatterer radius was varied from 0.1 to 0.6 km, but held constant within a given model. Q was assigned to horizontal planar layers in the model. Typically a two-layer model was used, in which a low Q was assigned to the upper 5 km and a higher Q was used at greater depths.

The emergent onset typical of blasts recorded in Alabama at station BKA is best matched by synthetic codas generated with a model that has small scatterers (100 m radius) and a low- Q surface layer ($Q=150$). The low- Q layer corresponds to the 2.0 km thick Paleozoic sediments. Figure 12 compares synthetic codas with an observed event. Codas with more impulsive onsets are matched by using models with 400-600 m scatterers and a $Q = 1500$ surface layer (Figure 13). Synthetic codas were generated for a wider range of model parameters by Craig (1990).

When geological contacts are rough, with irregularities having sizes comparable with wavelength, conventional normal-moveout techniques cannot explain observed data. We used the discrete-scatterer method to investigate the response of a layer of scatterers at depth. Figure 14 schematically shows the geometry and a few raypaths. A model was considered that contained scatterers only in layers at depths of 5 km and 40, and 45 km. The near-surface zone was highly attenuative ($Q=150$). At greater depths $Q=3400$ was used. The scattering response was again taken as a 14% velocity contrast. The model and corresponding synthetic seismogram are shown in Figure 15. The seismogram has a sharp onset, followed

by a fairly rapid decay (11.3 to 15s), which correspond to the direct wave and arrivals scattered in the near-surface zone. Arrivals from the deeper layers become noticeable shortly after 17 s and persist until the end of the trace. The character of the synthetic trace is unlike the expected response of a flat reflector, but very much like Moho reflections observed on COCORP lines.

The model of a 28 km deep earthquake is shown in Figure 16. The computed response is quite different from those of models which have a surface source (11) chiefly because the direct raypath from source to receiver is no longer confined to the near-surface zone. Q was specified as 1000 for the upper 20 km and 3000 for greater depths. The response of a basalt scatterer in a sandstone host was used as the scattering response. This is a fairly strong material contrast and was used in an effort to increase scattered amplitudes relative to the amplitude of the direct arrival. Synthetic seismograms were prepared for a series of models in which scatterer radius was varied from 100 to 600 m (Fig 17). Amplitudes increase with increased scatterer size, but in all cases they decay more rapidly with time after the direct wave than do observed data (Fig. 18).

The effect of scatterer spacing was investigated by comparing the synthetic codas generated using 5 km and 10 km spacing in otherwise identical models. A scatterer radius of 0.6 km was used in both cases. The coda that corresponds to the 5 km grid spacing was generated using the previous model (Fig. 16). The same source and receiver locations and duration were used to generate a grid of scatterers having a spacing of 10 km. A synthetic coda generated using this grid decays much more rapidly than does the coda generated using the 5 km spaced grid (Fig. 19).

10 Discussion and Conclusions

A model of heterogeneities in the earth's crust as a distribution of spherical scatterers was found to be effective in synthesizing the seismic P -wave coda. The model incorporates the complete frequency-dependent anisotropic scattering response for an elastic sphere embedded in an elastic host medium. Codas were synthesized by combining the scattered P and S waves from many scatterers distributed throughout the crust. The scattering model is particularly appropriate in regions where the geology cannot be accurately represented with smooth layers.

Computations were limited to singly-scattered wavelets. The validity of the single-scattering assumption can be tested by evaluating the mean free path (Sato, 1978) in the models above. Mean free path is given by $\ell = (n\sigma)^{-1}$, where n is the number density of scatterers and σ is the effective scattering cross-section. We chose from the model parameters used in simulations the values most likely to produce multiple scattering. These consisted of scatterer spacing $\Delta x = 5$ km, scatterer radius $a = 0.6$ km, and effective scattering cross-section equal to the geometric cross-section of the scatterer. The corresponding mean free path is 110 km, thus single scattering is a reasonable assumption in this work for synthetic codas with durations up to approximately 20 s.

Mie theory provides the exact solution for the scattered wavefield for any combination of frequency and material contrast and can be efficiently applied to seismic scattering problems. Scattering responses were demonstrated to vary strongly as a function of scattering angle and frequency. Radiation patterns and response spectra were prepared, using a P -wave source, for both scattered P and scattered S waves. For an elastic scatterer embedded in an elastic medium, a significant portion of incident P energy is converted to S -waves. For non-

dimensional wavenumber ka of the incident wave less than one, backscattering is stronger than forward scattering for both P and S waves. Within this range, as ka is increased, scattered amplitudes grow significantly but the shape of their radiation patterns changes very little. For larger ka , forward scattering becomes dominant.

Responses calculated using Mie theory were incorporated in the synthesis of P codas for geologic models containing several hundred scatterers. Simulations investigated the effects of scatterer size and spacing and source-receiver geometry on the onset and decay characteristics of seismograms. Synthetic codas were able to provide reasonable simulations of P -wave codas recorded from blasts and earthquakes in Alabama and Tennessee.

The marked difference in character between the synthetic seismograms prepared for the Alabama blasts and the Tennessee earthquakes is apparently due primarily to differences in the path geometry of the direct wave. The direct wave and nearly direct scattered waves from the Alabama surface source are selectively attenuated in the near-surface zone, whereas the direct and nearly direct paths from the deeper Tennessee source to the surface traverse much the same material as do the paths of scattered waves that arrive later in the coda.

P -wave codas of relatively deep-focus earthquakes recorded under a station have strong direct arrivals, relative to scattered waves. However, the ratio of the direct-wave amplitude to amplitudes in the coda is less than predicted by the synthetic seismograms. A model with more densely-spaced scatterers would improved the match between synthetic and observed data. An alternative is a model with lateral variations in scatterer density. If a zone of anomalously high scatterer density were to exist between source and receiver, waves traveling nearly direct paths

would be attenuated more than those traveling via the longer scattered paths that avoid the zone.

Computing resources may limit the precision and complexity of the model as dictated by scatterer spatial density, frequency bandwidth, and sampling rate. Timing precision will be affected by uncertainties in the location of source and by the assumption of minimum phase for the scattering response. Realistic synthetic codas were obtained in this study with constant velocity models and a uniform spacing of spheres of the same diameter. Improvement should be expected for more realistic crustal velocity models, although the commensurate demands of raytracing will add significantly to the computation time. Models could also be improved by using an appropriate random distribution of the location and size of scatterers.

Part of the motivation for this work lies in the hope that temporal variations in Q may prove to be detectable precursors to earthquakes. Accurate and regionally specific models of the coda are needed to detect and interpret temporal variations in Q . The model presented in this work provides a means for representing the seismic coda as a linear combination of scattered responses, and can assist in the development of inversion schemes that seek to determine scattering properties of a region from seismic codas.

Acknowledgements:

Support for the first and third authors was provided by the School of Earth and Atmospheric Sciences through Research and Teaching Assistantships. Seismic data and computing facilities were provided through the Georgia Tech Seismic Observatory and the support of the U. S. Nuclear Regulatory Commission, Office of Nuclear Regulatory Research, Earth Sciences Branch.

11 References

- Aki, K., 1969. Analysis of the seismic coda of local earthquakes as scattered waves, *J. Geophys. Res.* 74: 615-663.
- Aki, K., and B. Chouet, 1975. Origin of coda waves: Source, attenuation, and scattering effects, *J. Geophys. Res.*, 80, 3322- 3343.
- Aki, K., and P. Richards, 1980. *Quantitative Seismology, Theory and Methods*, Freeman.
- Arfken, G., 1970. *Mathematical Methods for Physicists*, 2nd ed. Academic Press, New York, 815 pp.
- Ben-Menahem, A. and Singh, S. J., 1981. *Seismic Waves and Sources*. Springer-Verlag, New York, 1108 pp.
- Blake, F. G., 1952. Spherical wave propagation in solid media, *J. Acoust. Soc. Amer.* 24: 211-215.
- Boas, M, 1966. *Mathematical Methods in the Physical Sciences*. Wiley, New York, 778 pp.

- Claerbout, J., 1976, *Fundamentals of Geophysical Data Processing*. McGraw-Hill, 274 pp.
- Craig, M. S., 1990. *A Discrete-Scatterer Model of the Seismic P Coda*, Ph.D. Dissertation, Georgia Institute of Technology, 131 pp.
- Dainty, A. M. and Toksöz, M. N., 1980. Seismic codas on the earth and the moon: A comparison, *Phys. Earth Planet. Inter.* 26: 250-260.
- Elmore, W. C. and M. A. Heald, 1969. *Physics of Waves*. McGraw-Hill; republished in 1985 by Dover, New York, 477 pp.
- Gaunard, G. C. and H. Überall, 1983. RST analysis of monostatic and bistatic acoustic echoes from an elastic sphere, *J. Acoust. Soc. Am* 73: 1-12.
- Herraiz, M. and A. F. Espinosa, 1987, Coda waves: A review, *Pageoph* 125: 499-577.
- Hulst, van de, 1957. *Light Scattering by Small Particles*. Wiley, New York. Republished in 1981 by Dover, New York, 470 pp.
- Mie, G., 1908. Beiträge zur Optik trüber Medien, speziell kolloidaler Metallösungen (Optics of turbid media), *Annalen der Physik*, 25: 377-445.
- Oppenheim, A. V. and R. W. Shafer, 1989. *Discrete-Time Signal Processing*. Prentice-Hall, Englewood Cliffs, New Jersey, 879 pp.
- Pao, Y-H, and C. C. Mao, 1963. Scattering of plane compressional waves by a spherical obstacle, *J. Appl. Phys.* 34, 493-499.
- Pilant, W. L., 1979. *Elastic Waves in the Earth*. Elsevier, Amsterdam, 493 pp.
- Rayleigh, J. W. S., 1896. *The Theory of Sound*, 2nd ed., Macmillan; Republished in

1945 by Dover, New York, v1: 480 pp, v2: 504pp.

Sato, H., 1977a. Energy propagation including scattering effects: Single isotropic scattering approximation, *J. Phys. Earth* **25**: 27-41.

Sato, H., 1977b. Single isotropic scattering model including wave conversions, simple theoretical model of the short period body wave propagation, *J. Phys. Earth* **25**: 163-176.

Sato, H., 1982. Coda wave excitation due to nonisotropic scattering and nonspherical source radiation, *J. Geophys. Res.* **87**: 8665-8674.

Sato, H., 1984. Attenuation and envelope formation of three-component seismograms of small local earthquakes in randomly inhomogeneous lithosphere, *J. Geophys. Res.* **89**: 1221-1241.

Snieder, R., 1988. Large-scale waveform inversions of surface waves for lateral heterogeneity; 1. Theory and numerical examples, 2. Application to surface waves in Europe and the Mediterranean, *J. Geophys. Res.* **93**: 12055-12080.

Stenzel, H., 1938. Über die von einer starren Kugel hervorgerufene Störung des Schallfeldes (On the disturbance of a sound field brought about by a rigid sphere), *Elektrische Nachrichten Technik* **15**: 71-78, radiation patterns reproduced in Clay and Medwin (1980), pp. 192-193.

Tie, An, 1987. *On scattering of seismic waves by a spherical obstacle*, Ph.D. Dissertation, Georgia Inst. of Tech., Atlanta, 126 pp.

Varadan, V. V. and V. K. Varadan, 1979. Scattering matrix for elastic waves. III. Application to spheroids *J. Acoust. Soc. Am.* **65**: 896-905.

Wu, R. and K. Aki, 1985. Scattering characteristics of elastic waves by an elastic heterogeneity *Geophysics* 50: 582-595.

Ying, C. F. and R. Truell, 1956. Scattering of a plane longitudinal wave by a spherical obstacle in an isotropically elastic solid, *J. Appl. Phys.* 27: 1086-1097.

Rock Type	α (km/s)	β (km/s)	ρ (g/cm) ³
Sandstone	5.0	2.7	2.5
Granite	5.7	2.9	2.67
Basalt	6.4	3.2	3.0

Table 1: Properties for typical geologic materials. $\alpha = P$ wave velocity, $\beta = S$ wave velocity, and $\rho =$ density (after Dobrin, 1976, pp. 456-458).

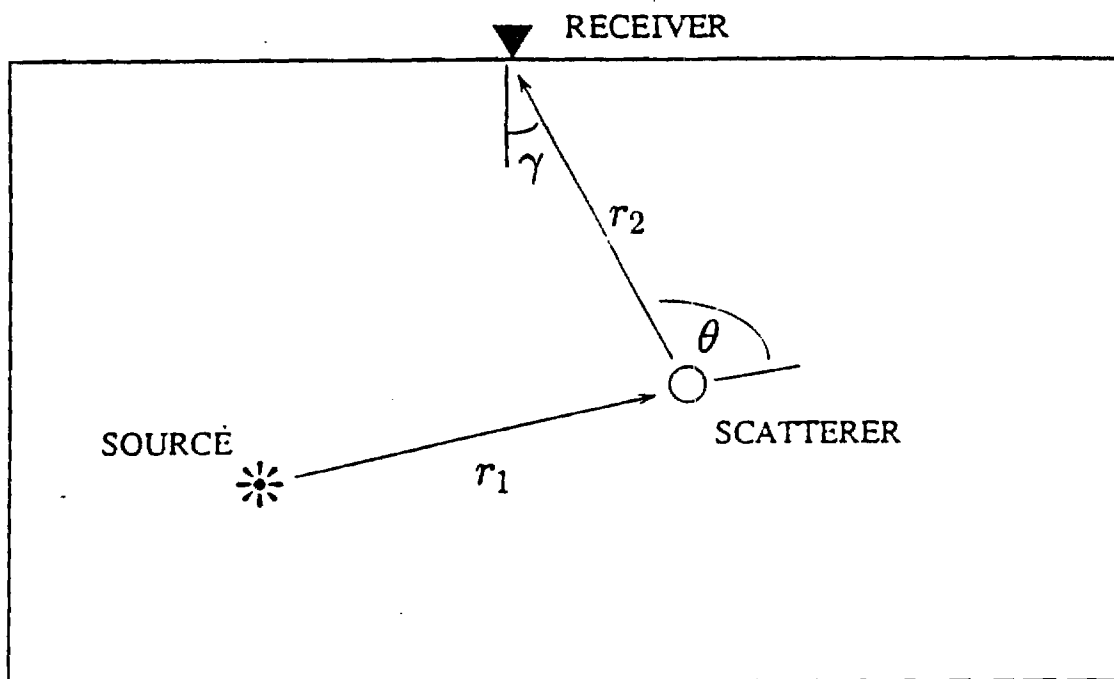


Figure 1: Scattering angle, θ , is measured in the plane of the source, scatterer, and receiver. Emergent angle is given by γ . The plane of source, scatterer, and receiver is vertical in this figure.

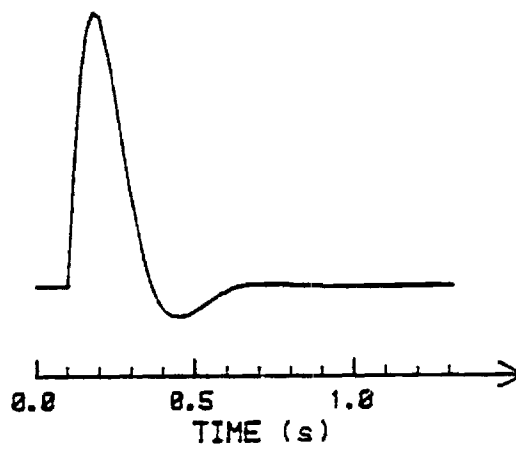


Figure 2: Source wavelet. $\sigma = 0.25$, $\rho = 2.67 \text{ g/cm}^3$, and $c = 6.0 \text{ km/s}$.

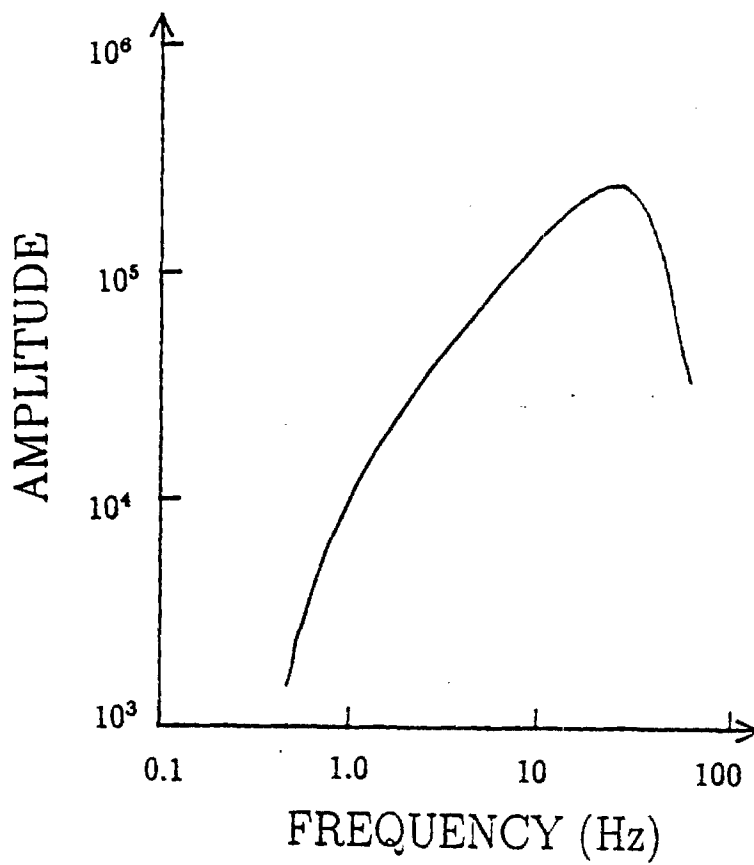
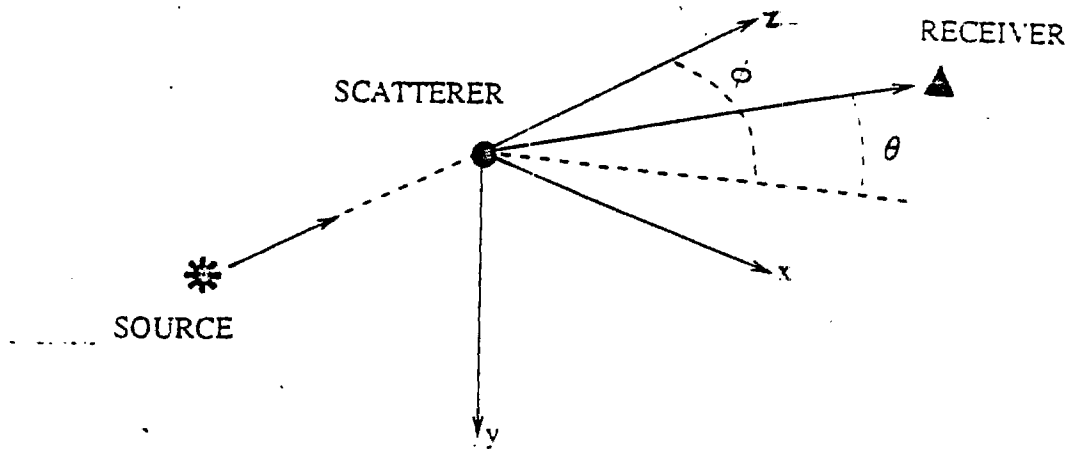
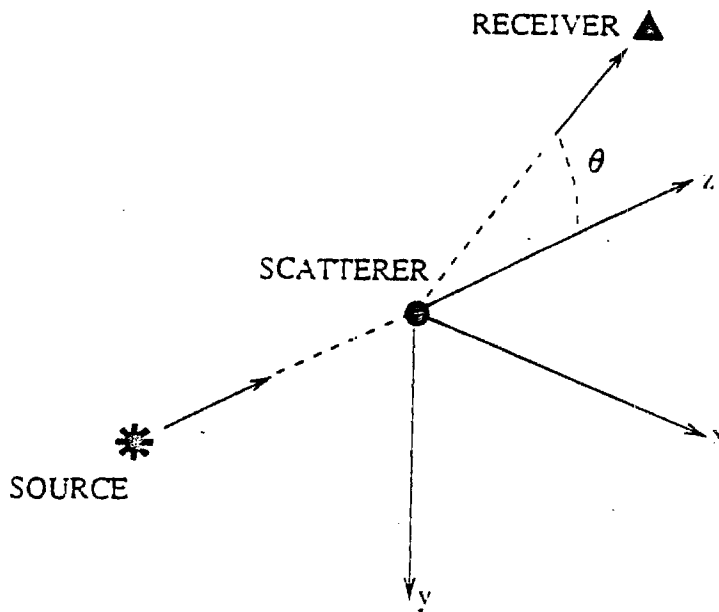


Figure 3: System response, Georgia Tech Seismic Network. Modulus, or amplitude spectrum.



3-D Coordinates



2-D Coordinates

Figure 4: Scatterer-based polar coordinate systems. Scatterer is located at the origin. The source, indicated by a star, is located on the negative z axis and the receiver is indicated by a triangle. The deflection of the ray path from scatterer to receiver is given by azimuthal angle ϕ and polar angle θ .

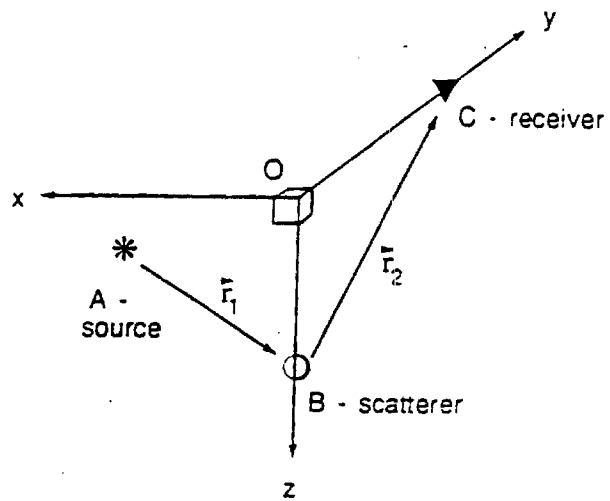


Figure 5: Coordinate system used to determine polarization of the scattered S -wave

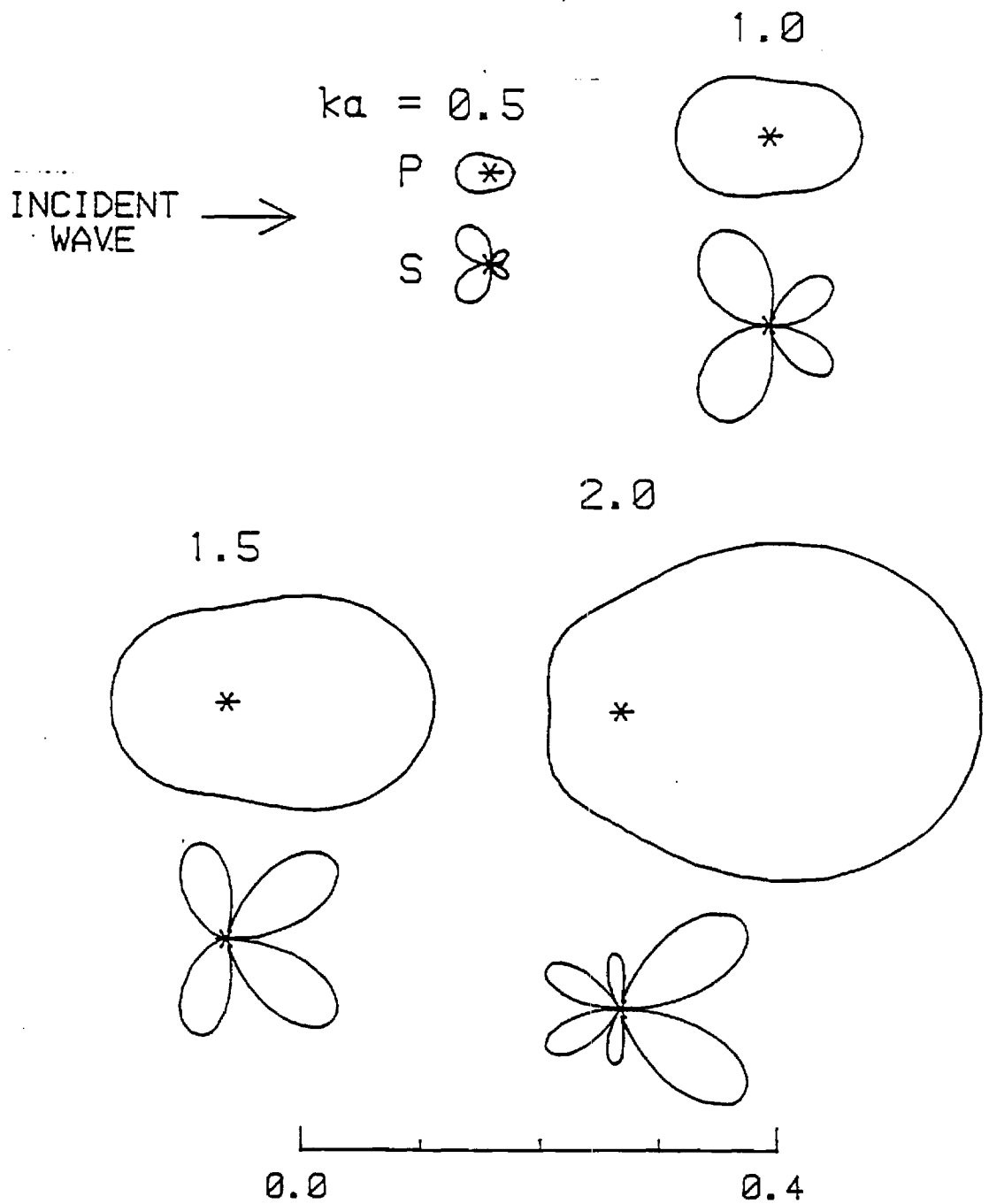


Figure 6: Radiation patterns, granite scatterer embedded in sandstone host. ka is non-dimensional wavenumber of P -waves in the host medium. Responses shown for $ka = 0.4, 0.6$ and 0.8 . The distance from the origin to the solid curve indicates the amplitude (modulus) of the scattered response.

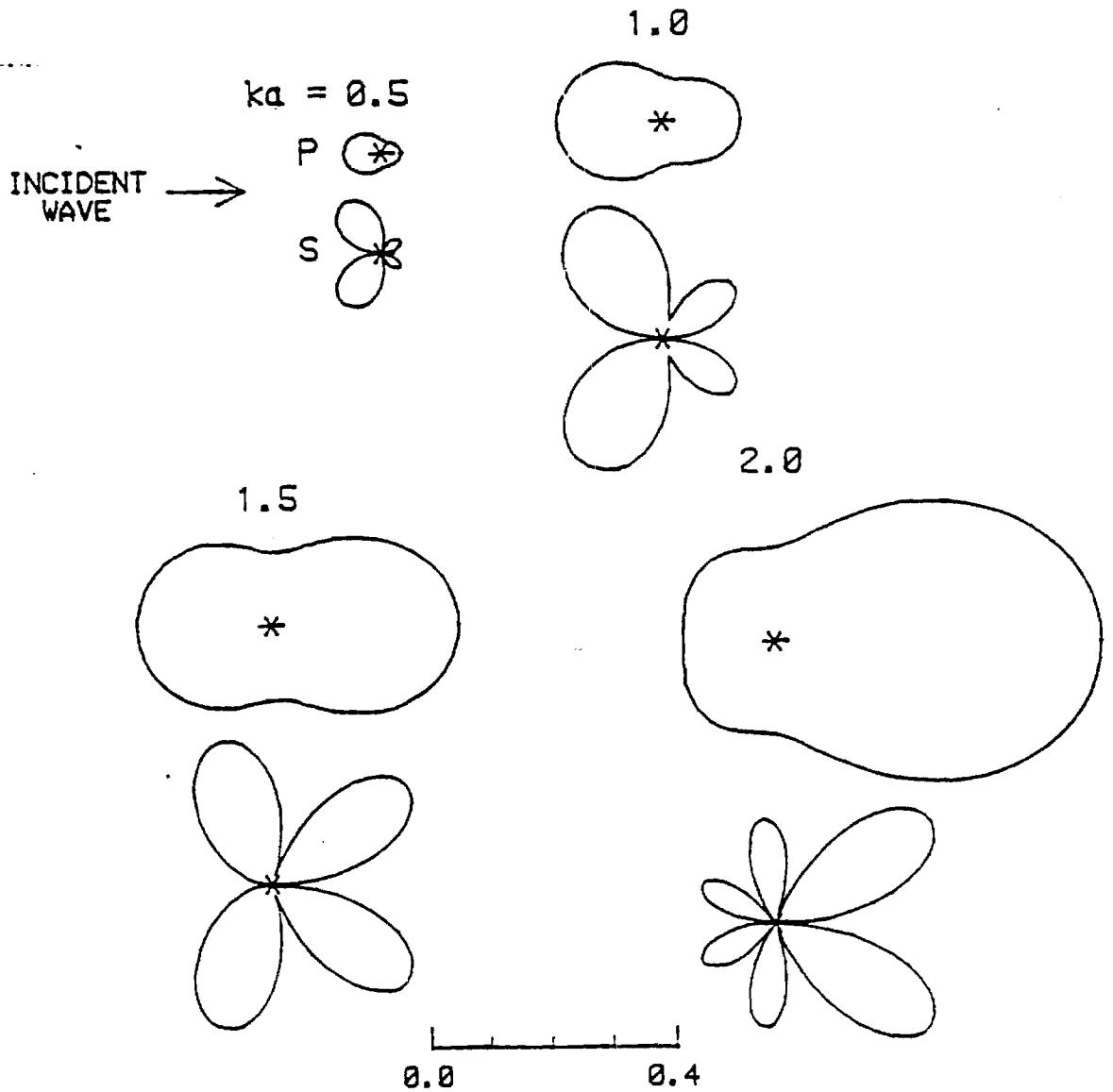


Figure 7: Radiation patterns, basalt scatterer embedded in sandstone host. ka is non-dimensional wavenumber of P -waves in the host medium. Responses shown for $ka = 0.4, 0.6$ and 0.8 .

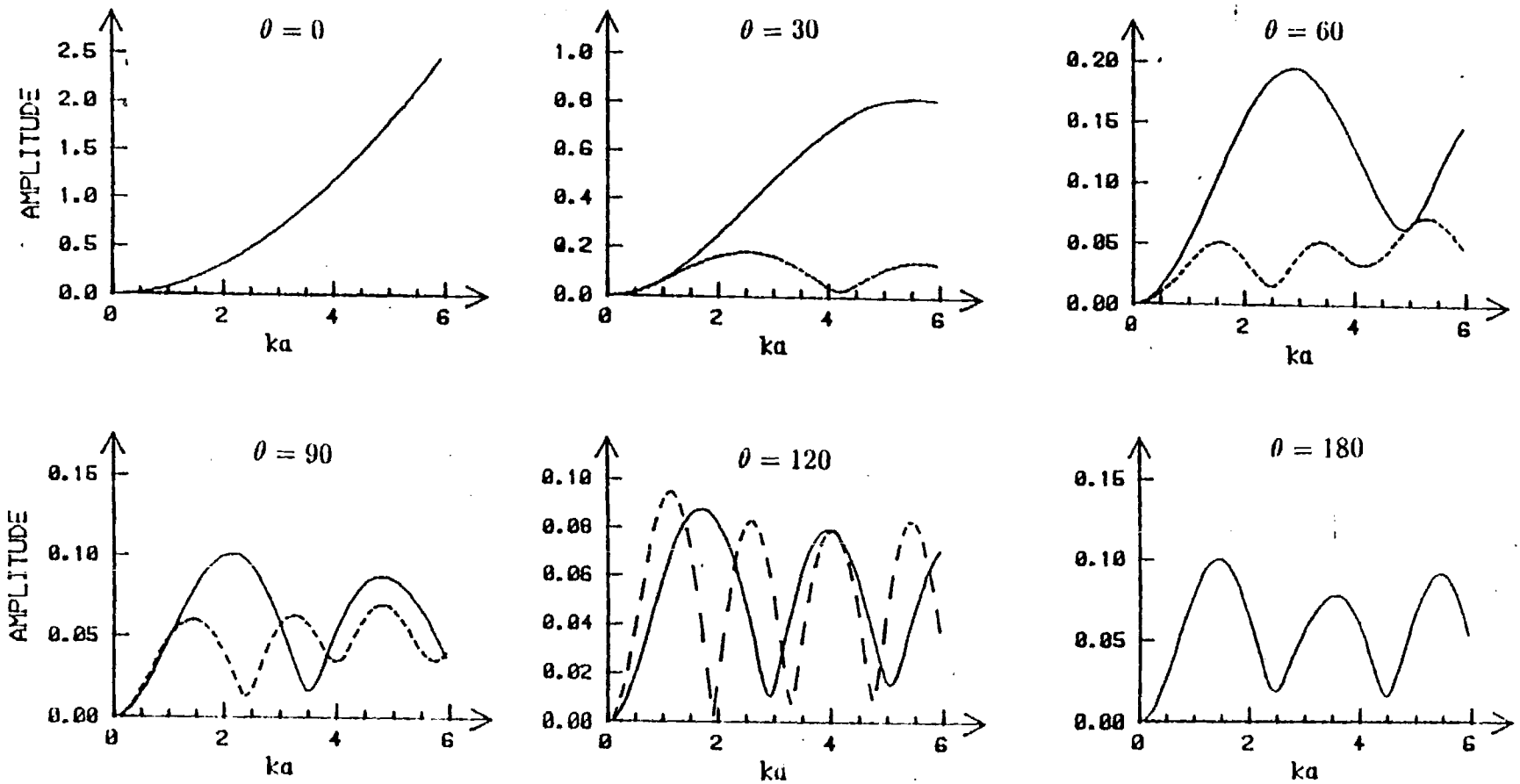


Figure 8: Scattered responses, granite scatterer in sandstone host. P responses are indicated by solid curve, S responses are dashed. ka indicates non-dimensional wavenumber of P -waves in the host medium. Note that the vertical scale varies among the plots.

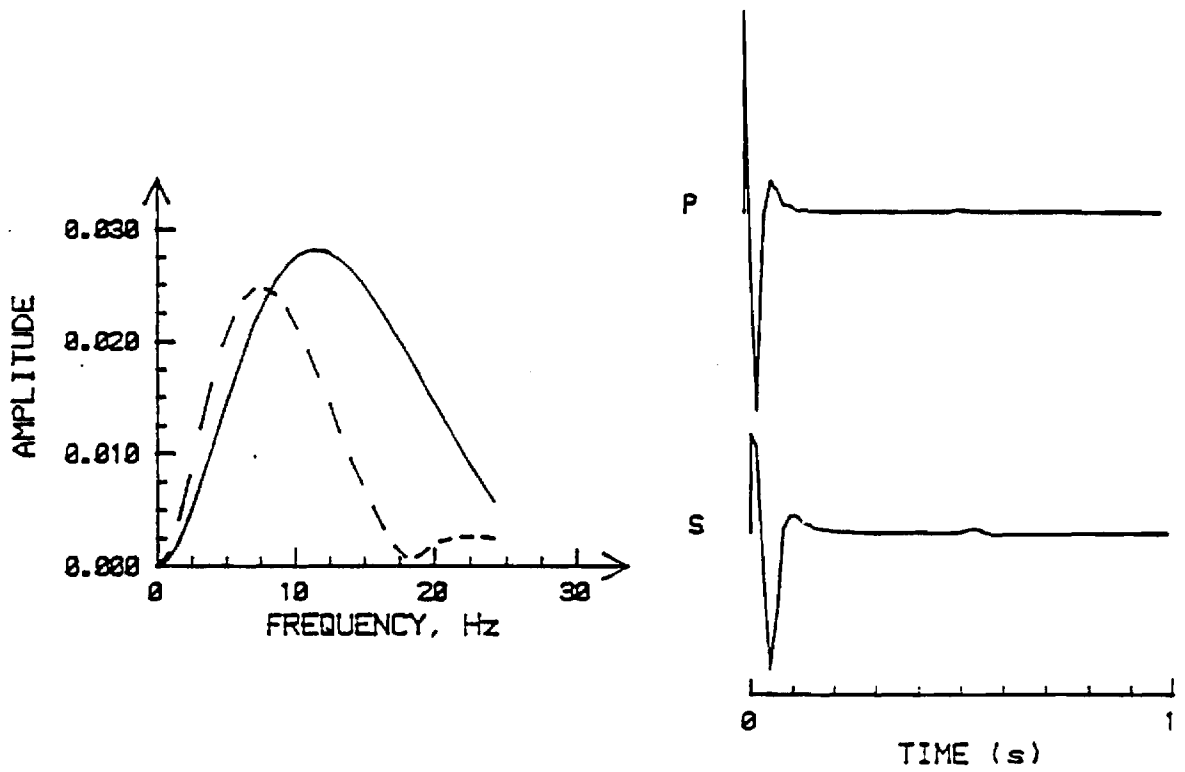


Figure 9: a. Products of attenuation operator and scattering response, P wave (solid) and S wave (dashed). b. Inverse Fourier transforms of their minimum-phase spectra.

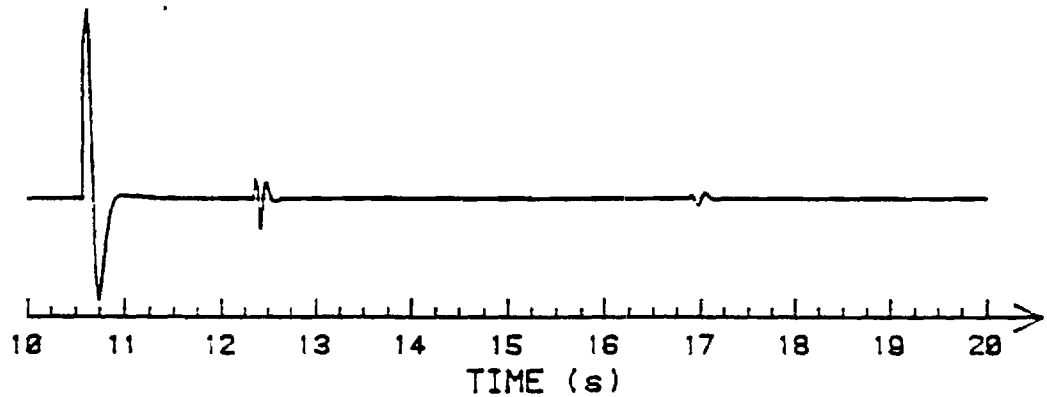
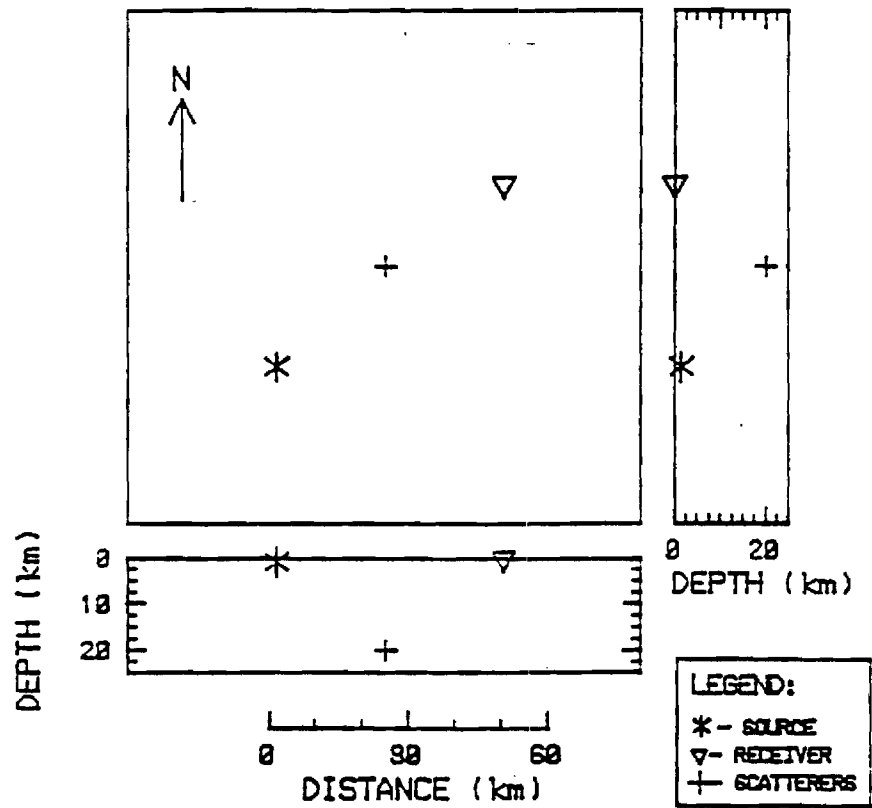


Figure 10: One-scatterer model and synthetic seismogram. The model is shown in plan view and two profiles. The direct wave, scattered *P*-, and scattered *S*-waves are shown in the seismogram.

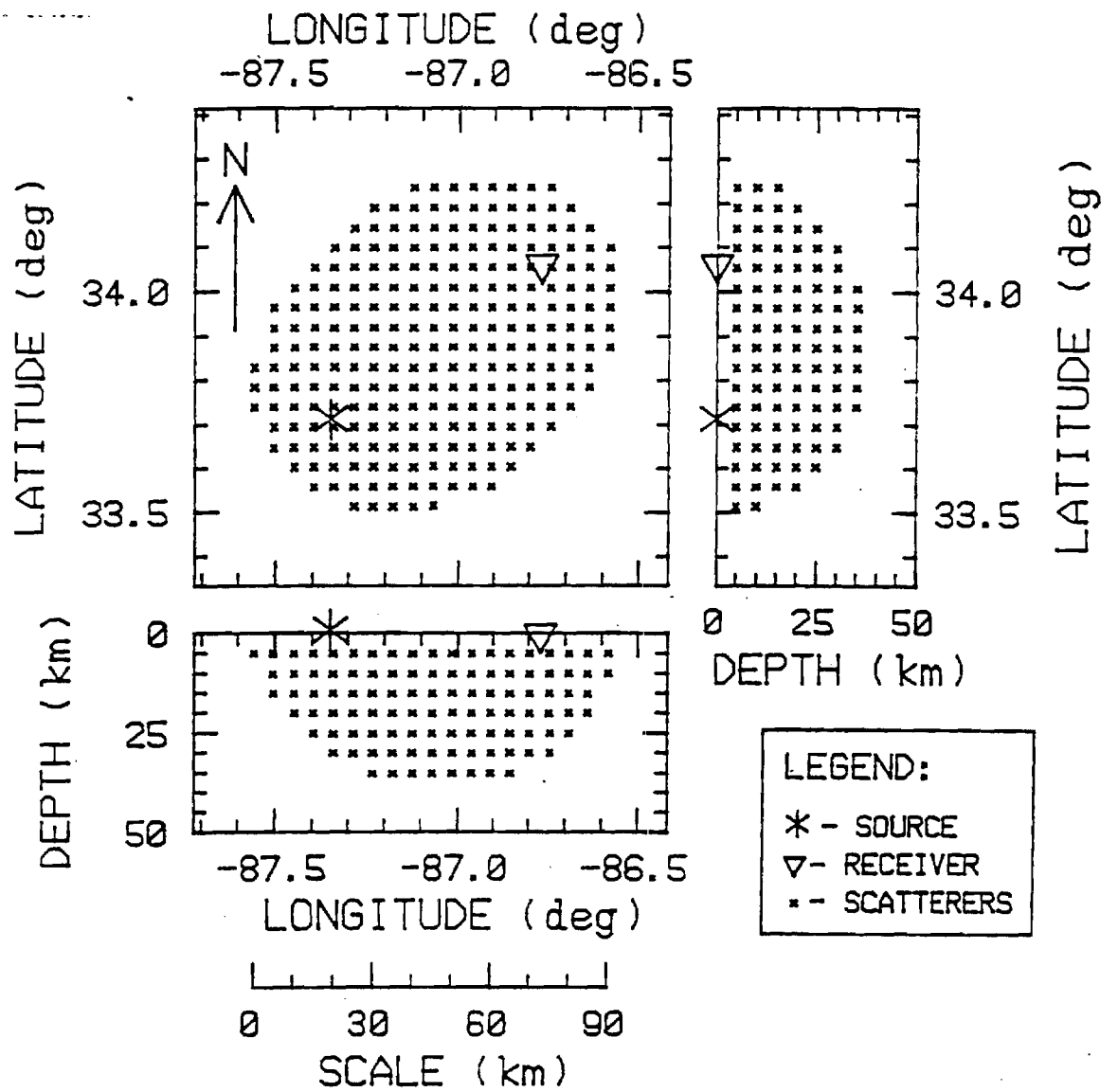


Figure 11: Alabama blast model, plan view and cross-sections. Source and receiver indicated with star and triangle. Scatterers to be considered in coda synthesis are indicated with pluses.

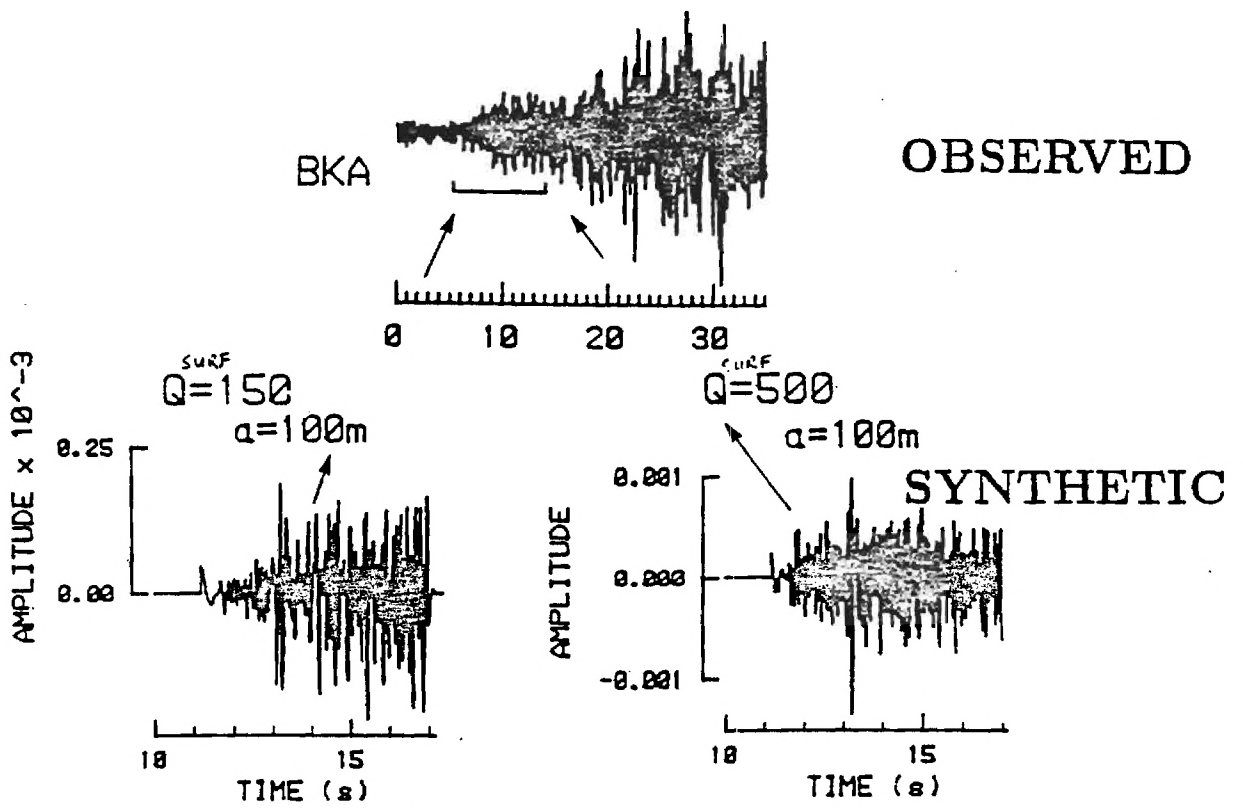


Figure 12: Comparison of observed blast (top), emergent onset, with synthetic seismograms (bottom). *P* coda in observed data is indicated by square bracket.

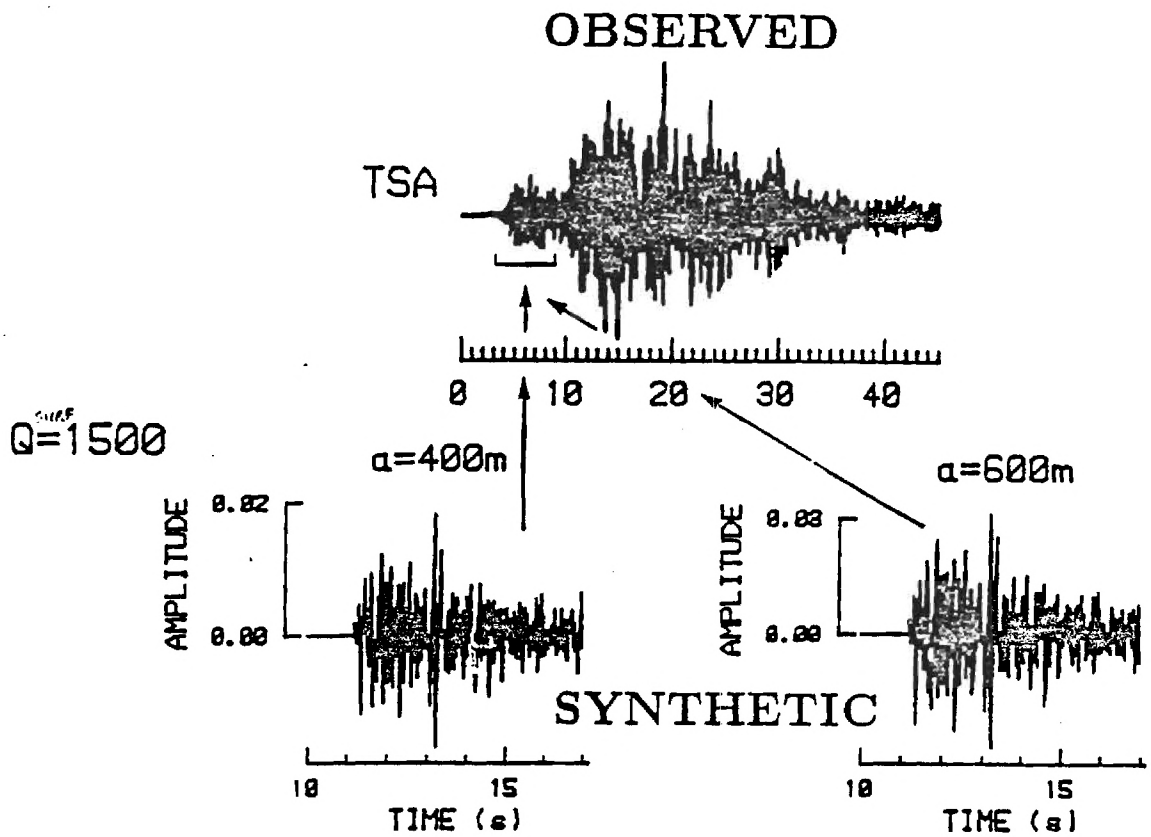


Figure 13: Comparison of observed blast (top), impulsive onset, with synthetic seismograms (bottom). *P* coda in observed data is indicated by square bracket.

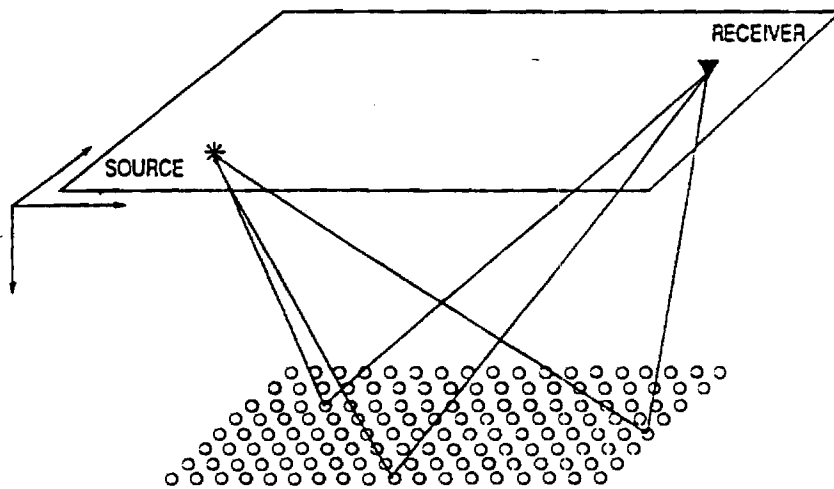


Figure 14: Schematic model for horizontal layer of scatterers. A few of the scattered raypaths are indicated.

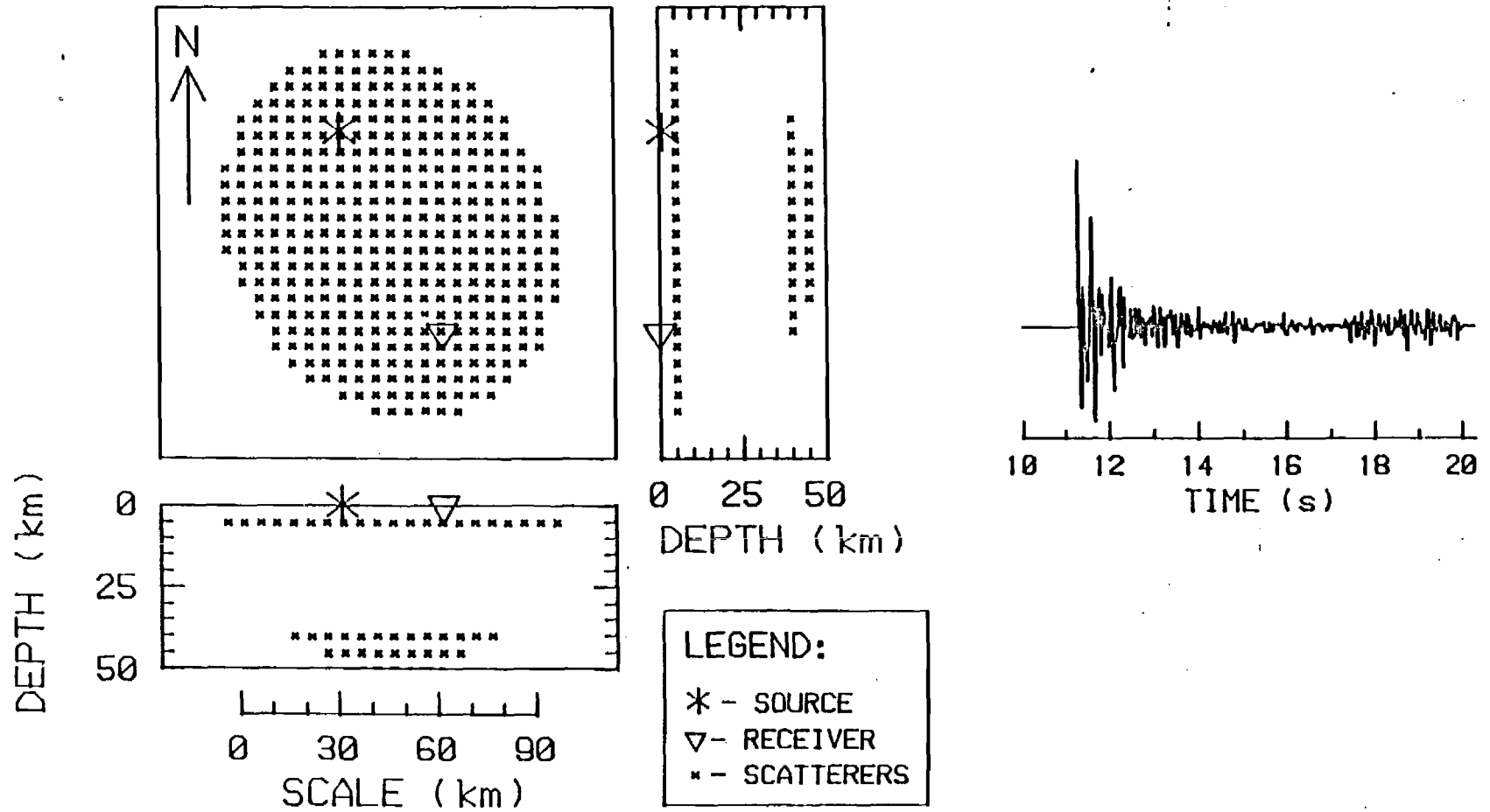


Figure 15: Model and synthetic seismogram for horizontal layer of scatterers.

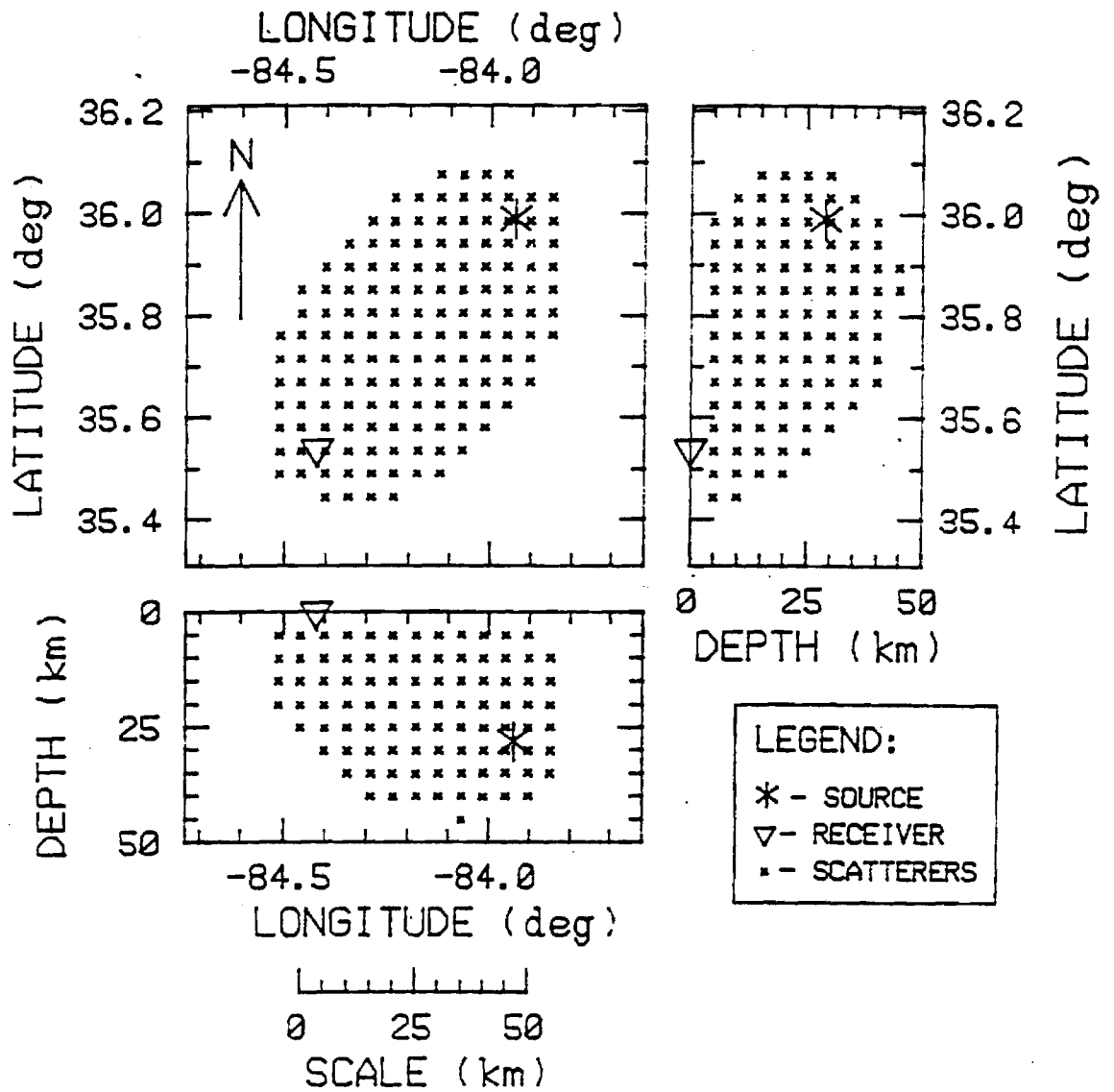


Figure 16: Earthquake model, plan view and cross-sections. Source and receiver indicated with star and triangle. Scatterers to be considered in coda synthesis are indicated with pluses.

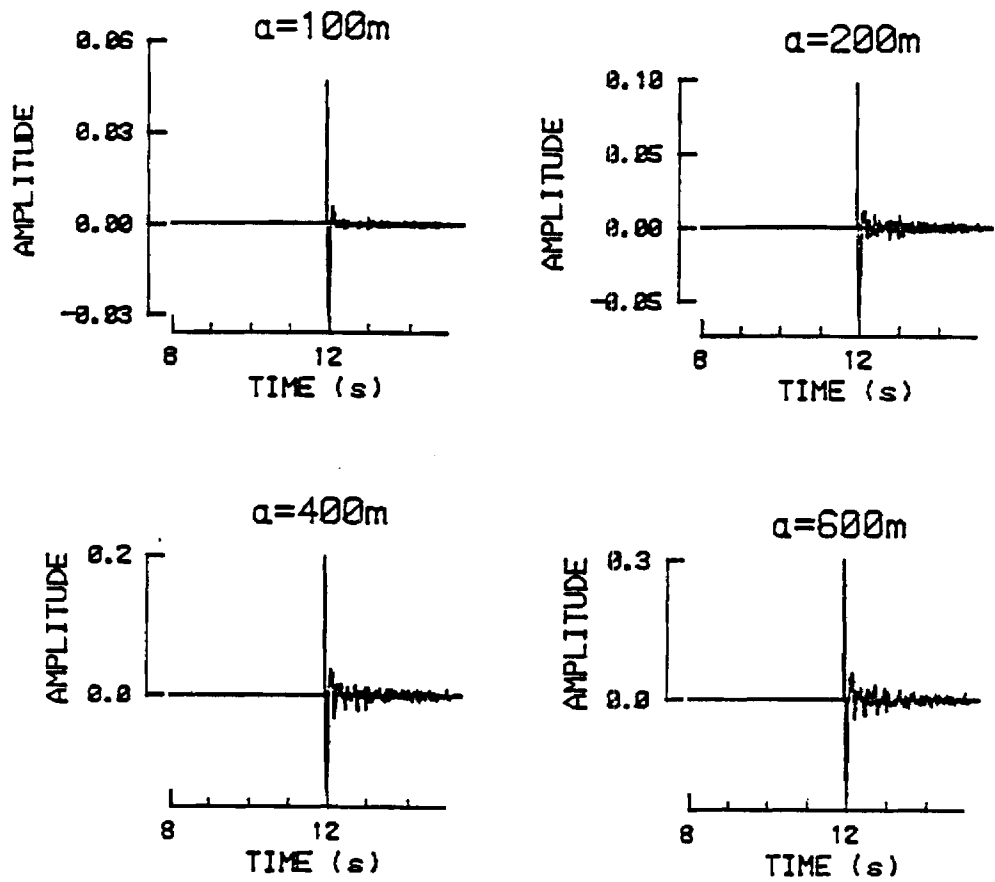


Figure 17: Synthetic seismograms generated using earthquake model, scatterer radius 100-600m.

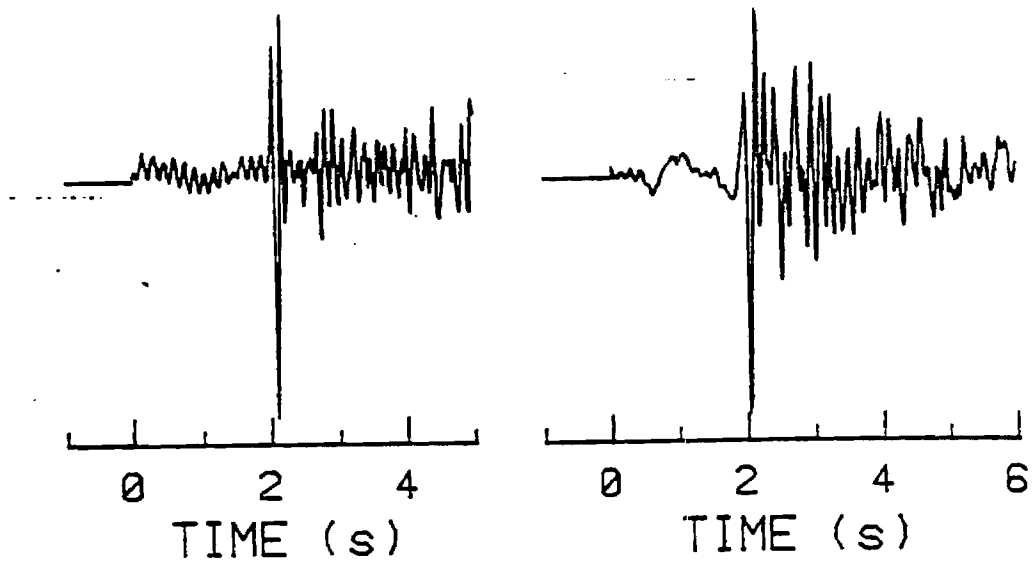


Figure 18: *P*-wave codas of earthquakes recorded in Tennessee

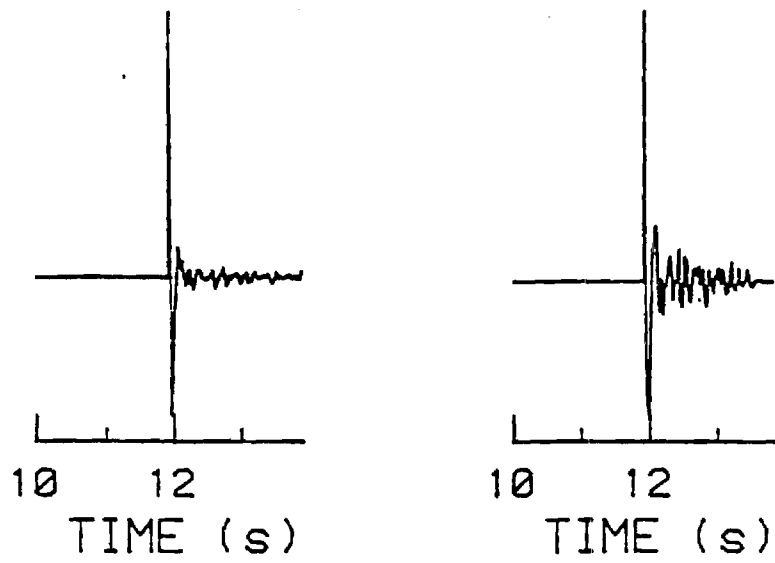


Figure 19: Synthetic seismograms generated using earthquake model, scatterer spacing 10 km (left) and 5 km (right).

APPENDIX B

A Model for Major Intraplate Continental Earthquakes

Leland Timothy Long
School of Geophysical Sciences
Georgia Institute of Technology
Atlanta GA 30332

Published in: Seismological Research Letters, Volume 59, No. 4,
October-December, 1988.

APPENDIX B

A MODEL FOR MAJOR INTRAPLATE CONTINENTAL EARTHQUAKES

Leland Timothy Long

ABSTRACT: Traditional paradigms of continental seismicity assert the stationarity of the earthquake process and a causal association of earthquakes with active faults, increasing levels of stress, and crustal structures, in a framework of Plate Tectonics. I propose, instead, that the seismicity associated with a magnitude six or greater intraplate continental earthquake is a transient phenomenon responding to a perturbation in crustal strength independent of existing faults and crustal structures. Regional plate stress may still provide the driving energy, but the causative stress is released by a perturbation in crustal strength in the vicinity of a major earthquake. The timing of a major earthquake and the characteristics of the associated seismicity may then be described by a sequence of five phases which are as follows: (1) Initiation. A major intraplate continental earthquake is initiated with a disturbance in the hydraulic or thermal properties of the crust below the epicenter. Such disturbances could be induced by the intrusion of a sill or by partial melting. (2) Strength corrosion. A corrosion in crustal strength follows the upward migration of fluids or heat from the area of recent disturbance. (3) Stress concentration. As a weakened central zone deforms in response to tectonic plate stress, stresses are concentrated in the surrounding rigid crust. (4) Failure. A major earthquake occurs when the stress surrounding the weakened core exceeds the crustal strength, either because the concentrated stresses are anomalously high or because the dispersing fluids have spread beyond the core. (5) Crustal healing. The final phase in the occurrence of a major intraplate continental earthquake is an extended aftershock sequence which is concentrated along the rupture zone of the main event. The occurrence of a major intraplate earthquake as described above releases the strain energy in a perturbed area. Additional major events would be unlikely until the strength has recovered sufficiently to equalize intraplate stress and permit a repeat of the cycle.

INTRODUCTION

The advent of Plate Tectonics has for many achieved the status of a Paradigm in the sense of Kuhn (1970). Although this assessment of the Plate Tectonics hypothesis is not immune from controversy (Mareschal, 1987), Plate Tectonics has achieved virtually universal acceptance and has for the last 20 years provided the earth science community with a basis for modeling and understanding the dynamic lithosphere. Present studies of

the continental and oceanic lithosphere consist largely of verifying the Plate Tectonics model through data acquisition and perfecting this model through the construction of sets of auxiliary hypothesis. A notable exception to the success of Plate Tectonics has been the lack of agreement on a generally acceptable model for major intraplate continental earthquakes. Hypothesis of diverse character (for examples see Dewey, 1985; Long et al., 1986) are yet to be rejected. Although the Plate Tectonics model deserves recognition for some measure of success (Dewey, 1988), formidable problems for its application to major intraplate continental earthquakes still exist because many observations, such as the sparsity of continually active surface ruptures, have not been reconciled with Plate Tectonics and because the existing models do not predict or explain isolated large earthquakes. Although Dewey (1988) does not see anomalies sufficient to imply an imminent revolution in seismotectonics, one might question whether the existing confusion in the understanding of intraplate continental earthquakes could suggest that the current routine science phase may be heading for a crisis, albeit only in intraplate seismotectonics, and whether at this time an examination of the application of commonly accepted paradigms to intraplate earthquakes might be in order.

For discussion purposes in this paper, a major intraplate earthquake or closely timed earthquake sequence is one with magnitudes greater than six and minimum fault rupture lengths on the order of 20 km. The Charleston, South Carolina, 1886, earthquake is such an event and the 1811-12 New Madrid sequence of at least 4 events would represent another. These and other major earthquakes are assumed to cause a failure of the strongest portion of the crust, which is typically in the depth range of 10 to 25 km. At these depths the tractional resistance to fault slip increases to the maximum stress sustainable in a viscous lower crust subject to a given strain rate (Chen and Molnar, 1983).

Intraplate continental earthquakes may be divided into two classes. The class containing large damaging earthquakes is the subject of the new model to be presented in this paper. These large events pose the dominant risk from intraplate continental earthquakes, but are limited to locations and time periods associated with a perturbation in the properties of the lower crust. The second class of events is dominated by small shallow earthquakes with limited seismic risk. The second class includes most of the shallow (0-10 km) focus earthquakes which can be attributed to many sources of stress or strength perturbation on existing shallow fractures. This class would include induced seismicity. These smaller shallow events play a role in this model for major earthquakes, as well as being widely distributed outside potential sites of major events.

In this paper I present alternatives or, perhaps, opposites to five paradigms in the seismotectonics of intraplate continental earthquakes and suggest a mechanism which is consistent with these alternatives. These alternatives are implicit in the basis for the proposed new model and question the extent that interiors of continental plates mimic the plate geometry and strength distributions of the more homogeneous oceanic plate and the extent that plate tectonics boundary phenomena can be transferred to intraplate tectonics. The model, if acceptable, could support the possibility that the alternate paradigms may be more appropriate for plate interiors. Also, the acceptance of this model could pose the possibility that adherence to the plate tectonics model has inhibited recognition of some dynamic processes in the lower crust that could play a large role in intraplate continental seismotectonics. If such a model can resolve inconsistencies in observations, explain why the old model does not work and predict new observations, then, perhaps, a change in our perspective of midplate continental seismotectonics is indeed in order.

FIVE PARADIGMS

Five paradigms for intraplate continental earthquakes are outlined in Table I. All have been questioned before and their degree of acceptance varies; but, in this paper a model is presented that simultaneously satisfies alternatives that are not generally accepted.

Paradigm 1: Earthquakes occur on active faults. This paradigm predates Plate Tectonics and holds that earthquakes occur through the release of stress accumulated on locked portions of active faults.

Alternative: Faults and related zones of weakness are created by the earthquake process and are not necessarily sites of future events. Faults are simply a manifestation of the earthquake process.

Paradigm 2: Earthquakes are the result of increases in deviatoric stress, released along faults or concentrated by structures in the crust.

Alternative: Earthquakes are a release of stress triggered by a decrease in strength which may be attributed to changes in physical properties of the crust.

Paradigm 3: The seismicity of the continental crust is associated with blocks of crust, major geologic structures, and their associated faults. The study of these structures should lead to an explanation for major earthquakes.

Alternative: The earthquake mechanism is independent of tectonic events and major geologic structures which are evident from studies of near-surface geology. The strength of the crust would be more dependent on depth than rock type and, perhaps, crustal strength would be controlled more by properties such as fluid content in the lower crust and upper mantle than by the rock type.

Paradigm 4: Short-term changes in pore-fluid pressure influence seismicity only in the vicinities of reservoirs.

Alternative: In this case the alternative is an expanded role for fluids in triggering earthquakes, including those at depth in the crust. This is the Hydroseismicity hypothesis as proposed by Costain et al. (1988).

Paradigm 5: Seismicity is a stationary process, with past events strongly suggesting the locations and magnitude distribution of events in the future. Locations of earthquakes in the past will continue to be active at the same rate.

Alternative: A major mid-plate earthquake and its aftershock sequence is a transient phenomena. Contemporary seismicity consists only of aftershocks from major past earthquakes and, as such, is of minimal utility in predicting future major events.

TABLE I Conventional Paradigms and Alternates.

<u>Conventional Paradigm</u>	<u>Alternate</u>
Active faults cause earthquakes	Earthquakes create faults
Increases in stress causes failure of crust	Change in strength causes failure
Crustal blocks and geologic structures control plate dynamics	Plate strength independent of block composition or block boundary
Reservoir induced seismicity is shallow and only near reservoirs	Hydraulic mechanism may occur anywhere "hydroseismicity"
Stationary process	Transient process

THE ALTERNATE MODEL

On discarding the traditional paradigms of intraplate continental seismicity and considering seismicity with the perspective of selected alternatives (or opposites), a model can be devised that describes the creation of a major earthquake and the characteristics of its associated seismicity. In this new model a major earthquake may be described as a sequence of five phases in the transient perturbation of the strength of the crust. The five phases are: (1) initiation, (2) strength

corrosion, (3) stress redistribution, (4) failure, and (5) crustal healing (see also Figure 1). I tender this model as an improvement over traditional paradigms for a description of the principal characteristics of zones of seismicity associated with a single major intraplate earthquake.

Phase 1 Initiation: The sequence of events leading to a major intraplate earthquake may be initiated with a disturbance in the hydraulic or thermal properties at Moho depths in a small portion of the continental crust. Such a disturbance could be induced by the intrusion of a sill or by partial melting. At the time of the initial disturbance, the strongest portion of the crust at a depth of 10 to 25 km cannot be penetrated by fluids from below. A horizontal zone of partial melt is formed and becomes a source for fluid and thermal perturbation of the overlying crust.

Evidence: During phase 1, the fluids generated in crustal underplating by intrusion of sills or partial melting in viscous deformation could create or enhance reflections from horizontal sills and provide direct evidence for the initiation of a major earthquake sequence. The existence of viscous deformation or multiple sills in the lower crust is suggested by the prominence of thin reflectors observed in deep crustal seismic reflection data (Allmendinger et al., 1987). Also, sills of molten material are observed at mid-crustal depths in areas of active tectonics (Brown et al., 1979). At Moho depths, studies suggest that a sharp reflecting Moho is the signature of recent tectonic activity and may be explained with the formation of sills. A reflecting Moho often is observed to truncate crustal structures of the most recent tectonic events, such as the vertical movements of the crust in the Basin and Range province (Klemperer et al., 1986). A possible association between seismicity and a sharp Moho (and hence recent tectonic activity) is suggested in the zone of active seismicity in southeastern Tennessee, where the Moho is clearly defined by reflections (Long and Liow, 1986), although the surrounding area is characterized by a gradational Moho (Owens et al. 1984).

Phase 2, Strength Corrosion: A corrosion in the strength of the lower crust could be caused by an upward migration of fluids or heat from the recently implanted sill or partial melting of the lower crust. The fluids may be driven by the higher temperatures of the sill or they may follow vertical tension cracks related to regional plate stress. Fluid pressures could vary between hydrostatic and lithostatic in sealed compartments controlled by a complex feedback among fluid flow, temperature, chemistry and strength.

A spatial variation in the crustal strength-versus-depth relation for the crust is generally accepted as an explanation

for differences in the maximum depth-of-focus of intraplate earthquakes (Chen and Molnar, 1983; Meissner and Strenhlau, 1982). Continental crust with earthquakes at a maximum depth of 5 to 15 km is characterized by high heat flow and recent tectonic activity. Continental crust with earthquakes at a depth of 15 to 25 km are characterized by limited tectonic activity and low heat flow. At shallow depths, the maximum possible stress is controlled by the mineralogical and physical properties of existing fractures, and Byerlee's law governing frictional strength versus depth. At depths below approximately 15 km the viscosity of the lower crust controls the ability to sustain stress. Increases in fluid content or temperature decrease the strength of the crust and shallow the zone of maximum possible stress. The corrosion of strength in a localized volume of the lower crust of a stable tectonic area could initiate seismicity by releasing regional compressive stress. This central zone or core of weakness would be a continuing zone of anomalous seismicity through phase 3. The dominant focal mechanism would be strike slip because the distortion of the weakened central zone, which would be analogous to the distortion in a hole in a plate, will keep the vertical axis the neutral axis. The corrosion of strength would imply preference over existing fault planes for new fault planes defined by the directions of maximum shear stress .

Evidence: Coda Q, which can be estimated using a space-time function for coda energy density, varies with seismic activity. Zones of anomalous Q are observed under volcanic regions and the Q value is observed to vary with the progress of a volcanic eruption (Fehler, et al., 1988). In China areas of low coda Q are associated with the largest earthquakes (Jin and Aki, 1988). In southeastern Tennessee coda Q was computed by the technique of Jin and Aki (1986). A simple inversion for Q structure suggests that azimuthal variations of coda decay can be explained by a zone of anomalously low coda Q (less than 100) in the area of southeastern Tennessee (see figure 2) which contains the largest and most numerous events (Long et al., 1987). This area exhibits a uniform strikeslip focal mechanism (Teague et al., 1986). The low coda Q suggests a perturbation in the fluid or fracture properties of the crust and the strikeslip focal mechanisms are consistent with the reaction of a central zone of weakness to regional plate stress. The presence of fluids in cracks and microcracks at depth in the crust explains (Al-Shukri and Mitchell, 1988) the association of enhanced earthquake activity with low velocity in the crust near the New Madrid seismicity.

Phase 3, Stress Concentration: The development of a central zone or core of weakness through a disturbance in the fluid and thermal properties is not sufficient in itself to cause a large earthquake. The area of developing weakness must also be under stress if energy is to be available for a large event. A likely source of the stress would be horizontal plate stress, usually

attributed to ridge push mechanisms. As a weakened central zone relaxes, stress is transferred to the surrounding more rigid crust where it is concentrated the greatest at the boundary of the core of weakness. In this phase, earthquake activity is greatest in the central zone, but surrounding the central zone earthquakes may occur with fault planes too small to rupture the strongest portion of the crust. These could represent stress adjustments on shallow planes of weakness, where the source of stress could be a reaction of the shallow crust to flexure about the deforming core of weakness. These events could also be triggered by a changing hydraulic regime.

Evidence: Finite element and theoretical models (Campbell, 1978) of a plate with core of weakness show increased stress surrounding the core. Stress within the core would be less, but uniform in its response to the regional stress. In this theoretical model the pattern of stress directions outside the core depend on the concentration at the boundary of the core and can include principal axes directions and magnitudes that deviate significantly from those of plate stress.

In southeastern Tennessee, a concentration of stress is suggested by the distribution of focal mechanisms (see figure 2). Inside the low coda Q area, which may coincide with a core of weakness, the dominant focal mechanism is strikeslip. Focal mechanisms outside this area show significant thrust and normal components. The pattern of seismicity in southeastern Tennessee is one of a concentration of activity in the vicinity of the low-Q area and activity becoming more diffuse with distance away from the central zone. The shallower events outside the core may represent a response of crustal zones above the maximum strength depth zone to distortion of the stress channel around the core of weakness.

Phase 4, Major Failure: A major earthquake occurs when the stress surrounding the central disturbed zone exceeds the strength of the crust, perhaps, because the dispersing crustal fluids have spread beyond the central disturbed zone and weakened the crust or because the stress load has shifted to the outside of the core of weakness. The geometrical pattern of the central zone and the dispersion of the fluid may determine the location and existence of the major earthquake. If the major earthquake occurs, at least two distinct patterns of faulting are possible. One pattern would consist of two near-vertical faults striking parallel to the direction of maximum shear stress of the regional field and extending away from diagonally opposite edges of the central core. These faults could be connected in the central zone by a fault or a series of faults in the complimentary direction. The other pattern would develop when deformation is resisted by a thinned strong portion of the crust above the core. In this case the major earthquake will occur on a reverse fault

with dimensions comparable to the size of the core of weakness.

Evidence: In the New Madrid seismic zone the pattern of aftershocks define two sub-parallel faults trending north-northeast and a connecting west-northwest sequence of faults (see figure 2). Various segments of these faults are believed to have ruptured during the sequence of four large events in 1811 and 1812. Hence, for the New Madrid earthquake zone, the contemporary pattern of faulting was developed through a sequence of earthquakes. The other pattern was exhibited by the Marryat Creek, Australia, earthquake (McCue *et al.*, 1987). The focal mechanism was strike slip with a thrust component which was more evident in the surface displacement.

Phase 5, Decay: The final phase in the occurrence of a major intraplate earthquake is an extended aftershock sequence. The fluids, no longer replenished by the hydraulic or thermal disturbance of the lower crust, dissipate from the core, subsequently increasing the strength of the crust and inhibiting additional earthquakes, except along the weakened fractures of the major event. Aftershock activity concentrates on the fault plane of the main event(s) and associated faults instead of in the core. Also, the amplified stress around the core is released, decreasing the overall level of stress and limiting the potential for additional significant activity.

Evidence: Most major earthquake areas in the eastern United States can be modeled as aftershock sequences. This is a controversial conclusion that is best illustrated by the Charleston seismicity. Seismologists generally accept the assumption that the immediate aftershock activity ended within a few years (Seaber and Armbruster, 1987); however, the felt events for the full 100 years are satisfied just as well by Omori's law for aftershocks (Long, 1982; Bollinger, 1983). Prior to 1886, the Charleston area showed little evidence of seismic activity.

DISCUSSION

Each phase of the proposed model suggests phenomena that could be observed with available geophysical techniques. Such observations could answer questions concerning the details of this mechanism. In phase 1 the strength and coherence of a reflecting Moho in an incipient seismic area could be an indication of recent underplating of the crust and evidence that new fluids or thermal perturbations are available to initiate the sequence of events leading up to a major intraplate earthquake. Variation in time of the Moho reflection amplitude, including the appearance of bright spots, could identify new locations of possible major events and answer questions concerning the rates

of fluid movement in the lower crust. In phase 2, the orientation of fractures with the direction of principal regional stress might be measured with shear-wave anisotropy. In phase 3 the depth distribution and focal mechanism of events surrounding the active central core should reflect the deformation and accumulation of stress. The dominant strike-slip focal mechanisms in the core of weakness suggests conditions that should continue to foster anisotropic behavior of the crust. Also, the central core should exhibit anomalously low Q. By identifying potential candidate seismic zones for phase 3, the areas of high risk may be restricted to a few areas where the pattern of seismicity suggests a potential for a major earthquake. In phase 4 the size and perhaps existence of the major event would be proportional to the magnitude of plate stress, as well as the size of the perturbed zone. In phase 5 the seismicity should exhibit a decay in activity typical of extended aftershock sequences.

The occurrence of a major intraplate continental earthquake as described in this model decreases the stress in the perturbed area. Additional major events would not be expected there again until the strength has recovered enough for a repeat of the cycle and until the regional plate stress has re-equilibrated. The rate of strength recovery is one unanswered question, but the time to recover half the strength must be on the order of an extended aftershock sequence. Incomplete recovery could provide paths for later intrusions, particularly if located over a recognized hotspot, and explain evidence for repeated major events in areas like New Madrid. Another unanswered question is the time required to progress through phase three. Evidence on the rate of movement of magma suggest this time could be on the order of years. Other unanswered questions concern the size of the lower crustal disturbance needed to trigger a major event and the certainty of the major event occurring in a seismic zone currently in phase three.

Many of the phenomena suggested above have not been observed, perhaps, in some cases because of a lack of data. However, many of the enigmas of major continental earthquakes, such as the pattern of epicenters in New Madrid, the lack of continuous seismic activity on the Meers fault, and the lack of continuous shear zones showing long-term deformation, are described by a model satisfying alternatives to traditional paradigms for continental seismicity. If such a model can resolve these and other inconsistencies in observations, explain why some aspects of the Plate Tectonics model do not work and predict new observations, then, perhaps, a change in our perspective of continental tectonics is indeed in order.

REFERENCES

- Allmendinger, R. W., K. D. Nelson, C. J. Potter, M. Barazangi, L. D. Brown, and J. E. Oliver (1987). Deep seismic reflection characteristics of the continental crust, Geology, 15, 304-310.
- Al-Shurri, H. J., and B. J. Mitchell (1988). Reduced seismic velocities in the source zone of New Madrid earthquakes, Bull. Seism. Soc. Am., 78, 1491-1509.
- Brown, L. D., P. A. Krumhansl, C. D. Chapin, A. R. Sanford, F. A. Cook, S. Kaufman, J. E. Oliver, and F. S. Schilt, (1979). COCORP seismic reflection studies of the Rio Grande rift, in Rieker, R. E., ed., Rio Grande rift: Tectonics and magmatism: Washington, D. C., American Geophysical Union, 169-184.
- Bollinger, G. A. (1983). Speculations on the nature of seismicity at Charleston, South Carolina, in Gohn, G. S., ed., Studies related to the Charleston, South Carolina, earthquake of 1886; Tectonics and Seismicity: U. S. Geological Survey Professional Paper 1313, T1-T11.
- Campbell, D. L. (1978). Investigation of the stress-concentration mechanism for intraplate earthquakes. Geophys. Res. Lett., 5, No. 6, 477-479.
- Chen, W. P., and P. Molnar (1983). Focal depth of intracontinental and intraplate earthquakes and their implications for the thermal and mechanical properties of the lithosphere, J. Geophys. Res., 88, 4183-4214.
- Costain, J.K., G.A. Bollinger, and J.A. Speer (1987). Hydroseismicity: a hypothesis for the role of water in the generation of intraplate seismicity, Seism. Res. Lett., 58, 41-64.
- Dewey, J.W. (1988). Hypocenter mapping and the extensibility of seismotectonic paradigms, (In Press) Proceedings, Univ. California Seismographic Stations. Centennial Anniversary Symposium, Univ. California Press, Berkeley.
- Dewey, J.W. (1985). A Review of Recent Research on the Seismotectonics of the Southeastern Seaboard and an Evolution of Hypotheses on the Source of the 1886 Charleston, South Carolina, Earthquake, U.S. Geological Survey NUREG/CR-4439.
- Fehler, M., P. Roberts, and T. Fairbanks (1988). A Temporal Change in Coda Wave Attenuation Observed During an Eruption of Mount St. Helens, Geophys. Res., 93, 4367-4374.
- Jin, Anshu, and K. Aki (1986). Temporal Change in Coda Q before

the Tangshan earthquake of 1976 and the Haicheng earthquake of 1975, Journal of Geophysical Research, 91, No. B1, 665-673.

Jin, Anshu, and K. Aki (1988). Spatial and temporal correlation between coda Q and seismicity in China, Bull. Seism. Soc. Am., 78, 741-769.

Klemperer, S. L., T. A. Hauge, E. C. Hauser, J. E. Oliver, and C. J. Potter (1986). The Moho in the northern Basin and Range, Nevada, along the COCORP 40°N seismic reflection transect, Geological Soc. Am. Bull., 97, 603-618.

Kuhn, T.S. (1970). The Structure of Scientific Revolutions (2nd ed.), University of Chicago Press, Chicago, 210 pp.

Long, L. T. (1982). Seismicity of Georgia, in Proceedings, Second Symposium on the Petroleum Geology of the Southeastern Coastal Plain, Information Circular 53, Georgia Geological Survey, Atlanta, Georgia, 202-210.

Long, L. T., and J.-S. Liow (1986). Crustal thickness, velocity structure, and the isostatic response function in the southern Appalachians, in Reflection Seismology: The Continental Crust; Geodynamics Series Volume 14. American Geophysical Union, Washington D.C., p. 215-222.

Long, L. T., R. E. White, and J. Dwyer (1986). The Charleston Earthquake Hypotheses - A Classification by Fundamental Tectonic Processes, Proceedings of the Third U. S. National Conference on Earthquake Engineering, August 24-25, 1986, Charleston, South Carolina, 25-32.

Long, L. T., J.-S. Liow, and F. B. Jones (1987). A technique for the inversion of coda Q; (abs.) Seismological Research Letters, 58, 101.

Mareschal, Jean-Claude (1987). Plate Tectonics: Scientific Revolution or Scientific Program, EOS Trans. Am. Geophys. Union 68, 532.

McCue, K., B.C. Barlow, D. Denham, T. Jones, G. Gibson and M. Michael-Leiba (1987). Another Chip Off the Old Australian Block, EOS, Trans., Am. Geophys. Union, 68, 609.

Meissner, R., and J. Strenhlau (1982). Limits of stress in continental crusts and their relation to the depth-frequency distribution of shallow earthquakes, Tectonics, 1, 73-89.

Owens, T. J., G. Zandt, and S. R. Taylor (1984). Seismic evidence for an ancient rift beneath the Cumberland Plateau, Tennessee: A detailed analysis of broadband teleseismic P

waveforms, J. Geophys. Res., 89, 7783-7795.

Seeber, L. and J. G. Armbruster (1987). The 1886-1889 aftershocks of the Charleston, south Carolina, earthquake: a widespread burst of seismicity, J. Geophys. Res. 92, 2663-2696.

Teague, A. G., G. A. Bollinger and A. C. Johnston (1986). Focal mechanisms analyses for eastern Tennessee earthquakes (1981-1983), Bull. Seism. Soc. Am., 76, 95-109.

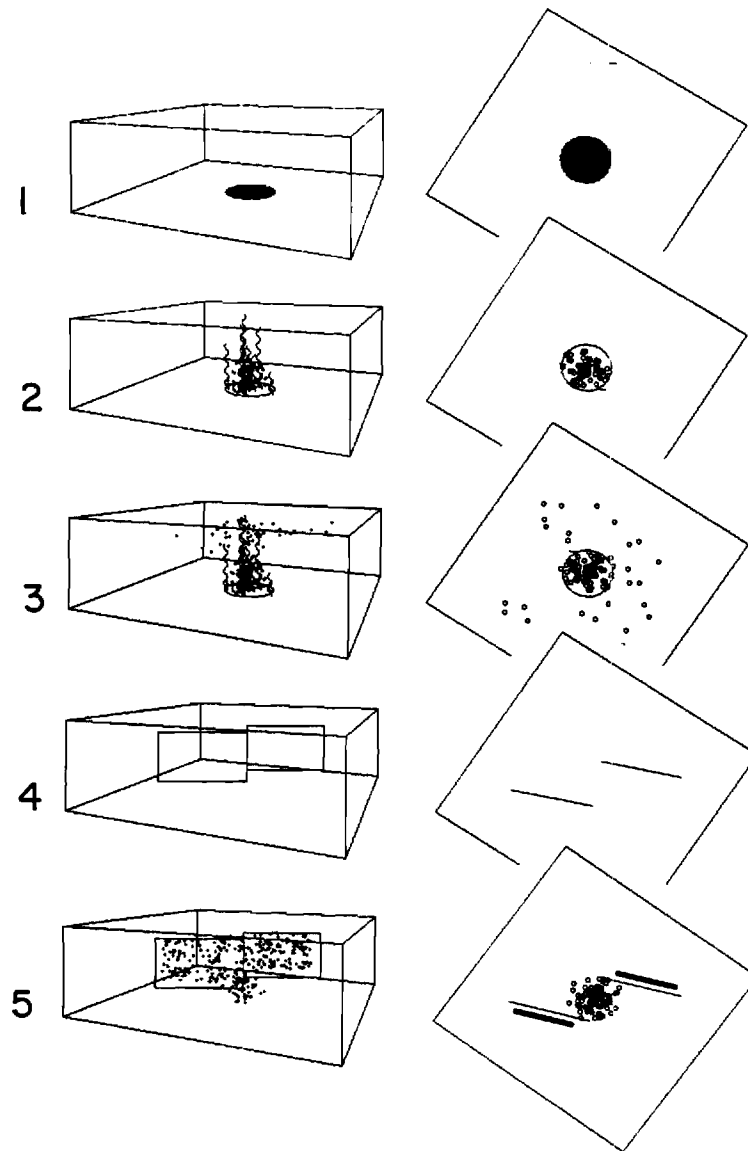


Figure 1. Illustration of the five phases of a major intraplate earthquake. 1) Initiation by underplating. 2) Strength corrosion by fluid and thermal diffusion. 3) Stress concentration as indicated by increased shallow seismicity (epicenters are small dots). 4) Failure along major faults (outlined by rectangles). 5) Crustal healing during an extended aftershock sequence.

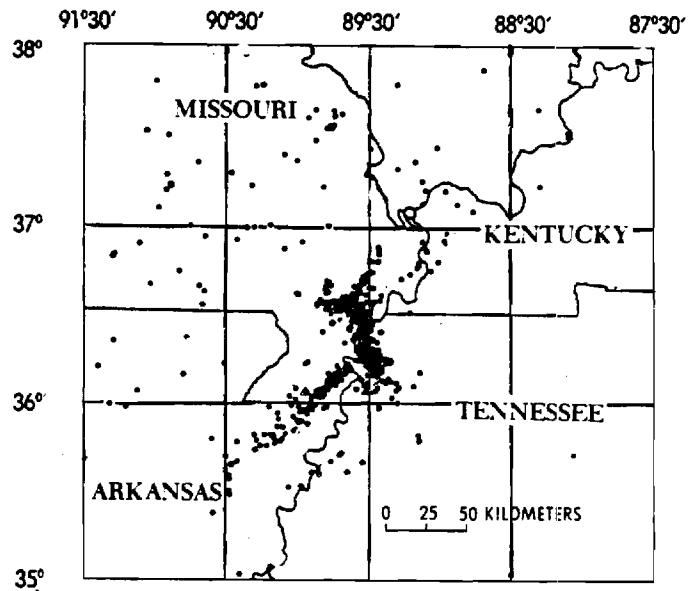
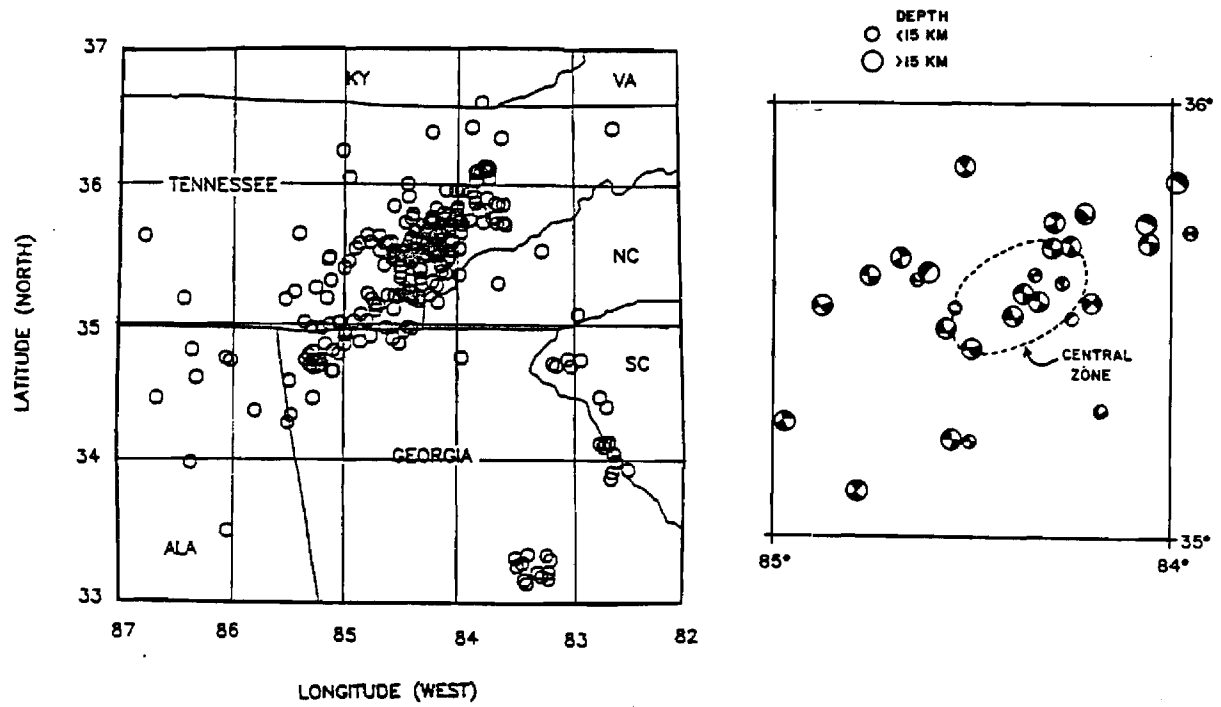


Figure 2. Pattern of seismicity and focal mechanisms for southeastern Tennessee; a possible example of phase 3. Pattern of seismicity for New Madrid; a possible example for phase 5.

APPENDIX C

A Local Weakening of the Brittle-Ductile Transition
can Explain Some Intraplate Seismic Zones

Leland Timothy Long and Karl-Heinz Zelt

Accepted for publication in Tectonophysics

APPENDIX C

A LOCAL WEAKENING OF THE BRITTLE-DUCTILE TRANSITION CAN EXPLAIN SOME INTRAPLATE SEISMIC ZONES

Leland Timothy Long and Karl-Heinz Zelt*

+ Now with Shell International, Den Haag, Netherlands

ABSTRACT: A decrease in the strength of a localized area of the lower crust would decrease the depth to the brittle-ductile transition and concentrate stress in the stronger elastic crust around and above the zone of decreased strength. Deformation within the zone of weakened lower crust would occur through viscous or dislocation creep in response to regional plate stress as well as by elastic failure in small earthquakes. Two-dimensional finite-element models of zones of weakness subjected to a regional plate stress predict stress amplification of 10 to 100 percent surrounding the local decrease in strength. A finite element model for an irregular zone of weakness in the lower crust can generate stress directions and relative magnitudes that satisfy the focal mechanisms and seismicity of southeastern Tennessee. An analysis of the displacements and stresses in the central area of decreased crustal strength suggests that strike slip faulting should dominate. Above this zone the strike slip faulting should exhibit a strong thrust component. The compression and extension of the crust surrounding the weakened zone at the level of the brittle-ductile transition predicts that the dominant strike slip faulting should exhibit components of normal faulting on the edges of the weak zone which are near a line through the weak zone parallel to the regional stress and reverse faulting on the edges which are near a line transverse to the regional stress.

The seismicity of southeastern Tennessee is diffused over a narrow elliptical zone trending northeast. The greatest concentration of activity is near the center. The central zone is characterized by deep-focus strike slip events with predominantly north or east striking nodal planes. These events are responding directly to compression in the direction of the regional compressive stress and extension perpendicular to the regional compressive stress within the weak zone. The uniformity of the focal mechanism solutions suggest that these earthquakes are not occurring on a random distribution of fractures and may be forming new faults. The area surrounding the central zone is characterized by focal mechanisms with larger components of reverse or normal fault movements. Events with normal components are dominant on the edges in line with the regional stress as predicted by the stress model for a weak central zone under stress. The agreement between observed earthquake focal mechanisms in southeastern Tennessee and models of crustal stress surrounding a zone of weakness suggests that these events may be

caused by a zone of weakness in the lower crust.

INTRODUCTION

Many hypotheses have been offered for major intraplate earthquakes and seismic zones (Dewey, 1985; Long, et al., 1986). Most efforts to identify hypotheses have concentrated on describing a causative structure common to active seismic zones; however, differences in the tectonic setting of seismic zones such as the southeastern Tennessee seismic zone and the aftershock zone of the 1886 Charleston, South Carolina, earthquake have made identification of common structures difficult. A pervading paradigm underlying most hypotheses is that the stresses generated by forces at plate boundaries and, possibly, by topographic or density loads reactivate preexisting faults or other weak structures. This study considers the response of weak zones in the lower crust to regional tectonic stress and compares crustal stress surrounding simulated weak zones with focal mechanism solutions for earthquakes in southeastern Tennessee.

The consistency of principal compressive stress directions in the interiors of crustal plates has long been recognized (McKenzie, 1969; Sbar and Sykes, 1973; Zoback and Zoback, 1980). Stresses in plate interiors exist in response to forces at mid-ocean ridges (Turcotte and Schubert, 1982, pg 287) and these forces can be transmitted over a large distance by the elastic lithosphere. Other forces associated with plate boundaries are those of slab-pull near subduction zones (Bott and Kusznir, 1984), forces associated with transform faults (Byerlee, 1978) and those related to viscous shear of asthenospheric convective flow (Richardson et al., 1979; Solomon et al., 1980; Fleitout and Froidevaux, 1982, 1983). Mareschal and Kuang (1987), and Kuang, et al. (1989) investigated the role of stresses from topographic and gravitational loading and concluded that variations in the stress field do to topography and density anomalies are comparable in magnitude to regional stresses generated by the forces of plate tectonics. They observed that zones of increased stress are consistent with the seismicity in southeastern Tennessee, but that the observed strike slip focal mechanisms could not be predicted with the same pattern of zones of higher stress. The maximum stresses associated with these forces are on the order of tens of MPa. In comparison, stresses required to cause brittle failure of the upper crust can range from 8 MPa at shallow depths to 9000 MPa in the lower crust (Meissner and Strehlau, 1982). Consequently, tectonic stresses alone cannot cause brittle failure unless the strength of the crust is low at the earthquake focus, usually assumed to be on an old fault.

The southeastern United States is situated within the North American Plate, where earthquakes of magnitude greater than 5.0

are rare and where the last major tectonic activity occurred in the Jurassic Period, during the opening of the Atlantic. In-situ stress measurements and earthquake focal mechanisms (Sbar and Sykes, 1973; Zoback and Zoback, 1980; Zoback, 1983) show that the greatest principal (compressive) stress in North America is horizontal and trends along the direction of plate motion, consistent with the regional stress originating from ridge push forces near the mid-Atlantic ridge. For southeastern Tennessee Zoback and Zoback (1980) predict northeast-southwest compression, consistent with 14 previously available focal mechanism solutions (Johnston et al., 1985; Teague et al., 1986).

Sykes (1978) proposed that intraplate earthquakes reactivate and follow preexisting zones of weakness, such as sutures developed in the Appalachian orogenic belt during the closing of the Proto Atlantic Ocean. Other cited zones of weakness which exhibit seismicity are the Ottawa-Bonnechere rift graben (Rankin, 1976) and the late Precambrian-early Paleozoic continental rift in the New Madrid area (Zoback, 1980). Talwani (1988) argued that major earthquakes prefer the intersection of zones of weakness. Other authors have stressed high-angle reverse motion on reactivated normal faults bordering Triassic basins along the eastern seaboard (Prowell and O'Connor, 1978; Reinhardt et al., 1984; Aggarwal and Sykes, 1978). Bollinger and Wheeler (1988) argued that the Giles county, Virginia, seismicity was best explained by reactivation of Iapetan normal faults.

These hypotheses do not explain the temporal and spatial clustering of earthquake epicenters in southeastern Tennessee and western North Carolina (Bollinger, 1973) or in the Charleston area. Estimates of recurrence rates from contemporary seismicity imply cumulative Quaternary displacements that are much larger than geological data can justify without invoking temporal clustering (Coppersmith, 1988). To explain the spatial clusters of seismicity in the eastern United States, attempts have been made to correlate earthquakes with mafic crustal units. These correlations are largely attempts to associate seismicity with concentrations of stress in the crust induced by inhomogeneous distributions of material properties. Fox (1970) was one of the first to speculate on the possible significance of the association of epicenters with mafic Paleozoic rocks in the Blue Ridge province. In studies of the Bowman and Charleston, South Carolina, seismicity, Long (1976) proposed a stress amplification mechanism that may explain seismicity near mafic intrusives and noted that the stress concentrations around or in an inclusion are a function of the ratio of the Young's modulus of the inclusion to that of the host, the shape of the inclusion and the applied stress. Kane (1977) extended the correlation of mafic intrusions with seismicity to other areas in the eastern United States. Long and Champion (1977) argued that earthquakes in the Charleston, South Carolina, area were better explained by stress amplification in or near a large mafic crustal intrusion

than by reactivation of the known faults. McKeown (1978) correlated the orientation of mafic intrusives with fault orientations and existing focal mechanism solutions for the New Madrid seismic zone and the southern Appalachian seismic zone. McKeown (1978) then used the stress calculations of Oudenhoven et al. (1972) to explain anomalous stress around solid inclusions. Whereas the above mentioned authors assumed intrusions stiffer than the surrounding plate, Campbell (1978) determined theoretical stress values associated with weakened intrusions. He suggested that mafic intrusions weakened possibly by serpentinization may concentrate stresses more than 200 percent above the regional values. The highest differential stress factor was found in the plate just outside the inclusion, implying that most or all brittle-failure earthquakes near a weak inclusion will occur in the plate nearby, not in the inclusion itself. The lack of a definitive association with seismicity has characterized all the mafic intrusion and stress concentration hypotheses. While they demonstrate the capability of variations in crustal rigidity to generate anomalous stress, many significant crustal units which should be anomalously rigid do not exhibit seismicity and the predicted stress distributions have not been confirmed with focal mechanisms

The discovery and improved understanding of the brittle-ductile transition at mid-crustal depths (Chen and Molnar, 1983; Meissner and Strehlau, 1982) has added a new dimension to discussions of stress distributions in the crust. They have shown that the depth to the brittle-ductile transition correlates with the maximum depth of earthquakes in continental interiors. A perturbation in the depth to the brittle-ductile transition due to the thermal effects of the cooling of a mid-crustal intrusion was investigated by Gettings (1988). He speculated that the residual thermal effects of an intrusives of late Miocene age or younger could cause shallowing of the brittle-ductile transition of 3 kilometers or more at the present and thus provide an area of possible stress amplification or concentration to explain the 1886 Charleston seismicity.

Long (1988) used the concept of a change in the properties of the brittle-ductile transition in the crust as the basis for a new hypothesis for major intraplate continental earthquakes. In Long's model the perturbation is caused primarily by the movements of fluids instead of the slower mechanism of thermal conduction. Long's (1988) model is based on a sequence of five phases. In the first phase of a major intraplate earthquake, the hydraulic or thermal properties of a portion of the continental crust at Moho depths is disturbed. Such a disturbance could be induced by the intrusion of a sill or by partial melting. In the second phase the upward migration of fluids or heat from the area of recent disturbance corrodes the strength of the crust near the brittle-ductile transition. As a weakened central zone deforms in response to regional stress during the third phase, stresses

are concentrated in the surrounding rigid crust. The fourth phase is the possible occurrence of a major earthquake when the stress surrounding the weakened central zone exceeds the crustal strength, either because the concentrated stresses are anomalously high or because the dispersing fluids have spread and weakened the crust outside the central zone. The final and fifth phase in the occurrence of a major intraplate earthquake is an extended aftershock sequence which concentrates near the fault plane of the main event.

The hypotheses of Long (1988) and Gettings (1988) are new in their use of a perturbed brittle-ductile transition and have not previously been confirmed by seismic data. In this study Long's (1988) model is tested by examining the stresses surrounding various shapes and sizes of a zone of crustal weakness within a compressed elastic crust. The magnitudes and directions of the principal stresses, which are computed using the finite element technique, are used to ascertain regions of likely seismicity and the relative location of strike-slip, normal and reverse focal mechanism solutions. In this study an attempt will be made to correlate the observed focal mechanism solution distribution for southeastern Tennessee with these computed crustal stresses,

SEISMICITY OF SOUTHEASTERN TENNESSEE

A dominant feature of the seismicity of the southeastern United States during the 1980's is the cluster of earthquakes in southeastern Tennessee. The relocation of over 296 earthquakes reveals a concentration of activity in the approximate center (84.3°W, 35.7°N) of the southeastern Tennessee seismicity (Fig 1) and fewer events in the surrounding elliptical seismic zone. Smaller and less active concentrations are found to the northeast near Maryville (84°W, 35.8°N) Tennessee (see Bollinger et al., 1976) and to the southwest in northwest Georgia (Long et al., 1986). Nearly continuous zones of seismicity extend from the center to the southwestern concentration in Georgia. Continuous linear zones of seismicity may also trend northwest across the seismic zone. One such alignment is located at the southwestern edge of the central cluster.

The directions of first motion and SV/P amplitude ratios were used to determine 41 single-event and two composite (two event) focal mechanism solutions for earthquakes in southeastern Tennessee and northern Georgia. The pertinent data for each event are listed in Table 1. The average location precision for two standard deviations is 5 km in depth and 3 km distance. Events were in the magnitude range of 1.7 to 3.9. The statistical estimate of confidence was developed by (Zelt, 1988) as an extension to the method of focal mechanism determination proposed by Guinn and Long, 1977. The significance is the probability that the first motions are not a random distribution.

The significance is based on the number of points, a test of the uniformity of the distribution of data points, the quality of the first motions and a Chi-square estimate of the goodness-of-fit. A confidence level of 0.9 suggests a probability of 0.10 that the observed first motions could be the result of random readings.

Over half of the focal mechanism solutions are strike slip and consistent with the 14 focal mechanisms reported by Johnston et al., 1985, and Teague et al., 1986. Of the remaining, eight are strike slip with a normal or reverse component, six are normal and five are reverse with a strike slip component. The measure of confidence of the focal mechanism solutions verify that for southeastern Tennessee and northwestern Georgia, solutions with large normal and reverse components exist with the same confidence level as the dominant strike-slip focal mechanism solutions. The depths of focus range from just below the base of the Paleozoic sediments at 8 km to 28.8 km and their average depth is 15 km. Figure 1 shows the distribution of these events with depth in a northeast-southwest profile. The average focal depth for strike-slip earthquakes is below the average at 17.3 ± 4.6 km. The average depth of earthquakes with normal or reverse focal mechanism solutions occurred near the average depth.

The central seismic zone (Fig. 1 and 2) is sampled by 18 focal mechanism solutions. Fourteen of these 18 events are either dominantly strike-slip or have a large strike-slip component. The dip of the B axis can be used as a measure of the deviation of the focal mechanism from pure strike slip. The dips of the null-axes (Fig 3), indicate that the most prominent zone of near-vertical dip, corresponding to pure strike-slip regimes, is the central cluster of the central seismic zone near 35.55N and 84.35W. This central cluster is flanked by regions of low B-axis dips, thus regions of normal or reverse components in their focal mechanisms. The two events that are anomalous in the central zone are shallow. Events further to the west and to the south-southwest are also nearly pure strike slip, but there are insufficient events to define anomalous focal mechanisms surrounding these events.

Focal mechanisms with prominent normal or reverse components are found near the outer edges of the central seismic zone. In order to determine which of the low B-axis dip regions corresponds to normal or reverse faulting, the dip of the tension axis was subtracted from the dip of the pressure axis for each solution (Fig. 4). This difference can range from -90° , corresponding to a pure reverse fault, to $+90^\circ$, corresponding to a pure normal fault. Values close to zero correspond to strike-slip mechanisms or near-vertical movement on vertical faults. The central cluster is dominated by strike slip faulting with reverse faulting. The northeast and southwest edges of the central zone are dominated by strike slip faulting with components of normal faulting. The general pattern of focal mechanisms in the cluster

of activity in southeastern Tennessee consists of earthquakes with reverse faulting in a central zone flanked by zones of normal faulting.

FINITE ELEMENT MODELS

Stress modeling in this study is based on the second order, multivariate finite element equations, outlined in Chapter 4.5 of Reddy (1984), with special emphasis on the plane elastic deformation of a linear elastic solid. The finite element technique divides the model space into a mesh of triangular elements which can approximate the physical properties of an arbitrarily complex two-dimensional media. The plates in this study are modeled using plane stress formalism in which the thickness is small compared to the dimensions in the plane. The meshes used in this study consisted of about 250 elements. The material types used are all isotropic. No body forces are applied and the model solutions are for elastic material properties. All stress magnitudes are based on a regional lithospheric stress of 5 MPA. Other values of stress can be obtained by scaling the computed stresses.

The intent of the finite element modeling is to estimate the distribution of stress at one instance during the third phase of Long's (1988) mechanism for major intraplate earthquakes. The distortion of weak crustal rock within a more rigid elastic crust is simulated in this study by assigning a lower Young's modulus to the weak zone. The weak zones are given circular and elliptical cross sections because these are expected to be similar to sills and other intrusive bodies. We considered smooth shapes appropriate for modeling the dispersion of fluids, a possible mechanism for weakening the crust. Two zones of weak material are used to simulate the geometry suggested by the focal mechanisms in the crustal volume of southeastern Tennessee.

The boundary conditions are designed to simulate a plate under compression. The left boundary is constrained to zero displacement. A normal force applied to the right boundary was tapered near the corner, producing minor irregularity in the stress field at the right edge. The side boundaries are constrained to zero normal displacement but are free to move tangential to the boundary. For the vertical cross section, one side boundary was made a free surface with no stress. Also, the elastic constants were set to a function of depth, leading to some irregularity in the stress field near the right boundary.

The average compressive stress of the entire grid is used to simulate crustal equilibrium without zones of weakness. When this average compressive stress is subtracted from the compressive stress of each individual point, changes in the form of plate extension and compression initiated by crustal weakening can be estimated in the rigid plate. In evaluating stresses

available for earthquakes occurring above the plate, changes in compressive stress in the plate may be more important than absolute values in establishing patterns of normal or reverse components in the faulting.

Single Large Circle

A single large circular zone provides a simple model for a weak zone in the lower crust (Fig 5). The universally compressive stress in both principal stress axis directions (Fig 6) is consistent with the boundary conditions and applied regional stress. The principal stresses exhibit changes in direction and magnitude near the boundary of the weak zone. Stresses vary by 50 percent near the boundary of the rigid crustal material and are 240 percent higher than in the material used to model the weak zone. The stresses can be divided into their deviatoric and dilatational components. The deviatoric stresses (Fig. 7) describe the stress available for shear failure in earthquakes. The regional compression and boundary conditions require extension perpendicular to the applied stress and compression parallel to the applied stress. Fig. 7 also shows little change in the directions of principal stress within the weak zone. The magnitude of deviatoric stress within the weak zone is only about 40 percent of the deviatoric stress on the boundary of the weak zone and is determined by the arbitrary choice of reduced values of the elastic constants used to simulate the weakened rock.

The changes in dilatation provide a measure of the extension and compression of the plate surrounding a transient weak zone. Fig. 8 represents the dilatation at each point with the dilatation of the entire grid subtracted. The geologic analogy would be the weakening of a portion of the crust, which is in an equilibrium state and a measure in change in compression or extension of the plate induced by the weak zone. The stresses indicate two zones of compression which are situated on the sides of the weak zone normal to the applied stress. The magnitude of the change is approximately twice the regional average. The increased dilatation of the weak zone should not be construed as extension because the change in material properties controls the stress. Instead, compression and hence thrust faulting would be expected in the remaining strong rocks above the deformed weak zone. The extension relative to a plate of uniform stress exists outside the weak zone on the sides in line with the applied stress. The extensional zones above the plate would be zones where normal faulting components would be expected in earthquake focal mechanisms. The compressional zones would be zones where earthquakes would exhibit components of reverse faulting.

In the central zone, the stress levels must decrease in parallel with the strength and are controlled by the distortion of the surrounding plate. Normally, compression is in line with

the regional stress and extension is normal to the applied stress. Consequently, any earthquakes occurring within the weak zone would have a vertical null axis and a strike slip focal mechanism.

Two Adjacent Circles

The stress model for two adjacent circles was chosen to be able to interpret the interaction of a system of sills or other types of weak zones within the crust and to model multiple weak zones delineated by focal mechanisms in southeastern Tennessee. The general properties of the stress field are similar to those of the single large circle. These general properties include the compression perpendicular to the applied stress and the relative extension on the edges of the weak zone parallel to the applied stress. The notable differences relate to increases in stress contrast that are proportional to the fraction of the total width of the model that contains the weaker material. For two circles aligned parallel to the maximum compressive regional stress (Fig 9), 10 km wide separation zone between the two circles is not a zone of stress concentration. The small separation allows a continuous weak zone of low stress from one circle to the other. Two circles aligned parallel to the regional stress, therefore, behave like a single irregularly shaped weak body.

For two circles aligned perpendicular to the applied stress, the finite element model predicts stresses similar to those for circles in line with the stress, except that the stress zone separating the two circular zones shows stress concentrations about 300 percent larger than in the surrounding elastic plate. In the deviatoric stress (Fig. 10) the elastic material separating the circles amplifies the applied stress instead of being absorbed in the weak zone as it is in the case of the circles aligned with the regional stress. The increased stress within the separation is explained by the direct application of the applied stress to the narrow zone of strong rock separating the two circles. Fig. 10 shows a distinct central zones for each weak zone surrounded by zones of higher stress. The patterns of stress are thus distinctly different in the vicinity of the weak zones and depend on the orientation of the complex weak zone in the regional stress.

Two circles located along a diagonal (45 degrees) relative to the applied stress show zones of deviatoric stress concentrations at the boundary of the circles including the zone separating the two circles. The stresses are of the same magnitude found for the other two-circle models. The deviatoric stresses (Fig. 11) show that two circular weak zones oriented diagonally to the applied stress remain independent zones of weakness and do not merge into a continuous weak zone. However, the deviatoric stresses on the connecting bridge are on the order of 100 percent greater than the average stress. This increase is significant in

that it suggests that irregularities within the central weak zone can generate significantly anomalous deviatoric stresses. Also, the diagonal orientation creates large intermediate zones of neither compressive nor extensional character immediately next to the circular weak zones. This can be seen to the right of the top circular weak zone and to the left of the bottom circular weak zone in Fig. 11. The diagonally aligned circles concentrate stresses between the two weak zones and provides a complex pattern of extensional and compressional zones.

Also, an ellipsoidal zone in various orientations was examined to simulate a continuous linear weak zone in an applied stress. The results are similar to those of the two adjacent circles with the exception that stress concentrations on the edges could be 50 percent greater. An ellipsoidal zone could represent perturbation of the strength of a fault zone by fluids. The deviatoric stresses for an ellipsoidal zone with its major axis parallel to the applied stress show negligible contrast with the surrounding stronger crust beside the weak zone. Stress concentrations appear only along the boundaries, particularly at the ends, of the ellipsoidal weak zone with its major axis perpendicular to the direction of applied stress with magnitudes similar to those of the two adjacent circles.

Crustal Perturbation in Vertical Profile

A perturbation of the strength of the lower crust leading to elastic or viscous deformation affects the stresses in the shallow crust. In order to evaluate the influence on stress above the weak zone, a vertical profile was examined. The surface sedimentary layers were added to assess the effects of sediments on stress in this shallow crust (Fig. 12). The model for the vertical profile differs from the model for crustal inclusions examined previously in that the top of the sediments is a free surface and the weak lower crust is simulated with lower elastic constants similar to those in the central weak zone. Also, the cross section is a two dimensional approximation to the three dimensional geometry of a shallowing of the brittle-ductile transition zone. The deviatoric stress (Fig. 13) shows a concentration of shear stress above the zone of perturbation. The deviatoric stresses are about 200 percent higher over a weakened crust than in the surrounding crust. The 200 percent increase is comparable to the largest shear stress observed in the analysis of stress amplification in a horizontal plate; the two weak zones at a diagonal to the applied stress. The direction and magnitude of the principal stress axes favor earthquakes on reverse faults above the weak zone. The low stress levels in the sediments show that low-velocity sedimentary basins are largely insulated from the stresses in the crust. The deeper sedimentary basins could contribute to the amplification of crustal stress by constricting the thickness of the stress channel. A large abrupt change in crustal structure can thus

concentrate stress in one area, which in this case is the zone between the sediments and the top of the weak zone.

CONCLUSIONS AND DISCUSSION

The combined inferences from stresses computed for a horizontal plate and a vertical cross section are that the focal mechanisms above the plate will exhibit stronger components of reverse and normal faulting than earthquakes in the plate. The orientation of principal axes and hence the inferred focal mechanisms is controlled by the central zone of weakened lower crust (fig. 15). In the weak zone of the horizontal plate the focal mechanisms should be strike slip. Stress concentrations at the edge of the weak zone can cause deviations of up to 30 degrees in the orientation of the principal axes. Above the weak zone, thrust or reverse motions are inferred. Above the plate surrounding the weak zone the distortion in the plate predict a pattern of extension perpendicular to the direction of greatest compressional regional stress near the edges of the weak zone parallel to the regional stress. Reverse faulting is expected near the edges of the weak zone normal to the regional field.

In southeastern Tennessee a pattern of earthquake focal mechanisms is observed that can be modeled by a mid-crustal weak zones as illustrated in figure 15. Two weak zones oriented at 45 degrees to the regional compressional stress give a better fit, but more focal mechanisms are needed to confirm the details. The factors that support a crustal weak zone are as follows:

- 1) The pattern of seismicity defines a concentration of activity in a central zone surrounded by lower levels of seismicity. The seismic zone is elongated to the northeast and southwest.
- 2) In the central zone the earthquakes below 15 km uniformly have strike slip focal mechanisms with northeast-southwest trending compressional axes. The stress model suggests that the stress directions in the weak zone should deviate only slightly from the regional stress field and that the null axis should be vertical.
- 3) The shallow events above the weak zone show large thrust components. The stress model for a vertical section predicts amplification above the weak zone.
- 4) All of the earthquakes in the central zone show some thrust component in agreement with the models showing compression in and above the weak zone.
- 5) The focal mechanisms for events surrounding the central zone depend on their position relative to the applied regional

stress. Events on the axis parallel to the regional stress show a normal component in the predominantly strike slip focal mechanisms, in agreement with the finite element stress model. The few events on the axis perpendicular to the regional stress show a thrust component. The decrease in seismicity on the axis perpendicular to the regional stress is consistent with the increased stress required to cause failure in a compressive regime.

The stress model and the observed seismicity in southeastern Tennessee may correspond to phase 3 of Long's (1988) five-phase hypothesis for major intraplate earthquakes. In phase 3 the weakened central zone is being deformed by regional compressive stress and the surrounding elastic crust is bearing the load no longer supported by the central zone. The regional compressive stress is required since without a regional stress the deformation of the central zone would not create the deviatoric stresses for the earthquakes. A local weakening of the crust by a perturbation of its hydraulic or thermal properties is required in order to trigger the events in zones where the crust is normally stronger and to allow concentration of the seismicity in limited seismic zones such as in southeastern Tennessee. In this model the seismicity exists by virtue of a decrease in strength, and not simply because a weak zone exists.

Variations in the P-axis orientation has sometimes been ascribed to the preferential failure of preexisting planes of weakness in a uniform stress field. The uniformity we observe for focal mechanisms in the central zone argues for a direct response to the direction of regional stress. The variations in focal mechanisms for shallow events and those in the surrounding elastic plate fit a pattern. Although existing faults may contribute to the scatter in our focal mechanisms in these zones, the general pattern is that predicted by stress models for a weakness in a plate subjected to regional stress.

The zone of weakness can be generated by perturbations in the hydraulic properties and/or thermal properties of the lower crust. Figure 15a is a simplified conceptual diagram showing the strength of the crust in tensional and compressive tectonic environments. A temperature increase (Fig. 15b) predicts a shallowing of the brittle-ductile transition. An increase in fluid content in the lower crust would create a localized decrease in the frictional strength. The change is more pronounced than that caused by a thermal perturbation and is also more pronounced in zones of crustal extension. In the southeastern Tennessee seismicity, the zones of predicted extension are those exhibiting the greater level of seismicity suggesting that a hydraulic perturbation is the more likely explanation for the seismicity. Also, the greater time and energy required to effect a thermal perturbation favor an explanation based on fluid movement.

The important conclusions from this analysis are as follows:

1) The focal mechanisms of earthquakes in southeastern Tennessee fit a pattern predicted by stress modeling of a zone of weakness in the lower crust.

2) The different orientations of focal mechanisms can be explained by inhomogeneity in stress.

3) The seismicity in southeastern Tennessee can be explained by a perturbation in the fluid properties of the lower crust.

ACKNOWLEDGMENTS

This research was supported primarily by the Nuclear Regulatory Commission, Office of Nuclear Regulatory Research. Supplemental support was provided by the Corps of Engineers, Savannah District, and the Tennessee Valley Authority. Computer time was provided by the School of Geophysical Sciences and the Advanced Computational Methods Center at the University of Georgia through the Supercomputing Support Group of the Office of Computing Services at the Georgia Institute of Technology.

REFERENCES

- Aggarwal, Y.P. and L.R. Sykes, 1978. Earthquakes, faults and nuclear power plants in southern New York, Science, 200, pp. 425-429.
- Bollinger, G.A., 1973. Seismicity of the southeastern United States, Bull. Seism. Soc. Am., 63, pp. 1785-1808.
- Bollinger, G.A., C.J. Langer and S.T. Harding, 1976. The Eastern Tennessee Earthquake Sequence of October through December, 1976, Bull. Seism. Soc. Am., Vol. 66, No. 2, pp. 525-547.
- Bollinger, G.A. and R. Wheeler, 1988. The Giles County, Virginia, seismic zone--Seismological results and geological interpretations, U.S. Geological Survey Professional Paper, 1355, U.S. Government Printing Office, Washington, D.C., 85pp.
- Bott, M.H.P. and N.J. Kusznir, 1984. The origin of tectonic stress in the lithosphere, Tectonophysics, Vol. 105, pp. 1-13.
- Byerlee, J., 1978. Friction of rocks, Pure and Applied Geophysics, 116, pp. 615-626.
- Campbell, D.L., 1978. Investigation of the stress concentration mechanism for intraplate earthquakes, Geophysical Research Letters, Vol. 5, No. 6, pp. 477-479.
- Chen, W.-P. and P. Molnar, 1983. Focal depths of intracontinental and intraplate earthquakes and their implications for the thermal and mechanical properties of the lithosphere, J. Geophys. Res., Vol. 88, pp. 4183-4214.
- Copersmith, K. J., 1988. Temporal and spatial clustering of earthquake activity in the central and eastern United States, Seismological Research Letters, Vol. 59, No. 4, pp. 299-304.
- Dewey, J.W., 1985. A review of recent research on the seismotectonics of the southeastern seaboard and an evaluation of hypotheses on the source of the 1886 Charleston, South Carolina, earthquakes, NUREG/ CR-4339.
- Fleitout, L. and C. Froidevaux, 1982. Tectonics and topography for a lithosphere containing density heterogeneities, Tectonics, Vol. 1, pp. 21-56.
- Fleitout, L. and C. Froidevaux, 1983. Tectonic stress in the lithosphere, Tectonics, 2, pp. 315-324.
- Fox, F.L., 1970. Seismic geology of the eastern United States, Assoc. Eng. Geologists Bull., 7, pp. 21-43.

Gettings, M.E., 1988. Variation of depth to the brittle ductile transition due to cooling of a mid-crustal intrusion, Geophysical Research Letters, Vol. 15, No. 3, pp. 213-216.

Guinn, S.A. and L.T. Long, 1977. A computer method for determination of valid focal mechanism solutions using P-wave first motions, Earthquake Notes, Vol. 48, No. 4, pp. 21-33.

Johnston, A.C., D.J. Reinbold, and S.I. Brewer, 1985. Seismotectonics of the Southern Appalachians, Bull. Seism. Soc. Am., Vol. 75, pp. 291-312.

Kane, M.F., 1977. Correlation of major eastern earthquake centers with mafic/ultramafic basement masses, U.S. Geol. Survey Prof. Paper 1028-O.

Kuang, Jian, L.T. Long, and J.C. Mareschal, 1989. Intraplate seismicity and stress in the southeastern United States, Tectonophysics, (in press).

Long, L.T., 1976. Speculations concerning Southeastern Earthquakes, mafic intrusions, gravity anomalies, and stress amplification, Earthquake Notes, Vol. 47, No. 3, pp. 29-35.

Long, L.T. and J.W. Champion, Jr., 1977. Bouguer Gravity Map of the Summerville-Charleston, South Carolina, Epicentral Zone and Tectonic Implications, Geol. Survey Prof. Paper 1028-K.

Long, L.T., 1988. A model for major intraplate continental earthquakes, Seismological Research Letters, Vol 59, No. 4, pp 273-278.

Long, L.T., R.E. White, and J. Dwyer, 1986. The Charleston earthquake Hypotheses - A classification by fundamental tectonic processes, Proceedings of the Third U. S. National Conference on Earthquake Engineering, August, 24-25, 1986, Charleston, South Carolina, pp 25-32.

Long, L.T., K.-H. Zelt, J.-S. Liow, R. Propes, J. Shand, D. Reinbold and B. Schechter. 1986. The North Georgia Earthquake of October 9, 1984, Earthquake Notes, Vol. 57, No. 3, pp 77-82.

Mareschal, J.C. and Jian Kuang, 1987. Intraplate Stresses and Seismicity: The role of topography and density heterogeneities, Tectonophysics, Vol. 132, pp. 153-162.

McKenzie, D.P., 1969. The relationship between fault plane solution for earthquakes and the directions of principal stresses, Bull. Seism. Soc. Am., Vol. 59, pp. 591-601.

McKeown, F.A., 1978. Hypothesis: Many earthquakes in the

central and southeastern United States are causally related to mafic intrusive bodies, Jour. Research U.S. Geol. Survey, Vol. 6, No. 1, pp. 41-50.

Meissner, R. and J. Strehlau, 1982. Limits of stresses in continental crusts and their relation to the depth-frequency distribution of shallow earthquakes, Tectonics, Vol. 1, No. 1, pp. 73-89.

Oudenhoven, M.S., C.O. Babcock, and W. Blake, 1972. A method for the prediction of stresses in an isotropic inclusion or orebody of irregular shape, U.S. Bureau of Mines, Report of Investigations 7645, 36 pp.

Prowell, D.C. and B.J. O'Connor, 1978. Belair fault zone: Evidence of tertiary fault displacement in eastern Georgia, Geology, Vol. 6, pp. 681-684.

Rankin, D.W., 1976. Appalachian salients and recesses: Late Precambrian continental breakup and the opening of the Iapetus Ocean, J. Geophys. Res., 81, pp. 5605-5616.

Reddy, J.N., 1984. An Introduction to the Finite Element Method, McGraw Hill Company.

Reinhardt, J., D.C. Prowell and R.A. Christopher, 1984. Evidence for Cenozoic tectonism in the southwest Georgia Piedmont, Geol. Soc. Am. Bull., Vol. 95, pp. 1176-1187.

Richardson, R.M., S.C. Solomon and N.H. Sleep, 1979. Tectonic stress in the plates, Rev. Geophys. Space Physics, 17, pp. 981-1019.

Sbar, M.L. and L.R. Sykes, 1973. Contemporary compressive stress and seismicity in eastern North America: an example of intraplate tectonics, Bull. Geol. Soc. Am., 84, pp. 1861-1882.

Solomon, S.C., R.M., Richardson, E.A., Bergman, 1980. Tectonic Stress Models and Magnitudes, J. Geophys. Res., 85, pp. 6086-6092.

Sykes, L.R., 1978. Intraplate seismicity, reactivation of preexisting zones of weakness, alkaline magmatism, and other tectonism postdating continental fragmentation, Rev. Geophys. Space Phys., 16, pp. 621-688.

Talwani, P, 1988. The intersection model for intraplate earthquakes, Seismological Research Letters, Vol. 59, No. 4, pp 305-310.

Teague, A.G., G.A. Bollinger, and A.C. Johnston, 1986. Focal Mechanism analyses for eastern Tennessee earthquakes (1981-

1983), Bull. Seism. Soc. Am., Vol. 76, No. 1, pp. 95- 109.

Turcotte, D.L. and Gerald Schubert, 1982. Geodynamics, Applications of Continuum Physics to Geological Problems, John Wiley & Sons, New York, 450 pp.

Zelt, Karl-Heinz, 1988. Investigation of the cause of earthquakes in southeastern Tennessee and northern Georgia using focal mechanisms and models of crustal stress, Ph.D. Thesis, Georgia Institute of Technology, Atlanta, Georgia, 231 pp.

Zoback, M.L. and M.D. Zoback, 1980. State of stress in the conterminous United States, J. Geophys. Res., Vol. 85, pp. 6113-6156.

Zoback, M.D., 1983. Intraplate earthquakes, crustal deformation and in situ stress, U.S. Geol. Survey, Open file Report 83-843, pp. 169- 178.

TABLE I. Earthquake locations and focal mechanisms.

Date YrMoDa	Origin Time	Lat. North	Long. West	Dur. Mag.	Depth km	# of pts.	Sig.	Tension Pressure		Null		P-T		
								az.	dip	az.	dip	az.	dip	
820130	12:39	35.80	83.94	2.8	18.8	9	0.76	38	47	221	43	130	1	-4
820224	12:10	35.72	84.29	1.3	20.4	8	0.69	189	7	283	27	86	62	20
820905	10:11	35.21	84.51	3.2	8.4	12	0.86	138	2	229	24	44	66	22
820924	21:57	35.68	84.24	3.2	14.0	12	0.78	161	25	257	14	14	61	-11
821214	06:35	35.29	84.17	2.4	9.1	11	0.81	312	8	51	47	215	42	39
821215	02:27	35.75	84.22	2.1	19.2	9	0.65	252	57	13	18	112	26	-39
830118	05:09	35.58	84.27	2.3	11.2	11	0.71	335	49	71	6	166	40	-43
830129	18:08	36.12	83.74	2.1	20.7	10	0.91	322	31	220	20	102	52	-11
830304	14:03	35.60	84.34	2.3	8.0	7	0.71	53	20	150	17	277	63	-3
830316	09:13	35.22	84.55	2.6	16.9	6	0.71	327	8	234	16	83	72	8
830405	03:17	35.54	84.19	2.1	18.8	7	0.96	176	16	266	3	6	74	-13
830526	12:30	35.67	84.27	2.5	14.6	12	0.88	146	4	54	19	247	71	15
831016	22:02	35.86	84.55	2.5	19.8	12	0.84	348	24	82	9	191	64	-15
840207	06:32	35.65	84.64	1.8	20.4	7	0.71	19	2	289	1	172	88	-1
840525	10:15	35.60	84.62	2.0	24.1	11	0.87	319	34	110	53	219	14	19
840830	16:26	35.55	84.35	3.1	21.1	16	0.96	142	12	59	3	315	78	-9
840830	16:41	35.55	84.35	2.4	18.0	7	0.99	331	7	239	16	84	72	9
841009	11:54	34.77	85.19	3.5	15.0	22	0.78	298	6	29	7	168	81	1
841107	09:31	35.59	84.64	2.0	18.7	14	0.71	308	40	199	21	88	43	-19
850309	14:29	35.03	85.03	2.5	9.7	12	0.68	8	6	277	8	134	80	2
850312	13:04	35.87	83.57	2.0	25.6	12	0.82	311	7	218	16	64	72	9
850410	10:53	35.72	84.06	2.3	22.0	11	0.53	14	24	226	62	110	13	38
850420	04:21	35.48	84.56	2.5	9.4	13	0.78	20	1	151	89	290	1	88
850712	18:20	35.20	85.15	3.0	19.6	10	0.60	123	17	216	9	333	71	-8
850815	17:31	35.67	83.95	1.8	12.5	8	0.78	100	3	190	2	314	86	-1
850924	00:01	35.68	84.05	1.7	19.1	9	0.88	140	10	233	16	19	71	6
851220	15:15	34.93	84.76	2.9	9.3	7	0.68	329	0	236	81	59	9	81
860107	01:26	35.60	84.76	3.1	17.5	24	0.95	107	11	198	4	308	78	-7
860127	06:44	35.88	83.65	2.6	15.0	11	0.83	289	8	21	17	175	71	9
860419	07:40	35.19	85.51	3.0	21.0	27	0.91	183	9	280	35	81	53	26
860423	07:18	34.79	85.30	1.8	19.1	8	0.60	120	2	24	70	211	20	68
860519	23:46	35.53	84.54	2.6	9.7	14	0.67	284	11	16	15	159	71	4
860602	07:46	35.43	84.50	2.5	18.6	14	0.87	132	32	31	17	277	53	-15
860624	19:22	35.98	83.94	2.8	28.8	14	0.67	131	1	40	41	222	49	40
860711	14:26	34.93	84.99	3.8	20.7	30	0.98	329	18	60	3	159	72	-15
860719	12:31	34.94	84.97	1.9	10.6	10	0.66	349	40	226	32	112	33	-8
860807	12:36	35.49	84.54	2.5	14.9	11	0.49	285	15	25	32	174	54	17
860819	20:51	36.26	85.01	2.9	20.0	13	0.73	112	20	244	62	15	19	42
861115	12:08	35.88	83.82	2.0	16.4	9	0.70	172	2	81	7	278	83	5
870112	18:56	35.50	84.25	2.1	14.8	9	0.85	320	23	121	65	227	7	42
870222	10:35	36.39	84.21	2.8	19.0	14	0.81	314	2	44	1	161	88	-1
870327	01:26	35.60	84.76	3.9	17.5	35	0.99	323	4	53	6	199	83	2
870901	23:02	35.51	84.40	3.2	16.9	17	0.99	304	20	41	18	170	63	-2

The significance measure is based on the number of points, the distribution of data points, quality of first motions and SV/P ratios, and a Chi-square estimate of goodness of-fit.

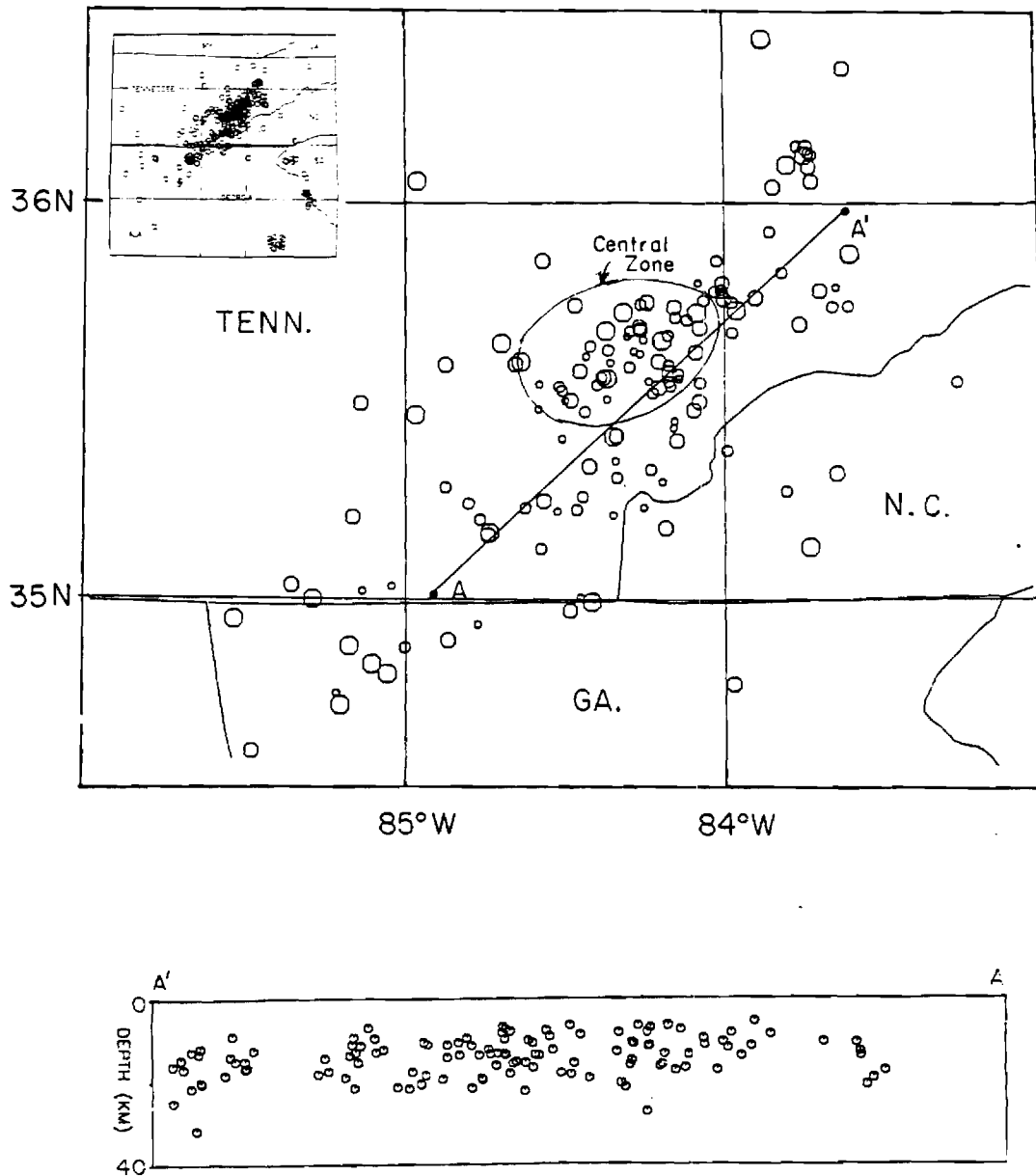


Figure 1. Seismicity of southeastern Tennessee. The events shown have been relocated with station corrections applied and represent a select subset of the observed data in southeastern Tennessee.

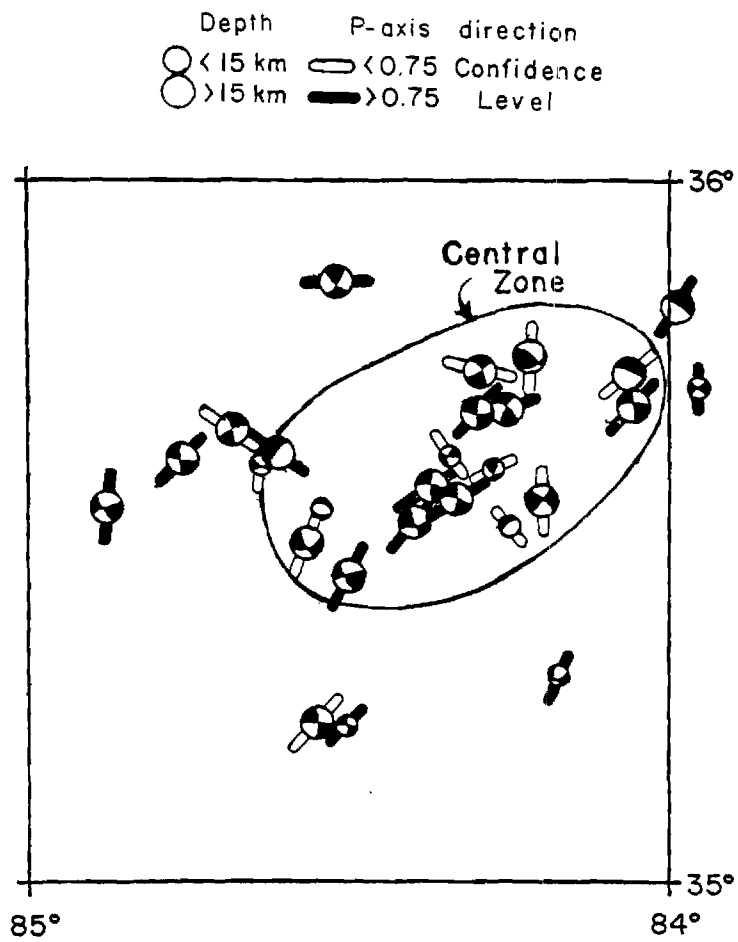


Figure 2. Focal mechanism solutions and epicenters in the central zone. The bar indicates the horizontal projection of the P-axis. Events with confidence levels above 0.75 are solid.

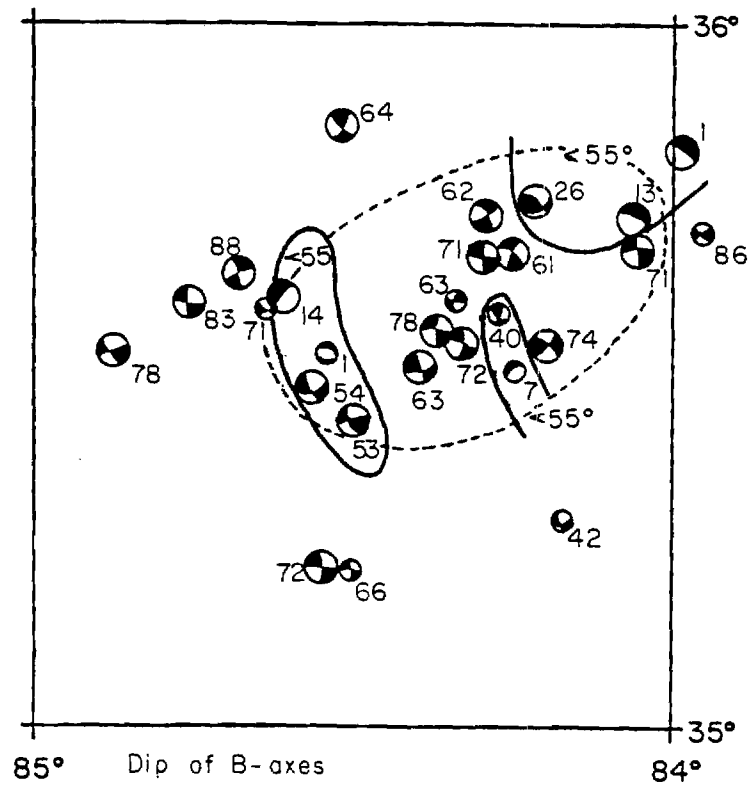


Figure 3. Dip of the B axis of the focal mechanism solution for the central zone. The dip of the B axis indicates deviation from pure strike slip motion.

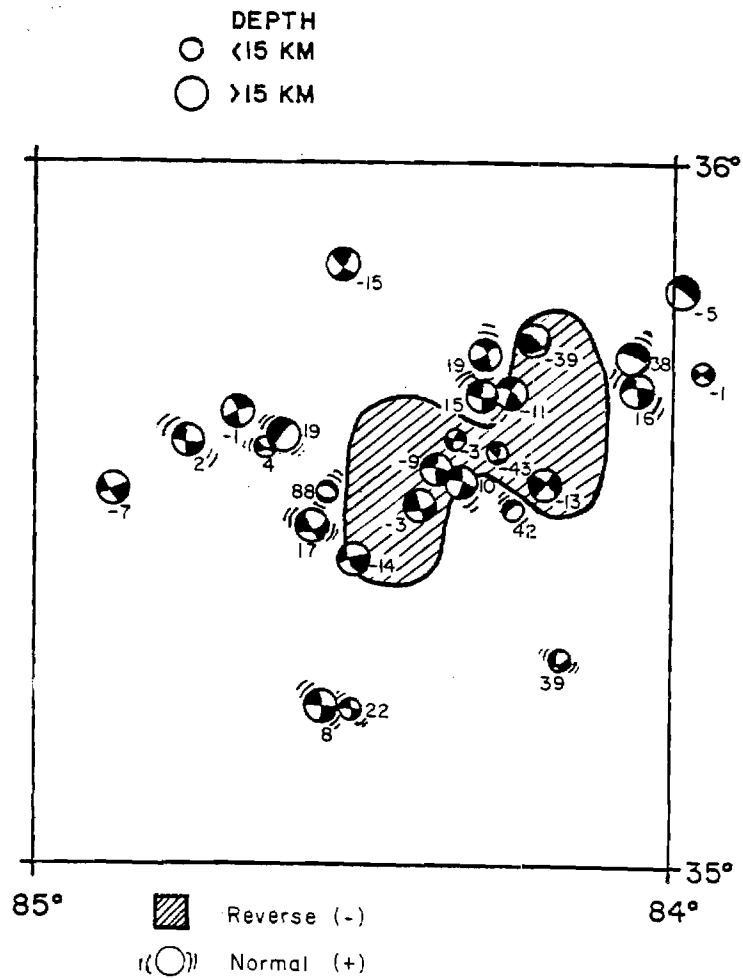


Figure 4. Difference between the dip of the tension axis and the dip of the pressure axis. Negative values suggest reverse faulting and positive values suggest normal faulting components in the predominant strike slip focal mechanisms.

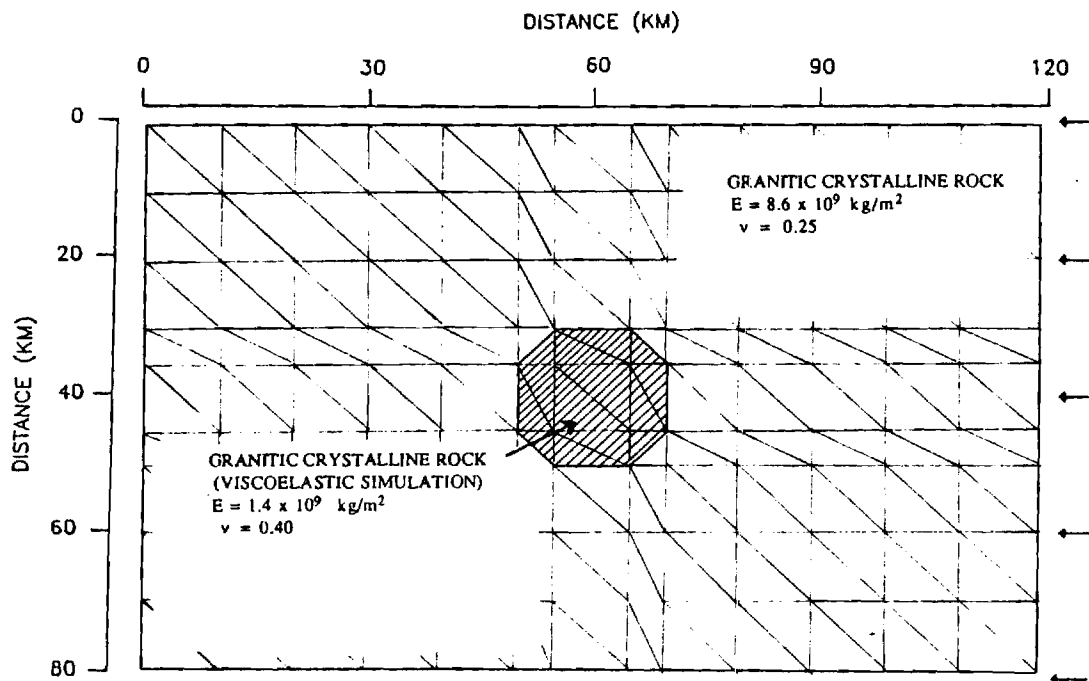


Figure 5. Model for a single circular zone of weakening in a horizontal crustal plate.

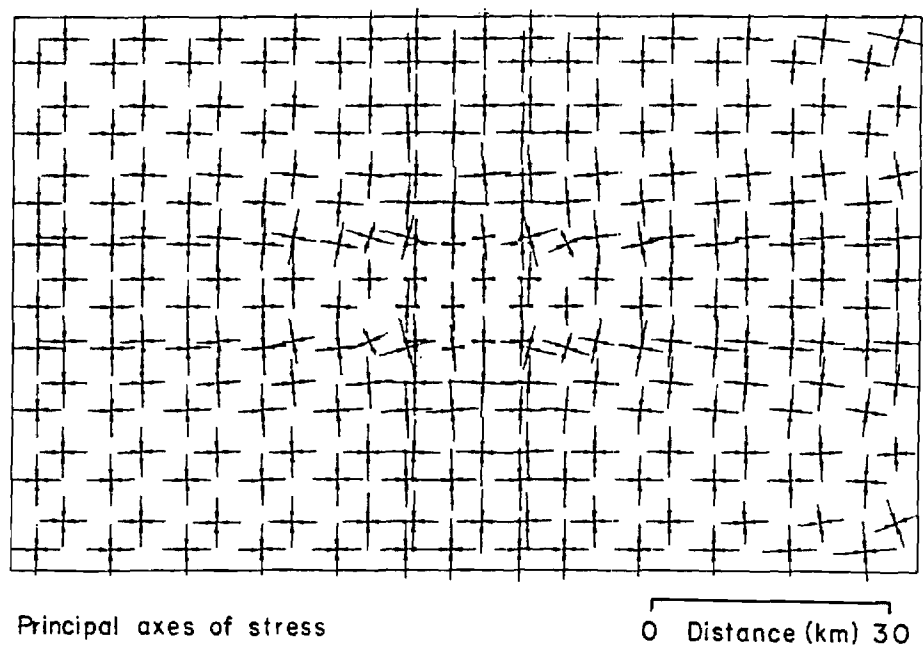


Figure 6. Stress surrounding a weak circular zone in a horizontal crustal plate. Arrows indicate principal stress directions and magnitudes. The force applied to the right boundary was tapered at the edges, leading to some irregularity in the stress directions along the right edge.

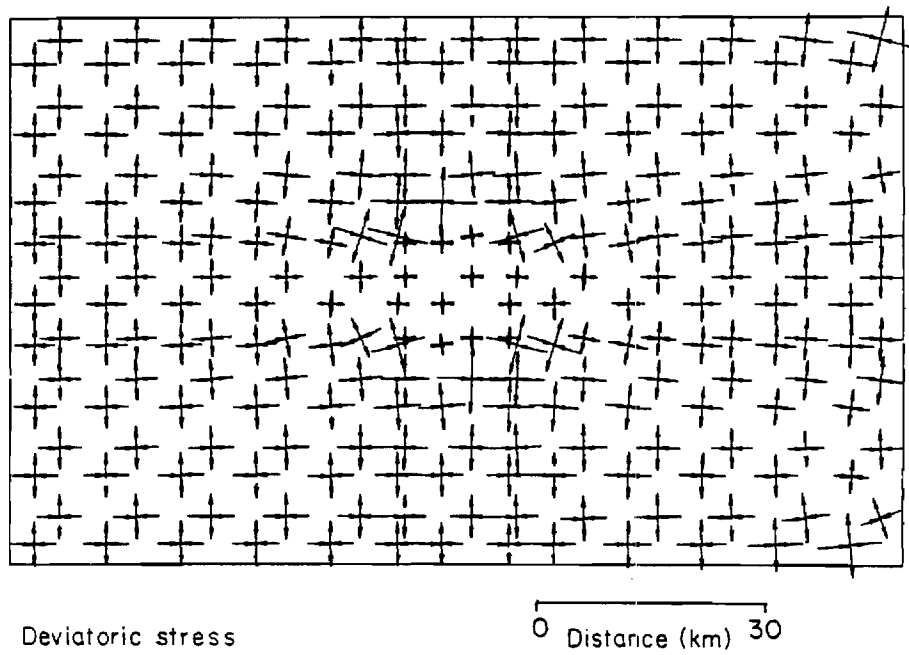


Figure 7. Deviatoric stresses surrounding a weak zone in a horizontal crustal plate. Contours are in MPa.

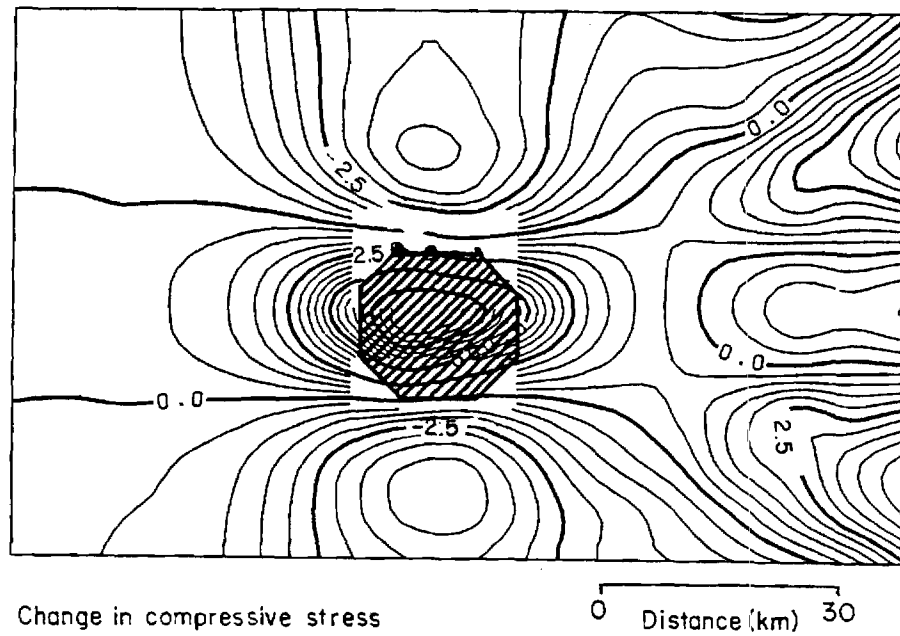


Figure 8. Dilatation surrounding a weak zone in a horizontal crustal plate.

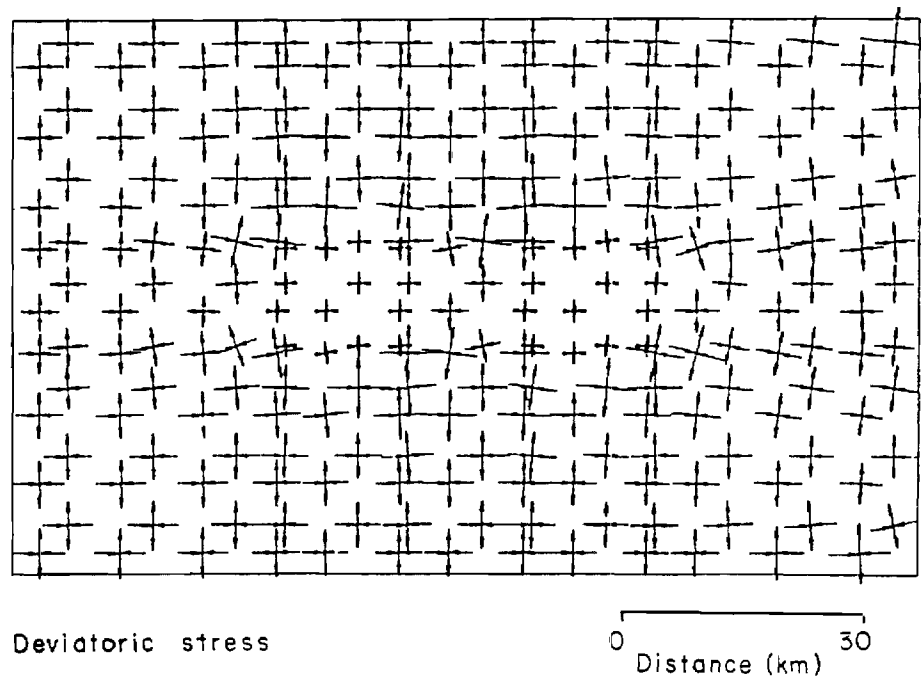


Figure 9. Deviatoric stress for two circular zones of weakened crust aligned parallel to the applied stress.

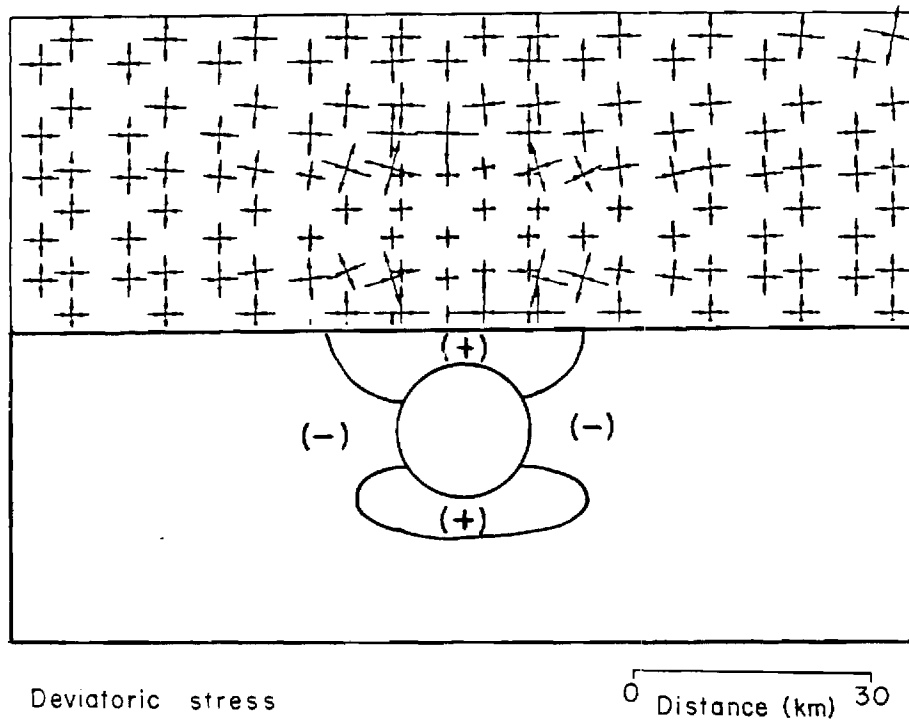


Figure 10. Deviatoric stress for two circular zones of weakened crust aligned perpendicular to the applied stress.

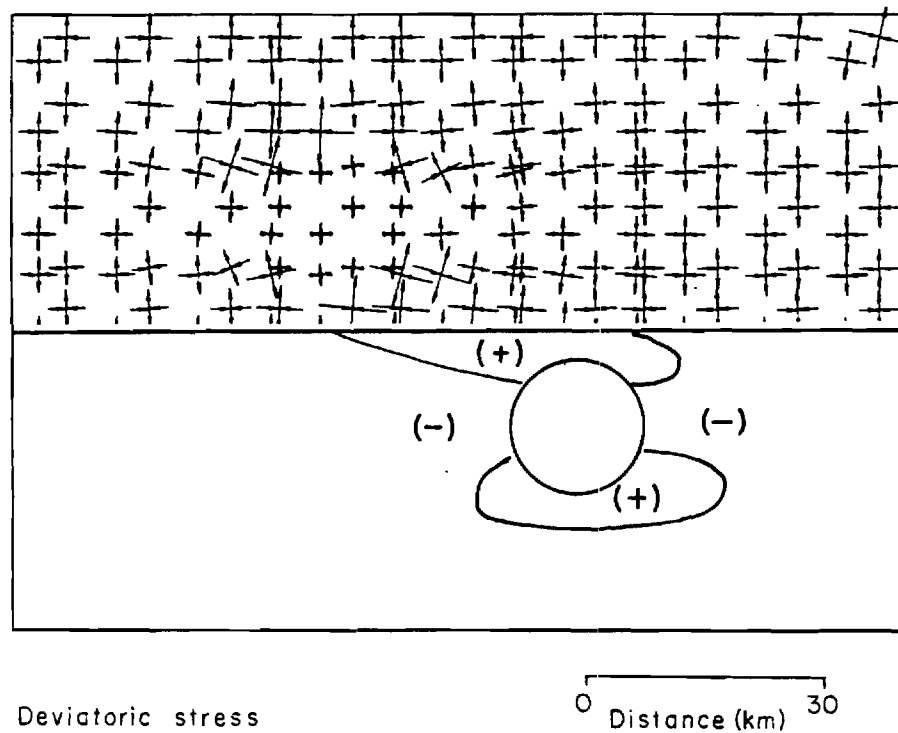


Figure 11. Deviatoric stress for two circular zones of weakened crust aligned at 45 degrees to the direction of applied stress.

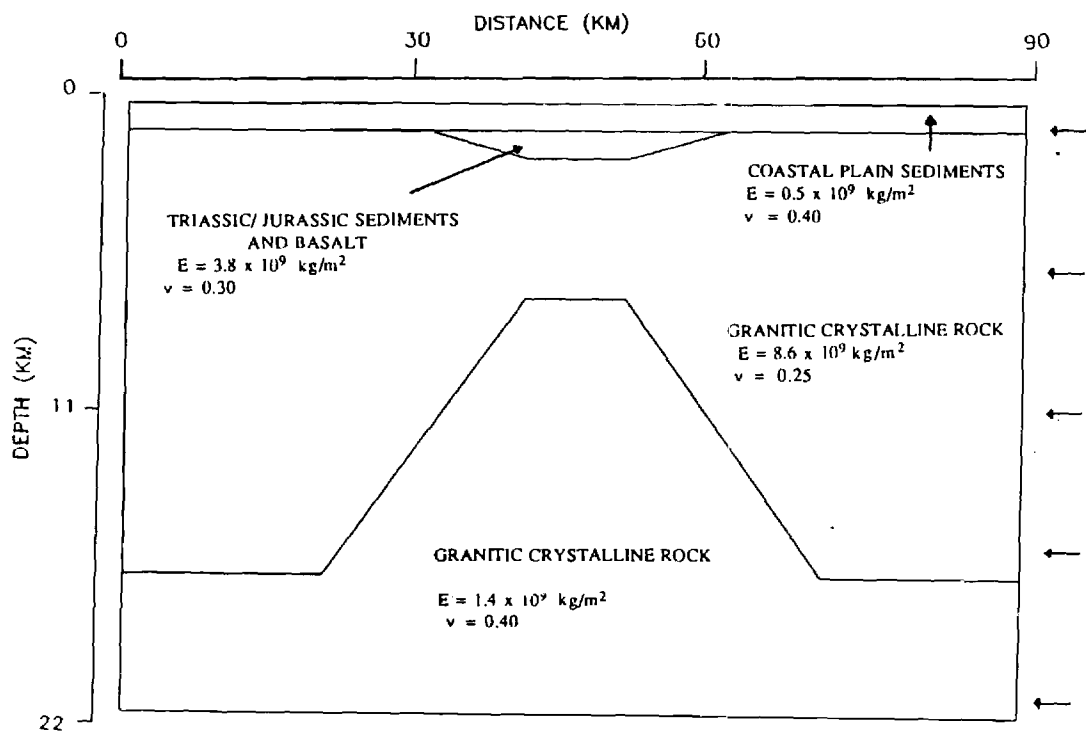


Figure 12. Geologic model for a vertical profile across a zone of weakness in the crust.

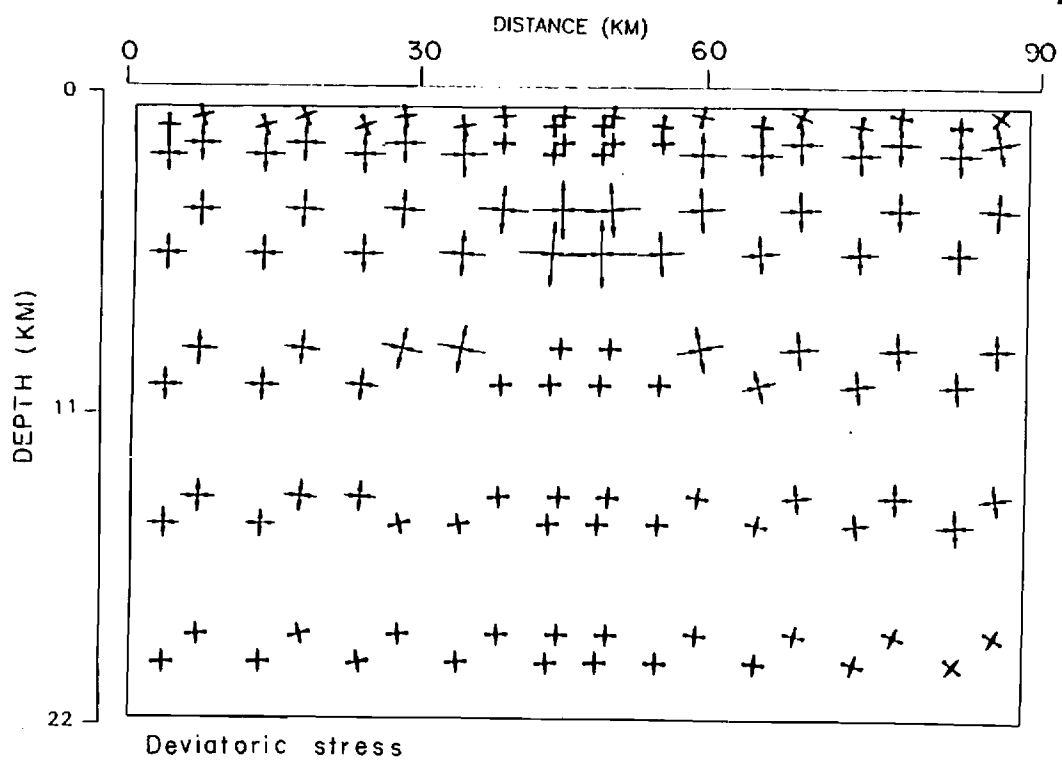


Figure 13. Deviatoric stress in a vertical section across a zone of weakness in the crust. See figure 12 for the model parameters. The top boundary is a free surface. Weak material is simulated across the bottom as well as in the weak zone. Forces applied to the right side were constant so that the differential response of the elastic properties of the shallow and deep crust leads to some irregularity in the stresses near the right boundary.

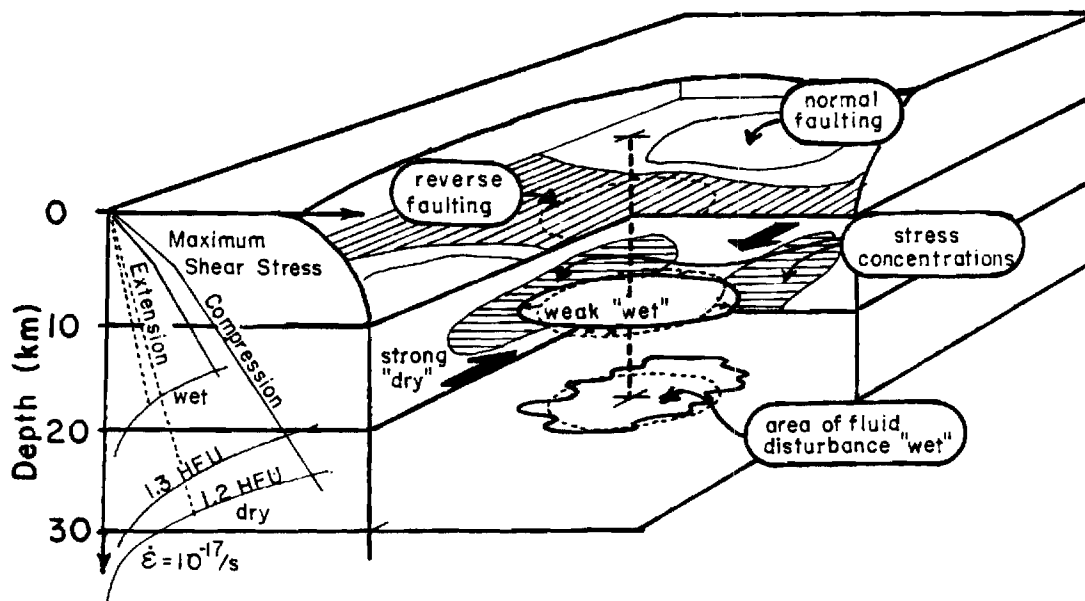


Fig. 14. Model for crustal stress surrounding a zone of weakness in the lower crust. The simplified conceptual diagram showing changes in the strength of the crust induced by thermal and fluid disturbances in the lower crust, is adapted from Meissner and Strehlau (1982).